Earth-Science Reviews 95 (2009) 1–52

Contents lists available at ScienceDirect

Earth-Science Reviews

journal homepage: www.elsevier.com/locate/earscirev

Quantitative paleoenvironmental and paleoclimatic reconstruction using paleosols

Nathan D. Sheldon [a,*], Neil J. Tabor [b]

[a] Department of Geological Sciences, University of Michigan, 2534 CC Little, 1100 N. University Ave., Ann Arbor, MI 48109, USA
[b] Department of Earth Sciences, Southern Methodist University, P.O. Box 750395, Dallas, TX 75275, USA

ARTICLE INFO

Article history:
Received 8 April 2008
Accepted 15 March 2009
Available online 27 March 2009

Keywords:
paleosols
paleoclimate
paleoenvironments
isotopes
geochemistry
pedogenesis

ABSTRACT

Paleosols (fossil soils) are preserved throughout the geologic record in depositional settings ranging from alluvial systems to between basalt flows. Until recently, paleosols were studied using primarily qualitative methods. In recent years, paleopedology has shifted from a largely qualitative field based on comparisons with modern analogues to an increasingly quantitative endeavor. Some of this change has been a result of applying existing techniques to new materials, but many of the innovations have been the result of applying new techniques to new materials, including thermodynamic modeling of soil formation, isotope geochemistry, and applications of empirical relationships derived from modern soils. A variety of semi-quantitative and quantitative tools has been developed to examine past weathering and pedogenesis, and to reconstruct both paleoenvironmental and paleoclimatic conditions at the time that the paleosols formed. Though it is often not possible to achieve the same temporal resolution as with marine records for paleoclimatic reconstructions, proxies based on paleosols are potentially a much more direct means of making paleoclimatic reconstructions because soils form at the Earth's surface, in direct contact with the atmospheric and climatic conditions at the time of their formation. Paleoclimatic and environmental properties that may be reconstructed using the new proxies include provenance, weathering intensity, mean annual precipitation and temperature during pedogenesis, nutrient fluxes into and out of the paleosols, the atmospheric composition of important gases including CO_2 and O_2, the moisture balance during pedogenesis, the soil gas composition, reconstructed vegetative covering, and paleo-altitude.

Contents

1. Introduction . . . 2
2. Qualitative methods . . . 4
 2.1. Taxonomic and stratigraphic approaches . . . 4
 2.2. Semi-quantitative methods . . . 5
  2.2.1. Compaction . . . 5
  2.2.2. Ichnology . . . 6
3. Quantitative methods overview . . . 7
4. Clay mineralogy of soils and paleosols . . . 7
 4.1. Occurrence of clay minerals . . . 7
5. Whole rock geochemistry . . . 8
 5.1. Analytical methods . . . 8
 5.2. Provenance and pedogenesis . . . 8
  5.2.1. Major element ratios and pedogenic processes . . . 8
  5.2.2. Major element weathering indices . . . 10
  5.2.3. Trace element ratios . . . 11
  5.2.4. Rare earth elements . . . 12
 5.3. Mass-balance calculations . . . 13
  5.3.1. Pedogenesis and diagenesis . . . 13
  5.3.2. Precambrian atmospheric CO_2 from mass balance . . . 14
 5.4. Paleotemperature . . . 15

* Corresponding author. Tel.: +1 734 647 7569.
E-mail address: nsheldon@umich.edu (N.D. Sheldon).

0012-8252/$ – see front matter © 2009 Elsevier B.V. All rights reserved.
doi:10.1016/j.earscirev.2009.03.004

5.5. Paleoprecipitation . . . 16
5.5.1. Content of Fe–Mn nodules in vertisols . . . 16
5.5.2. Depth to Bk horizon . . . 16
5.5.3. Bw/Bt horizon geochemistry . . . 17
5.6. Long-term chemical weathering . . . 17
6. Thermodynamic approaches . . . 18
6.1. Simple versus complex systems . . . 18
6.2. Single-equation approaches . . . 18
6.2.1. Precambrian atmospheric CO_2 . . . 18
6.2.2. Earliest Triassic soil formation . . . 20
6.3. Multiple-equation approaches . . . 20
7. Stable isotope approaches . . . 22
7.1. Stable isotopic composition of pedogenic minerals as paleoenvironmental proxies . . . 22
7.1.1. Mineral-water isotope fractionation and the jargon of stable isotope geochemistry . . . 22
7.1.2. Stable isotope fractionation factors of common pedogenic minerals . . . 23
7.1.3. Relationship between hydrogen and oxygen isotopes in continental waters . . . 25
7.2. Carbon in soils . . . 25
7.2.1. One-component soil CO_2 . . . 25
7.2.2. Two-component soil CO_2 . . . 26
7.2.3. Three-component soil CO_2 . . . 27
7.3. Soil and paleosol carbonate . . . 27
7.3.1. Pedogenic calcite $\delta^{18}O$ values . . . 27
7.3.2. Pedogenic siderite as a proxy for soil moisture $\delta^{18}O$ values . . . 30
7.4. $\delta^{13}C$ values of soil carbonate . . . 30
7.4.1. Calcite from one-component of soil CO_2 . . . 30
7.4.2. $\delta^{13}C$ of pedogenic siderite . . . 31
7.4.3. Calcite derived from 2-component soil CO_2 mixing . . . 31
7.4.4. Soil carbonates formed by mixing of three-components of soil CO_2 . . . 35
7.5. $\delta^{18}O$ and δD of hydroxylated minerals . . . 36
7.5.1. Origin of residual deposits . . . 37
7.5.2. Variations in soil moisture $\delta^{18}O$ and δD values . . . 37
7.5.3. Single-mineral paleotemperature estimates . . . 38
7.5.4. Mineral-pair $\delta^{18}O$ values . . . 40
7.6. Paleo-vegetation/paleo-photosynthesis . . . 40
8. Future approaches and challenges . . . 41
8.1. Boron isotopes . . . 41
8.2. Energy balance models . . . 42
8.3. “Clumped isotope” paleothermometry . . . 43
9. Summary . . . 44
Acknowledgements . . . 44
Appendix A. Supplementary data . . . 44
References . . . 44

1. Introduction

Increasing recognition of paleosols (fossil soils; Fig. 1) in non-marine strata has opened up new types of paleoenvironmental and paleoclimatic reconstructions. While good quantitative paleoclimatic data may be obtained from plant fossil assemblages using either nearest living relative (e.g., Leopold and Clay-Poole, 2001; Utescher and Mosbrugger, 2007) or leaf morphometric approaches (e.g., Wolfe, 1994; Uhl et al., 2007), those approaches yield snap shots of past environments and are relatively rare in the fossil record. Paleosols preserved in continental basins on the other hand, raise the possibility of long-term, fairly continuous paleoclimatic records, potentially with a temporal resolution that equals that of marine proxy records (e.g., Retallack et al., 2004b; Sheldon and Retallack, 2004; Retallack, 2007). The last point is crucial because unlike most marine proxies, which are fundamentally indirect climatic records, paleosols formed at the Earth's surface, in direct contact with climatic and environmental conditions that prevailed at the time of their formation. Potentially then, paleosol-based proxies could be among the most powerful tools for reconstructing past environments. Until recently, paleopedology (the study of paleosols) was largely a qualitative science that relied on the recognition of features similar to modern soils that allowed for a “nearest living relative” comparison. That is, a paleosol was identified as indicating an ancient grassland if it had features similar to a modern grassland (Fig. 2). This approach still underlies most paleopedology, but has some fundamental limitations, namely the need for taxonomic uniformitarianism. Continuing on with the grassland example, the origin of grasses is most likely in the Cenozoic (e.g., Strömberg, 2002). However, paleosol-based estimates for the origin of grasslands as evidenced by Mollisol-like paleosols range from Eocene to Miocene (Retallack, 1997a,b, 2001a,b) depending on the strictness of one's taxonomy. Furthermore, others (Terry, 2001) have described Oligocene-age paleosols as “Mollisols” without meaning to connote that a grassland ecosystem was present. On the other hand, there are some types of paleosols found in the Earth's past for which there are imperfect analogues (e.g., Retallack, 1997c; Sheldon, 2005), or for which there is no appropriate modern analogue owing to different environmental and ecological conditions in Earth's past. For example, weathering at the Earth's surface was occurring in the Precambrian (e.g., Driese, 2004; Sheldon, 2006b), but under the influence of microbial enhancement only in the absence of higher plants.

The emergence of new quantitative techniques for reconstructing various paleoenvironmental and paleoclimatic conditions using whole rock and isotopic geochemistry has fundamentally changed the field of paleopedology. Proxies for variables ranging from levissage to mean annual precipitation to the composition of the paleo-atmosphere at the time of the paleosols' formation have now been developed. Some of the approaches that we describe in this review have been widely applied, others have not but could have wider applicability. We also attempt to “gaze into the crystal ball” to evaluate

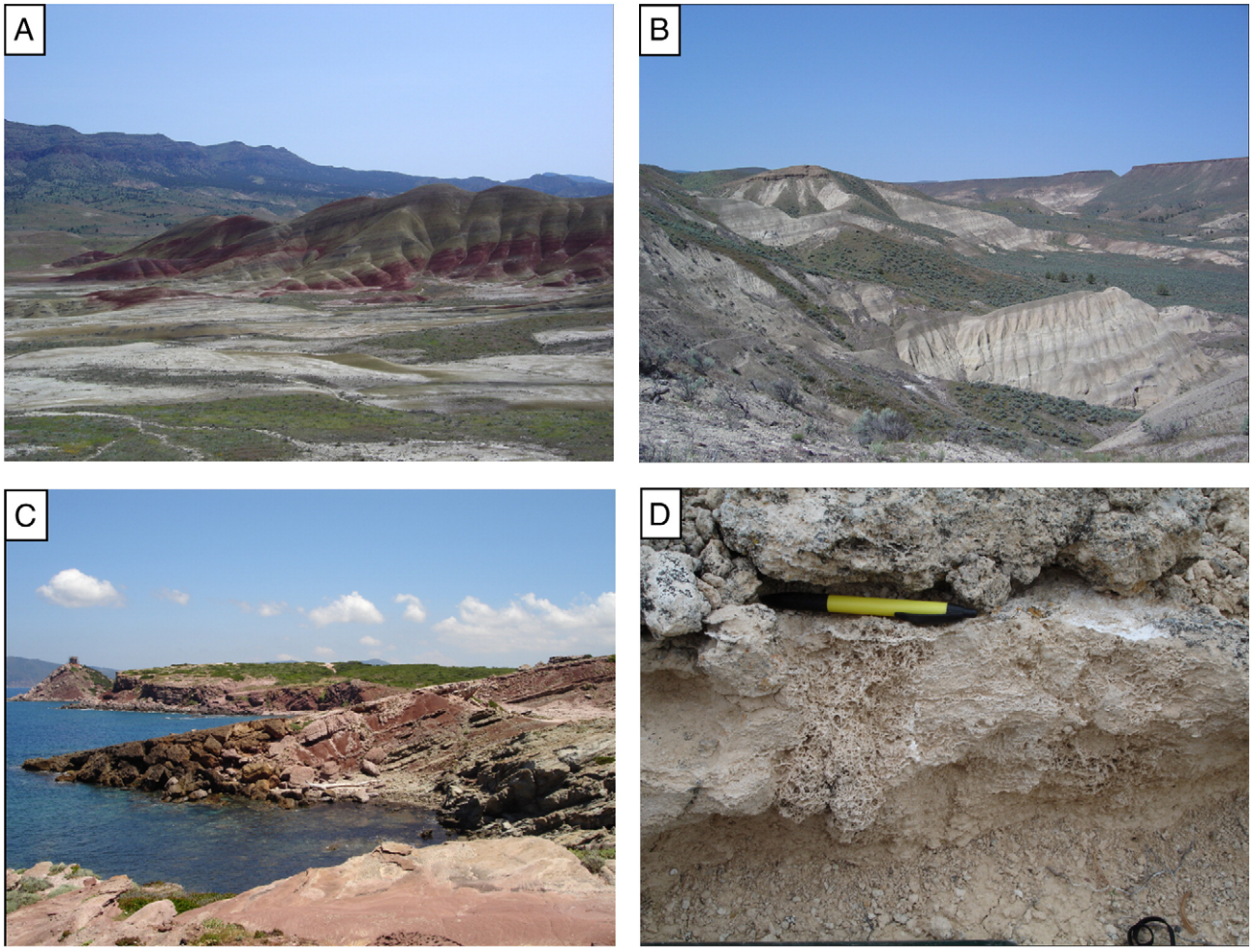

Fig. 1. Photos of representative paleosols. A) Painted Hills Unit, Eocene, Oregon. Dominated by Alfisol-like paleosols. B) Mascall Formation overlook, Miocene, Oregon. Near-mollic Inceptisol-like paleosols. C) Classic "red beds" from the Permian Cala del Vino Formation, Sardinia. D) Close-up of root mat carbonate rhizoliths, Renova Group, Montana.

some future directions and some ways in which existing proxies may be extended. In general, no single proxy for weathering processes or past environmental conditions, or single type of quantitative data is without limitations. Therefore, a multi-proxy approach is key both to giving the investigator the widest possible range of information, but also to ensure reproducibility of her/his results. Thus, the approach

Fig. 2. Comparison between modern soil and paleosol equivalent. A) Modern xeric Mollisol, southwestern Montana; B) late Miocene xeric Mollisol, central Oregon.

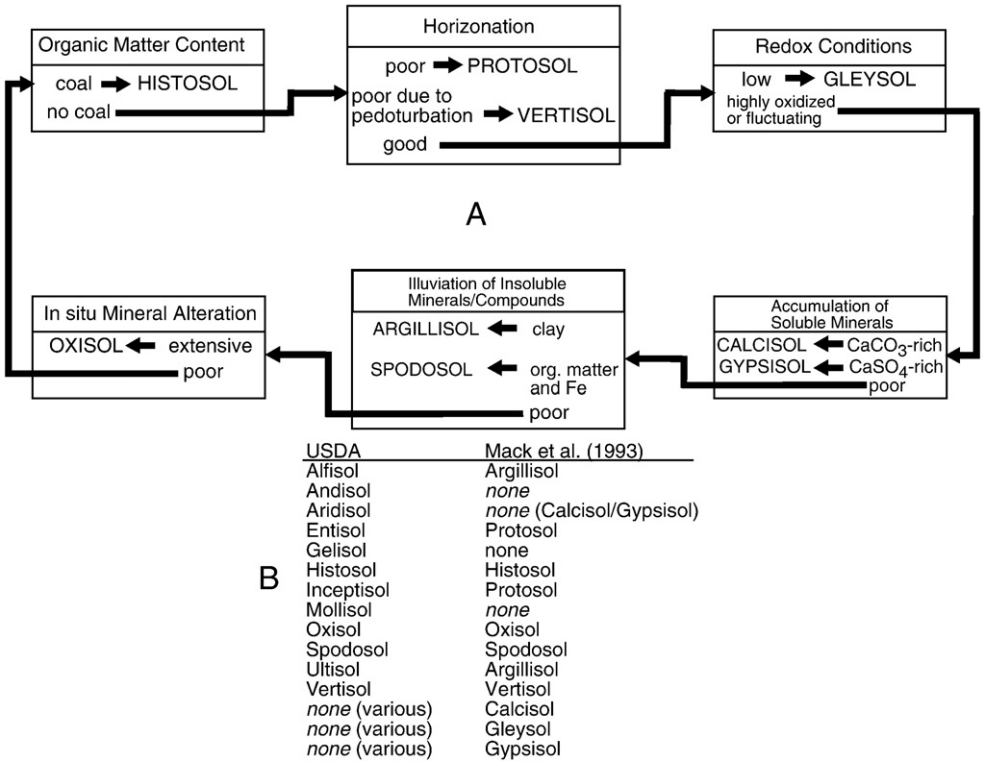

Fig. 3. Comparing taxonomic schemes. A) Paleosol-specific classification scheme; B) equivalent taxonomic units, modern soil Orders are from Soil Survey Staff (2006). Part A is modified after Mack et al. (1993).

that has emerged, and that we endorse here, is to try to quantify past pedogenic processes and the environmental conditions present at the time that the soils formed, with taxonomy and "nearest living relative" analogues of paleosols serving as an important additional tool rather than as the focal direction.

2. Qualitative methods

2.1. Taxonomic and stratigraphic approaches

There is a long history of using qualitative methods to describe paleosols and to characterize the paleoclimatic and paleoenvironmental conditions in which the paleosols formed. These qualitative methods include both taxonomic and stratigraphic approaches, and still form an important template of basic information onto which the newer quantitative methods are applied. While it is beyond the scope of this review to look at those approaches in any exhaustive fashion, interested readers are directed to earlier review papers by Retallack (1991) and Kraus (1999) that detail many of the commonly applied approaches to paleosol taxonomy whether using modern analogues (Retallack and Germán-Heins, 1994), modern taxonomy (pedotype approach; e.g., Retallack, 1994), or paleosol-specific taxonomy (e.g., Mack et al., 1993). The fundamental difference is that the paleosol-specific taxonomy is a hierarchical system that relies primarily on observable features in the paleosols (Fig. 3; Table 1), whereas the modern analogue and modern soil taxonomic approaches attempt to identify a larger number of characteristics and may require the investigator to abandon their *sensu stricto* usage because some key modern taxonomic features (e.g., cation exchange capacity) are not preserved by paleosols. Fig. 3 also includes a list of taxonomic equivalents between the modern soil and paleosol-specific taxonomic schemes.

Stratigraphic approaches to the study of paleosols include applications of sequence stratigraphy and of the pedofacies concept (e.g., Kraus, 1999). Sequence stratigraphy is a conceptual framework for evaluating depositional systems in terms of the balance between accommodation space for deposition and basin filling processes. It assumes cyclical deposition due either to fluctuating climatic conditions or sea level cyclicity. Sequence stratigraphy has been fairly widely applied in continental, paleosol-bearing sections on both deep-time geologic (various, e.g., McCarthy and Plint, 2003; Atchley et al., 2004; Cleveland et al., 2007; Ruskin and Jordan, 2007; Mack et al., in revision) and Quaternary (Kemp et al., 2006) time scales. The pedofacies concept advocated by Kraus and others (Bown and

Table 1
Paleosol taxonomic modifiers (Mack et al., 1993).

Modifier	Feature
Albic	Presence of an eluvial (E) horizon [Fe and Al compounds accumulated]
Allophanic	Presence of allophone or other amorphous Si and Al compounds
Argillic	Presence of illuvial [downward transported] clay
Calcic	Presence of pedogenic carbonate
Carbonaceous	Presence of dark organic matter, but not coal
Concretionary	Presence of globules with concentric fabric
Dystric	Low base status as indicated by relative paucity of chemically unstable grains such as feldspars and volcanic rock fragments
Eutric	High base status as indicated by the abundance of chemically unstable grains such as feldspars and volcanic rock fragments
Fragic	Subsurface horizon that was hard at the time of soil formation (e.g., root traces and burrows terminate or are diverted at this horizon; hard pan)
Gleyed	Evidence of periodic waterlogging such as drab hues, mottles of drab colors and yellow, red, or brown, presence of pedogenic pyrite or siderite
Gypsic	Presence of vadose gypsum or anhydrite
Nodular	Presence of globules with undifferentiated internal fabric; typically composed of carbonate, silica, or Fe-oxides
Ochric	Presence of a light-colored A horizon
Salic	Presence of pedogenic salts more soluble than gypsum (e.g., halite)
Vertic	Presence of decimeter-scale dessication cracks, wedge-shaped peds, hummock and swale structures (gilgai micro-relief), slickensides, or clastic dikes
Vitric	Presence of relict or actual volcanic glass shards or pumice

Kraus, 1987; Kraus, 1987; Kraus, 1997) is based on the idea that paleosol formation should be viewed in terms of the depositional processes and system that it formed in (as individual facies within the depositional system), rather than as an independent entity. Summing up their findings from the Eocene Willwood Formation briefly, paleosol maturity should increase with distance away from a fluvial channel, going from Entisol-like (Protosol) paleosols immediately adjacent to the channel to more well-developed paleosols on more distal areas of the floodplain (Bown and Kraus, 1987; Kraus and Aslan, 1993; Kraus, 1997). Flood frequency (i.e., recurrence interval), flood intensity (e.g., proportion of the floodplain inundated), and rate of accommodation space creation (denudation/subsidence) are important controlling variables (Kraus, 1999). More recent applications of the pedofacies concept have found more complex maturity-floodplain position relationships (Hamer et al., 2007b), but the general concept appears widely applicable. Applications of sequence stratigraphy and the pedofacies concept are particularly important in long-term paleoclimatic studies, because paleosol maturity has often been used to indicate climatic intensity (references in Retallack, 2001b; Retallack et al., 2000). While maturity and weathering intensity may indicate climatic conditions (Retallack and Germán-Heins, 1994), they could equally indicate long formation times and floodplain stability (Kraus, 1997). Cyclical changes to the depositional system are probably due to short-term climate fluctuations or to locally magnified effects based on global drivers such as Milankovitch cyclicity (e.g., Retallack et al., 2004b), and need to be taken into account when reconstructing past climatic and environmental conditions. The approach advocated by Buck and Mack (1995), Sheldon et al. (2002), Sheldon and Retallack (2004), and Sheldon (2006c) is to compare only paleosols of similar maturity and similar inferred physiographic setting (i.e., similar pedofacies) when reconstructing past climatic conditions. By confining proxy-based reconstructions of paleo-precipitation and paleo-temperature to moderately to well-developed paleosols (Inceptisol-like to Alfisol-like), those authors have reconstructed past climatic conditions that very closely match reconstructions based on fossil floras (Sheldon et al., 2002; Sheldon and Retallack, 2004). Close consideration of data quality and recognition of alluvial stratigraphy often lead to fairly substantial differences in climatic histories (e.g., Terry, 2001 versus Retallack, 1983), so careful understanding of stratigraphic and facies relationships is critical.

2.2. Semi-quantitative methods

2.2.1. Compaction

Sheldon and Retallack (2001) presented a straightforward method for evaluating the effects of compaction on paleosols and for decompacting soils to their original thickness at the time of their formation. That paper also reviewed previous attempts to make the same types of calculations from Retallack (1994) and Caudill et al. (1997), both of which mis-estimated compaction of shallowly buried paleosols, and demonstrated the issues associated with those previous methods. The decompaction method of Sheldon and Retallack (2001) can only be considered to be semi-quantitative because it relies on accurate taxonomic description of the paleosols in order to determine the correct constants to use in the generalized equation.

Soils and their associated sediments are compactable because they include some porosity between the individual constituent grains. How compactable a given soil or sediment type will be is a function of their solidity (the fractional complement to porosity):

$$S_i = \frac{\rho_d}{\rho_s} \tag{1}$$

where ρ_d is the dry bulk density of the soil and ρ_s is the solid grain bulk density of the material that was weathered to form the soil. For most soils, ρ_s will be 2.5–2.9 g cm^3, where 2.7 g cm^3 is a reasonable value for clay-rich soils (Sheldon and Retallack, 2001; Table 2). The compaction of a given soil is given by:

$$C = \frac{S_i}{S_b} \tag{2}$$

where S_b is the burial solidity, which should exceed S_i for a material that has been compacted, thus giving $C<1$. For normally pressured sections, the generalized compaction equation of Sclater and Christie (1980) may be used as a starting point:

$$F = F_0 e^{-kD} \tag{3}$$

where F is the fractional burial porosity, F_0 is the initial porosity, D is the burial depth expressed in km, and k is an empirically derived curve-fitting constant (for equation, see Sheldon and Retallack, 2001). Because porosity is the complement of solidity (i.e., $F_0 = 1 - S_i$ and $F = 1 - S_b$), Eq. (2) can be combined with Eq. (3) and re-arranged to give compaction (C) as follows:

$$C = \frac{-S_i}{\left[\frac{F_0}{e^{kD} - 1}\right]} \tag{4}$$

Fig. 6 depicts compactibility differences among some common soil orders with burial depth using constants for S_i, F_0, and k from Table 2. The method has been widely applied both to long sequences of paleosols (e.g., Sheldon and Retallack, 2004; Cleveland et al., 2007) and to individual paleosols for paleoclimatic (e.g., Prochnow et al., 2006; Retallack, 2007) and paleoaltimetry (e.g., Takeuchi et al., 2007) applications. In general, this method gives results that closely match independent estimates of compaction, though the results depend in part on accurate taxonomic description of the paleosols because there is a wide range in the properties of analogous modern soils (Table 2).

Table 2
Paleosol decompaction constants.

Substrate	Density	Range	σ	S_i	F_0	k
Marine (Sclater and Christie, 1980)						
Shale	1.07	–	–	0.37	0.63	0.51
Sand	1.35	–	–	0.51	0.49	0.27
Chalk	0.81	–	–	0.30	0.70	0.71
Shaley sand	1.18	–	–	0.44	0.56	0.39
Soil types						
Alfisol (n =46)	1.68	1.33–1.97	0.16	0.65	0.35	0.15
Andisol (n =26)	0.79	0.44–1.50	0.27	0.30	0.70	0.71
Aridisol (n =24)	1.60	1.39–1.76	0.09	0.62	0.38	0.17
Entisol (n =3)	1.61	1.60–1.64	–	0.62	0.38	0.17
Histosol (n =13)	0.07	0.04–0.10	0.02	0.06	0.94	2.09
Inceptisol (n =41)	1.32	0.65–1.92	0.39	0.51	0.49	0.27
Mollisol (n =50)	1.42	0.85–1.91	0.25	0.55	0.45	0.23
Oxisol (n =31)	1.30	0.96–1.46	0.11	0.50	0.50	0.29
Spodosol (n =20)	0.97	0.30–1.87	0.47	0.37	0.63	0.52
Ultisol (n =38)	1.50	0.97–1.84	0.27	0.58	0.42	0.20
Vertisol (n =380)	1.80	1.55–2.06	0.16	0.69	0.31	0.12
Modern floodplain (Nadon and Issler, 1997)						
Inorganic silts and clays						
Mean (Liquid limit <50)[a]	–	–	–	0.635	0.365	0.16
Mean (Liquid limit >50)[b]	–	–	–	0.511	0.489	0.27
Sands						
Mean[c]	–	–	–	0.692	0.308	0.12

Note: Units of density and range are g cm^{-3}. Units on k are $\times 10^{-5}$ cm^{-1}. Original sources for the paleosol data contained in the table are given in Sheldon and Retallack (2001).

[a] Silts (n = 61) and clays (n = 261); porosity ranges from 35.72% to 37.34%.

[b] Silts (n = 9) and clays (n = 61); porosity ranges from 46.96% to 50.80%.

[c] Clean (graded; n = 20), clean (poorly graded; n = 62), silty sands (n = 153), and clayey sands (n = 88); porosity ranges from 30.10% to 31.59%.

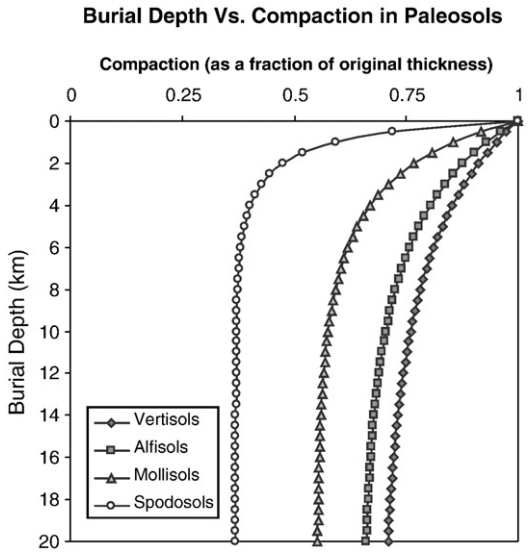

Fig. 4. Compactibility of different soil orders.

To give one specific example, Retallack (1986) used ptygmatically folded clastic dikes in the ~2.2 Ga Hekpoort paleosol to estimate that it had been compacted to 67–73% of its original thickness. Sheldon and Retallack (2001) used Eq. (4) and constants for a Vertisol (Retallack, 1986; Driese et al., 2005) from Table 2 to estimate compaction to 72–76% of original thickness given independent constraints on burial depth.

The primary disadvantages to the approach of Sheldon and Retallack (2001) are that it requires accurate soil taxonomy and that it requires a fairly accurate estimate of the burial overburden. Because the differences in compactibility among different soil orders can be fairly large (Fig. 4), accurate taxonomic identification is very important. Similarly, most of the compaction predicted by Eq. (4) occurs within burial depths of 4 km or less, with very little change among deeply buried paleosols. Thus, uncertainty in burial depth of even 500 m for shallowly buried paleosols would have a large effect on the calculated compaction.

2.2.2. Ichnology

A number of recent workers have begun integrating continental ichnology with studies of paleosols (e.g., Genise et al., 2004; Kirkland, 2006; Kraus and Hasiotis, 2006; Laza, 2006; Hamer et al., 2007a,b), and trace fossils have been key to understanding some early ecosystems (e.g., Feakes et al., 1989; Retallack and Feakes, 1987). A wide variety of animal and plant traces have been identified (e.g., Hasiotis, 2004) that are useful in paleoenvironmental reconstructions using paleosols. In particular, rhizolith or root trace density (Fig. 1D) and penetration depth have been used to understand vegetation type and density (O'Geen and Busacca, 2001; Retallack, 2007) and to characterize the paleohydrological setting (Kraus and Hasiotis, 2006). In marine settings, a semi-quantitative ichnofabric index has been created (Droser and Bottjer, 1986) that looks at total bioturbation density. Attempts to apply this method to paleosols have been relatively rare and as Genise et al. (2004) point out, well-developed

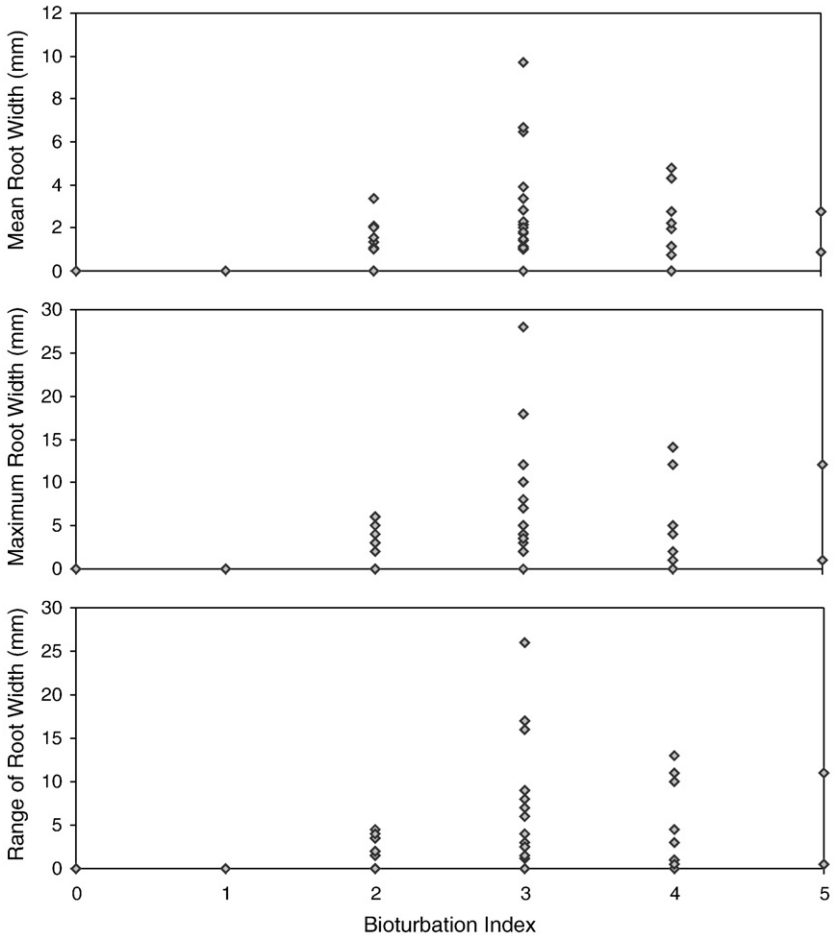

Fig. 5. Bioturbation index versus root size in paleosols. Data are from N.D. Sheldon and J.M.M. Hamer (unpublished). See text for discussion.

paleosols may be nearly devoid of bioturbation and poorly developed paleosols may be very heavily bioturbated, so the definitions appropriate to a marine setting do not necessarily apply to a continental setting. In part, this is due to fluctuating water tables and redox conditions in continental settings. Whereas hydrological and chemical conditions in a marine setting may be relatively uniform over long periods of time, they may fluctuate on very short time scales in continental settings (i.e., seasonally), which affects both the creation and preservation of ichnofabric. Furthermore, bioturbation in paleosols may be the result of either animals or plants, so care is needed to delineate both types. For example, while most animals in continental settings (exceptions are bivalves or gastropods) are unlikely to burrow down past the level of the water table, plant roots are very likely to extend to that depth beneath the surface. An example of an attempt to use ichnology semi-quantitatively rather than qualitatively may be found in Fig. 5 using previously unpublished data collected from Miocene paleosols in Montana formed on fine-grained overbank flood deposits. Working independently, one half of the team (N.D. Sheldon and J.M.M. Hamer) measured various root trace parameters (mean diameter, maximum diameter, range of root diameter at a given stratigraphic level) and the other half of the team made semi-quantitative assessments of the degree of bioturbation made by animals throughout a 60 m section (Fig. 5). This approach yielded a couple of interesting results. The highest mean root diameters, maximum root diameter (and by extension maximum plant size), and maximum range of root diameters are associated with moderate degrees of bioturbation, suggesting that while some bioturbation helps plant communities to become established, heavy bioturbation may impede growth of high stature plants, instead favoring low stature or fast-growing plants. The data also skew toward mid-range root diameters in heavily bioturbated paleosols and only small roots (with a small size range) are found in weakly bioturbated paleosols (Fig. 5). While more work is needed to confirm these results and to extend them to other depositional settings, these results suggest that there is considerable scope for integrating semi-quantitative as well as qualitative ichnological data with studies of paleosols.

3. Quantitative methods overview

In recent years, paleopedology has shifted from a largely qualitative field based on comparisons with modern analogues to an increasingly quantitative endeavor. Some of this change has been a result of applying existing techniques to new materials (Sections 4 and 5 below, clay mineralogy and whole rock geochemistry), but many of the innovations have been the result of applying new techniques to new materials, including thermodynamic modeling of soil formation, isotope geochemistry, and applications of empirical relationships derived from modern soils. Paleoclimatic and environmental properties that may reconstructed using the new proxies include provenance, weathering intensity, mean annual precipitation and temperature during pedogenesis, nutrient fluxes into and out of the paleosols, the atmospheric composition of important gases including CO_2 and O_2, reconstructed vegetative covering, and paleoaltitude.

4. Clay mineralogy of soils and paleosols

The clay size fraction in soils is operationally defined as the population of grains and crystals that are <2 μm equivalent spherical diameter (e.s.d.; e.g., Soil Survey Staff, 1975). In a strict sense, therefore, clay minerals can be any mineral in the soil that is <2 μm e.s.d. In practice, however, the term clay minerals usually refers to finely crystalline minerals that result from pedogenic alteration, and most commonly is applied to phyllosilicates, oxides, and oxyhydroxides. It has long been recognized that soil clay minerals are correlated with climate factors, such as temperature and water availability in the soil, because these factors strongly affect the amount and effectiveness of chemical weathering in the soil profile. The correlation of soil clay mineralogy with climate conditions has been reviewed extensively in numerous studies over the past five decades (e.g., Jackson, 1964; Pedro, 1982; Wilson, 1999), and this contribution makes no attempt to provide a thorough review of this subject. Earlier reviews suggest generally that clay mineralogy follows a weathering pattern, from hot and humid to cool and dry, in the order kaolinite → smectite → vermiculite → chlorite and mixed-layer phyllosilicates → Illite and mica. We provide below a brief summary of methods for clay mineral identification, and the occurrence of kaolinites and smectites in soil and paleosol profiles. This reflects that these two phyllosilicates are among the most abundant minerals that have been identified in paleosols, and therefore also most commonly have undergone quantitative geochemical analysis.

4.1. Occurrence of clay minerals

Kandite minerals, a group of 1:1 phyllosilicates, are recognized by a basal $d(001)$ spacing of ~7 Å that expands to 10 Å upon solvation with hydrazine and Dimethylsulfoxide (DMSO; Jackson and Abdel-Kader, 1978; Calvert, 1984). Kaolinite and Halloysite are common pedogenic minerals in soil profiles (Wilson, 1999), although halloysite is not a common constituent of paleosol profiles (Srodon, 1999). Pedogenic kaolinites form in well-drained and acidic soils with moderate silica activity and very low base cation activity in soil solutions (Dixon, 1989). This corresponds generally with soil formation in warm and humid climate. Kaolinite-dominated soil profiles are frequently associated with oxide and oxyhydroxide minerals such as goethite, hematite and gibbsite (e.g., Bárdossy et al., 1977; Tardy et al., 1990a,b). Kaolinite may also occur as a minor constituent in soils dominated by 2:1 phyllosilicates (Nash et al., 1988). Kaolinite is an abundant clay mineral in paleosol profiles that formed in paleotropical sites (e.g., Retallack and Germán-Heins, 1994; Gill and Yemane, 1996; Tabor and Montañez, 2004; Jacobs et al., 2005). Notable dissimilarities between modern pedogenic kaolinites and geological deposits include finer grain size, greater degree of disorder, and small amounts of isomophous substitution of Fe for Al in modern soil kaolinites (e.g., Herbillon et al., 1976). This may indicate that at least some diagenetic transformations occur in kaolinites.

Smectites, a large group of 2:1 phyllosilicate minerals, are recognized by a basal $d(001)$ spacing of ~12–14 Å which expands to ~18 Å in response to Mg-saturation and glycerol solvation, or expansion to ~20 Å upon glycol solvation (Moore and Reynolds, 1996). Montmorillonite and bedellite are the most common smectite minerals in soils and paleosols, and both minerals permit a substantial amount of isomorphous substitution in the tetrahedral and octahedral layers (Wilson, 1999; Tabor et al., 2004a,b; Tabor and Montañez, 2005). Pedogenic smectite forms in poorly drained soils characterized by high pH, with high chemical activity of silica and basic cations (Borchardt, 1989). This corresponds generally to intermittently poorly drained environments, including monsoonal and xeric climates characterized by strongly seasonal precipitation. Smectite-dominated soil profiles are frequently associated with hematite and calcite.

The clay size fraction in soils and paleosols is seldom composed of a single mineral. Rather, it typically includes mixtures of phyllosilicate, Fe- and Al- (oxyhydr) oxides, quartz and occasionally feldspars that cannot easily be separated from each other. As a result, mineralogical and geochemical characterization of discrete minerals in the soil (or paleosol) clay size fraction is complicated. Three approaches have been used to address complex clay mineral mixtures: (1) Adopt assumptions about the composition of minerals in the mixtures that are not under study in order to calculate an end-member composition for the mineral of interest (e.g., Bird and Chivas, 1988a,b; Lawrence and Rashkes Meaux, 1993), (2) ignore complications that may arise

from variability in mineral content of the clay size fraction (Tabor et al., 2004a,b), or (3) utilize non-routine physical and chemical separation (Munsterman and Kerstholt, 1996; see also review of separation techniques in Gilg and Sheppard, 1996) or spectroscopic techniques (Tabor and Montañez, 2005) in order to delineate the relative concentrations of different minerals in the clay-size fraction.

5. Whole rock geochemistry

5.1. Analytical methods

Paleosols may be analyzed as "whole rocks" in a manner similar to other geological materials. Typically, this involves the use of either X-ray fluorescence (XRF) or inductively coupled plasma optical/atomic emission spectroscopy (ICP-OES/AES) or mass spectrometry (ICP-MS). Both types of analyses offer different advantages and disadvantages. XRF analysis is non-destructive, offers a wide variety of major (from fused glasses), and trace and rare Earth (from pressed pellets), is relatively low-cost, and offers both precise and accurate results. Disadvantages of XRF analysis include "fussy" sample preparation that involves measurement of sample masses to many decimal points of precision, slow machine run times, and a lack of availability as many universities have shifted to ICP-based analysis because it can be used on a wider range of materials (e.g., soils and water too). Though neither ICP-OES/AES nor ICP-MS offer easily the full range of elements that can be analyzed by XRF, the combination of both techniques yields a similar suite. Other advantages include relatively "unfussy" sample preparation, low-costs, and quick analysis times. Disadvantages include the need to use both techniques to get adequate precision for the full suite of elements that are typically of interest, that ICP analysis is a destructive technique, Si volatilization in the presence of HF, and the use of highly reactive HF and/or perchloric acid to achieve sample dissolution.

One common problem with studies of paleosols is in having a well-constrained parent material to analyze as well. As will be discussed below, many of the geochemical proxies that have been proposed for analyzing past climatic and environmental conditions and past pedogenic processes are based on comparison with the chemical composition of the protolith/parent material. Thus, regardless of analytical methodology, it is very important that complete profiles (i.e., at least one sample of each horizon) including C or R horizon samples be collected whenever possible.

5.2. Provenance and pedogenesis

A number of different proxies based on whole rock geochemical analyses (Table 3) have been proposed for evaluating pedogenic processes in paleosols (see Retallack, 1997a,b,c). Most are based on ratios between different elements (Table 3), but in general, little justification has been given in the literature for why particular elemental ratios are meaningful. We are hoping to rectify that situation in this review by presenting clear examples of how and why (Table 3) different pedogenic processes may be evaluated using elemental geochemistry. By convention, major element data are presented as weight percentages of oxides and trace elements as ppm. From there, the convention is to convert the raw abundances into moles by dividing the weight percentage (or ppm) by the molecular mass (Table 4) before the equations are solved. For all of the geochemical functions that we present, the molar rather than oxide equivalent for a given element is shown (i.e., Ca rather than CaO, Na rather than Na_2O, etc.; Table 3).

Table 4
Molar masses.

Molecular masses of common oxides and elements	
Oxide/element	Molar mass ($g\ mol^{-1}$)
Al_2O_3	101.96
Ba	137.3
CaO	56.08
Ce	140.12
K_2O	94.2
La	138.91
Lu	175
MgO	40.32
MnO	60.94
Na_2O	61.98
Nb	92.9
Nd	144.2
P_2O_5	189.94
Rb	85.47
SiO_2	60.09
Sm	150.4
Sr	87.6
Th	232.04
TiO_2	79.9
U	238
Yb	173
Zr	91.22

5.2.1. Major element ratios and pedogenic processes

"Major elements" refers to the primary rock-forming elements Ca, Fe, K, Mg, Na, along with Al, O, and Si as building block elements for silicate minerals, and minor amounts of Mn, P, and Ti (Li, 2000). Typically, major element concentrations are measurable in terms of weight percent. The rock-forming elements can be separated according to redox sensitivity ($Fe^{2+/3+}$ and $Mn^{2+/3+/4+}$), valence (Ti^{4+} or P^{5+}), or chemical affinity (K and Na versus Ca and Mg). In particular, chemical affinity is useful because the majority of CO_2 consumption during weathering (e.g., Sheldon, 2006d) involves the monovalent alkali (K and Na) and divalent alkaline earth elements (Ca and Mg).

Table 3
Molecular weathering and pedogenesis ratios.

Ratio	Formula	Rationale	Pedogenic process
Major elements			
ΣBases/Al	$\frac{\Sigma Bases}{Al}$	ΣBases = Ca + Mg + Na + K Common rock-forming alkaline and alkaline earth elements are lost relative to Al during pedogenesis	Hydrolysis
Base loss	Base/Ti	Base cations (Ca, Mg, Na, K) should be leached during weathering at normal pH conditions and Ti accumulated	Leaching
Clayeyness	Al/Si	Al accumulated as clay minerals form	Hydrolysis
Gleization	FeO/Fe_2O_3	Fe^{2+} is most common and mobile under reducing conditions, whereas Fe^{3+} is immobile under oxidizing conditions	Oxidation
Provenance	Ti/Al	Ti is most readily removed by physical weathering, Al by chemical weathering	Acidification (~pH)
Salinization	$\frac{K + Na}{Al}$	Alkali elements accumulate as soluble salts not removed	Salinization
Trace elements			
Leaching	Ba/Sr	Sr solubility >Ba solubility	Leaching/hydrolysis
Parent Material	La/Ce, Sm/Nd, U/Th	Different parent materials have different initial trace element ratios prior to pedogenesis, but most of those elements are immobile during weathering, so the paleosol ratio should approximate the parent material ratio	Acidification (~pH)

For example, the large atomic radius alkali elements fit into different sites in minerals than the somewhat smaller alkaline earth elements. Observations of modern weathering of basalt parent soils suggest that the alkaline earth elements (which are also associated with more mafic minerals) weather more readily than the alkali elements (Chadwick et al., 1999), a pattern also observed in paleosols with a basaltic parent (see Section 5.3.1 for details; Sheldon, 2003; Tabor et al., 2004a; Sheldon, 2006c,d), though laterites formed on basalt do not necessarily conform to this rule of thumb (Hill et al., 2000). Elemental ratios are favoured over simple single-element measurements because the absolute abundance of an element within a soil/paleosol can vary dramatically over small spatial scales (e.g., between horizons), because the textural heterogeneity common in soils/paleosols can give rise to chemical heterogeneity, and because more process information is gained by looking at how two or more elements change with respect to one another.

Examples of commonly applied major element ratios used to explain individual pedogenic processes are given in Table 3. Proxies for hydrolysis include ΣBases/Al (see Section 5.2.2) and Al/Si. Al/Si is thought to be a measure of "clayeyness" because Al accumulates in clay minerals relative to a silicate mineral parent. The ratio was first proposed (though inverted from the present form) by Ruxton (1968) and has been widely applied (various, e.g., Retallack et al., 2000; Prochnow et al., 2006; Sheldon, 2006b; Hamer et al., 2007b). Among the applications of the Al/Si ratio is the confirmation of field classification of Bt horizons (Sheldon, 2005; Hamer et al., 2007b) and as a measure of provenance (e.g., Sheldon, 2006a). The primary weakness of applying the Al/Si ratio is that it is difficult to account for syn-formational additions of Si due to aeolian processes, although by looking at a suite of elements that are also prone to windborne addition (i.e., other commonly occurring crustal elements; alternatively, with REE, see Ziegler et al., 2007), it is often possible to distinguish that process from pedogenic changes.

The gleization ratio, Fe^{2+}/Fe^{3+}, is the most commonly applied major element ratio for understanding oxidation, though others have been proposed as well (see Retallack, 2001b for examples) based on Mn or on some combination of Fe and Mn. Gleization is sometimes used interchangeably with hydromorphism, and refers to the *in situ* reduction of Fe and Mn due to waterlogged conditions (Bockheim and Gennadiyev, 2000). As with other major element ratios, it is important to consider the parent material chemical composition (e.g., Driese et al., 2003) because the initial, unweathered gleization ratio may be very different for different parent materials. For example, unweathered basalt will typically have a gleization ratio in excess of 2, whereas samples from well-drained paleosols derived from basalt will typically have gleization ratios much less than 0.5 (Sheldon, 2003) owing to oxidation during weathering. Sayyed and Hundekari (2006) found a similar pattern, with gleization ratios in unweathered basalts of 4–5, and values generally <1 for modern soils and paleosols derived from basalt. Driese (2004) also presented a similar result when comparing modern and Precambrian Vertisols. An additional application of the gleization ratio has been to look at redox changes across mass extinction events. In the earliest Triassic, southern hemisphere high-paleolatitude Gondwanan paleosols consistently show higher gleization ratios (i.e., more reduced conditions) than their latest Permian predecessors, coincident with Permian-Triassic extinction, and often over the space of cms (Retallack, 1999; Sheldon, 2006a). This has been interpreted to represent a very rapid (<10,000 year; Retallack and Jahren, 2008) shift to highly reducing soil gas conditions. Given that paleosols above and below the boundary represent wetland settings (which should be fairly reduced anyway), this change is striking (Sheldon, 2006a). The primary weakness of applying the gleization ratio is one of constraining the timing of the reduction of Fe^{3+} to Fe^{2+}, because groundwater movement during early diagenesis (i.e., typically reducing waters) or exposure of the paleosol profiles to oxidizing waters during uplift and exposure could, theoretically at least, change the ratio. Ways to account for this possibility include careful characterization of the Fe-bearing minerals using petrography, SEM, or microprobe analysis, field observations of redoximorphic features in the paleosol (Kraus and Aslan, 1993), and mass-balance calculations (see Section 5.3.1 for details) of both redox-sensitive and redox-insensitive elements to look for evidence of diagenetic changes.

Salinization (Table 3) is the process by which otherwise mobile elements (K and Na) accumulate as soluble salts in a soil or paleosol. Examples of this process can be found fairly commonly in modern (e.g., Buck et al., 2006), Cenozoic (e.g., Hartley and May, 1998), and Mesozoic (e.g., Lawton and Buck, 2006) soils and paleosols that form in arid regions or deserts. Older examples are much more rare because salts are often removed by diagenesis, leaving evaporite mineral pseudomorphs rather than the original minerals. The salinization ratio may also be related to mean annual temperature in some settings (see Section 5.4; Sheldon et al., 2002), and though other ratios have been proposed (see Retallack, 2001a,b), only this one has been widely applied. However, salinization is not one of the most reliable pedogenic process indicators because of differences in behaviour between in K and Na during pedogenesis. In general, Na is less subject to diagenetic redistribution (Retallack, 1991). To verify salinization results, investigators should also look for other aridity indicators such as pedogenic carbonate nodules and physical presence of evaporite minerals in hand specimen or thin section.

Leaching may be quantified in paleosols using a base loss ratio where the abundance of a given base is divided by the abundance of Ti. This approach, though simple, bypasses the problem associated with full mass-balance calculations of needing to measure or estimate bulk density values for paleosol and parent material samples (see Section 5.3). In particular, it may be valuable for paleosols recovered from deep drilling cores where there is a limited amount of material available and using some of it for bulk density measurements (which are effectively destructive if the clod-paraffin method is used) is not possible (Sheldon, 2006c). The keys to using base loss ratios are that they must be plotted as a function of depth because different horizons should show different elemental behaviour, and that multiple elements need to be plotted, included both alkali and alkaline earth elements to capture the full range of pedogenic processes. P/Ti may also be plotted as a rough guide to paleo-fertility. This approach has been applied to basalt-parented paleosols thus far (Tabor et al., 2004a; Sheldon, 2006c), but should in theory, be widely applicable. The primary potential problem with this approach is with low-Ti parent materials, because then relatively minor differences in Ti content could show apparently large differences in pedogenesis. Thus, this approach to quantifying leaching works best for paleosols that have igneous or metamorphic parent materials, and less well for paleosols that formed on limestone or relatively quartz-rich parent materials.

The Ti/Al ratio is particularly useful as a provenance indicator because Ti contents may be quite variable among different types of rocks, even as Al contents are relatively constant (e.g., granite vs. basalt; Li, 2000). In general, the more mafic the parent material, the higher the Ti/Al ratio will be (Fig. 6; Maynard, 1992). Furthermore, because both elements are relatively immobile, the ratio should remain constant during pedogenesis at near-neutral pHs (5.5–8), and should also be constant as a function of depth within a paleosol (Sheldon, 2006a). At near-neutral conditions, Al is slightly more mobile than Ti (Li, 2000), and Al can be mobilized significantly in older soils (e.g., >150 Ka, Kurtz et al., 2000). Ti and Al are most mobile under acidic pH conditions, so the ratio should also potentially shift from the parent material value according to the pH at the time of formation. Neither element is redistributed readily by diagenesis, so the Ti/Al ratio should be a reliable indicator of provenance even for Precambrian paleosols if they formed at near neutral pH conditions and had short to moderate (<100 Ka) formation times, though potentially, it also may be used as paleo-weathering intensity measurement in paleosols that do not exhibit constant values with

depth in the profile (see below). Applications of the Ti/Al ratio include confirming similar provenance for latest Permian and earliest Triassic paleosols in a study of weathering intensity changes across the boundary (Sheldon, 2006a), to compare modern and Precambrian weathering of Vertisol-like paleosols (Driese et al., 2007), to compare provenance between different pedotypes and potential sediment source areas using Oligocene–Miocene paleosols (Hamer et al., 2007b), and to infer parent material homogeneity in Precambrian paleosols (e.g., Rye and Holland, 2000).

Fig. 6 depicts the Ti/Al ratio as a function of depth for various weakly- to moderately-developed paleosols that formed on different types of parent material. In each case, the mean parent material value is very close to the values at any position within the profile (i.e., nearly constant depth profile), and both mudstone and sandstone parents are characterized by low Ti/Al ratios. In contrast, basalt-parented paleosols show somewhat more variability with depth due typically to a minor component of ash and/or sediment, but also significantly higher Ti/Al ratios throughout the profiles. Taken together, these results suggest that the Ti/Al ratio is a reliable indicator of provenance (e.g., Stiles and Stensvold, 2008).

An example of using the Ti/Al ratio to examine weathering intensity is found in Fig. 7. In contrast to the moderately developed basalt-parented paleosols results shown in Fig. 6, the paleosols in Fig. 7 show significantly reduced Ti/Al ratios in the upper part of their profiles. The paleosols in Fig. 6 are all identified as being Inceptisol-like or Andisol-like (Protosol), whereas the more developed paleosols in Fig. 7 are all identified as being Alfisol-like (Argillisol). Closer inspection of the chemical data of Sheldon (2003, 2006d) indicates that both Ti and Al have been lost, but that Ti has been more extensively lost. In thin section, Ti-bearing minerals like rutile and Fe-oxides show minimal alteration. This suggests that the Ti loss at the top of the paleosols profiles is due to physical removal rather than chemical dissolution. That idea is further supported by the fact that the highest Ti/Al ratios are in the parental basalt. If Ti has been dissolved and transported within the profile downward into the B horizon of the paleosols, then that accumulation would result in the highest Ti/Al ratios at that level, which is not observed in any of the profiles. The primary weaknesses of this approach are with low Ti parent materials and in differentiating between chemical and physical removal of either Ti or Al during pedogenesis, though petrography/SEM studies offer a means to account for the second problem.

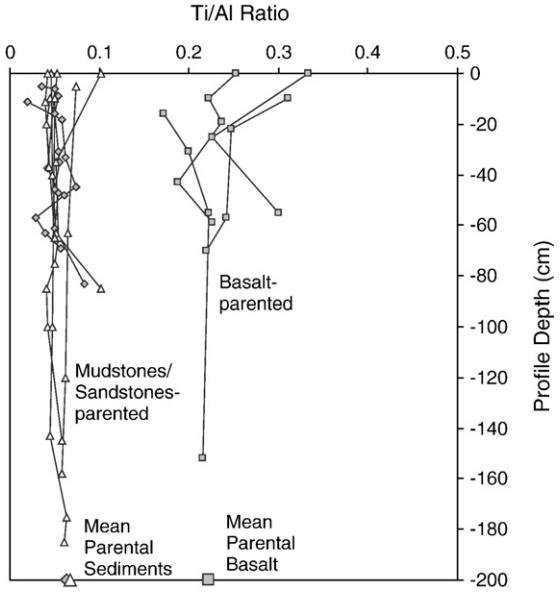

Fig. 6. Ti/Al ratios for moderately developed paleosols. Squares are basalt-parented Quaternary paleosols; data are from Sheldon (2006c). Diamonds are for sandstone-parented latest Permian and earliest Triassic paleosols; data are from Sheldon (2006a). Triangles are from mudstone-parented Eocene and Oligocene paleosols; data are from Sheldon et al. (2009).

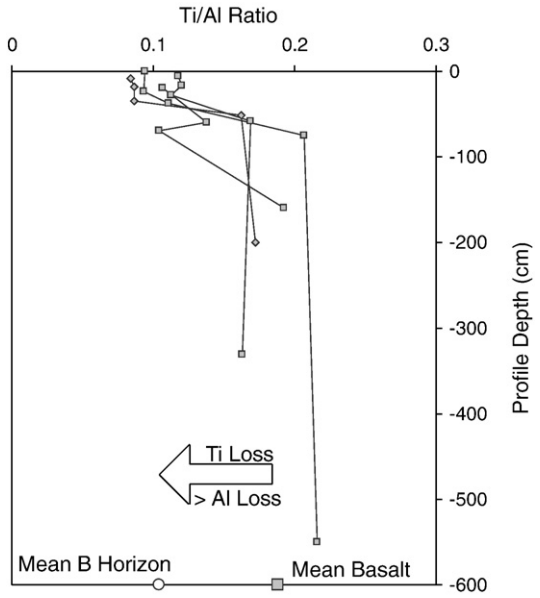

Fig. 7. Ti/Al ratios for well-developed paleosols on basalt. Data are from middle Miocene paleosols (Sheldon, 2003, 2006d).

5.2.2. Major element weathering indices

The other primary use of major element geochemistry has been to identify single indices that quantify the totality of weathering processes. The first of these was proposed by Nesbitt and Young (1982) and is called the "chemical index of alteration" or CIA:

$$\mathrm{CIA} = 100 \times \frac{\mathrm{Al}}{\mathrm{Al} + \mathrm{Ca} + \mathrm{K} + \mathrm{Na}} \quad (5)$$

where each of the elemental concentrations is coverted to moles. The CIA is a measurement of the weathering of feldspar minerals and their hydration to form clay minerals. As clay content increases Al should also increase, whereas Ca, K, and Na contents should decrease, leading to higher CIA values. For example, a pure sample of microcline ($KAlSi_3O_8$) would have a CIA value of 50. If it was weathered to form pure illite (which has a chemical formula similar to muscovite [$KAl_3Si_3O_{10}(OH)_2$]), the CIA value would increase to 75. Similarly, if the illite was completely leached of K and kaolinite was formed, the CIA value would further increase up to 100. Depending on the parent material chemistry, CIA changes during weathering may be quite large or relatively small. For example, tholeiitic basalt has CIA values of 40–45 (Sheldon, 2003); the formation of Alfisol-like paleosols (Argillisols) on tholeiitic basalts of the Columbia River Flood Basalt group under temperate conditions gave rise to B horizon CIA values of 60–70 (Sheldon, 2003). Parent materials that have already been cycled as sediments or which are clay-rich in the first place may start out with CIA values of 60–70, with weathering leading to even higher values. In general, the CIA is most useful for silicate rocks because a typical limestone would have very low Al levels to start with and thus, a very low CIA value that might not change appreCIAbly during pedogenesis.

More recent authors (Maynard, 1992; Fedo et al., 1995) have been concerned about post-burial addition of K by metasomatism and have modified the CIA to account for metasomatism by removing K from their modified CIA expressions in different ways. A second potential issue with K arises from illitization of clay minerals (e.g., smectites) in

sub-metamorphic burial conditions. This is particularly important for Paleozoic and older paleosols because smectite is meta-stable and may be altered to illite in the presence of K-rich pore waters. Nonetheless, unless there is evidence of K metasomatism or illitization (and this is primarily of interest in metamorphosed areas or with very old, i.e., Precambrian, paleosols) from petrography or some other method, the CIA is a good tool for evaluating chemical weathering and for comparing different paleosols. Both the CIA-K of Maynard (1992) and PIA of Fedo et al. (1995) of B horizons in soils are well-correlated with mean annual precipitation (see Section 5.5; Sheldon et al., 2002), so the primary recent use of the CIA-K has been for estimating paleoclimatic conditions (e.g., Nordt et al., 2006; Hamer et al., 2007a,b).

One final consideration with this type of weathering index is that there is one piece of nomenclatural confusion that has been propagated through the literature. The "chemical index of weathering" (CIW; Harnois, 1988) and CIA-K (Maynard, 1992) were developed for different purposes (Harnois (1988) was concerned about the inconsistent behaviour of K during pedogenesis, and Maynard (1992) was concerned about K addition by metasomatism), but, nevertheless, involve the same equation:

$$\mathrm{CIW(CIA-K)} = 100 \times \frac{\mathrm{Al}}{\mathrm{Al}+\mathrm{Ca}+\mathrm{Na}} \tag{6}$$

Retallack (various, e.g., 2001b; see Colman, 1982) has advocated a slightly different weathering index because while CIA and its variants give a good accounting of feldspar weathering, other types of minerals are not necessarily captured by that index, in particular Mg-bearing minerals. The ΣBases/Al ratio (Table 3) is designed to overcome this and is calculated with the following expression (again, using molecular values for each element):

$$\frac{\sum \mathrm{Bases}}{\mathrm{Al}} = \frac{\mathrm{Ca}+\mathrm{K}+\mathrm{Mg}+\mathrm{Na}}{\mathrm{Al}} \tag{7}$$

The ΣBases/Al ratio is susceptible to the same potential issues with metasomatically altered paleosols as the CIA, but again, unless there is some reason to suspect post-burial alteration, the ratio may be used to describe weathering of paleosols. ΣBases/Al has been used for a variety of purposes including characterizing weathering intensity (e.g., Retallack, 1999; Bestland, 2000; Retallack and Krull, 1999; Sayyed and Hundekari, 2006) and for taxonomic purposes (Sheldon et al., 2002). Sayyed and Hundekari (2006) compared a variety of weathering ratios including the ΣBases/Al ratio to examine differences between near-modern and Cretaceous weathering on "red bole" and "green bole" paleosols formed on Deccan Traps basalt flows. A ΣBases/Al ratio of 0.5 is a statistically significant dividing line between Alfisols (>0.5; dystric Argillisols) and Ultisols (<0.5; eutric Argillisols); that criterion is roughly equivalent to the Soil Survey Staff (2006) base saturation criteria of 35% to separate between base-rich Alfisols and base-poor Ultisols (Sheldon et al., 2002). An example where that criterion was applied can be found in Sheldon (2005), who used it to confirm a field identification of Alfisol-like paleosols. In addition, Clechenko et al. (2007) discuss a thick paleosol associated with the Paleocene–Eocene boundary as being comparable to a modern Ultisol. Using data from their paper (their Table 1), an average ΣBases/Al of 0.3 is obtained for the paleosols, lending additional support to this criterion as a means for distinguishing between paleo-Alfisols and paleo-Ultisols. A further application of the ΣBases/Al ratio can be found in Perez-Huerta and Sheldon (2006), who used it to examine how short-term sea level (i.e., glacio-eustatic) changes affected nutrient availability in shallow marine settings where the ΣBases/Al ratio was used to represent the fluctuating continental input derived from soils.

Darmody et al. (2005) presented two other measurements of chemical weathering that they applied to modern soil formation with granitic parent materials:

$$\mathrm{WI-1} = \frac{\mathrm{Si}+\mathrm{Ca}}{\mathrm{Fe}+\mathrm{Ti}} \tag{8}$$

$$\mathrm{WI-2} = \frac{\mathrm{Si}+\mathrm{Ca}}{\mathrm{Fe}+\mathrm{Ti}+\mathrm{Al}} \tag{9}$$

Darmody et al. (2005) found strong positive correlations between WI-1, WI-2, and Si/Al [1/"clayeyness" (Section 5.2.1)], and strong negative correlations with the CIW of Harnois (1988), suggesting that all of the ratios were capturing weathering intensity. To date, Eqs. (8) and (9) have not been widely applied to paleosols. One exception is Kahmann et al. (2008), who compared results between a number of indices and found that WI-1 and WI-2 were in relatively poor concordance with other weathering indices and also with estimates of mean annual precipitation derived from CIA-K values (see Section 5.5.3). However, the parent material being studied by Kahmann et al. (2008; sediments) was very different than that being studied by Darmody et al. (2005). Thus, at this point, results using Eqs. (8) and (9) are equivocal and more testing is needed to determine if the relationships that Darmody et al. (2005) found are widely applicable or only apply to cases with granitic parent materials.

5.2.3. Trace element ratios

Trace element abundances vary considerably among different paleosol types and parent materials. In general, to be useful a trace element must be present at the 10 s–100 s ppm level, because the analytical uncertainty using either XRF or ICP is a couple of ppm. As with major elements, ratios between trace elements are favoured both as means of normalizing differences but also because different elements are gained or lost due to different pedogenic processes. Trace element geochemistry in paleosols has been used for a variety of applications including examining weathering intensity (e.g., Kahmann et al., 2008), evaluating leaching (Sheldon, 2006a; Retallack, 2001a,b, 1999), and for provenance (Hamer et al., 2007b; Sheldon et al., 2009; Sheldon, 2006a). The most commonly used ratio is Ba/Sr, which is thought to represent leaching behaviour during weathering (Table 3; Sheldon, 2006a; Retallack, 2001b), where higher values represented more leaching. Both are alkaline earth elements and have similar atomic radii and similar chemical affinities, but Sr is significantly more soluble than Ba (Vinogradov, 1959), so under most conditions it will be leached more readily. Thus, a heavily leached paleosol should have relatively lower Ba/Sr ratios near the top of the profile and relatively high Ba/Sr ratios lower in the profile if a B horizon is present (Sheldon, 2006a). The Ba/Sr ratio has been used to characterize leaching behaviour in paleosols throughout the geologic record including Precambrian (Retallack and Mindszenty, 1994), Permian–Triassic (Krull and Retallack, 2000; Sheldon, 2006a), and Cenozoic (Terry, 2001) examples. There are two potential weaknesses of applying the Ba/Sr ratio. First, the chemical behaviour of Ba is less well understood than Sr, particularly in soils. Second, different parent materials have variable initial concentrations (and textures due to different mineral composition), so relatively minor changes in absolute abundance in samples with small initial amounts could be interpreted as intensive leaching when the process was of relatively little importance.

An additional trace element ratio that is potentially useful is U/Th (Table 3). U and Th are both actinide elements; This typically more abundant in most potential parent rocks except for limestones (e.g., Li, 2000). Th and U are both relatively immobile during weathering except under intense conditions (Li, 2000), or where there is a strong

redox gradient, because while U^{4+} is insoluble under oxidizing conditions, U^{6+} is soluble. Thus, during weathering, a few scenarios are possible that may give insight into both provenance and pedogenesis. The first is that U is leached away during pedogenesis and Th remains, leaving the upper horizons of the soil/paleosols with lower U/Th ratios than the parent material. This would indicate very intense weathering and a strong redox gradient. If the U is redistributed by lessivage rather than leached away, then the U/Th ratio should be highest in Bw/Bt horizons, and elevated relative to the parent material ratio (e.g., supporting data from Sheldon, 2006a). Alternatively, if pedogenesis was not very intense and there was no significant redox gradient, then the U/Th ratio should be constant with depth in a soil (e.g., data in Condie et al., 1995). Measurements of modern weathering suggest that the second scenario, U redistribution and accumulation in soils, is most likely (van der Weijden and van der Weijden, 1995; Pett-Ridge et al., 2007). Examples in paleosols can be found among diverse settings, including basalt-parent laterites (Kisakürek et al., 2004) and sandstone-parented Inceptisol-like palesols (Sheldon, 2006a). However, Pett-Ridge et al. (2007) also demonstrate that U that has accumulated in paleosols that are more than 150 Ka old is largely derived from atmospheric deposition (i.e., aerosols) rather than from weathering of the parent material. Thus, the U/Th ratio is probably most useful in paleosols with short-moderate formation times (see Section 5.3.1 for ways to address this in paleosols).

Another trace element of interest is Nb, which is a transition metal that exhibits similar chemical behaviour to V, Ti, and Zr, all of which are typically relatively immobile during weathering. Kurtz et al. (2000) studied a climosequence of soils developed on Hawaiian basalts that range in age from 0.3 to 4100 Ka, and found that Nb and Ta were essentially completely immobile during weathering whereas other refractive elements including Zr, Al, Hf, and Th all displayed at least some limited mobility, particularly in the older soils. Because Nb is more abundant than Ta, it is preferable as an immobile index element in mass balance calculations (see Section 5.3). Kahmann et al. (2008) found that Nb was also the least immobile element during pedogenesis of Mississippian paleosols when compared with a whole suite of different refractory elements and suggested that Nb could be used as an index element to evaluate gains and losses of other elements during pedogenesis.

5.2.4. Rare earth elements

The rare earth elements (REE) are the lanthanide series elements (atomic numbers 57–71). The REE have similar atomic radii and all share a trivalent state (though some are divalent and monovalent as well), and some are not particularly rare relative to other transition metals (e.g., Ce; Tyler, 2004). They may be separated according to mass into light REE (LREE; atomic masses <153: La, Ce, Pr, Nd, Sm, and Eu) and heavy REE (HREE; atomic masses >153: Gd, Tb, Dy, Ho, Er, Tm, Yb, and Lu). As with the Earth's crust, LREE are typically more abundant than HREE in soils. REE values are typically normalized and reported relative to some common standard such as the North American Shale Composite (NASC; Li, 2000) or to chondritic meteorites (Nakamura, 1974). The solubility of the REE elements is typically low at near neutral pHs (Li, 2000; see Wimpenny et al., 2007 for discussion on pH effects on REE and platinum group elements), with increasing solubility resulting from more acidic pHs (Tyler, 2004). Their leaching behaviour varies according to regional humidity. Extremely humid climates with acidic soils (Spodosols and laterites, e.g., Oxisols) may be leached of REE more than other elemental constituents (Tyler, 2004), but otherwise, REE tend to accumulate during weathering (e.g., Zhang et al., 2007). Also, evidence for leaching of REE in laterites is equivocal, because a number of studies have found that they actually accumulate even in those intensely weathered settings (e.g., Walter et al., 1995; Koppi et al., 1996; Nesbitt and Markovics, 1997; Braun et al., 1998; Hill et al., 2000), suggesting perhaps that podzolization leaches REE, but not in most cases of lateritization. Kahmann et al. (2008) also found a strong relationship between clay content and trace element and REE accumulation even in Histosol-like paleosols (low pH, low Eh), lending further support to the idea that under most conditions, REEs will accumulate during pedogenesis. Thus, one application of REE chemistry to is assess weathering intensity, because if the formation times are similar, a more intensely weathered soil will show more enrichment in REE than a less intensely weathered soil (all other conditions being equal; Sheldon, 2006a). Sheldon (2006a) used REE data (among other indicators of leaching) to argue that there was a significant enhancement in chemical weathering across the Permian–Triassic boundary based on a nearly order of magnitude increase in abundance in both LREE and HREE in earliest Triassic paleosols as compared with latest Permian paleosols. Another application of this general principle (i.e., accumulation of REE during weathering) comes from a basalt-parented chronosequence in which Zhang et al. (2007) found the following relationship relating *ΣREE* (ppm) to formation time:

$$\text{Age}\left(10^4\text{years}\right) = \left(\frac{\Sigma\text{REE} - 105.2}{1.082}\right) \tag{10}$$

where $R^2 = 0.95$ for the empirical relationship. Though this relationship is probably only applicable to basalt-parented paleosols because of differences in initial (i.e., parent material) REE concentrations, the high precision that they report suggests that similar chronofunctions could be developed for other parent materials as well.

Another potential application of REE geochemistry is as a means for determining provenance (Table 3). Sheldon (2006a and supplemental data) has proposed that the molecular ratios of Sm/Nd, La/Ce, and Yb/Lu are useful as a means for determining provenance because the elements in each pair are both relatively abundant in most potential silicate parent materials and because the solubility of all of the elements is similar. As with the U/Th ratio, under moderate weathering conditions, constant Sm/Nd, La/Ce, and Yb/Lu ratios would be expected in paleosol profiles when plotted against depth. Given the similar chemical behaviour of each of those element pairs, the paleosol value should match the parent material value quite closely if there are no additional sources of sediment (e.g., aeolian addition) and if they are derived from a common protolith. Thus, by comparing Sm/Nd, La/Ce, and Yb/Lu ratios as a function of paleosol depth, Sheldon (2006a) confirmed results from Ti/Al ratios that indicated that although there was a substantial increase in paleosol and sediment maturity across the Permian–Triassic boundary it could not be attributed to a shift in provenance, and was instead due to enhanced chemical weathering and leaching (based on total REE abundance and Ba/Sr ratios). These REE ratios for provenance are therefore useful both as a check on other provenance indicators and as an independent means for assessing other processes such as aeolian addition of dust.

A final paleosols REE proxy that has been proposed is to use REE "fingerprinting" to identify fossil bones associated with particular paleosol horizons. This was proposed as a means for National Parks to determine whether or not bones for sale in rock and gem shops had been poached from National Park lands. Trueman (1999) proposed that because the ionic radii of trivalent REEs are similar to Ca^{2+}, they should be readily incorporated into bone apatite during early diagenesis. Applying this general principle, Metzger et al. (2004) found that REE signatures of bones, though highly variable within a site, were significantly enhanced compared to sites without paleosol formation. They further found that the greater degree of pedogenesis, the higher the HREE concentration was within bones, regardless of soil horizon, and that fossil bone REE signatures from different depositional environments and different types of paleosols were distinguishable. There is some overlap in REE values between similar sites and similar paleosols, so while it is probably not possible to "fingerprint" sites to an absolute

certainty, fossils collected from different paleoenvironments including paleosols should be distinguishable.

In general, the difficulties with applying different REE geochemical proxies are the same. First, though many REEs may be obtained by relatively conventional means (XRF or ICP-MS), there is additional cost relative to major element geochemistry. Second, many potential soil and paleosol parent materials are relatively low in REE prior to pedogenesis, so only a long formation time or relatively intense weathering will result in easily decipherable REE patterns. Third, though elemental ratios show some promise, individual REEs are not useful because it is the pattern of their distribution both between samples, and relative both to some standard (NASC or chondrites) and to the parent material chemistry.

5.3. Mass-balance calculations

5.3.1. Pedogenesis and diagenesis

Many geologic and pedogenic processes can be most easily discussed in terms of which elements are involved in a given process and how their abundance and distribution changed as the soil developed from the protolith. One common method of assessing gains and losses of various elements in soils is through constitutive mass balance (see Brimhall and Dietrich (1987); Chadwick et al. (1990)). Mass balance calculations have also been used extensively with paleosols to understand pedogenesis (various, e.g., Driese et al., 2000, 2007; Bestland, 2002; Sheldon, 2003, 2005; Hamer et al., 2007b). Mass balance can be reduced to two concepts, strain (ε) of an "immobile" element and transport (τ) of a second element with respect to the immobile element. While a more thorough discussion may be found in any of the original references mentioned above, the basic concept is that if elements that were immobile during weathering can be identified then it is possible to assess losses and gains of mobile elements compared to the immobile element. This has in it the underlying assumption of open system transport, that is, that mass may be lost or gained by the system. In real terms, the gains and losses of elements could be due to a variety of physical and chemical processes. For example, the loss of a given element could represent pedogenic processes while the addition of another element could be from aeolian processes. The open system mass-transport function for element j in the weathered sample (w) is defined as follows:

$$\tau_{j,\mathrm{w}} = \left[\frac{\rho_{\mathrm{w}} C_{j,\mathrm{w}}}{\rho_{\mathrm{p}} C_{j,\mathrm{p}}}\right]\left[\varepsilon_{i,\mathrm{w}} + 1\right] - 1 \tag{11}$$

where ρ_{w} is the density of the weathered material, $C_{j,\mathrm{w}}$ is the chemical concentration (weight percentage) of element j in the weathered material, ρ_{p} is the density of the parent material, and $C_{j,\mathrm{p}}$ is the chemical concentration (weight percentage or molar mass) of element j in the parent material. In many cases, ρ_{w} values must either be assumed based on modern analogues or adjusted from measured values to take into account compaction of the paleosol (Eq. (4); Sheldon and Retallack, 2001) after its formation. If $\tau_{j,w} = 0$ (i.e., element w was immobile), then $\varepsilon_{i,w}$ can be solved for separately, thus bypassing volume (as in the classical definition of strain) as follows:

$$\varepsilon_{i,\mathrm{w}} = \left[\frac{\rho_{\mathrm{p}} C_{j,\mathrm{p}}}{\rho_{\mathrm{w}} C_{j,\mathrm{w}}}\right] - 1 \tag{12}$$

where $\varepsilon_{i,\mathrm{w}}$ is the strain on immobile element i in the weathered sample. Selection of immobile elements is often made on the basis of theory rather than observations: Ti, Nb, Al, and Zr are typically assumed to be immobile during weathering. However, it is possible to assess the immobility by comparing the relative mobilities of a supposedly immobile element assuming that another element is immobile (Chadwick et al., 1990). For example, one could plot $\tau_{\mathrm{Ti,w},\varepsilon(\mathrm{Zr})}$ against $\varepsilon_{\mathrm{Zr,w}}$ and $\tau_{\mathrm{Zr,w},\varepsilon(\mathrm{Ti})}$ against $\varepsilon_{\mathrm{Ti,w}}$ to determine which element was truly immobile during weathering. If more than one element shows similar immobility, then the usual convention is to use the more abundant element. Thus, while Nb is immobile in most settings, if Zr is similarly immobile, it would be the element of choice for the calculations because it is typically 5+ times as abundant. An additional consideration with the selection of putatively immobile elements for use in mass balance calculations is the texture of the paleosols. For example, Stiles et al. (2003) found lower $\varepsilon_{\mathrm{Ti}}$ values than $\varepsilon_{\mathrm{Zr}}$ values in a modern climosequence, where the Zr resided almost exclusively within the sand and coarse-size fractions of the soils while Ti resided preferentially in smaller size fractions. There was little chemical weathering of the Zr-bearing zircons evident in SEM as compared with Ti-bearing minerals, so the lower $\varepsilon_{\mathrm{Zr}}$ values represent physical, rather than chemical weathering, and preferential removal of larger grain sizes. Thus, Stiles et al. (2003) advocate using Ti as the immobile element in clay-dominated soils and paleosols and Zr as the immobile element in coarser-grained soils and paleosols.

To illustrate some of these concepts, an example using data from Sheldon (2003) is presented. The middle Miocene Picture Gorge Subgroup is part of the Columbia River flood basalt province; between Picture Gorge flows, a variety of paleosols have been preserved including Alfisol-like (Argillisol) and Histosol-like paleosols (Sheldon, 2003). For the Picture Gorge paleosols, Zr was determined to be the least mobile of the typically immobile elements (Fig. 8; as compared with Ti and Nd). $\varepsilon_{\mathrm{Zr}}$ values indicate slight addition of Zr, but significant loss of Ti (τ_{Ti}). This pattern indicates that Zr is more immobile than Ti because an element (Zr in this case) that is chemically immobile and only redistributed by physical weathering processes should accumulate during regular pedogenesis. If the plot is reversed ($\varepsilon_{\mathrm{Ti}}$ versus τ_{Zr}), unrealistic addition (200% addition) of both elements is indicated, because there are virtually no Ti- or Zr-bearing minerals observed in thin section (Sheldon, 2003, 2006d). Thus, for other mass balance calculations Zr is used as the immobile element. The gains or losses of alkali (K, Na, Rb) and alkaline earth elements (Ca, Mg, Sr) can then be calculated and plotted as a function of depth for a typical Picture Gorge paleosol (Fig. 9). Ca and Na were lost extensively throughout the profile with more than 80% of Ca and 60% of Na removed relative to the parental basalt (Fig. 9A), a pattern similar to modern basalts (Chadwick et al., 1999) and other basalt-parented paleosols (Sheldon, 2006c). In contrast, both K and Rb were added to the paleosols relative to the basaltic parent, except deep in the profile (Fig. 9B). Rb addition is systematically higher than K addition, a pattern that was interpreted by Sheldon (2003) as indicating airborne addition of volcanic ash from a local source. Given that both elements have the same chemical affinities, if the addition of both elements was instead due to metasomatism, the τ values would be equal (Sheldon, 2003). Plants use K as an important cellular electrolyte, whereas Rb is not a biologically important cation, so the difference between the two should represent

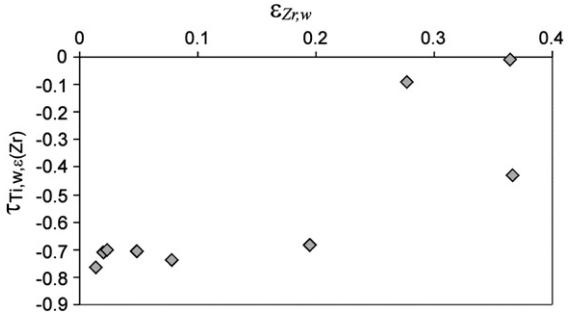

Fig. 8. Immobile element determination.

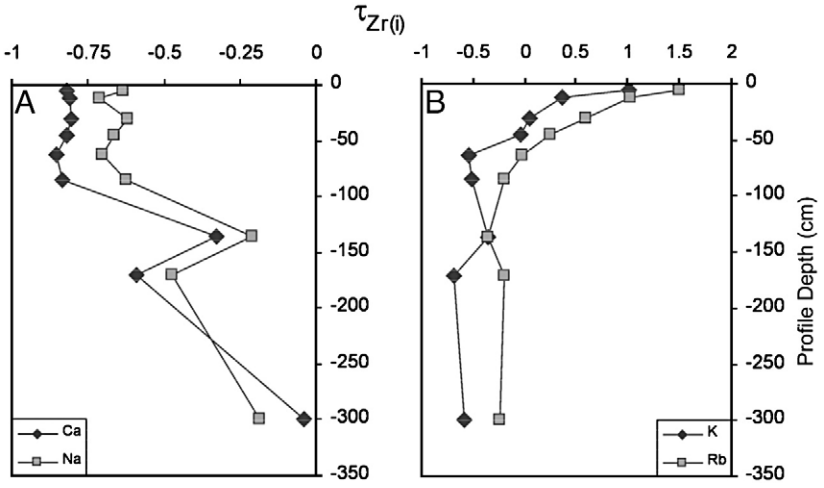

Fig. 9. Mass-balance of major and trace elements. Ca and Na are lost throughout the profiles, whereas both K and Rb were added.

pedogenesis. The equation for delineating pedogenesis from addition is:

$$\Delta_P = \tau_K - \tau_{Rb} \quad (13)$$

where Δ_P is the change in K due to pedogenesis. Fig. 10 shows Δ_P values as a function of depth in the same paleosol in Fig. 9B. The adjusted K loss is now similar to that of Na, another alkali element, which is similar to the pattern observed in modern basalt-parented soils (Chadwick et al., 1999). Thus, mass balance may be used to differentiate between different pedogenic processes and sources of elemental additions and losses.

The obvious limitation to applying any type of mass balance calculation is being able to demonstrate that one or more elements was immobile or nearly immobile during weathering. Because true immobility is unlikely, the relative degree of immobility is important. $\varepsilon_{i,w}$ values of ± 0.4 indicate limited mobility, but ideally, unless there is a strong basis for inferring addition or removal by physical weathering processes, values closer to 0 are preferable. For example, when volcanic rocks weather, many of the mafic minerals (e.g., olivine, pyroxene, plagioclase feldspar) chemically weather readily under most pH conditions, whereas rutile (TiO_2) will only be removed by physical weathering except at very acidic pH conditions. Thus, addition of Ti^{4+} is unsurprising in that case and the relative degree of enrichment will in fact be tracking pedogenesis, and at least indirectly, giving weathering intensity. If on the other hand $\varepsilon_{Ti,w}$ is less than 0 in the same setting, that suggests that some erosion of the paleosol has taken place or that there has been down-profile translocation of the Ti-bearing minerals. Distinguishing between those processes is key to understanding how that paleosol developed. Therefore, care is needed in selecting and testing "immobile" elements to ensure that they truly represent pedogenic immobility.

The other factor that is important in considering mass balance results is the role that formation time plays. Short duration, intense weathering may result in similar elemental gains and losses as long duration, low intensity weathering. Tightly constraining formation times for paleosols, in particular for pre-Quaternary paleosols, is very difficult, though a few methods have been proposed that are independent of chemical composition (cf. Sections 5.2.3–5.2.4; Birkeland, 1999; Retallack, 2001a,b; Sheldon, 2003; Retallack, 2005b). For example, Sheldon (2003) used data from Markewich et al. (1990) to propose the following relationship relating formation time (T_f in years) to Bt horizon thickness (T_{Bt}):

$$T_f = 17.07\,(T_{Bt})^2 + 645.8\,(T_{Bt}) \quad (14)$$

where $R^2 = 0.87$, no error function was calculated because the relation falls apart for very long-formation times. Retallack (2005b) did something similar for Bk horizons where he found a relationship between soil age (A in Ka) and nodule size (S in cm):

$$A = 3.92S^{0.34} \quad (15)$$

where $R^2 = 0.57$ and the standard error is 1.8 Ka. While these chronofunctions hold some promise for paleosols with either Bt or Bk horizons, they are both based on relatively few data ($n = 10$ for Sheldon, 2003; $n = 9$ for Retallack, 2005b) and many soil/paleosols types lack those particular horizons. Semi-quantitative relationships discussed in Birkeland (1999) also offer some promise for at least making appropriate order-of-magnitude age estimates, but significantly more work is needed in this area.

5.3.2. Precambrian atmospheric CO_2 from mass balance

Because Precambrian paleosols formed at the Earth's surface, in direct contact with the atmosphere at the time of their formation, they are considered to be one the best lines of evidence for determining the composition of the Precambrian atmosphere (e.g., Zbinden et al., 1988; Holland and Zbinden, 1988; Rye et al., 1995; Rye and Holland, 1998; Retallack, 2001b; Sheldon, 2006b). The three gases of primary interest are CO_2 and CH_4 (Pavlov et al., 2000, 2003) as greenhouse gases that allowed the Earth to overcome the "faint young Sun" paradox (Kasting, 1993) early in its history, and O_2, because there is

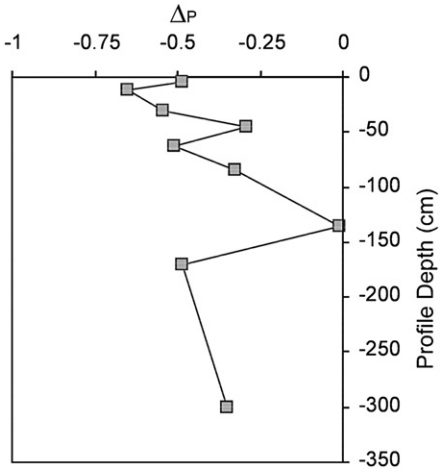

Fig. 10. True K mass balance.

extensive evidence to suggest that O_2 levels increased substantially at ~2.3 Ga ago (various; Bekker et al., 2004 and references therein). Understanding the "faint young Sun" paradox is one of the fundamental questions in Earth Sciences, because with significantly reduced solar insolation, the Earth should have been completely glaciated if there was not significantly higher levels of greenhouse forcing than at present (Kasting, 1993).

As will be discussed further below in Section 6.2, one of the difficulties of reconstructing CO_2 and CH_4 levels is to divorce the method from assumptions about precisely what level of oxygen was present. For example, Holland and Zbinden (1988) discuss a method that looks at the balance between O_2 and CO_2 as indicated by weathering processes in a ~1.1 Ga old paleosol in the form of a ratio between CO_2 and O_2 consumption. Of potentially wider applicability is a method for calculating CO_2 levels that is independent of any assumptions about the atmospheric O_2 level. Sheldon (2006b) presented such a model based on mass-balance calculations (see Section 5.3.1) of silicate weathering that related elemental weathering to atmospheric CO_2 levels.

During silicate weathering, total CO_2 consumption can be approximated by the following reactions:

$$MgO + 2CO_2 + H_2O \rightarrow Mg^{2+} + 2HCO_3^- \quad (16)$$

$$CaO + 2CO_2 + H_2O \rightarrow Ca^{2+} + 2HCO_3^- \quad (17)$$

$$Na_2O + 2CO_2 + H_2O \rightarrow 2Na^{+} + 2HCO_3^- \quad (18)$$

$$K_2O + 2CO_2 + H_2O \rightarrow 2K^{+} + 2HCO_3^- \quad (19)$$

where, for example, each mole of base cation (e.g., MgO) liberated requires two moles of CO_2 (e.g., Holland and Zbinden, 1988). Although other elements are weathered, with few exceptions (e.g., a quartz arenite) the parent rock concentration of the bases in reactions (17–20) are at least 1–2 orders of magnitude larger than any other mobile element. Because K may be remobilized metasomatically and accumulated in paleosols after burial (e.g., Maynard, 1992), it has to be dealt with differently than Ca, Mg, and Na, typically by assuming that K mass transfer values should be equal to Na mass transfer values or potentially, by using Eq. (14).

Mass transfer values (Eq. (12)) for each of those individual cations can be transformed into mass fluxes as follows:

$$m_{j,\mathrm{flux}}\left(\mathrm{g\ cm^{-2}}\right) = \rho_p \frac{C_{j,p}}{100} \int_{Z=0}^{Z=D_{j,w}} \tau_{j,w\,(z)}\, dZ \quad (20)$$

where Z is the depth in the soil profile and $D_{j,w}$ is the total depth of the profile (e.g., Chadwick et al., 1990). Given that many Precambrian paleosols have been deeply buried and show evidence of significant compaction (e.g., Retallack, 1986 showed ptygmatically folded quartz dikes), it is necessary to decompact the paleosols to their original thickness $D_{j,w}$ using Eq. (4). After the compaction-corrected mass fluxes are calculated for each individual base cation and coverted to moles, because 2 mol of CO_2 are required to liberate each mole of base cation (Eqs. 17–20) the total flux of CO_2 required for the observed weathering (M) is given by:

$$M\left(\mathrm{mols\ CO_2\ cm^{-2}}\right) = 2\sum m_{j,\ \mathrm{flux}} \quad (21)$$

Soils do not form instantaneously, so to calculate a true flux value, M must be divided by time (T). With limited biological productivity as in the Precambrian, the time-averaged flux (M/T) is a product of two distinct sources of CO_2, CO_2 in the atmosphere being added by rainfall to the soils (X_{rain}), and CO_2 added by direct diffusion into the soils (X_{diff}). Holland and Zbinden (1988) quantified X_{rain} and X_{diff} as follows:

$$\frac{M}{T}\left(\mathrm{mol\ cm^{-2}\ yr^{-1}}\right) = X_{\mathrm{rain}} + X_{\mathrm{diff}} \approx pCO_2\left[\frac{K_{CO_2} r}{10^3} + \kappa\frac{D_{CO_2}\alpha}{L}\right] \quad (22)$$

where pCO_2 is the partial pressure of atmospheric CO_2 (atm), K_{CO_2} is the Henry's Law constant for CO_2, r is rainfall rate (cm yr^{-1}), D_{CO_2} is the diffusion constant for CO_2 in air (0.162 $cm^2\ s^{-1}$; CRC Handbook), α is the ratio of diffusion constant for CO_2 in soil divided by the diffusion constant for CO_2 in air (discussed below), L is the depth to the water table, and κ is a constant which is the ratio of seconds in a year divided by the number of cm^3 per mol of gas at standard temperature and pressure (1.43×10^3 (s cm^3)/(mol year)). There is no explicit term including any CO_2 processes involving a terrestrial biosphere (i.e., it is assumed to play a negligible role), a point that was further discussed by Sheldon (2006b), but which is a reasonable simplifying assumption (however, see Yapp and Poths, 1993). Eq. (23) also assumes that the CO_2 diffusion constant and gradient are constant with depth, and that the partial pressure of atmospheric CO_2 is much larger than the partial pressure of CO_2 at the water table (depth = L). Eq. (23) can be rearranged to solve for atmospheric pCO_2 as follows:

$$pCO_2 = \frac{M}{T\left[\frac{K_{CO_2} r}{10^3} + \kappa\frac{D_{CO_2}\alpha}{L}\right]} \quad (23)$$

Thus, by quantifying M using direct measurements of paleosol mass balance and estimating T and L, it is possible to calculate the partial pressure of atmospheric CO_2 at the time the paleosols formed. Sheldon (2006b and supplemental materials) discusses the uncertainties in the model assumptions, but in general, only T is poorly constrained and makes a significant (>10%) difference to the calculated pCO_2 value.

Among the results of applying this mass-balance paleobarometer were that the pCO_2 value ~2.2 Ga ago was $23\frac{\times}{3}^3$times present atmospheric levels (PAL), an amount insufficient to overcome the "faint young Sun" paradox at that time, that similar pCO_2 values persisted until at least 1.8 Ga ago, and that much lower pCO_2 values were present by 1.1 Ga ago (Sheldon, 2006b). Each of those conclusions was based on analysis of multiple contemporaneous or near-contemporaneous paleosols. The finding that pCO_2 levels at ~2.2 Ga ago were insufficient to overcome the "faint young Sun" paradox is further supported by atmospheric modeling results (Pavlov et al., 2000, 2003), which also suggest the need for an additional greenhouse gas such as CH_4. The third conclusion, of relatively low pCO_2 levels (<10 PAL) ~1.1 Ga ago is also supported by recent results from a completely independent proxy, a paleobarometer derived from calcified cyanobacteria (Kah and Riding, 2007). Thus, if a reasonable estimate for T may be made, then this method appears to be very useful for estimating Precambrian pCO_2.

5.4. Paleotemperature

In addition to isotopic paleothermometers (see Section 7 below), there have been recent attempts to develop paleothermometry based on empirical relationships relating mean annual temperature (MAT) to the geochemical composition of modern soils. Using data from Marbut (1935) and modern measurements of MAT, Sheldon et al. (2002) proposed the following relationship between MAT and salinization of a Bw or Bt horizon (Table 3):

$$T(^\circ\mathrm{C}) = -18.5S + 17.3 \quad (24)$$

where the standard error (SE) is ±4.4°C, S is salinization (Table 3), and $R^2 = 0.37$ for the empirical fit. The underlying principle is that alkali elements (K and Na) are typically accumulated in desert settings, which usually have relatively low MAT (even if they are seasonally or daily high). Thus, paleosols with high salinization ratios should have low MAT values. The relationship is applicable to lowland settings and moderate soil formation times (<100 Ka). It is not applicable to hillslope, montane, wetland, or tropical (e.g., laterites) paleosols (Sheldon et al., 2002). A second Inceptisol-specific (~Protosol) relationship between MAT and "clayeyness" (Al/Si; Table 3) of the Bw or Bt horizon has also been proposed:

$$T(^{\circ}\mathrm{C}) = 46.9C + 4 \quad (25)$$

where the SE is ±0.6 °C, C is clayeyness (Table 3), and $R^2 = 0.96$ (Sheldon, 2006c) for the empirical fit. Though Eq. (24) is relatively imprecise, the relationship is highly significant (t-test = 8.5154, F-test = 72.58) and when applied to appropriate paleosols, gives results that are consistent with paleotemperature estimates based on leaf-margin and nearest living relative estimates from plants (Sheldon et al., 2002; Sheldon and Retallack, 2004; Sheldon, 2009). It has been applied to Cenozoic (Sheldon et al., 2002; Sheldon and Retallack, 2004; Hamer et al., 2007b), Mesozoic (Retallack, 2005a), and Paleozoic (Sheldon, 2005) paleosols. The more precise Inceptisol-only Eq. (25) is potentially applicable over a wider range of estimated paleotemperatures, though Inceptisol-like paleosols are typically rare at very high or very low MAT conditions. Nonetheless, it also gives paleotemperature results that are consistent with independent estimates based on fossil floras and faunas (Hamer et al., 2007a). The Inceptisol paleothermometer has been applied to Quaternary paleosols from Hawai'i (Sheldon, 2006c), Miocene paleosols (Hamer et al., 2007a), and Eocene–Oligocene transition paleosols (Sheldon, 2009). The primary weakness of both element-based paleothermometers is that a variety of processes, including some not related to temperature, may alter chemical composition, so care is needed not to overinterpret results based solely on these approaches. As with many of the proxies that we are discussing, if possible, results should be verified using multiple proxies.

5.5. Paleoprecipitation

A variety of different quantitative proxies have been developed for estimating mean annual precipitation (MAP). Water availability is one of the key factors in determining the relative effectiveness of many pedogenic processes. For example, leaching of base cations is limited in arid settings (Retallack, 2001b) and enhanced in humid settings (e.g., Sayyed and Hundekari, 2006). A variety of different paleoprecipitation proxies have been developed, all based on empirical relationships derived from modern soils. Each of the proxies that we will discuss is based on the properties of a single horizon or soil feature, so which proxy is most appropriate for a given setting will depend on what type of paleosol is being analyzed. Examples to be discussed include proxies based the iron content of Mn nodules in Vertisols, the depth to a Bk horizon below a paleosol surface, and the chemical composition of a Bw/Bt horizon.

5.5.1. Content of Fe–Mn nodules in vertisols

Stiles et al. (2001) studied a modern climosequence developed on the Texas Gulf Coastal Plain. Most of the soils there are Vertisols forming under modern MAP ranging from 800 to 1500 mm yr^{-1} (Stiles et al., 2001). They also observed that Fe–Mn nodules were common in the soils and hypothesized that the iron content corresponds to mean annual precipitation values (Fe_{TOT} as a whole number % value, i.e., 20, not 0.2):

$$P\left(\mathrm{mm\ yr^{-1}}\right) = 654.4 + 31.5\ \mathrm{Fe_{TOT}} \quad (26)$$

where $R^2 = 0.92$ for the empirical relationship (Stiles et al., 2001). They then applied the relationship to Fe–Mn nodules in Paleozoic paleosols, yielding inferred moisture regime results that correspond well with field characteristics of the paleosols and with qualitative observations based on comparisons to modern analogues. Stiles et al. (2001) did not find that their results correspond well to estimates based on depth to the Bk horizon (see Section 5.5.2) and found the Bk depth generally underestimated the modern known precipitation values. This method seems to be viable for paleo-Vertisols, however, it is unclear how common authigenic Fe–Mn nodules are given that there are relatively few reported occurrences (see references in Stiles et al., 2001), so its applicability may be somewhat limited.

5.5.2. Depth to Bk horizon

$CaCO_3$ is highly soluble and both Ca^{2+} and CO_3^{2-}/HCO_3^- are readily mobilized both in groundwater and in soil solutions, so the presence of $CaCO_3$ in a soil or paleosol indicates at least some degree of aridity (perhaps just seasonally), because under wetter conditions carbonate would not be stable or form authigenically. Jenny and Leonard (1935) and Jenny (1941) first recognized that there was a relationship between the depth below the surface of modern soils to their Bk horizon (carbonate-bearing) and MAP in Great Plains soils. Arkley (1963) further expanded observations of the relationship by considering more arid Mojave Desert settings and found the same relationship. Retallack (1994) combined Jenny's (1941) and Arkley's (1963) data and other literature data ($n = 317$ in total) and fit a regression line to it that related depth to the Bk horizon to MAP. That relationship was widely applied to paleosols ranging in age from Paleozoic to the Quaternary (e.g., examples in Retallack et al., 2000; Retallack, 2001b). Factors to consider before applying the relationship to paleosols include erosion of the paleosols prior to burial, post-burial compaction, and the effect of elevated atmospheric CO_2 levels (models of Bk horizon formation suggest that they will form deeper in the profile at significantly elevated CO_2 levels; McFadden et al., 1991). Erosion may be dealt with through careful stratigraphy and consistent application of the proxy (e.g., tops of soils are always measured from the surface that the highest root traces emanate down from). Compaction may be dealt with as described above (see Section 2.2.1). There are many means of reconstructing past CO_2 levels including using isotopic data from paleosols (see Section 7.4.3.1). In general though, this is only a concern for Ordovician–Silurian and Jurassic–Cretaceous paleosols (e.g., Berner and Kothavala, 2001), and for some Precambrian paleosols (Sheldon, 2006b).

Royer (1999) questioned whether the proxy worked by looking at 1168 Bk-bearing soils from the NRCS database and finding only a weak relationship between Bk depth and MAP. He proposed a simpler test, namely that soils receiving less than 760 mm yr− 1 would be Bk-bearing and those receiving more than 760 mm yr^{-1} would not have Bk horizons. Retallack (2000) pointed out a number of issues in Royer (1999) that merit reconsideration of those findings. The soils used in Retallack's (1994) study were tightly constrained to have similar characteristics (e.g., horizonation, age, degree of development), a factor ignored by Royer (1999), who simply used presence/absence of a Bk horizon as his sole criterion. For example, according to Retallack (1994), the relationship only applies to moderately developed soils (i.e., with carbonate nodules, not wisps or caliche layers) formed on unconsolidated parent material (e.g., alluvium or loess) in lowland settings, and which were undisturbed by human activity. Hundreds of Royer's (1999) soils did not conform to one or more of these criteria, so it is unsurprising that he did not find the same relationship. Royer's (1999) second result (a Bk-horizon isohyet at 760 mm yr^{-1}) probably also gives only weak guidance because the Bk-bearing/Bk-free isohyet is at different precipitation values in many modern settings on different continents (Retallack, 2000). Nonetheless, in part due to that criticism, Retallack (2005b) substantially expanded his database to include 807 soils with a slightly revised relationship:

$$P\left(\mathrm{mm\ yr^{-1}}\right) = -0.013D^2 + 6.45D + 137.2 \quad (27)$$

where the SE is ±147 mm yr^{-1}, and $R^2 = 0.52$ for the empirical relationship. Using a subset ($n = 675$) of the newly compiled database, Retallack (2005b) also defined the following relationship for mean annual range of precipitation (MARP):

$$\mathrm{MARP} = 0.79T + 13.7 \quad (28)$$

where the SE is ±22 mm yr^{-1}, $R^2 = 0.58$ for the empirical relationship, and where T is the thickness the paleosol with carbonate nodules (i.e., Bk horizon thickness; in cm). Application of this new MAP relationship gives results comparable to estimates from B horizon geochemistry (see Section 5.5.3) and paleobotanical results where the paleosols conform to all of the criterial listed above (Retallack, 2007; Sheldon, 2009). However, it should be noted that there are some modern soil orders that are still not represented within the modern soil proxy data set. For example, Nordt et al. (2006) point out that there are essentially no Vertisols in the dataset and that no data exists to quantify the differences in Bk depth between micro-highs and micro-lows in Vertisols, an important consideration given cm- to dm-scale micro-relief in most Vertisols. Furthermore, Vertisols (which often form in strongly seasonal or monsoonal climates) often preserve dispersed carbonate throughout the profile. Nordt et al. (2006) found that equation of Retallack (1994) was poor at predicting MAP in a modern Vertisol climosequence when microhighs were used and somewhat effective when microlows were used (though only to Bk depths of 117 cm or less), but that a different equation fit their data better and that Retallack's (1994) equation systematically underestimated MAP. For a given soil/paleosol, the predicted MAP using Eq. (27) is not substantially different than Retallack's (1994) earlier fit to the data, which suggests that Eq. (27) is not useful for paleo-Vertisols either. Thus, though Eq. (27) is potentially very broadly applicable, care must be taken to use it only with appropriate paleosols types (i.e., not Vertisols), parent material textures (alluvium or loess), and with an understanding of the geologic age, setting (lowlands), and burial history (i.e., decompacted values) of the paleosols.

5.5.3. Bw/Bt horizon geochemistry

During weathering of silicate rocks, minerals such as feldspars are broken down to form clay minerals by hydrolysis and acid attack reactions (see Section 5.2.2). Water availability is one of the key controls on the rate of these reactions, so given the same amount of time, more clay should be formed under a wetter climatic regime than a dry one (Birkeland, 1999; Retallack, 2001b). Thus, Sheldon et al. (2002) used the soil database of Marbut (1935) and modern measurements of MAP to propose the following relationship between CIA-K of Bw and Bt horizons (Eq. (6); Maynard, 1992) and MAP:

$$P\left(\mathrm{mm\ yr^{-1}}\right) = 221.1e^{0.0197(\mathrm{CIA-K})} \quad (29)$$

where the SE is ±181 mm yr^{-1}, and $R^2 = 0.72$ for the empirical fit. They also proposed two other proxies for MAP, one based on ΣBases/Al for the Bw or Bt horizons (Table 3):

$$P\left(\mathrm{mm\ yr^{-1}}\right) = -259.3\mathrm{Ln}\left(\frac{\Sigma\mathrm{Bases}}{\mathrm{Al}}\right) + 759 \quad (30)$$

where the SE ±235 mm yr^{-1}, and $R^2 = 0.66$ for the empirical relationship. The other is a Mollisol-specific MAP relationship where:

$$P\left(\mathrm{mm\ yr^{-1}}\right) = -130.9\mathrm{Ln}(C) + 467 \quad (31)$$

where the SE is ±156 mm yr^{-1}, C is the molar ratio Ca/Al of the B horizon, and $R^2 = 0.59$ for the empirical relationship.

Bw and Bt horizons are used because: 1) they form over long periods of time, making their chemical composition a function of equilibrium processes rather than kinetic ones; 2) long formation times also ensure that short-term climatic volatility (e.g., El Niño) does not overprint the long-term conditions; 3) there should be a clear difference between the parent material weathering ratio value and the B horizon value if the proxy is applicable (e.g., for CIA-K, there should be at least a 5–8 unit difference), and if the values are very close, then the proxy is not applicable. Though the original database of Marbut (1935) had a wide range of soil types in it, the relationships are not considered applicable for paleosols with near surface carbonates or evaporite minerals, for hillslope or montane settings, or for laterites (Sheldon et al., 2002). Eqs. (29) and (30) are both useful over a range of precipitation values between 200 and 1600 mm yr^{-1}. For example, a CIA-K value of 100 (e.g., pure kaolinite) gives a MAP estimate of 1585 mm yr^{-1}, and a CIA-K value of 0 (i.e., no Al present at all) gives a MAP estimate of 221 mm yr^{-1}. For paleosols with very well-developed Bk horizons, Eq. (30) is favoured over Eq. (30) because it gives more consistent results when applied to modern soils; for other types of paleosols Eq. (29) is preferred both because it is more precise and more accurate.

Eq. (29) has been widely applied to paleosols of a wide range of ages including Paleozoic (e.g., Driese and Ober, 2005; Driese et al., 2005; Sheldon, 2005) and Mesozoic (e.g., Prochnow et al., 2006) paleosols, and has proven particularly useful for Cenozoic (e.g., Hamer et al., 2007a,b; Kraus and Riggins, 2007; Retallack, 2007; Sheldon, 2009; Sheldon et al., 2009) paleosols where diagenesis can be discounted more easily than for the older paleosols. Two separate lines of evidence suggest that Eq. (29) is a particularly useful proxy for MAP. The first is that it produces MAP estimates that are consistent with independent paleobotanical estimates based on leaf-margin analysis (Sheldon et al., 2002; Sheldon and Retallack, 2004; Retallack et al., 2004a; Retallack, 2007; Sheldon, 2009) and nearest-living relatives (Retallack et al., 2004a,b; Hamer et al., 2007a,b; Sheldon et al., 2009). The second is that it generally successfully predicts modern, measurable MAP in soil climosequences (Driese et al., 2005; Nordt et al., 2006), even for soil types (i.e., Vertisols) that are not represented by many soils in the original Marbut (1935) database. For arid and semi-arid settings, it also gives results that are consistent within error of estimates based on Bk horizon depths (e.g., Sheldon and Retallack, 2004), though typically gives systematically slightly "wetter" results.

In general, Eq. (29) is the most well-supported proxy for MAP based on paleosols, however, it must be carefully applied according to the criteria listed above and wherever possible, multiple proxies (e.g., Bk depth or paleobotanical estimates) should also be used to confirm the results. Another important consideration is to be sure that high CIA-K values are not simply due to inheritance from chemically mature parent materials. Thus, a useful guideline based on observations from the original Marbut (1935) database is that there should be at least a 5–8 unit difference in CIA-K values between the paleosol's parent material value and its B horizon value depending on the field taxonomic description of the paleosol (at least 5 units for weakly to moderately developed Orders, >5 units for moderately to strongly developed Orders). One final consideration is the role that topography may play in limiting the applicability of Eq. (29). Rasmussen and Tabor (2007) show a generally poor correspondence between CIA-K and MAP for some parent materials (though good for others) along transects of increasing elevation in the Sierra Nevadas. Sheldon et al. (2002) specifically limited the applicability of Eq. (29) to lowland settings. The results of Rasmussen and Tabor (2007) confirm this and serve as a good reminder that proxies should be applied carefully in settings for which they were not defined.

5.6. Long-term chemical weathering

Another potential application of whole rock geochemistry is to quantify long-term change in chemical weathering. In many continental basins, long sequences of paleosols spanning many millions of

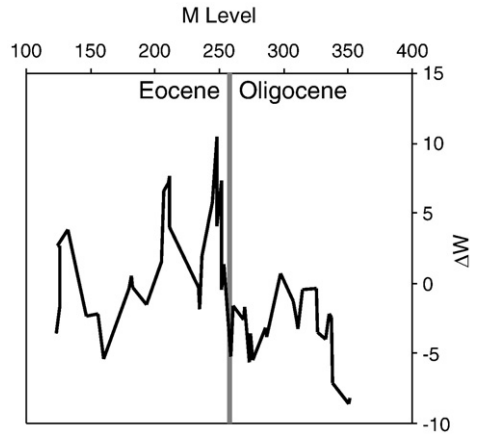

Fig. 11. Quantifying long-term chemical weathering. The values of ΔW shown are based on the 3-pt. running average of 54 chemical analyses collected from a ~250 m section. The level of the Eocene–Oligocene transition is known from mammalian biostratigraphy.

years are preserved (e.g., Sheldon and Retallack, 2004; Prochnow et al., 2006; Retallack, 2007; Sheldon, 2009). By using the same weathering ratio, measured from the same horizon in comparably developed paleosols (e.g., all Alfisol-like paleosols), it is possible to characterize changes in the chemical weathering environment. A new parameter ΔW can be derived as follows using CIA (Eq. (5)) as the weathering index:

$$\Delta W = \mathrm{CIA}_x - \mu_{\mathrm{CIA}} \tag{32}$$

where ΔW is the deviation in weathering for a given paleosol (CIA_x) relative to the mean degree of weathering for the whole sequence (μ_{CIA}). Fig. 11 shows how ΔW changed across the Eocene–Oligocene transition for a relatively poorly dated section in the Ebro Basin (Spain). Ongoing work by L. Cabrera, M. Garces, and E. Diaz will refine the chronology using magnetostratigraphy, but the level of the Eocene–Oligocene transition is already know from mammalian biostratigraphy (L. Cabrera, pers. comm.). Though the record is variable through time, it is nonetheless clear that there was a significant decline in chemical weathering across the Eocene–Oligocene transition (Sheldon, 2009). The mean Eocene value of ΔW is +2.82 for Eocene, whereas it is −3.60 for the Oligocene. Given that μ_{CIA} is 14.2 for that whole section, those ΔW changes represent a shift from about 20% enhanced weathering to −25% reduced weathering across the boundary; a very substantial change in chemical weathering. Similar results obtained using the same method on North American Eocene–Oligocene transition paleosols were reported by Sheldon and Retallack (2007). Thus, this approach may be a very powerful tool for evaluating changes in pedogenesis, weathering, and climate in Earth's past. By using ΔW rather than CIA_x values, it is possible to obviate over-reliance on single data points and also to determine which CIA_x values represent outliers to the pedogenic history of an area, and also removes one of the potential weaknesses of the approach, namely uncertainties about which pedogenic processes were responsible for changes to single elements.

6. Thermodynamic approaches

6.1. Simple versus complex systems

Reconstruction of paleoenvironmental and paleoclimatic conditions using thermodynamic modeling is a relatively recently developed quantitative tool for studying paleosols with approaches ranging from simple single equation models (e.g., Rye et al., 1995; Hessler et al., 2004) to complicated multi-equation models designed to simulate as many pedogenic processes as possible (Sheldon, 2006d). The primary weakness of all of the thermodynamic models employed to date is that they have not considered reaction kinetics, instead relying on simplifying assumptions to account for kinetic effects. For example, Sheldon (2006d) used a computer model to suppress quartz formation during his model runs of paleosol formation because at low temperatures (e.g., Earth's surface conditions), quartz formation is very slow and most silica instead is present as amorphous silica or chalcedony (Palandri and Reed, 2001). Including kinetics is the next logical step, but represents a fairly substantial increase in model complexity.

So far, thermodynamic models have been used primarily to try to reconstruct paleo-atmospheric conditions. Specifically, they have been used to try to model Precambrian atmospheric conditions (Rye et al., 1995; Hessler et al., 2004; Ohmoto et al., 2004) at the time that a given sedimentary deposit or paleosol was formed. Though the limitations of the existing models will form the primary basis of this review, the general approach has merit and has been relatively underutilized. In particular, the multiple equation approach, when coupled with other proxy data, could yield significant results.

6.2. Single-equation approaches

6.2.1. Precambrian atmospheric CO_2

The first single-equation approach was proposed by Rye et al. (1995), who were studying the ~2.2 Ga old Waterval Onder paleosols, preserved on top of the Hekpoort Basalt of South Africa (Retallack, 1986). Rye et al. (1995) suggested that the equilibrium relationship between siderite and reduced iron-silicates (SIS herein) in paleosols could be used to constrain Precambrian atmospheric pCO_2. They argued that reduced iron-silicates should form rather than siderite if pCO_2 is low, so the absence of siderite is taken as evidence of low pCO_2 levels. As a model iron-silicate, greenalite was selected by Rye et al. (1995) because it is a low-temperature metamorphic iron-silicate suitable to Precambrian paleosols, many of which have been altered by greenschist facies metamorphism at T ≥300 °C (Rye and Holland, 2000). Greenschist metamorphism would not remove siderite, because it is not decarbonated under common conditions of metamorphism up to, and including, greenschist facies metamorphism (Rye et al., 1995). The governing equation used by Rye et al. (1995) is as follows:

$$\mathrm{Fe_3Si_2O_5(OH)_{4(green)}} + 3\mathrm{CO_{2(g)}} = 3\mathrm{FeCO_{3(sid)}} + 2\mathrm{SiO_{2(aq)}} + 2\mathrm{H_2O}. \tag{33}$$

They used thermodynamic data from Eugster and Chou (1973) to calculate the phase boundary shown in Fig. 12. In their paper, Rye et al. (1995) allowed that Eugster and Chou's (1973) data for greenalite were poorly constrained. Their original SIS CO_2 paleobarometer gives an upper limit of ~100 times present atmospheric CO_2 levels based on equilibrium between siderite and greenalite.

There are a number of theoretical and geological issues (see a thorough discussion in Sheldon, 2006b) with the simple model of Rye et al. (1995) for determining Archean atmospheric pCO_2 from paleosols. To summarize: 1) using a single equilibrium relationship for all Archean and Proterozoic paleosols is misleading because the mineral assemblage present is not the same in all Precambrian paleosols; 2) greenalite does not form authigenically in soils and so represents the metamorphic rather than pedogenic assemblage; a better iron-silicate mineral choice would be berthierine, which did form as part of the pedogenic assemblage at Waterval Onder (Retallack, 1986); 3) Rye et al. (1995) measured *in situ* carbon dioxide in banded iron formations (BIFs) as a check on their thermodynamic model results, but that provides only weak guidance because the chemistry of a soil formed at the Earth's surface bears little resemblance to the chemistry of a BIF formed in the ocean, in part because decomposition of organic matter leaves the effective

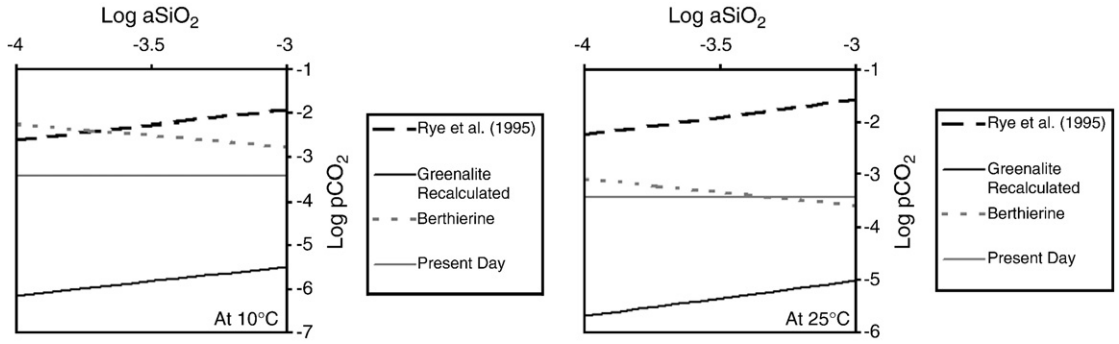

Fig. 12. Single-equation phase diagram for Fe-bearing mineral authigenesis in the ~2.2 Ga Hekpoort paleosol.

pCO_2 of the deep ocean about three times that of the surface ocean (Kasting, 2004); 4) Even when a pedogenically realistic mineral assemblage is used (substituting berthierine for greenalite, see below), estimated carbon dioxide levels are inconsistent with geologic evidence; 5) the oldest occurrence of siderite in a paleosol, which the SIS paleobarometer would indicate formed under conditions of atmospheric CO_2 greater than 60–100 times present levels, is ~0.98 Ga, a time for which there is no independent evidence of CO_2 levels that high (e.g., Retallack and Mindszenty, 1994); 6) anoxic weathering experiments involving the dissolution of Fe-biotite yielded no siderite even at very high pCO_2 levels (=1 atm; >2000 PAL) where Rye et al.'s (1995) model would predict siderite stability (Murakami et al., 2004).

Fig. 12 (modified after Sheldon, 2006b) is a phase diagram that shows Rye et al.'s (1995) result along with a recalculated phase boundary for their SIS paleobarometer using more up to date thermodynamic data for greenalite drawn from the computer program SUPCRT92 (Johnson et al., 1992; with data from E. Shock as compiled in Soltherm by M. Reed). The up-to-date phase boundary gives a significantly different result including Precambrian pCO_2 levels estimated to be only significantly lower than present atmospheric pCO_2 levels (PAL) over a reasonable range of $aSiO_{2\ (aq)}$, rather than higher as would be expected based on other geological criteria (Sheldon, 2006b). At quartz saturation ($aSiO_{2\ (aq)} = 10^{-4.047}$), a condition common in most modern surface waters, an atmospheric pCO_2 of just $10^{-5.72}$, or 0.006 PAL is predicted (Fig. 12). Greenalite does not form pedogenically and is instead a common greenschist facies metamorphic mineral (which is not present in the mineral assemblage at Waterval Onder; Retallack and Krinsley, 1993), so perhaps a similar SIS paleobarometer using the pedogenic mineral assemblage would be more effective. Berthierine (thermodynamic data from Fritz and Toth (1997)) is a serpentine group ferrous iron silicate that forms in chemically reducing conditions but rarely as a soil mineral (e.g., Sheldon and Retallack, 2002), and which is part of the mineral assemblage of the ~2.2 Ga old Waterval Onder paleosols (Retallack and Krinsley, 1993). An expression for equilibrium between berthierine and siderite and kaolinite can be written as follows:

$$Fe_2Al_2SiO_5(OH)_{4(bert)} + SiO_{2(aq)} + 2CO_{2(g)} = 2FeCO_{3(sid)} + Al_2Si_2O_5(OH)_{4(kaol)} \quad (34)$$

where kaolinite is inferred to have been part of the pre-metamorphic mineral assemblage (Retallack and Krinsley, 1993; Rye and Holland, 2000). Calculated pCO_2 levels are higher than for the recalculated SIS paleobarometer of Rye et al. (1995), and close to present day values at a range of temperatures (Fig. 15). That value represents a maximum pCO_2 value because the berthierine at Waterval Onder is not a pure end member. Thus it would have an activity of less than one, further lowering the calculated pCO_2 level. The choice of Al-mineral is relatively unimportant as calculations based on gibbsite instead of kaolinite (not shown) also result in pCO_2 values below present day conditions (Sheldon, 2006b).

Equilibrium modeling using greenalite or berthierine SIS paleobarometers suggests one of two conclusions, either Precambrian pCO_2 levels were much lower than expected and comparable to present atmospheric levels, or the whole approach is oversimplified and unreliable. Given the "faint young Sun" paradox (Kasting, 1993), such low levels are difficult to reconcile with the need for a much stronger than present Precambrian greenhouse. Furthermore, by simplifying atmospheric composition down to a single chemical reaction there is a risk of over-interpreting the absence of evidence of a single mineral phase, in this case siderite.

A similar model based on massive siderite beds in BIFs prior to ~1.8 Ga (i.e., Ohmoto et al., 2004) inverts the logic of Rye et al. (1995) to suggest that the presence siderite in the BIFs implies pCO_2 values in excess of 100 PAL and that the inhibiting factor in siderite formation after 1.8 Ga was near modern pO_2. However, Ohmoto et al. (2004) assert that siderite stability requires $pO_2 = 10^{-60\pm5}$, a value well below any existing estimate for the Precambrian, but as Sleep (2004) correctly points out, even at the naturally maintained pO_2 minima ($pO_2 = 10^{-13}$) reaction kinetics dictate that oxidation processes are unlikely to inhibit siderite formation. Furthermore, even at the present day pO_2 value of 0.21, siderite formation in near-modern soils is not restricted (e.g., Achyuthan, 2003) to poorly aerated settings as Ohmoto et al. (2004) asserted. Thus, even if pO_2 levels were relatively high (a minority viewpoint held by Ohmoto et al., 2004), siderite should form at the Earth's surface when pCO_2 is significantly elevated. In addition, BIFs can only provide weak guidance for Earth surface and atmospheric conditions because they formed below storm wave base under conditions of enhanced pCO_2 relative to the surface as a result of the decomposition of organic matter (Kasting, 2004).

A final thermodynamic approach to reconstructing Precambrian atmospheric pCO_2 levels is based on equilibrium modeling of the formation of mineral rinds on sub-aerially deposited pebbles (Hessler et al., 2004). Hessler et al. (2004) considered three possible equilibrium relationships that might apply to the formation of the carbonate rinds, which, in contrast to the other SIS paleobarometers, involve no iron silicate rather than no siderite. They calculated a minimum pCO_2 of 2.51×10^{-3} bars (~6.8 PAL). That scenario requires an unusual geologic setting in which iron silicates are very unstable at the Earth's surface (Sheldon, 2006b). If iron silicates were instead stable, the estimated pCO_2 minimum is significantly higher, though still insufficient to account for the "faint young Sun" (Kasting, 1993). Without more investigation into iron silicate stability and Archean weathering conditions it is not clear which of the two scenarios is most likely. Furthermore, it is also unclear how common siderite coated pebbles (*sans* iron silicates) are in the geologic record, and thus how often they may provide a useful pCO_2 constraint. However, where appropriate, the Hessler et al. (2004) thermodynamic model appears to provide a useful constraint.

Thus, results from attempts to reconstruct Precambrian pCO_2 levels using single-equation thermodynamic models are at best

equivocal at this point. Thermodynamic models in general oversimplify the problem of estimating Precambrian pCO_2 levels, and by slightly changing starting assumptions (e.g., SIS paleobarometers of Rye et al., 1995; Ohmoto et al., 2004; Sheldon, 2006b) or thermodynamic data (e.g., Sheldon, 2006b) vastly different conclusions may be drawn. Extreme caution is thus advocated in their application, because the mostly widely cited one (Rye et al., 1995) has a number of fundamental flaws, and other approaches (Hessler et al., 2004) may have only limited application to relatively rare sedimentary occurrences. Instead, as discussed in Section 5.3.2, a mass-balance model for reconstructing Precambrian pCO_2 levels is favored because it gives reproducible results consistent with geologic evidence, is independent of assumptions about pO_2 values, and takes into account both pedogenic and diagenetic processes (Sheldon, 2006b).

6.2.2. Earliest Triassic soil formation

One of the primary weaknesses of the single-equation approach to Precambrian conditions is the amount of uncertainty about the original pedogenic mineral assemblage. Given that model interpretations were based on the presence/absence of a single mineral at a single site, it is unsurprising that inconsistent results were obtained. Those uncertainties decrease with younger rocks, with settings that are better understood, and with model approaches that rely on the mineral assemblage that is actually present rather than on some theoretical assemblage. The key with any model is the ability to evaluate it successfully against "real" data. Thus, a single-equation approach applied to a well-characterized geologic setting has a greater chance of success. Sheldon and Retallack (2002, 2003) have used a single-equation equilibrium model to examine pedogenic processes in well-studied (Retallack and Krull, 1999; Krull and Retallack, 2000; Retallack et al., 2005; Sheldon, 2006a) earliest Triassic paleosols in Antarctica. Krull and Retallack (2000; see also Sarkar et al., 2003) presented organic matter $\delta^{13}C$ data that was interpreted to represent a significant methane release event coincident with the Permian–Triassic extinction, possibly due to destabilization of seafloor clathrates or to diking of permafrost fields (Retallack and Jahren, 2008). C cycle modeling by Berner (2002) suggests that large isotopic excursions can only be caused by introduction of methane (i.e., Siberian Traps volcanism was ruled out). Because methane oxidizes on very short time scales (7–24 years in the present atmosphere), local reduction may occur in relatively confined settings such as soils. The earliest Triassic of Antarctica was characterized by waterlogged soils (Sheldon, 2006a) that were essentially coal swamp environments without peat accumulation (Retallack et al., 1996) that could be termed "clastic swamps." The unusual serpentine group mineral berthierine was also present (Sheldon and Retallack, 2002, 2003), a strong indicator of chemically reducing conditions (see references in Sheldon and Retallack, 2002). Thus, Sheldon and Retallack (2002, 2003) used an equilibrium model based on the following equation to examine if the presence of berthierine gives a useful constraint on paleoenvironmental conditions at the time of its formation:

$$Al_2S^2i_2O_5(OH)_{4(Kaol)} + Fe_2O_{3(Hem)} + \frac{1}{4}CH_4 = Fe_2Al_2SiO_5(OH)_{4(bert)} + SiO_{2(aq)} + \frac{1}{2}H_2O_{(aq)} + \frac{1}{4}CO_{2(aq)} \quad (35)$$

Assuming pure minerals and a dilute solution (i.e., $aH_2O \approx 1$), the following equilibrium relationship was developed (using data from the SOLTHERM database; see Palandri and Reed, 2001) that allowed them to model the conditions that would result from elevated methane levels:

$$\frac{a_{SiO_{2(aq)}} p^{\frac{1}{4}}CO_2}{p^{\frac{1}{4}}CH_4} = K = 10^{-1.673}(25\ ^\circ C) \quad (36)$$

Over a realistic temperature range (10–25 °C), a variety of methane scenarios (2–100× present levels) were examined (see Fig. 1 of Sheldon and Retallack, 2003). At $aSiO_{2(aq)}$ values comparable to modern surface waters ($10^{-4.047}$), very high soil gas pCO_2 values (>1000 PAL; modern tropical soils often exceed 100 PAL, Brook et al., 1983) are indicated for all of the methane scenarios. This result provides an explanation for the "post-apocalyptic greenhouse" paleosols observed in Antarctica (Retallack and Krull, 1999), which included paleo-Ultisols forming at >65°S even though modern Ultisols are limited to ±45° N or S today by giving evidence for short-term exceptionally high soil gas pCO_2 levels (Sheldon and Retallack, 2002, 2003; Sheldon, 2006a). Evidence for these short-term chemically reducing but highly acidic soil gas conditions at high paleo-latitudes is now widespread for the earliest Triassic, with nine berthierine-bearing localities in Antarctica and Australia, including all of the paleosol-bearing Antarctic sequences that have been widely studied (Sheldon, 2006a).

This type of application of thermodynamic modeling (i.e., in concert with whole rock geochemical and isotopic data), where there is geological evidence to "aim at", is much more effective than the more theoretical approaches that have been applied to Precambrian paleosols. Thermodynamic modeling of soil and paleosol formation does represent a potentially powerful tool, but less so when used exclusively and in scenarios where there is relatively little additional proxy data to work with. For Phanerozoic paleosols, this is less likely to be a problem than for Precambrian ones, and in places where the diagenetic setting is well understood, single-equation thermodynamic modeling is likely to give additional insight into unusual mineral assemblages observed in paleosols, but probably should not be used as a "standalone" proxy any more than for the Precambrian.

6.3. Multiple-equation approaches

Soils are potentially excellent proxy records of environmental conditions because they form in direct contact with the atmosphere. As a result, gas contents in soils equilibrate with atmospheric gases. However, due to soil respiration, soil pCO_2 may be up to 100–200 times higher than that of the atmosphere (Brook et al., 1983; Volk, 1987) in tropical settings, with generally lower concentrations in temperate settings. The minimum soil pCO_2 level expected is that of atmospheric pCO_2, which corresponds to no biological productivity. Elevated soil pCO_2 values are associated with high-biomass systems or with waterlogged settings where diffusive loss of soil pCO_2 to the atmosphere (if soil pCO_2 > atmospheric pCO_2) is inhibited. Thus, well-drained soils with low to moderate productivity will generally have low soil pCO_2, but still somewhat greater than atmospheric pCO_2.

Because atmospheric pCO_2 level cannot be lower than the soil pCO_2 levels under open-system exchange, equilibrium modelling of abiotic weathering reactions can constrain minimum atmospheric pCO_2 levels (Sheldon, 2006d) if the weathering environment is well-understood. To illustrate this, we will summarize Sheldon's (2006d) efforts to model the formation of intra-basaltic paleosols preserved between middle Miocene Columbia River Flood Basalt Province flows. In other words, if present levels of pCO_2 are sufficient to create the observed degree of weathering in these paleosols, then it is likely that paleo-atmospheric pCO_2 levels were also at near-modern levels because biota can only serve to enhance the degree of weathering. This approach is somewhat indirect, but the thermodynamics of microbial and plant interactions during weathering are still poorly understood.

The computer program CHILLER (e.g., Palandri and Reed, 2001) allows users to calculate heterogeneous equilibrium of gas–mineral–water systems. CHILLER forces equilibrium with different water and gas mixtures by treating gases as homogeneous minerals. Each of the different gas compositions is thus a separate "mineral", with separate thermodynamic behaviour. In other words, a water-rock system in equilibrium with present atmospheric conditions is in equilibrium with the "minerals" called "fCO_2 – 3.5" (CO_2 fugacity = $10^{-3.5}$) and "fO_2 – 0.7" (O_2 fugacity = $10^{-0.7}$). To look at a range of possible pCO_2

levels, new CO_2 "minerals" were created for 0.1, 1, 3, 5, 10, 15, and 20 times present atmospheric levels (PAL) assuming a present day atmospheric pCO_2 of $10^{-3.5}$ (for dilute mixtures, e.g., CO_2 in the atmosphere, $f \approx p$). All equilibrium K values are from the SOLTHERM database (construction of the database is outlined in Palandri and Reed, 2001). The basic equation that controls the availability of CO_2 is:

$$H_2O_{(aq)} + CO_2(g) = HCO_3^-(aq) + H^+_{(aq)}. \quad (37)$$

From here, a K value may be calculated from the following (where a represents activity):

$$K = \frac{a_{HCO_3^-}\, a_{H^+}}{f_{CO_2}\, a_{H_2O}} \quad (38)$$

Rearranging that expression (Eq. (39)) and taking the Log_{10} of both sides (Eq. (40)) permits calculation of a new K value (here called K^*) that can be used to force equilibrium with a given atmospheric CO_2 value.

$$\left(f_{CO_2}\right)K = \frac{a_{HCO_3^-}\, a_{H^+}}{a_{H_2O}} \quad (39)$$

$$\text{Log } K^* = \text{Log}\left(f_{CO_2}\right) + \text{Log}K = \text{Log}\ \frac{a_{HCO_3^-}\, a_{H^+}}{a_{H_2O}} \quad (40)$$

For example, to create a new CO_2 gas "mineral" that corresponds to present-day atmospheric conditions (i.e., $pCO_2 = 10^{-3.5}$ bars), the following expression would be used:

$$\text{Log } K^* = 10^{-7.818} + 10^{-3.5} \quad (41)$$

For the modeling, O_2 fugacity/pressure was kept constant at present levels, which is reasonable because oxygen levels are thought to have been roughly constant throughout the Cenozoic. CHILLER may be used to examine different water-rock ratios by "titrating" rock into a water of a given composition (i.e., rainwater) and by outputting how that water changes composition in response to the addition of rock. If precipitation is approximately constant through time, then there should be a systematic decrease in the amount of water that reacted with the parental basalt with increasing depth in the profile (Sheldon, 2006d). Thus, by graphing results depicting ascending water-rock ratios from the top down, an artificial soil profile may be modeled (Sheldon, 2006d). These artificial profiles obtained for equilibrium with different CO_2 levels (0.1–20 PAL) can then be compared with actual geochemical data on mass balance and the mineral assemblage from Sheldon (2003).

The rainwater composition used in the modeling may be found in Sheldon (2006d). Because rainwater is very fresh (i.e., has low salinity and low total-dissolved solids), most of the cations available for reactions come from the rock(s) being weathered. Pedogenesis is dominated by the breakdown of base-bearing minerals either by hydrolysis (e.g., potassium feldspar being weathered to illite) or by acid attack that liberates cations for use by plants and microbes. An example of the latter type of reaction would be the dissolution of the plagioclase feldspars albite or anorthite:

$$NaAlSi_3O_{8\ albite} + 4H^+ = Na^+ + Al^{3+} + 3SiO_{2(aq)} + 2H_2O \quad (42)$$

$$CaAl_2Si_2O_{8\ anorthite} + 8H^+ = Ca^{2+} + 2Al^{3+} + 2SiO_{2(aq)} + 4H_2O \quad (43)$$

where the resulting species are all aqueous. Acid attack reactions consume H^+ ions, thereby raising the pH of the system, and providing a long-term control on atmospheric pCO_2 (e.g., Berner, 2004). While HCO_3^- is the most stable carbon-bearing species at near neutral pH values (5.5–8), CO_3^{2-} becomes the most stable species at higher pH values (>8). This change leads to the precipitation of carbonate minerals such as calcite, siderite, and ankerite. However, all of the interflow paleosols of the Picture Gorge Subgroup are carbonate-free, so the first appearance of carbonate minerals can be taken to represent the end point of the realistic weathering reaction (Sheldon, 2006b).

Atmospheric pCO_2 values of 0.1, 1, 3, 5, 10, 15, and 20 PAL were used in model calculations, where 0.1 PAL is an extreme case used to represent the sub-modern pCO_2 levels suggested by Pagani et al. (1999) and Royer et al. (2001a,b). All model calculations were for 25 °C temperature conditions, which is within 10 °C of paleotemperature estimates from the paleosols themselves (Sheldon, 2003, 2006d) and paleobotanical estimates (Graham, 1999). Using a reaction temperature of 25 °C has the additional advantage of being the temperature at which most thermodynamic data are best-constrained. All model calculations were run over the range of 0.001–10 g of rock added to a kilogram of water, or 10^{-3} to 10^{1} g of rock titrated. In all cases, calcite precipitated before the end of the titration run. Taking into account both kinetic factors and the temperature, a number of zeolite and high-temperature minerals were suppressed from forming in the calculations.

A thorough description of the model results (including mineralogical data) may be found in Sheldon (2006d), but to illustrate what the model outputs look like and how they are comparable to other tools for assessing pedogenesis, Fig. 13 compares model results for Ca^{2+} and Na^+ in the soil water solution with mass balance results (see Section 5.3 for the method) obtained from the type section of middle Miocene Ilukas pedotype, which is found throughout the Picture Gorge Subgroup (Sheldon, 2006d). Weathering is typically most intense near the surface of a soil and declines rapidly with increasing depth and decreasing permeability (both initial and as a direct result of plant-rock interactions). Therefore, with the titration of progressively more rock into solution we would expect an increase in the activity (and by extension, molality) of a given cation. This pattern is observed in the model calculations for Na^+ and Ca^{2+} (though the same result was found for other common base cations; Sheldon, 2006d). In addition, to reproducing the expected cation distributions indicated by mass-balance calculations, the model also produced reasonable pH values for Alfisol-like (Argillisols) paleosols, and produced reasonable water-rock ratios during pedogenesis relative to a calculated "real" water-rock ratio based on estimates of MAP (Sheldon, 2006d).

The 10 PAL model run was also favored as the most likely scenario because only the 10 PAL case produced a significant amount of Mg^{2+}. That value represents an upper limit to pCO_2 though, because higher pCO_2 values result in dolomite precipitation and dolomite is not observed in the paleosols and is unlikely to form in any soils for kinetic reasons (Capo et al., 2000). That the 10 PAL case best matches the geologic evidence raises the question of how much of that total pCO_2 is due to atmospheric pCO_2 and how much is due to soil productivity. Using the world soil pCO_2 map of Brook et al. (1983), modern soils like the Picture Gorge Subgroup paleosols have 3–8 PAL soil pCO_2. If one assumes that 10 PAL is the total soil pCO_2, from both atmospheric and soil respiration sources necessary to produce the Picture Gorge Subgroup paleosols, then atmospheric pCO_2 likely ranged from 2 to 7 PAL for the transient middle Miocene climatic optimum (Sheldon, 2006d). Even at the low end of that range, it is likely that sub-pre-Industrial atmospheric pCO_2 levels, as suggested by Pagani et al. (1999), are too low. Furthermore, a value of 2–4 PAL is consistent with estimates from stomatal index (Retallack 2002; Kürschner et al., 2008) and mass-balance modelling (Berner and Kothavala 2001; though cf. Berner, 2005). The model results do not preclude the possibility of very low atmospheric pCO_2 coupled with non-analogous biotic productivity in the Ilukas paleosols (i.e., unusually high productivity forests). However, that scenario is unlikely because the flora and fauna of the middle Miocene was not substantially different from a modern one (e.g., Janis et al., 2002), so it is more likely that modern-analogue forests have comparable productivity to their Miocene

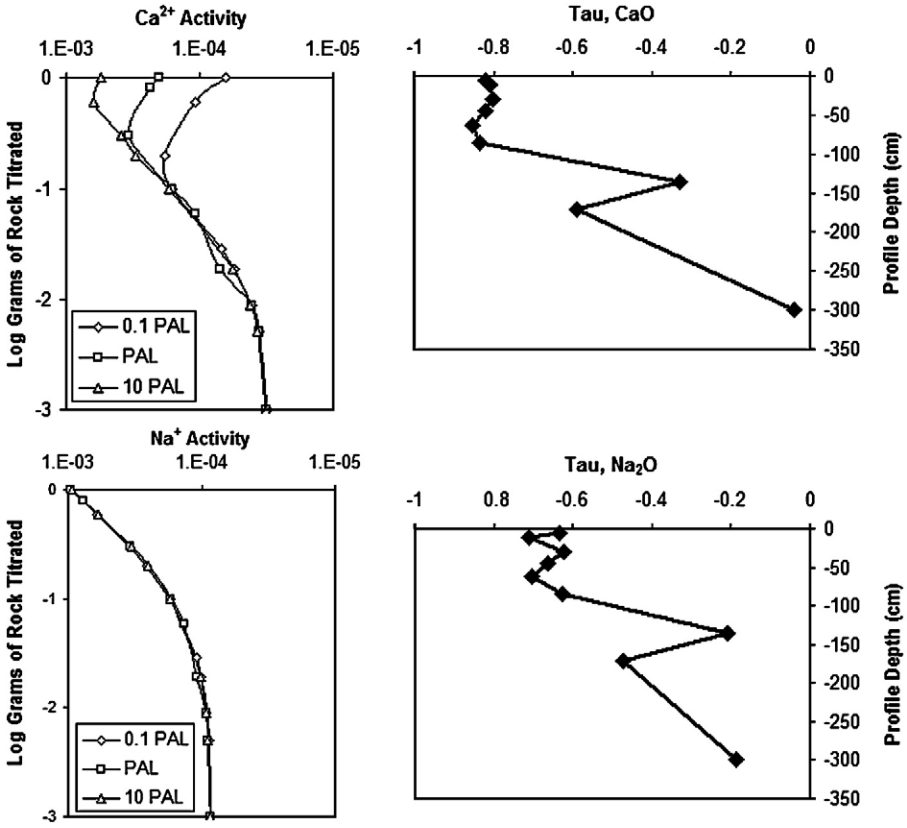

Fig. 13. Multi-equation thermodynamically-derived profile versus mass-balance calculations.

counterparts. Therefore, these results are suggestive that the middle Miocene warm event was due, at least in part, to elevated atmospheric pCO_2 (Sheldon, 2006b).

The multi-equation thermodynamic approach thus potentially gives a wide range of information about both pedogenic environment and the climatic conditions under which the modeled paleosol(s) formed. Potential limitations include poorly constrained parent material chemistry and poorly constrained vegetative covering. However, in areas where both are known (e.g., paleosols formed on volcanic units or at unconformities with associated floras or clear taxonomic identifications), this approach is viable. Furthermore, for pre-vascular land plant paleosols, it presents an excellent potential research tool because one of the two primary limitations is removed.

7. Stable isotope approaches

7.1. Stable isotopic composition of pedogenic minerals as paleoenvironmental proxies

The stable isotope values of pedogenically-formed minerals have the potential to provide paleoenvironmental information such as the isotope composition of soil waters (e.g., Vitali et al., 2002; Tabor and Montañez, 2002, 2005; Tabor et al., 2002, 2004a,b), paleotemperature (Yapp, 1993a, 2000; Delgado and Reyes, 1996; Savin and Hsieh, 1998; Vitali et al., 2002; Tabor and Montañez, 2005; Gilg, 2003; Tabor, 2007), the isotope values of gases in the soil (Cerling and Quade, 1993; Cerling et al., 1991; Koch et al., 1995; Yapp, 2001a,b; Fox and Koch, 2003; Behrensmeyer et al., 2007), and the partial pressure of soil and tropospheric gases (Cerling, 1984; Quade et al., 1989; Cerling, 1991; Yapp and Poths, 1996; Mora et al., 1996; Ekart et al., 1999; Tabor et al., 2004a,b). The utility of soil authigenic minerals as proxies of paleoenvironmental conditions requires: (1) relatively well-known temperature-dependent stable-isotope mineral-water fractionation factors, (2) isotopic equilibrium, or near equilibrium, at the time of mineral crystallization, (3) closed-system conditions for structurally-bound elements since the time of mineral formation, (4) water-dominated environments of crystallization, and (5) knowledge of the relationship between the isotope of interest in the mineral and the medium (e.g., H_2O, CO_2) from which it was derived. Considering that the vast majority of waters on the continents have a meteoric origin, that processes that govern the global meteoric water line and mixing of gases between the soil and atmosphere are similar, and the low solubility of most paleosol minerals, conditions (4) and (5) have been likely fulfilled and constant for minerals that form in well-developed soils since at least the advent of vascular plants during Silurian time (Gregory, 1991; Yapp and Poths, 1991, 1992; Yapp, 2001a,b; Came et al., 2007). Requirements (1) through (3) are specific to the mineral of interest and its paragenesis. In particular, requirement 1 is critical to drawing paleoenvironmental inferences from the stable isotope value of soil minerals.

7.1.1. Mineral-water isotope fractionation and the jargon of stable isotope geochemistry

In this work, we consider variation among stable isotopes of oxygen, hydrogen and carbon in soil media, and in solid materials that occur in paleosol profiles. Herein, we consider the two most abundant isotopes of oxygen, hydrogen, and carbon: ^{16}O and ^{18}O, ^{1}H and ^{2}H, ^{12}C and ^{13}C. Isotopes of these elements may be partitioned, or fractionate, differently among the reactants and products of chemical reactions. In general, reactions involving these isotopes are mass-dependent (i.e., the process in question discriminates against the higher mass isotope to some degree). Isotope fractionation is depicted by the chemical equilibrium constant of a chemical reaction that includes isotope exchange:

$$\text{Mineral}-{}^{16}\text{O} + \text{H}_2{}^{18}\text{O} \leftrightarrow \text{Mineral}-{}^{18}\text{O} + \text{H}_2{}^{16}\text{O}. \quad (44)$$

The fractionation of ^{16}O and ^{18}O among the reactants and products is described by the alpha value (α):

$$^{18}\alpha_{\text{mineral}} = \frac{\frac{^{18}O_{\text{mineral}}}{^{16}O_{\text{mineral}}}}{\frac{^{18}O_{H_2O}}{^{16}O_{H_2O}}} \quad (45)$$

where $^{18}\alpha$ is the oxygen isotope fractionation factor. The hydrogen and carbon isotope fractionation factors are noted by $^{D}\alpha$ and $^{18}\alpha$, respectively. α values for isotope exchange reactions are very small, which indicates that, in the absence of a more energetic reaction such as dissolution and precipitation, isotope exchange will not occur. That is, the isotope composition of a mineral is stable, and will remain unchanged, after it has formed. Fractionation of ^{18}O and ^{16}O between a mineral and water can vary, but changes in α are principally related to the temperature of reaction such that:

$$10^3 \ln\alpha_{\text{mineral}-H_2O} = \frac{A}{T^2} + \frac{B}{T} + C \quad (46)$$

where A, B, and C are constants which describe the behavior of an isotope for a specific mineral-water system, and T is temperature in K. Note, however, that the quantity B/T does not appear in many isotope fractionation equations. A list of fractionation equations for common pedogenic minerals is given in Table 5.

Measurement of the isotope composition is usually reported with respect to the difference between the measured $^{18}O/^{16}O$ value of the sample with respect to the measured $^{18}O/^{16}O$ value of a standard. These reported values, called δ ("delta") values, are calculated as:

$$\delta X = \left(\frac{\frac{^{heavy}X_{\text{sample}}}{^{light}X_{\text{sample}}}}{\frac{^{heavy}X_{\text{standard}}}{^{light}X_{\text{standard}}}} - 1 \right) \times 1000 \quad (47)$$

where X is the element under consideration (C or O for example), $^{\text{heavy}}$ and $^{\text{light}}$ refer to the concentration of heavy and light isotopes, respectively, of element X in the sample and standard. δ values are reported in per-mil units (parts per thousand), which is denoted by the symbol, "‰". Conventional presentation of δ values are δD for hydrogen, $\delta^{13}C$ for carbon and $\delta^{18}O$ for oxygen. The standard that is used for reporting δD and $\delta^{18}O$ values is Standard Mean Ocean Water (SMOW), whereas the standard used for reporting $\delta^{13}C$ values is PeeDee Belemnite. Therefore both SMOW and PDB have δ values that are defined as 0‰ when referenced with respect to themselves.

7.1.2. Stable isotope fractionation factors of common pedogenic minerals

A significant amount of research has focused upon measurement and determination of stable isotope fractionation factors (see reviews by Hoefs, 1997; Valley et al., 1986; Savin and Lee, 1988; Chacko et al., 2001; Sharp, 2007). Table 5 presents the stable isotope fractionation factors (values of $10^3\ln\alpha$) of common soil-forming minerals, as determined from laboratory syntheses, isotope exchange reactions and natural experiments. At temperatures that reflect soil formation in the presence of liquid water (~0–30 °C; Yapp, 2001a,b; Tabor and Montañez, 2005), the majority of mineral-water oxygen isotope fractionation factors ($10^3\ln^{18}\alpha$) have positive values, which indicates that ^{18}O is enriched in the mineral product (Table 5; Fig. 14A). Carbonates and silicates have the largest (~25–35) and Fe(III)-oxides the smallest (~0–15) $10^3\ln^{18}\alpha$ values, and Al- and Mn-oxides have intermediate values. In addition, $10^3\ln^{18}\alpha$ values decrease with higher temperatures for all minerals considered herein. Minerals with little or no ionic substitution, such as low-Mg calcite and kaolinite ($Al_2Si_2O_5(OH)_4$) have relatively invariant $10^3\ln^{18}\alpha$ values under isothermal conditions. Mineral groups that permit a great deal of metal-cation substitution, such as 2:1 phyllosilicate minerals, result in variable $10^3\ln^{18}\alpha$ values under isothermal conditions (Savin and Lee, 1988). For example, Tabor and Montañez (2005) reported the chemistry of smectites from Permian–Pennsylvanian-age paleosol profiles that correspond to differences in isothermal $10^3\ln^{18}\alpha$ values > 1‰ among samples, whereas Koster and others (1999) determined that nontronite ($Na_{0.3}Fe^{3+}{}_2(Si,Al)_4O_{10}(OH)_2$) $10^3\ln^{18}\alpha$ values are ~4‰ lower than Fe-rich $10^3\ln^{18}\alpha$ values. This highlights the importance of accurate mineralogical and chemical characterization of pedogenic minerals in order to interpret appropriately the meaning of their $\delta^{18}O$ values.

All mineral-H_2O hydrogen isotope fractionation factors ($10^3\ln^{D}\alpha$; Table 5; Fig. 14B) considered herein have negative values, indicating that ^1H is enriched in the mineral product. Goethite has the most negative (~−100), whereas gibbsite has the most positive (~−5), $10^3\ln^{D}\alpha$ values, and phyllosilicates have intermediate values. Within analytical uncertainty, goethite and gibbsite $10^3\ln^{D}\alpha$ values do not

Table 5
Light stable isotope fractionation equations for common soil-formed minerals.

Reaction	$10^3\ln^{18}\alpha$	$10^3\ln^{D}\alpha$	$10^3\ln^{13}\alpha$	Reference
$H_2O(l)$–$H_2O(v)$	$1.137*10^6/T^2-0.4156*10^3/T-2.0667$	$28.844*10^6/T^2-76.248*10^3/T+52.612$		Majoube, 1971
Calcite-H_2O	$2.78*10^6/T^2-2.89$		$-2.988*10^6/T^2+7.6663*10^3/T-2.4612$	(O'Neil et al., 1969; Kim and O'Neil, 1997)
Calcite-CO_2	$18.03*103/T-32.42$			
Siderite-H_2O	$3.13*10^6/T^2-3.50$			Carothers et al. (1988)
Siderite-CO_2	See Fig. 17			
Goethite-H_2O	$1.63*10^6/T^2-12.3$			(Yapp, 1990; Yapp, 1987a,b; Bao and Koch, 1999; Muller, 1995)
	$1.907*10^3/T-8.004$	−99.8		
	$2.76*10^6/T^2-23.7$			
Hematite-H_2O	$1.63*10^6/T^2-12.3$			(Yapp, 1990; Clayton and Epstein, 1961; Bao and Koch, 1999)
	$0.413*10^6/T^2-2.56$			
	$0.542*10^6/T^2-5.221$			
	$0.733*10^6/T^2-6.194$			
Gibbsite-H_2O	$2.04*10^6/T^2-3.61*10^3/T+3.65$	−5.1		(Vitali et al., 2000, 2001)
Boehmite-H_2O	$2.11*10^6/T^2-4.4$	XXX		Bird et al. (1992)
Kaolinite-H_2O	$2.76*10^6/T^2-6.75$	$-2.2*10^6/T^2-7.7$		Sheppard and Gilg (1996)
Smectite-H_2O	$2.60*10^6/T^2-4.28$ Sum of metal-oxygen bonds	$-2.2*10^6/T^2-7.7+(2*Al-4*Mg-68*Fe)$		(Delgado and Reyes, 1996; Savin and Lee, 1988; Sheppard and Gilg, 1996)
Illite/smectite-H_2O		$-19.6*10^3/T+25$ (0–120 °C) $-45.3*10^3/T+94.7$ (0–150 °C)		(Yeh, 1980; Capuano, 1992; Hyeong and Capuano, 2004)

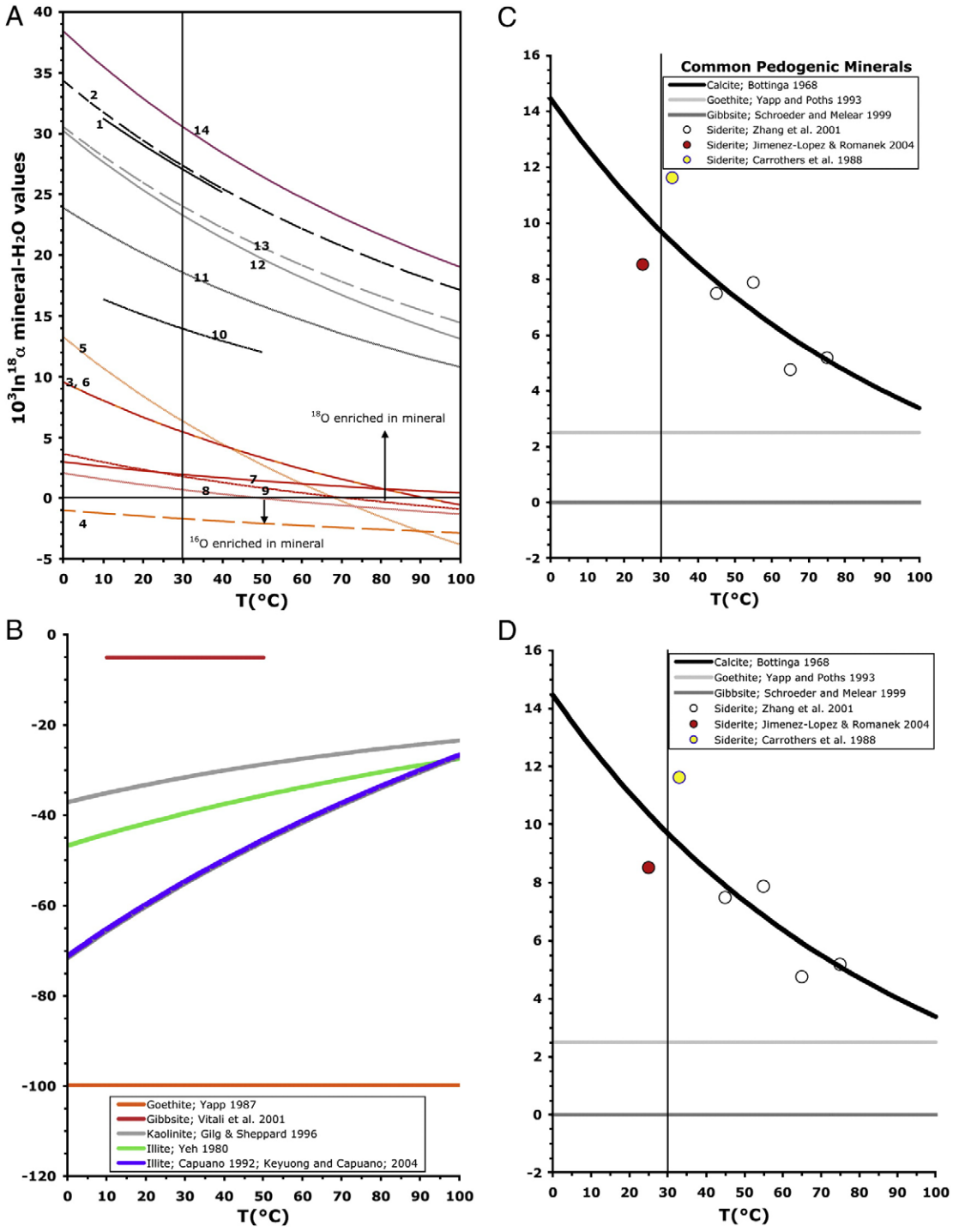

Fig. 14. (A) Cross plot of $10^3\ln^{18}\alpha$ values versus temperature (°C) for common pedogenic minerals. 0 °C is shown as the lower limit, because it assumed that liquid water is required for chemical reaction and formation of pedogenic minerals. Thin black vertical line at 30 °C is the approximate upper limit of soil temperatures based on mean annual surface air temperatures from weather stations in the International Atomic Energy Association (IAEA) global network for isotopes in precipitation database (Rozanski et al., 1993). Arabic numbers within graph indicate studies which reported the $10^3\ln^{18}\alpha$ value: 1 = calcite, Kim and O'Neil (1997); 2 = calcite, O'Neil et al. (1969); 3 = goethite, Yapp (1990); 4 = geothite, Bao and Koch (1999); 5 = goethite, Muller (1995); 6 = hematite @ pH = 1–2, Yapp (1990); 7 = hematite, Clayton and Epstein (1961); 8 = hematite @ pH = 1–2, Bao and Koch (1999); 9 = hematite @ pH = 8–9, Bao and Koch (1999); 10 = Gibbsite, Bird et al. (1994a); 11 = boehmite, Bird et al. (1992); 12 = Kaolinite, Sheppard and Gilg (1996); 13 = smectite, Delgado and Reyes (1996); 14 = siderite, Carothers et al. (1988). See Text for discussion. (B) Cross plot of $10^3\ln^D\alpha$ values versus temperature (°C) for common hydroxylated pedogenic minerals. See text for discussion. (C) Cross plot of $10^3\ln^{13}\alpha$ values versus temperature (°C) for common pedogenic minerals. See text for discussion.

vary with temperature, although goethite $10^3\ln^D\alpha$ values do vary according to Al substitution for Fe in the crystal lattice (Feng and Yapp, 2008). Phyllosilicates exhibit temperature dependence, where $10^3\ln^D\alpha$ values decrease with higher temperatures (Fig. 14B). In addition, 2:1 phyllosilicate $10^3\ln^D\alpha$ values vary according the concentration of octahedrally-coordinated metal cations, where $10^3\ln^D\alpha = -2.2 * 10^6 / T^2 - 7.7 + (2 * \mathrm{Al} - 4 * \mathrm{Mg} - 68 * \mathrm{Fe})$ (Suzuoki and Epstein, 1976; Gilg and Sheppard, 1996; Tabor and Montañez, 2005). This effect could result in isothermal $10^3\ln^D\alpha_{\text{smectite-H2O}}$ values that differ by ~70‰, although Tabor and Montañez (2005) found that the chemistry among 14 different Permian–Pennsylvanian paleosol smectites accounted for isothermal $10^3\ln^D\alpha_{\text{smectite-H2O}}$ variability no greater than ~5‰.

Mineral-CO_2 carbon isotope fractionation values ($10^3 \ln^{13}\alpha$; Table 5; Fig. 21) for calcite (Bottinga, 1968) and the Fe(CO_3)OH group in solid solution with goethite (Yapp and Poths, 1993) are positive, indicating that ^{13}C is enriched in the mineral product, whereas mineral-bound C that is apparently in solid solution with gibbsite (Tabor and Yapp, 2005a,b) shows no fractionation with respect to gaseous CO_2 (i.e., gibbsite and CO_2 $\delta^{13}C$ values are equivalent; Schroeder and Melear, 1999). Calcite-CO_2 $10^3 \ln^{13}\alpha$ values decrease with increasing temperature (Fig. 14A), whereas goethite-CO_2 and gibbsite-CO_2 $10^3 \ln^{13}\alpha$ values do not exhibit temperature dependence (Yapp, 2001a,b). Although siderite-CO_2 $10^3 \ln^{13}\alpha$ values appear to follow closely those for calcite-CO_2, siderite-CO_2 $10^3 \ln^{13}\alpha$ values are too poorly studied at this time to be expressed as a temperature-dependent fractionation equation (see Fig. 14C).

7.1.3. Relationship between hydrogen and oxygen isotopes in continental waters

The vast majority of continental surface waters are meteoric in origin (Dansgaard, 1964; Gat and Bowser, 1991). That is, surface waters are derived from the atmosphere as precipitation (rainfall and snow). The main source of meteoric water is vapor derived from evaporation of ocean water, which has maintained mean $\delta^{18}O$ values near 0‰ (±2‰) for most of the Phanerozoic (Gregory, 1991; Yapp and Poths, 1992; Tabor, 2007; Eiler, 2007). Over the continents, the oxygen and hydrogen isotope values of rainfall follow a Rayleigh-type distillation, whereby subsequent rain-out events have progressively more negative oxygen and hydrogen isotope values. The rain-out process is driven principally by cooling of the air-mass (Dansgaard, 1964; Fig. 15), which may arise from vertical thermal uplift, physical transport over high-altitude sites (e.g., mountains), or latitudinal transport to cooler sites (e.g., Rozanski et al., 1993; Clark and Fritz, 1997). The oxygen and hydrogen isotope values of rainfall are strongly correlated, and may be approximated by the equation for the meteoric water line (Craig, 1961): $\delta D = 8 * \delta^{18}O + 10$. While there is abundant evidence for short-term departures from the meteoric water line (e.g., Gat and Bowser, 1991; Krishnamurthy and Bhattacharya, 1991; Lawrence and White, 1991), the long-term weighted mean of precipitation $\delta^{18}O$ and δD values indicates that the aforementioned equation for meteoric water is an accurate representation of isotopes in the meteoric water cycle. Considering that timescales for significant accumulation of authigenic minerals in soil profiles range from 10^3–10^5 years, it is generally assumed that Craig's (1961) meteoric water line equation is an accurate representation of precipitation that rained upon, and percolated through, the soil profile (e.g., Yapp, 1993a, 2001a,b; Delgado and Reyes, 1996; Ferguson et al., 1999; Savin and Hsieh, 1998; Vitali et al., 2001; Tabor and Montañez, 2002, 2005; Tabor et al., 2002; Tabor, 2007; Gilg, 2003).

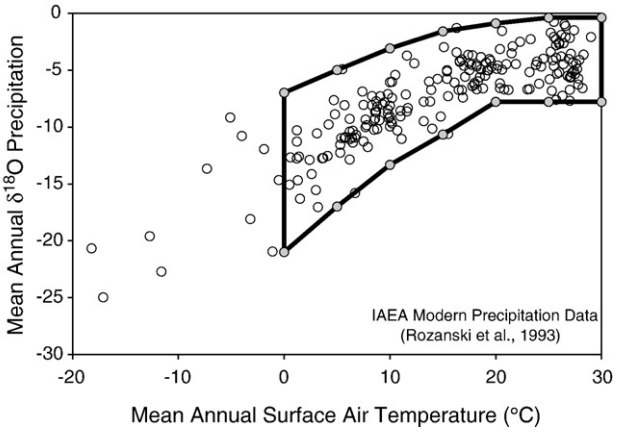

Fig. 15. Cross plot of weighted mean annual $\delta^{18}O$ values versus mean annual surface air temperature for 209 weather stations from the International Atomic Energy Association (IAEA) global network for isotopes in precipitation database (Rozanski et al., 1993). The points upon the polygon that surround data points above 0 °C are used to construct a modern surface domain for hydroxylated minerals. See text for discussion.

In fact, both the $\delta^{18}O$ and δD values of rainfall are correlated with surface air temperature (e.g., Fig. 15 — IAEA Database from Rozanski et al., 1993). Based upon previous studies of meteoric precipitation $\delta^{18}O$ and δD values, Criss (1999; see also Dansgaard, 1964) arrived at the following correlation: $\delta^{18}O_{MAP} \approx 0.695_{MAT(°C)} - 13.6$, where MAP is the weighted mean annual precipitation and MAT is the mean annual surface atmospheric temperature. This general correlation indicates that precipitation $\delta^{18}O$ values will decrease by ~0.7‰ with each °C fall in temperature. Given the relation between altitude, latitude, and temperature, Criss (1999) also presented empirical relationships between precipitation $\delta^{18}O$ values and altitude, $\Delta\delta^{18}O \approx 2 \pm 1‰\ km^{-1}$, as well as latitude, $\Delta\delta^{18}O \approx 0.2 \pm 0.1‰\ 100\ km^{-1}$. Criss (1999) emphasizes, however, that these relationships are only rough approximations, and as will be discussed in subsequent sections, application of these observed relations to the isotope composition of paleosol minerals (paleosol calcite, for example) as a means of paleoclimatic reconstruction should be avoided or used with extreme caution.

7.2. Carbon in soils

The $\delta^{13}C$ value of pedogenic minerals may be directly related to the $\delta^{13}C$ value of CO_2 in the local soil environment (Cerling, 1984; Quade et al., 1989; Schroeder and Melear, 1999; Schroeder et al., 2006). However, soils may be characterized by mixing of one, two, or three components of soil CO_2, which can result in significantly different $\delta^{13}C$ values of soil CO_2 and the resulting soil mineral. The three CO_2 components are derived from (1) oxidation of *in situ* organic matter, (2) tropospheric CO_2, and (3) dissolution of pre-existing carbon-bearing minerals such as carbonate in the soil (Yapp, 2001a,b, 2002). Based upon geological and chemical arguments, the conditions of soil CO_2 mixing in the paleosol at the time of mineral crystallization must be assessed in order to interpret appropriately the environmental significance of mineral $\delta^{13}C$ values (e.g., Quade et al., 1989; Hsieh and Yapp, 1999; Tabor et al., 2004a,b; Tabor and Yapp 2005b; Tabor et al., 2007), and to determine whether the minerals formed in the presence of one, two, or three components of soil CO_2.

7.2.1. One-component soil CO_2

In a strict sense, soils with only one component of CO_2 form under a chemically closed-system, but it is also useful to include in this category soils which form under semi-closed systems (e.g., Gluyas, 1984; Tabor et al., 2007). Chemically closed or semi-closed conditions arise in settings where gaseous diffusion between the soil and the troposphere is limited, usually as a result of poorly drained, waterlogged conditions within the soil profile. Diffusion from the troposphere (including CO_2) to the soil is limited, and aqueous O_2 in the soil is quickly consumed by oxidation of organic matter (Feng and Hsieh, 1998). Yet, oxidized carbon species ($CO_{2(aq)}$, HCO_3^-, CO_3^{2-}) may still be liberated from closed system soils at pH levels permissive of carbonate precipitation (~pH = 5.5–8.5; Irwin et al., 1977; Gluyas, 1984) in the following types of reactions:

$$SO_4^{2-} + 2CH_2O \rightarrow H_2S + 2HCO_3^- \quad (48)$$

$$SO_4^{2-} + 2CH_2O \rightarrow HCO_3^- + HS^- + H_2O + CO_2. \quad (49)$$

Under these conditions, both bicarbonate and resulting carbon-bearing minerals will have $\delta^{13}C$ values that are equivalent to that of the oxidizing organic matter in the closed-system soil. For example, given that C_3 plant organic matter has $\delta^{13}C$ values ranging from approximately − 20 to − 33‰ (mean = − 27‰; see Section 7.6), carbon-bearing-mineral $\delta^{13}C$ values in a closed system soil profile will have $\delta^{13}C$ values ranging from − 20 to − 33‰. Soil profiles forming under semi-closed conditions will result in more positive calcite $\delta^{13}C$ values (because

tropospheric CO_2 is isotopically heavier; ~− 6.5 to − 8.0‰ during the Holocene), but will be isotopically more negative than $\delta^{13}C$ values of the same mineral that forms in a 2- or 3-CO_2 component soil. Minerals that may result from one-component soil CO_2 mixing include calcite (Tabor et al., 2007) and siderite (Mozley and Carothers, 1992; Mozley and Wersin, 1992; McMillan and Schwertmann, 1988; Ludvigson et al., 1998; White et al., 2005). It is less likely that carbon-bearing minerals that require oxidizing conditions (e.g., Fe(CO_3)OH in goethite; Yapp, 2001b) or free drainage (e.g., occluded CO_2 in gibbsite; Bárdossy and White, 1979; Schroeder and Melear, 1999) will form in soils characterized by one component of soil CO_2.

7.2.2. Two-component soil CO_2

Two-component soil CO_2 mixing assumes that the only two sources contributing to soil CO_2 are CO_2 from the open atmosphere (tropospheric CO_2) and CO_2 from *in situ* oxidation of biological carbon in the soil. Steady-state solutions to the one-dimensional Fickian diffusion equation yield reasonable representations of $\delta^{13}C$ values of soil CO_2 with depth in modern soils characterized by mixing of two sources of CO_2 (Cerling, 1984). In these models, the pCO_2 and $\delta^{13}C$ value of Earth's atmosphere is the upper boundary condition, and there is a depth-dependent CO_2 production term that describes the oxidation of organic carbon in the soil. Above a characteristic CO_2 production depth within the soil, both the concentration and $\delta^{13}C$ of soil CO_2 will progressively approach values of the Earth's atmosphere. Thus, CO_2 in soil gas can be generally regarded as a mixture of two isotopically distinct end-members in these soils: atmospheric CO_2 and CO_2 derived from *in situ* oxidation of soil organic matter (Fig. 16). As mentioned earlier, soil organic matter $\delta^{13}C$ values are principally determined by (1) the $\delta^{13}C$ of CO_2 in the global troposphere and (2) the photosynthetic pathway employed by primary producers within the soil profile. Therefore, for times in the geological past when C_3 photosynthesis was the dominant floral metabolism (pre-Miocene time; see 8.6) and soil organic matter $\delta^{13}C$ exhibited minimal temporal or spatial variation (e.g., Tabor et al., 2004a,b; Peters-Kottig et al., 2006; Montañez et al., 2007), stratigraphic changes in mineral $\delta^{13}C$ values among paleosol profiles may indicate either (1) variations in soil productivity (i.e., the concentration of CO_2 derived from *in situ* oxidation of organic matter) or (2) changes in atmospheric pCO_2. In this regard, $\delta^{13}C$ values of carbon-bearing pedogenic minerals which formed in the presence of two-component soil CO_2 mixing have the potential to provide information about (1) paleoecology and (2) the concentration of CO_2 in ancient atmospheres. Pedogenic minerals which provide geochemical records of two-component soil CO_2 mixing include calcite (Cerling, 1991; Mora et al., 1996; Yapp and Poths, 1996; Ekart et al., 1999; Tabor et al., 2004a, b), goethite (Yapp, 1987a,b; Yapp and Poths, 1992, 1993, 1996; Yapp, 2004; Tabor et al., 2004a,b; Tabor and Yapp, 2005a), and gibbsite (Schroeder and Melear, 1999; Tabor and Yapp, 2005a,b; Schroeder et al., 2006). Of these minerals, only the geochemistry of calcite and goethite are sufficiently understood to permit estimates of atmospheric pCO_2. Both pedogenic calcite and goethite are relatively abundant in the terrestrial stratigraphic record, and thus have the potential to provide a relatively continuous Phanerozoic record of paleoatmospheric pCO_2 (see Section 7.4.3.1; Ekart et al., 1999) that may be cross-checked by independent proxy methods (Yapp and Poths, 1996; Tabor et al., 2004a,b).

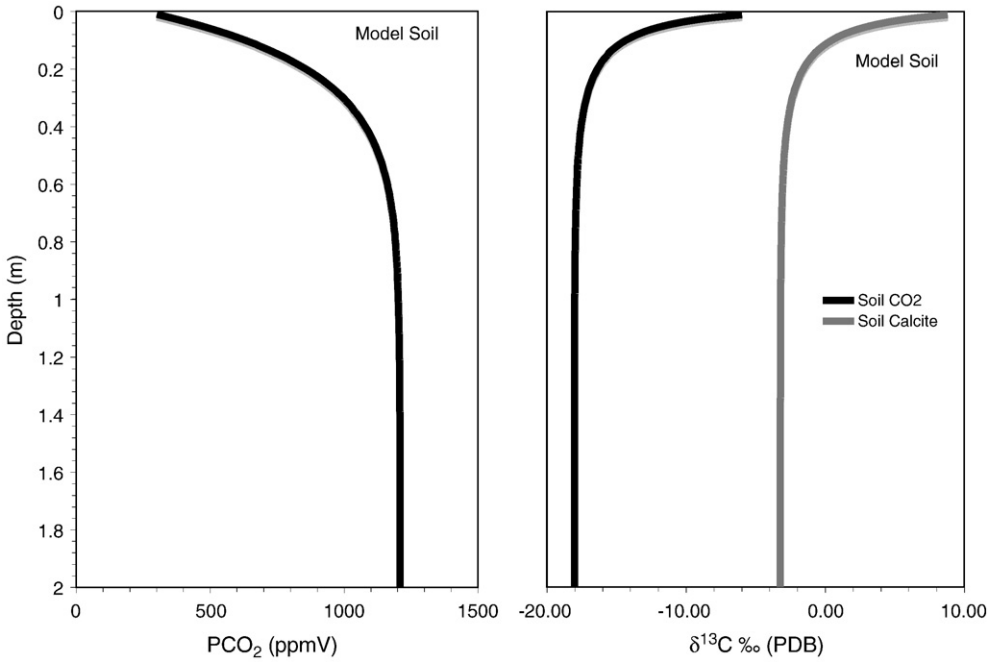

Fig. 16. Steady-state model plot of soil depth in meters versus (A) soil CO_2 concentration and (B) $\delta^{13}C$ values of soil CO_2 and pedogenic calcite. Solution to the soil CO_2 concentrations assumes Fickian, one-dimensional diffusion, of the form

$$pCO_2 = \left(\frac{(\phi / D_s) \times \left(1 - e^{-z/Z}\right)}{22} * 10^6\right) + 300$$

where ϕ is the production rate of CO_2 in the soil in gC $cm^{-3}h^{-1}$, D_s is the diffusion coefficient for gas through the soil, z is depth in meters in the soil, and Z is a scaling depth in meters, also called the characteristic production depth of CO_2 (Cerling, 1991) in the soil. This model soil is calculated with $\phi = 0.00002$ gC $cm^{-3}h^{-1}$, $D_s = 0.0001$, and $Z = 0.2$, and 300 ppmV as the upper boundary limit of the soil (i.e., a tropospheric pCO_2 of 300 ppmV). Soil CO_2 $\delta^{13}C$ values were calculated as a mass balance of tropospheric CO_2 (300 ppmV through profile) with $\delta^{13}C$ value of − 6.5‰ (a reasonable pre-industrial age value; Schlesinger, 1997) and CO_2 from oxidation of organic matter (variable concentrations) with $\delta^{13}C$ value of − 6.5‰ (i.e., organic matter $\delta^{13}C = -26.4$‰). Soil calcite $\delta^{13}C$ values were calculated using the CO_2-calcite carbon isotope fractionation equation of Bottinga (1968) with assumed calcite crystallization temperatures of 25 °C and mildly alkaline soil solution. See Text for discussion.

7.2.3. Three-component soil CO_2

On the basis of geological and chemical arguments, several studies have concluded that three-component CO_2 mixing relations can exist in various soils (Hsieh and Yapp, 1999; Yapp, 2001a,b; 2002; Tabor et al., 2004a,b; Tabor and Yapp, 2005b,c). As in 2-component CO_2 mixing, 3-component mixing assumes soil CO_2 is represented by sources contributed from oxidation of organic matter and the global troposphere, but includes also a third component of CO_2 contributed from dissolution of pre-existing carbonate in the soil profile. Although carbonate may have very negative $\delta^{13}C$ values in rare instances (e.g., one-component CO_2 mixing; Yemane et al., 1989; Tabor et al., 2007; Coney et al., 2007), CO_2 that is produced from dissolution of carbonate generally is enriched in ^{13}C relative to atmospheric CO_2 or CO_2 derived from oxidation of organic matter (e.g., Hoefs, 1997; Criss, 1999; Sharp, 2007). As a result of these mixing relationships, pedogenic minerals that form in 3-component soil CO_2 mixing systems are characterized (and for the most part recognized) by $\delta^{13}C$ values more positive than 1- or 2-component soil CO_2 mixing. Pedogenic minerals which may form in the presence of mixing of 3 soil CO_2 components include goethite (Hsieh and Yapp, 1999; Yapp, 2001a, 2002; Tabor et al., 2004a,b; Tabor and Yapp, 2005b,c), gibbsite (Tabor and Yapp, 2005a,b), and possibly calcite.

7.3. Soil and paleosol carbonate

Precipitation of carbonate in soil profiles is related to evapotranspiration, acidity of soil solution, temperature, and availability of metal cations (Ca^{2+}, Fe^{2+}, Mg^{2+}). Carbonates may form in virtually any climate and soil drainage class (e.g., Whelan and Roberts, 1973; Soil Survey Staff, 1975, 2003; Semeniuk and Meagher, 1981; Franzmeier et al., 1985; Buol et al., 2003; Aslan and Autin, 1998; Retallack, 2001a,b; Schaetzl and Anderson, 2005). In poorly drained, swampy and anoxic environments, pedogenic siderite ($FeCO_3$) is common (McMillan and Schwertmann, 1988; Ludvigson et al., 1998) and calcite may also form (Whelan and Roberts, 1973; Aslan and Autin, 1998; Tabor et al., 2007). However, pedogenic calcite is typically associated with well-drained soil profiles in sub-humid, semi-arid, and arid climates (e.g., Soil Survey Staff, 1975; Machette, 1985; McFadden and Tinsley, 1985; Buol et al., 2003; Schaetzl and Anderson, 2005; Srivastava et al., 2002) characterized by relatively low rainfall (~<800 mm/yr; Jenny, 1941; Arkley, 1963; Gile et al., 1966; Retallack, 1994; Royer, 1999) and high evapotranspiration (Thornthwaite, 1948; Srivastava et al., 2002). In these well-drained, dry-climate soils, aqueous Ca^{2+} ions derived from dissolution of minerals are transported downward into the soil profile until precipitated as carbonate or removed from the soil through the groundwater system (Ekart et al., 1999; Tabor et al., 2006).

Macroscopic forms of pedogenic carbonate-accumulation occur as filamentous, nodular, tubular, and completely indurated and massive or laminated horizons (Gile et al., 1966; Machette, 1985). Petrographic studies indicate that pedogenic carbonate crystal fabrics are dominantly micrite, with lesser amounts of microspar, sparite, needle fiber, radial-fibrous and radiaxial textures (Deutz et al., 2002, 2001; Brewer, 1976; Loisy et al., 1999; Fig. 17). Although it is apparent that many different crystal morphologies may form in modern soils, non-micrite crystal textures in paleosol profiles are frequently suspected of post-pedogenic (i.e., diagenetic) alteration (e.g., Cerling, 1991; Ekart et al., 1999; Deutz et al., 2001, 2002).

Pedogenic carbonate mineralogy is overwhelmingly dominated by low-magnesium calcite (Jenny, 1941; Brewer, 1976; Freytet and Verrecchia, 2002; Sparks, 2003). Therefore, the majority of stable-isotope based paleoenvironmental and paleoclimatological reconstructions from paleosol carbonate focus upon low-magnesium calcite (e.g., Cerling, 1991; Ekart et al., 1999). However, other pedogenic carbonate minerals have been reported in rare cases. Mineralogical studies of soil and paleosol carbonates have also identified dolomite, trona, ankerite, and siderite (Postma, 1983; McMillan and Schwertmann, 1988).

Kohur et al. (1995) identified microcrystalline dolomite from a soil profile within a saltpan soil in Alberta, Canada. Dolomite has also been identified in weakly developed soils forming upon basaltic parent materials in Hawaii, U.S.A. (Capo et al., 2000; Whipkey et al., 2002). Ankerite nodules have also been identified in paleosol profiles that underwent marine flooding (Mack et al., in revision). Trona ($Na_2CO_3 \cdot NaHCO_3 \cdot 2H_2O$) has also been reported from shallow subsurface horizons of floodplain soils of Uttar Pradesh, India (Datta et al., 2002). The origins of pedogenic dolomite, ankerite and trona are not entirely clear, but they are likely related to high chemical activity of aqueous Mg^{2+}, Fe^{2+}, and Na^{+} in soil solution in conjunction with rapid evapotranspiration of soil water, and they are considered to represent exceedingly rare phenomena. As a result, the occurrence of dolomite and ankerite in paleosol profiles is usually attributed to diagenetic processes exclusive of pedogenesis.

Pedogenic siderite has been identified in modern soil-forming environments (Postma, 1981, 1982; Stoops, 1983; Landuyt, 1990; Brewer, 1964) and paleosol profiles (Matsumoto and Iijima, 1981; Leckie et al., 1989; Mozley and Carothers, 1992; Brown and Kingston, 1993; Baker et al., 1996; Ludvigson et al., 1998; Jacobs et al., 2005; White et al., 2005). The presence of siderite in a soil or paleosol profile indicates formation in a reducing environment, low concentrations of aqueous sulfate, circum-neutral pH, and soil pCO_2 greater than 100,000 ppmV (Pearson, 1979; Postma 1982; Bahrig, 1989; Pye et al., 1990). Although siderite is a common diagenetic alteration product (e.g., Mozley, 1988; Mozley and Carothers, 1992), microspherulitic siderite (Spencer, 1925; see Fig. 17) appears to be strongly associated with pedogenesis in poorly drained, waterlogged soils (Stoops, 1983; Landuyt, 1990; Browne and Kingston, 1993; Ludvigson et al., 1998; Ufnar et al., 2002, 2004; White et al., 2001, 2005; Jacobs et al., 2005).

7.3.1. Pedogenic calcite $\delta^{18}O$ values

The $\delta^{18}O$ value of calcite is related to the $\delta^{18}O$ value of the water from which it is derived, and the temperature of mineral crystallization (see equation of O'Neil et al., 1969 in Table 5). The potential of calcite oxygen isotope ratios as a paleotemperature proxy has been recognized for a very long time (McCrea, 1950; Epstein et al., 1953). Early studies acknowledged that $\delta^{18}O$ values of soil (Salomons et al., 1978; Magaritz and Amiel, 1980; Magaritz et al., 1981; Rabenhorst et al., 1984; Cerling, 1984; Quade et al., 1989; Cerling and Quade, 1993) and paleosol (Quade et al., 1989; Mack et al., 1991; Yapp and Poths, 1996) calcite are probably related to temperature of crystallization, but that its utility as a temperature proxy might be confounded by the effects of variable rainfall $\delta^{18}O$ values at isothermal sites (e.g., Fig. 15; Cerling and Quade, 1993; Stern et al., 1997; Tabor and Montañez, 2002) and modification of soil water $\delta^{18}O$ values by evapotranspiration (Cerling, 1984; Mack et al., 1991; Stern et al., 1997; Tabor et al., 2002; Mack and Cole, 2005; Tabor and Montañez, 2005; Behrensmeyer et al., 2007; Tabor, 2007). In spite of these complicating factors, paleosol calcite $\delta^{18}O$ values are still perceived as a useful indication of soil moisture $\delta^{18}O$ values (Cerling, 1984; Quade et al., 1989; Cerling and Quade, 1993; Stern et al., 1997).

7.3.1.1. Pedogenic calcite as a proxy for soil moisture $\delta^{18}O$ values. Several important studies have used the $\delta^{18}O$ values of paleosol calcite as a monitor of rainfall $\delta^{18}O$ values. Quade et al. (1989) observed a large shift toward more positive paleosol calcite $\delta^{18}O$ values in Miocene strata from Northern Pakistan that were deposited ~7 Myr before present. This positive oxygen isotope shift was subsequently identified in other areas around Asia (Stern et al., 1997; Sanyal et al., 2004; Behrensmeyer et al., 2007), and is interpreted to represent changing atmospheric circulation conditions (and precipitation $\delta^{18}O$ values) over the Indian subcontinent, and intensification to the modern Asian monsoon system. In a large study of Miocene–Pleistocene

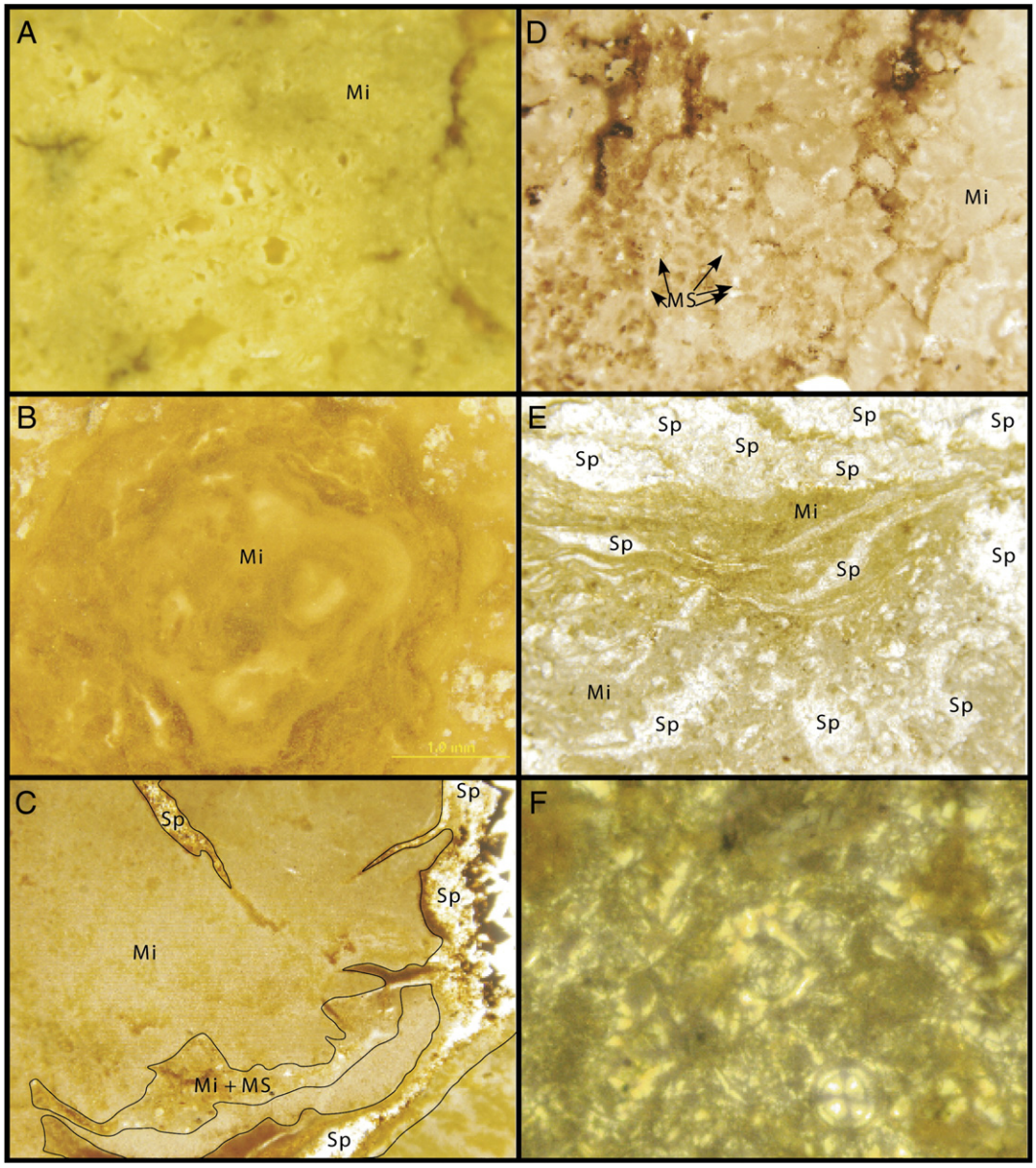

Fig. 17. Photomicrographs of paleosol carbonates. Mi = micrite, Sp = Sparite, MS = microspar (A) Nearly pure microcrystalline calcite (micrite; gray areas) that occludes mudstone from the matrix (red areas) in an Upper Triassic (Carnian) paleosol carbonate nodule of the Ischigualasto fm., Argentina. The area shown is appropriate for sampling, and determination of $\delta^{18}O$ and $\delta^{13}C$ values, in order to approximate environmental conditions during pedogenesis. Field of view is 2 mm. (B) Nearly pure micrite from a cross-section of a vertically oriented rhizolith in a paleosol from the Middle Permian Quanzijie fm, Xinjiang Province, Northwest China. The area shown is appropriate for sampling, and determination of $\delta^{18}O$ and $\delta^{13}C$ values, in order to approximate environmental conditions during pedogenesis. The red areas are colored by stain from potassium ferricyanide, which indicates low-magnesium calcite. The light gray areas are gypsum. Scale bar is 1 mm. (C) Domains of (1) micrite, (2) veins of sparry calcite, and (3) mixed micrite, microspar and Fe-oxide in a paleosol nodule from the Late Triassic (Carnian) Ischigualasto fm., Argentina. $\delta^{18}O$ and $\delta^{13}C$ values from domains of sparry calcite and mixed microspar and micrite are inappropriate, whereas $\delta^{18}O$ and $\delta^{13}C$ values from domains of micrite are appropriate, for sampling and measurement of oxygen isotope values in order to approximate environmental conditions during pedogenesis. Field of view is 4 mm. (D) Clotted micrite (dark areas) that is finely intergrown with microspar (light areas) from a paleosol nodule in Cretaceous (Kimmeridgian) strata of the Democratic Republic of Congo. Dark areas are stained by Fe-oxides. Field of view is 0.5 mm. While the areas of clotted micrite are appropriate for oxygen and carbon isotope analysis in order to approximate pedogenic conditions, very fine intergrowth of microspar and micrite makes sampling of the appropriate phase very challenging, and likely only feasible via a computer-assisted drill system. (E) Lamellar micrite intercalated with sparry calcite from a horizontal rhizolith in the Middle Permian Moradi fm., Niger. Field of view is 2 mm. While areas of micritic calcite are appropriate for sampling and oxygen and carbon isotope analysis in order to interpret environmental conditions during pedogenesis, domains of micrite are relatively narrow, and divided by complex networks of sparry and microspar cements. Samples such as this should be avoided for isotopic analysis, or employ a computer-assisted drill system. Sampling. (F) Sphaerosiderites in claystone matrix from an Upper Oligocene paleosol in Chilga Woreda, northwestern Ethiopia. Siderite spherules such as these are appropriate for carbon and oxygen isotope analysis in order to interpret environemtnal conditions during pedogenesis. (For interpretation of the references to colour in this figure legend, the reader is referred to the web version of this article.)

paleosols from the mid-continent, U.S.A., Fox and Koch (2004) suggested that long-term trends in calcite $\delta^{18}O$ values appear to track changes in rainfall $\delta^{18}O$ values related global-scale paleoclimate factors, where the most positive $\delta^{18}O$ values occur in strata from the mid-Miocene climatic optimum, and a stepped trend toward more negative $\delta^{18}O$ values occurs in post mid-Miocene samples during the interval of Late Cenozoic cooling, and northern hemisphere glaciation. Levin and others (2004) observed a positive ~5.5‰ shift in $\delta^{18}O$ values of paleosol calcite occurring in ~4.5 Ma strata of southern Ethiopia which they attributed to climatic change possibly including closure of the Indonesian seaway, long-term uplift of the East African highlands, and aridification of eastern Africa. Koch et al. (2003) noted a small positive $\delta^{18}O$ shift of approximately 1‰ in the Bighorn Basin, Wyoming, U.S.A., that is synchronous with the Paleocene–Eocene

Thermal Maximum. This positive oxygen isotope shift was attributed to increased evapotranspiration, changing $\delta^{18}O$ value of meteoric water from the airmasses over that site, or changes in the seasonality of rainfall.

In a regional study of uppermost-Pennsylvanian and lowermost-Permian paleosols spanning ~10° of tropical paleolatitude in western Pangea, Tabor and Montañez (2002) noted a northward trend toward more negative $\delta^{18}O$ values, from ~ − 0.5‰ at the paleoequator to ~ − 8‰ at 10°N paleolatitude. A similar, but smaller, pattern of northward ^{18}O depletion was observed in co-occuring pedogenic phyllosilicates and Fe-oxides. The collective pattern of pedogenic mineral $\delta^{18}O$ values was interpreted to represent reverse equatorial flow, and occurrence of monsoonal atmospheric circulation patterns over western equatorial Pangea. The stratigraphic pattern of paleosol calcite $\delta^{18}O$ values in Texas, U.S.A. preserves a 5‰ shift toward more positive values through the Lower Permian, which was interpreted to represent decreasing rainfall, onset of aridity, and increased evaporative enrichment of ^{18}O in soil waters (Tabor et al., 2002). Subsequent paleotemperature estimates derived from independent proxies suggest that most of the temporal pattern of ^{18}O enrichment in calcite was related to evapotranspiration (Tabor and Montañez, 2005; Tabor, 2007).

Given the observed correspondence among rainfall $\delta^{18}O$ values, temperatures and elevations, many studies have used paleosol calcite $\delta^{18}O$ values as a proxy of paleoelevation (Garzione et al., 2000, 2004; Currie et al., 2005; Rowley and Currie, 2006; DeCelles et al., 2007; see recent review by Rowley and Garzione, 2007; Quade et al., 2007). In these studies, paleoelevation estimates are based typically upon measurements of rainfall $\delta^{18}O$ values and surface air temperatures along modern elevation transects. These modern data permit estimates of calcite $\delta^{18}O$ values that would result along the modern elevation transect, and the $\delta^{18}O$ value of paleosol calcite is compared directly with the modern calcite $\delta^{18}O$ "lapse-rate" curve to arrive at an estimate of paleoelevation. Isotope-based proxies of paleoelevation have been reviewed extensively in recent years (Rowley and Garzione, 2007; Quade et al., 2007), and the reader is referred to those studies for a more thorough treatment of paleoelevation reconstructions.

In general, paleoelevations derived from paleosol calcite $\delta^{18}O$ values are seemingly robust (i.e., reproducible and consistent within a given setting) and consistent with other structural and geodynamical data, but the choice of lapse-rate model greatly affects the absolute paleoelevation values that are reconstructed and the amount of uncertainty in the estimates. In particular, the authors note that studies that reconstruct paleoelevations using pedogenic carbonates typically contain little other information about the paleosols in question because they are generally focused instead on the tectonic implications of the calculated paleoelevation values. Collection and inclusion in papers of additional photographic documentation, taxonomic classification, and documentation of the suitability of the pedogenic nodules should be goals of future paleoelevation studies, even if the information is presented primarily as Data Repository items. Those types of information and application of additional paleoclimatic proxies for MAT and MAP could only strengthen the interpretations of paleoelevation and could also serve as an important additional test of how reasonable the reconstructed paleoelevation estimates are. For example, if a paleo-Ultisol (Argillisol; typically free of any pedogenic carbonate) is identified as having been formed at a paleo-elevation of 5500 m, then either the taxonomic description or the lapse rate model must be incorrect based on the present-day distribution of soil types (Soil Survey Staff, 2006).

7.3.1.2. Pedogenic calcite $\delta^{18}O$ values as a proxy of paleotemperature. Dworkin et al. (2005) was the first study that attempted to formalize paleosol calcite $\delta^{18}O$ values as a quantitative indicator of soil paleotemperature. Dworkin et al. (2005) presented two different equations to relate the $\delta^{18}O$ value of pedogenic calcite to temperature of crystallization from Cretaceous-age paleosol profiles in western Texas, U.S.A. The first equation (Eq. (50) below) is a third-order polynomial that relates the observed parametric correlation between air temperature from the entire International Atomic Energy Association (IAEA) data set (Rozanski et al., 1993) to pedogenic calcite via the oxygen isotope fractionation equation between water and calcite (O'Neil et al., 1969; see Table 5). The second equation (Eq. (51) below) is derived from the empirical relationship that was measured between pedogenic calcite $\delta^{18}O$ values ($\delta^{18}O_{cc}$) and measured mean annual surface air temperature from soils located in interior continental sites (Cerling and Quade, 1993):

$$0 = -0.50T^3 + (\delta^{18}O_{cc}(‰, \mathrm{SMOW}) + 152.04)T^2 - 2.78 \times 10^6 \quad (50)$$

and

$$(2)\delta^{18}O_{cc}(‰, \mathrm{PDB}) = 0.49T - 12.65. \quad (51)$$

This method of paleotemperature estimation has also been applied to calcite $\delta^{18}O$ values from Upper Triassic (Prochnow et al., 2006) and Cretaceous (Nordt et al., 2003) paleosols.

The analytical uncertainty of the temperature estimates reported by Dworkin et al. (2005) is ~±0.5 °C (1σ), which reflects only the analytical uncertainty of the $\delta^{18}O$ measurement for calcite (~0.1 to 0.2‰) and no other potential sources of error. Considering an analytical uncertainty equivalent to ±0.5 °C, Eqs. (50) and (51) indicate that paleotemperature estimates based on paleosol calcite $\delta^{18}O$ values are indistinguishable from one another between ~12° and 20 °C, corresponding to $\delta^{18}O_{cc\text{-}PDB}$ values ranging from − 2.9‰ to − 6.7‰. Pedogenic carbonate $\delta^{18}O$ values above or below these values will result in significantly different temperature estimates from Eqs. (50) and (51). However, the method of Dworkin et al. (2005) does not take into account two potentially important effects (1) variable rainfall $\delta^{18}O$ values among isothermal sites (see Fig. 15) and (2) change of soil water $\delta^{18}O$ values (and resultant calcite $\delta^{18}O$ values) from meteoric water via evaporation.

Fig. 15 shows the $\delta^{18}O$ value of meteoric precipitation versus the corresponding mean annual surface air temperature for 222 stations from the IAEA global precipitation database (Rozanski et al., 1993). Precipitation $\delta^{18}O$ varies among isothermal sites by ~10‰ to 5‰, which would be approximately the same range of $\delta^{18}O$ values of calcite that results from those waters among those sites. These results indicate that temperature estimates based on soil calcite $\delta^{18}O$ values should have an uncertainty no better than ±5 °C (Ferguson et al., 1999). Note that this uncertainty does not consider additional complications, such as modification of meteoric water $\delta^{18}O$ values in the soil by evaporation.

The effect of evaporation on soil moisture $\delta^{18}O$ values is related to relative humidity (h) as water molecules move from the liquid to vapor phase (Gonfiantini, 1986). No change in soil moisture $\delta^{18}O$ values will result at $h = 100\%$, and the greatest enrichment of ^{18}O (more positive $\delta^{18}O$ values) in soil water will occur at $h = 0\%$. During calcite crystallization in the soil, relative humidity during evaporation is somewhere between these two extremes (Sparks, 2003). The practical consequence of evaporation from the soil is that soil water is driven toward heavier $\delta^{18}O$ values than the $\delta^{18}O$ values of rains that originally percolated into the soil. The evaporation effect, and ^{18}O enrichment of soil moisture, is enhanced in the shallowest parts of the soil and during the driest time of year (e.g., Fig. 18); where and when soil carbonate is most likely to form (McFadden and Tinsley, 1985). However, ^{18}O enrichment of soil water is attenuated at depth, and closely approximates the mean $\delta^{18}O$ value of meteoric precipitation (Fig. 18). Considering these spatial relationships, only those calcite samples from the lowest parts of soil and paleosol profiles should be used to estimate meteoric water $\delta^{18}O$ values (Quade et al., 1995). Nevertheless, for instances where paleotemperature and paleoprecipitation $\delta^{18}O$ values have been determined by independent proxies, paleosol calcite $\delta^{18}O$ values indicate that soil moisture $\delta^{18}O$ values may have been altered by evaportion by as much as +5 to +7‰

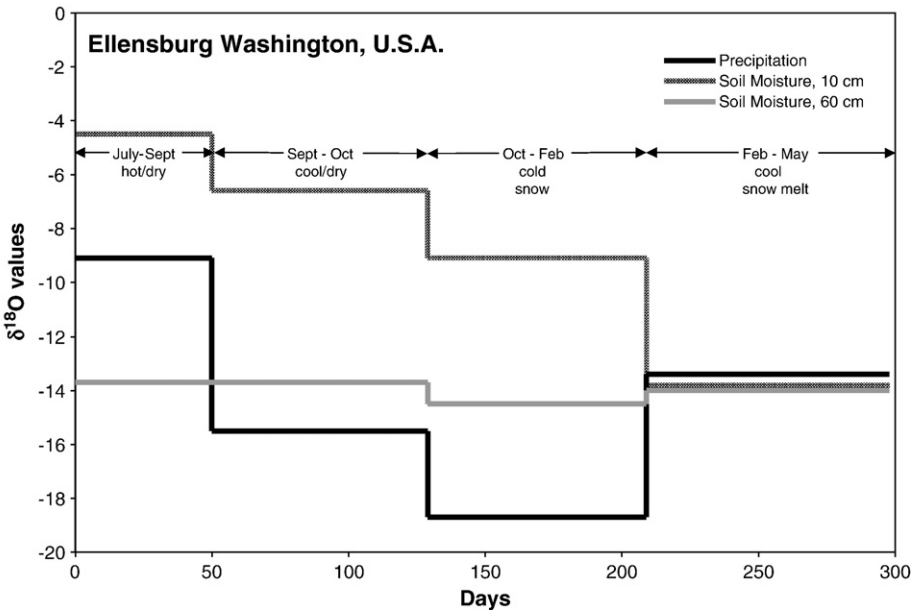

Fig. 18. $\delta^{18}O$ values of meteoric precipitation (black line), soil moisture at 10 cm, and soil moisture at 60 cm depth in a modern soil profile in Ellensburg, Washington U.S.A., versus progressive days of analysis (Robertson and Gazis, 2005). The shallowest sample level (10 cm) of the profile has soil water $\delta^{18}O$ values significantly more positive (~9‰) $\delta^{18}O$ values than that of mean annual precipitation values, whereas the deepest sample level (60 cm) of the profile has $\delta^{18}O$ values very near that that of the mean $\delta^{18}O$ value of precipitation. See text for discussion.

(Tabor and Montañez, 2005; Tabor 2007). Because of all of these factors, paleosol calcite $\delta^{18}O$ values should probably be avoided as a proxy of paleotemperature.

7.3.2. Pedogenic siderite as a proxy for soil moisture $\delta^{18}O$ values

Pedogenic sphaerosiderites exhibit $\delta^{18}O$ values ranging from ~0‰ to −18‰ (PDB; Baker et al., 1996; Ludvigson et al., 1998; White et al., 2001; Ufnar et al., 2002, 2004). However, siderite $\delta^{18}O$ values typically exhibit a narrow range of intra-profile values (<2‰), which is interpreted to reflect relatively stable (invariant) temperatures and mean $\delta^{18}O$ value of local groundwater that flood the soil profile (Ludvigson et al., 1988; White et al., 2001; Ufnar, 2002, 2004). Nevertheless, because the $\delta^{18}O$ value of siderite is related to two variables (T and $\delta^{18}O$ of H_2O), one variable must be assumed, or determined by an independent means, in order to determine the other (as is the case with pedogenic calcite). In their treatment of sphaerosiderite $\delta^{18}O$ values from paleosols that defined a mid-Cretaceous paleolatitudinal transect from ~35° to 55°N, White et al. (2001; Ludvigson et al., 1998; Ufnar et al., 2002, 2004) used the predicted mean annual surface air temperatures from General Circulation Models (GCM) for Middle Cretaceous time (Barron, 1989; Barron et al., 1989; Poulsen, 1999) in order to estimate groundwater and meteoric precipitation $\delta^{18}O$ values. Sphaerosiderite $\delta^{18}O$ values indicate significantly more negative $\delta^{18}O$ values (4.0–4.3‰) of mid-Cretaceous meteoric precipitation than modern isolatitudinal sites. Based upon the well-known relationship in the modern hydrological cycle, that coastal precipitation shows ~− 2‰ shift for every additional 100 mm of precipitation per month, White et al. (2001) hypothesized that these sphaerosiderite-producing soils formed in the presence of ~2400 to ~2600 mm of precipitation per yr along the coastlines of the North American Cretaceous interior seaway.

Other examples of sphaerosiderite in paleosol profiles have been described from high-latitude Permo-Carboniferous (Brown and Kingston, 1993; Faure et al., 1995) and Triassic strata (Retallack, 1976) as well as tropical Paleogene strata (Jacobs et al., 2005; Fig. 17). They typically occur in clastic strata that are associated with coal measures. In this regard, sphaerosiderite may be an abundant paleopedogenic mineral in both time and space, which is limited to poorly drained environments, and that has gone largely unnoticed as a useful proxy of paleoclimate. If so, $\delta^{18}O$ values of paleopedogenic sphaerosiderites have the potential to become an important paloeclimate proxy which represents pedogenic environments that are generally exclusive of pedogenic calcite.

7.4. $\delta^{13}C$ values of soil carbonate

7.4.1. Calcite from one-component of soil CO_2

The closed-system, one-component soil CO_2 model of calcite crystallization is not normally considered in soil systems, but is frequently associated with early diagenetic marine and lacustrine calcites that are characterized by very negative $\delta^{13}C$ values (e.g., Irwin et al., 1977; Gluyas, 1984; Scotchman, 1991). Calcites that precipitate via one component, chemically closed or semi-closed, conditions will have $\delta^{13}C$ values no more than 14.8‰ heavier than *in situ* soil organic matter. This reflects that open-system oxidation of soil organic matter, in the absence of contribution of isotopically heavier CO_2 from the global troposphere, results in (at least) 4.4‰ diffusive enrichment, and an additional ~10.4‰ carbon isotope enrichment from gaseous CO_2 to calcite due to carbon isotope fractionation between carbonate species (at mildly alkaline pH; Bottinga, 1968).

Evidence for calcite formation in the presence of one soil CO_2 component is sparse. However, a study of waterlogged soils in the Atchafalaya Swamp, Louisiana, U.S.A. demonstrated that calcite $\delta^{13}C$ values can be less than − 20‰, and therefore did not crystallize under open-system exchange with tropospheric CO_2 (Whelan and Roberts, 1973). In this regard, calcite precipitation in the presence of one soil CO_2 component may be a reasonably common occurrence in swampy, waterlogged soil and paleosol profiles. Given the sedimentary bias toward preservation of low-lying and poorly-drained landscapes, there may be also a bias toward preservation of paleosol calcite that forms via one component of soil CO_2.

As mentioned above, calcite crystallization in the presence of one CO_2 component is related to dysoxic or anoxic conditions in poorly drained soil profiles. Therefore, at field scale, one-component soil calcites may be associated with profiles that exhibit drab or redoximorphic soil matrix colors and weak or no development of soil structure (Vepraskas, 1992). However, soil and paleosol colors are strongly susceptible to change after burial (e.g., Retallack, 1991), therefore very negative calcite $\delta^{13}C$ values may be the most diagnostic characteristic of a one-component soil CO_2 system. Examples of paleosol calcite that have been interpreted to form in the presence of one component of soil CO_2

are also rare. However, paleosol calcite $\delta^{13}C$ values from Upper Permian and Lower Triassic strata of the Karoo Supergroup are characterized by drab colors, poor soil structural development, and calcite $\delta^{13}C$ values as low as − 24‰ (Yemane et al., 1989; Macleod et al., 2000; Retallack et al., 2003; Smith and Botha, 2005; Tabor et al., 2007; Melezhik et al., 2007; Coney et al., 2007). Although the meaning of the very negative $\delta^{13}C$ calcite values in the Karoo basin has been interpreted to represent different processes (e.g., Oceanic links, marine-derived methane; Macleod et al., 2000), they may possibly represent crystallization in the presence of one soil CO_2 component (Tabor et al., 2007).

7.4.2. $\delta^{13}C$ of pedogenic siderite

Pedogenic sphaerosiderite is characterized by a large range of $\delta^{13}C$ values, from ~+8‰ to − 45‰, and intraprofile sphaerosiderite $\delta^{13}C$ values preserve a range of $\delta^{13}C$ values that vary by as much as 30‰. As mentioned above, formation of sphaerosiderite in soils is associated with saturated, anoxic soil profiles that are conducive to methanogenic bacteria (Faure et al., 1995; Ludvigson et al., 1998; White et al., 2001). Kinetic carbon isotope fractioantion between CO_2 and CH_4 that is generated by methanogenesis ($10^3 \ln {}^{13}\alpha CO_2\text{–}CH_4$) ranges from ~40‰ to 60‰, and may produce CO_2 with $\delta^{13}C$ values as positive as 7‰ (Whiticar et al., 1986; Faure et al., 1995). Therefore, sphaerosiderites with the most positive $\delta^{13}C$ values (> − 5‰; Irwin et al., 1977) may represent CO_2 that was generated directly from methanogenesis, whereas more negative $\delta^{13}C$ values may result from (1) closed-system, one-component CO_2 mixing as described above (see Section 7.2.1) and/or (2) possible additional contributions of CO_2 derived from oxidation of methanogenic CH_4 (Irwin et al., 1977; Faure et al., 1995; Ludvigson et al., 1998). Because of its complex behaviour, no significant contributions to paleoclimate reconstruction have been made from sphaerosiderite $\delta^{13}C$ values.

7.4.3. Calcite derived from 2-component soil CO_2 mixing

Two-component models assume that the only sources contributing to soil CO_2 are CO_2 from the troposphere and CO_2 derived from *in situ* oxidation of biological carbon in the soil. Under steady-state conditions of Fickian diffusion, calcite $\delta^{13}C$ values are expected to exhibit progressively more positive values upward through the soil or paleosol profile (see discussion of 2-component soil CO_2 mixing in Section 7.2.2). The vast majority of studies of soil and paleosol calcite carbon isotopes have sought to interpret $\delta^{13}C$ values within the context of a 2-component soil CO_2 mixing model. This reflects, in large part, that 2-component soil calcite $\delta^{13}C$ values may permit estimation of paleoatmospheric pCO_2.

Two-component soil CO_2 mixing requires free drainage for oxidation of organic matter and open-system exchange with the global troposphere. As a result, paleosol calcite samples associated with profiles that lack gley colors, redoximorphic accumulations such as hematite or manganese nodules, and that exhibit well-developed soil structure are generally regarded as appropriate paleosols for estimation of paleoatmospheric pCO_2 from calcite $\delta^{13}C$ values (Ekart et al., 1999). Furthermore, paleosol matrix should be non-calcareous in order to avoid possible inheritance of detrital carbonate $\delta^{13}C$ values, and carbonate texture and mineralogy other than microcrystalline calcite (micrite) should be avoided, as they are possibly diagenetic alteration products not reflective of conditions during soil formation. Any inferences about paleoatmospheric pCO_2 values from inappropriate samples should be disregarded.

7.4.3.1. Estimates of paleoatmospheric pCO_2. The $\delta^{13}C$ values of pedogenic calcite and coexisting organic matter may be used to estimate atmospheric pCO_2 via the following two-component CO_2 mixing equation (Yapp and Poths, 1996):

$$\delta^{13}C_{m(cc)} = \left(\delta^{13}C_{A(cc)} - \delta^{13}C_{O(cc)}\right)(C_A/C_S)_{cc} + \delta^{13}C_{O(cc)} \quad (52)$$

Other equations for the solution of paleoatmospheric pCO_2 from pedogenic mineral $\delta^{13}C$ values have been presented (Cerling, 1991, 1999; Mora et al., 1996; Ekart et al., 1999; Montañez et al., 2007), but they all consider the same variables, and result in similar pCO_2 estimates. $\delta^{13}\,C_{m_{(cc)}}$ is the measured $\delta^{13}C$ value of pedogenic calcite. The $\delta^{13}C$ values subscripted with "*A*" and "*O*" are the $\delta^{13}C$ values of calcite formed solely in equilibrium with CO_2 derived from the atmosphere and from oxidation of soil organic matter, respectively. The subscript "(cc)" indicates calcite. C_A refers to the concentration of CO_2 gas in the soil if the only contribution to soil CO_2 were from the atmosphere. C_S is the actual concentration of CO_2 that was present in the soil. The value for $(\delta^{13}\,C_{A_{(cc)}} - \delta^{13}\,C_{O_{(cc)}})$ is assumed to be +16‰ (Yapp and Poths, 1991, 1992, 1993, 1996), because it represents the approximate difference between the estimated $\delta^{13}C$ values of pre-industrial atmospheric CO_2 (− 6.5‰) and recent C_3 continental biota (−27‰), after the latter value is adjusted for the diffusive 4.4‰ enrichment in $\delta^{13}C$ in the biologically-derived CO_2 of the soil (Cerling et al., 1991). Note that other $(\delta^{13}\,C_{A_{(cc)}} - \delta^{13}\,C_{O_{(cc)}})$ values have been suggested (e.g., ~13.7‰, Arens et al., 2000), but differences in this quantity result in relatively minor differences in estimated pCO_2 values (Yapp and Poths, 1991; Tabor et al., 2004a,b).

$\delta^{13}C_{O(cc)}$ values may be estimated from measured $\delta^{13}C$ values of co-existing organic matter within the paleosol profiles (Tabor et al., 2004a,b; Montañez et al., 2007). $\delta^{13}C_{O(cc)}$ values should be at least 14.8‰ heavier than the $\delta^{13}C$ value of oxidizing organic matter in open-system soils characterized by mixing of two components of CO_2 (Tabor et al., 2007). This reflects the diffusive 4.4‰ enrichment in $\delta^{13}C$ in the biologically-derived CO_2 (Cerling et al., 1991), as well as an additional 10.4‰ carbon isotope enrichment from gaseous CO_2 to calcite due to carbon isotope fractionation between carbonate species (at mildly alkaline pH; Bottinga, 1968). However, Bowen and Beerling (2004) suggest that $\delta^{13}C$ values of organic matter remaining in paleosol profiles may result in an overestimate of respired soil CO_2 $\delta^{13}C$ (and $\delta^{13}C_{O(cc)}$), and a significant underestimate of atmospheric pCO_2. If Bowen and Beerling (2004) are correct, then use of fossil organic matter $\delta^{13}C$ values for $\delta^{13}C_{O(cc)}$ provides minimum estimates of atmospheric pCO_2 rather than absolute estimates.

Because the activity of CO_3^{2-} in calcite is fixed at unity, pedogenic calcite does not, by itself, contain a proxy record of the partial pressure of soil CO_2 (however, pedogenic goethite does, see Section 7.4.3.3). Therefore, at this time, the concentration of soil CO_2 (C_S) must be assumed in order to estimate paleoatmospheric pCO_2 values from paleosol calcite. These assumptions are constrained by available *in situ* measurements of soil CO_2 in modern calcite-producing soils.

The concentration of soil CO_2 is a function of soil depth, soil respiration rate (or biological productivity), and diffusivity of the soil medium (Boynton and Reuther, 1938; Boynton and Compton, 1944; Wood and Petraitis, 1984; Quade et al., 1989; Soloman and Cerling, 1987). Soil CO_2 concentrations vary from near atmospheric pCO_2 concentrations (a modern value of ~350 ppmV; Keeling et al., 1995) at the interface with the overlying troposphere to higher, nearly constant, values beneath a characteristic production (z) depth in the soil. The location of the characteristic production depth in the soil is determined by soil respiration rate (or soil productivity) and the diffusivity of the soil medium. Soil diffusivities typically range from 2% to 50% of that for free air (Glinski and Stepniewski, 1985). In general, more moist and clay-rich soils have lower diffusivities, whereas drier and sandier soils have higher diffusivities (Rolston, 1986).

Soil respiration rates, which represent production of CO_2 from oxidation of organic matter in the soil, appear to (1) primarily reflect a logarithmic correlation with ambient atmospheric and soil temperatures up to at least 32 °C (Anderson, 1973; Knapp et al., 1998; Fang et al., 1998; Fang and Moncrief, 2001), and (2) secondarily respond to soil moisture availability, although this appears to only be applicable when soil biota are at or near drought conditions (Brook et al., 1983). Therefore, characteristic production depths for highly productive soils

with low diffusivity occur only a few centimeters below the soil surface, whereas low productivity soils with high diffusivity have much deeper characteristic production depths, possibly as deep as 30–50 cm below the soil surface (Wood and Petraitis, 1984; Quade et al., 1989; Cerling and Quade, 1993; Yapp and Poths, 1992 Schroeder and Melear, 1999). Furthermore, soil media with lower diffusivity will be characterized by higher $S(z)$ values than low diffusivity counterparts. Moreover, due to variations in productivity of soil biota, soils from warm climates will have higher $S(z)$ values than cool climate counterparts, and soils with abundant soil moisture will have higher $S(z)$ values than their drought-phase counterparts. For example, Breecker et al. (2009) have recently monitored $S(z)$ values for modern semi-arid soils in New Mexico and found that there was significant seasonal variation between about 500 and 2000 ppmv, which was in turn reflected by seasonal variations in $\delta^{13}C$ and $\delta^{18}O$. Pedogenic carbonate formation occurred simultaneously with $S(z)$, $\delta^{13}C$, and $\delta^{18}O$ minima, which suggests that the carbonate is not recording mean growing season conditions and that there is therefore a seasonal bias in the formation of pedogenic carbonates.

Although modern 2-component soil CO_2 concentrations range from little more than ambient tropospheric concentrations (~500 ppmV; Wood and Petraitis, 1984) to as much as 21% of the soil atmosphere (210,000 ppmV; Yamaguchi et al., 1967; Brook et al., 1983), soils that are characterized by mixing of two soil CO_2 components, and which contain *in situ* accumulations of calcite, appear to be limited to a range of soil CO_2 concentrations from about 1000–8000 ppmV (de Jong and Schappert, 1972; Brook et al., 1983; Wood and Petraitis, 1984; Soloman and Cerling, 1987; Quade et al., 1989). This range of soil CO_2 concentrations reflects the relatively low productivity of soils characterized by calcite crystallization (Schlesinger, 1997). Note however, that this very low range of soil pCO_2 also reflects that modern tropospheric pCO_2 is low, and contributes very little (~300 ppmV) to total soil pCO_2. For times when tropospheric pCO_2 was significantly higher than modern (e.g., 2000–3000 ppmV; Eocene, Paleocene, Cretaceous; Yapp and Poths, 1996; Yapp, 2004; Tabor and Yapp, 2005a), soil CO_2 in calcareous soils likely had a correspondingly higher concentration (3000–11,000 ppmV).

Ekart et al. (1999) assumed soil CO_2 concentrations of 5000 ppmV for 758 paleosol calcite samples representing ~400 million years time. Nordt et al. (2002) assumed a range of soil CO_2 concentrations from 4000 to 6000 ppmV for paleosols from Upper Cretaceous and Lower Paleogene strata in Alberta, Canada. Prochnow et al. (2006) assumed soil CO_2 concentration to be 4000 ppmv for "arid to semiarid" paleosol calcite and 5000 ppmv for "subhumid" paleosol calcite samples from Triassic profiles in Utah, U.S.A. However, if the lower overall $S(z)$ values and seasonal bias recorded in modern semi-arid soils in terms of $S(z)$ was comparable in the geologic past, then it is likely that many of the paleoatmospheric pCO_2 estimates in the literature are overestimates (Breecker et al. (2009), so care is needed in considering records from arid to semi-arid settings.

In their treatment of Permo-Carboniferous paleosols from the southwestern United States, Montañez et al. (2007) assumed that calcite samples taken from morphologies indicative of long-term net soil moisture deficiency, such as Calcisols (Mack et al., 1993), were characterized by generally low and invariant $S(z)$ values, whereas calcites from paleosol morphologies consistent with less soil moisture deficiency, such as calcic Argillisols, were characterized by relatively high and invariant $S(z)$ values, and calcite samples collected from paleosol morphologies that are indicative of significant variability in soil moisture availability, such as calcic Vertisols, were characterized by a larger range of $S(z)$ values. Finally, the lithology of the paleosol profiles (sandstone, siltstone, mudstone and claystone) was assumed to have affected the soil pCO_2. Montañez et al. (2007) used the following ranges of $S(z)$ values for paleoatmospheric pCO_2 estimates: (1) sandstone-dominated Calcisols are lowest, ranging from 1000–3000 ppmV, (2) siltstone-dominated Calcisols range from 1500 to 4000 ppmV, (3) mudstone-dominated Calcisols range from 2000 to 5000 ppmV, (4) mudstone-dominated Vertisols range from 3200 to 7500 ppmV, (5) claystone-dominated calcic Vertisols range from 4000 to 8000 ppmV, and (6) mudstone-dominated calcic Argillisols are highest, ranging from 6000 to 9000 ppmV.

The importance of the assumed soil pCO_2 values (C_S values) cannot be overstated, as the resulting atmospheric pCO_2 estimates vary proportionately with them (Cerling, 1991; Ekart et al., 1999; Royer et al., 2001a,b; Tabor et al., 2004a,b). Therefore, until an independent means of estimating soil CO_2 concentration (see Section 8.1 for a possible method for this) at the time of calcite crystallization in a paleosol profile becomes available, this parameter will remain an effectively unknown value, and will continue to limit the utility of paleosol calcite $\delta^{13}C$ values as proxy of atmospheric pCO_2.

Cerling (1991, 1992) were the first studies to demonstrate the potential of paleosol calcite $\delta^{13}C$ values as a proxy of atmospheric pCO_2, in which it was suggested that Cretaceous atmospheric pCO_2 was significantly higher than modern values. This was followed by several important studies of Paleozoic paleosol calcites, which appeared to delineate a first-order trend of decreasing atmospheric pCO_2 from ~15–20 PAL in the Early Paleozoic to near PAL in the Late Carboniferous (Mora and Driese, 1993; Mora et al., 1996). These Paleozoic studies were especially important at the time of publication, because they were among the first geochemically-based pCO_2 proxy data for comparison with carbon mass flux model pCO_2 estimates (Berner, 1991; Berner and Kothavala, 2001), and the two different model estimates appeared to agree with one another.

Ekart et al. (1999) compiled the first temporally extensive dataset of two-component paleosol calcite $\delta^{13}C$ values. Ekart et al. (1999) presented results for 758 $\delta^{13}C$ analyses that represented each time period since the advent of vascular plants (~400 million years BP; Fig. 19). The results of that study largely agreed with estimated paleoatmospheric pCO_2 from carbon mass flux models, but Ekart et al. (1999) also noted a significant disparity between pCO_2 estimates from the two proxy methods for the Permian. There have been dozens of additional studies of paleosol calcite $\delta^{13}C$ values since the compilation provided by Ekart et al. (1999). Fig. 19 presents 2615 pedogenic calcite $\delta^{13}C$ values (black crosses), ranging in age from Devonian to Recent (~415–0 My), which were compiled from the literature. This compilation includes results only from those studies that presented paleosol micrite $\delta^{13}C$ values in a Table or Appendix (see caption in Fig. 19 for sources). Also shown in Fig. 19 are the best fit and 95% confidence interval for terrestrial vascular plant organic matter $\delta^{13}C$ values that is based upon analysis of 2148 different samples, which range from Devonian to Late Cretaceous (Strauss and Peters-Kottig, 2003). Because of complications related to the evolution and prominence of C_4 photosynthesizers in landscapes characterized by soils that accumulate calcite, the following discussion is limited to pre-Cenozoic data. Furthermore, the authors emphasize that the following discussion is intended only as a demonstration of how models of 2-component soil CO_2 mixing can be applied to paleosol calcite data, and it is not intended for any specific inferences to be drawn about variations in paleoatmospheric pCO_2.

Assuming that organic matter $\delta^{13}C$ values in Fig. 19 accurately represent the $\delta^{13}C$ values of organic matter in the soils from which calcite $\delta^{13}C$ values are derived, they can be used to define an effective lower limit for calcite $\delta^{13}C$ values that are permissive of two-component soil CO_2 mixing. This lower limit calcite $\delta^{13}C$ value (thick red line marked by 0 PAL) is 14.8‰ more positive than contemporaneous paleosol organic matter, which reflects 4.4‰ diffusive enrichment of CO_2 $\delta^{13}C$ values derived from oxidation of organic matter, as well as an additional 10.4‰ carbon isotope enrichment from gaseous CO_2 to calcite due to carbon isotope fractionation between carbonate species (at mildly alkaline pH; Bottinga, 1968). Calcite $\delta^{13}C$ values that are more negative than this lower limit provide negative estimates of

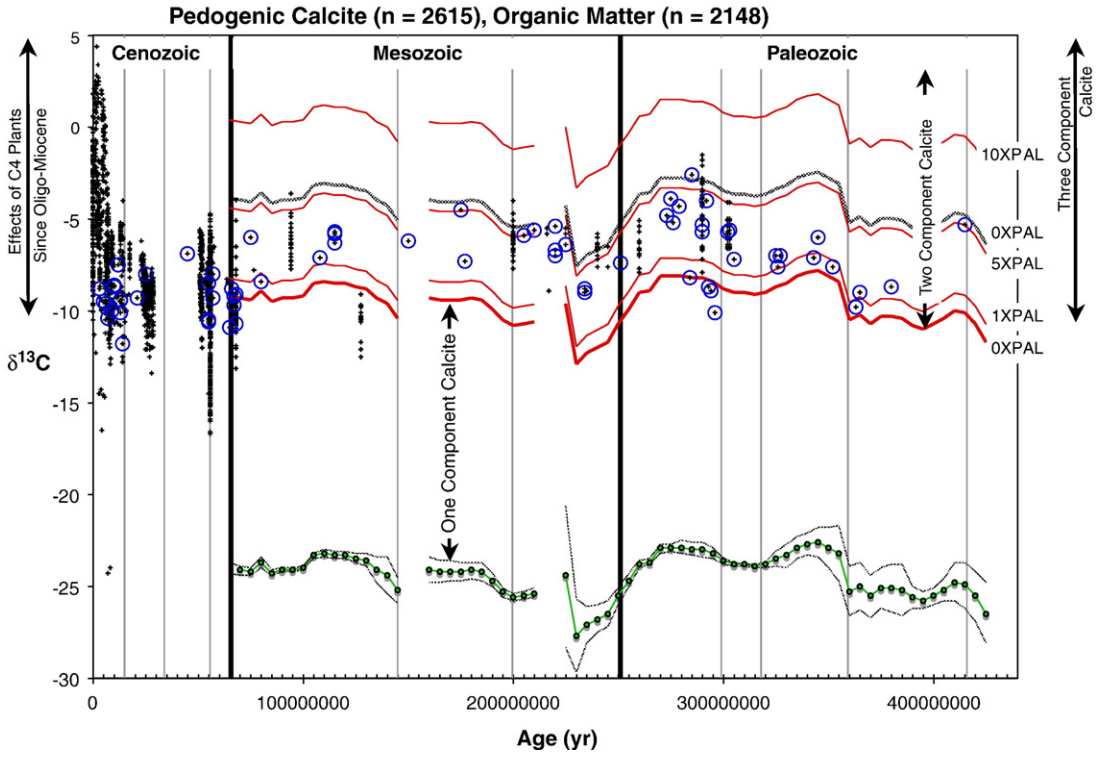

Fig. 19. Cross plot of $\delta^{13}C$ values of paleosol calcite samples (crosses and blue open circles) and vascular plant total organic matter versus age (in years). This dataset consists of 2615 calcite and 2148 organic matter data points compiled from peer-reviewed, published literature. Although many more pedogenic calcite and organic matter data points have been reported in the literature, only samples that (1) have radiometric, paleomagnetic or biostratigraphic age constraints and (2) are tabulated are included herein. Calcite d13C values are divided into open blue circles that represent the review data of Ekart and others (1999) and black crosses, which represent calcite d13C values from various studies (Srivastava, 2001; Magaritz et al., 1981; Deutz et al., 2001; Schlesinger, 1985; Quade et al., 2004; Quade and Cerling, 1995; Fox and Koch, 2003; Dever et al., 1988; Sinha et al., 2006; Cerling, 1992; Clyde et al., 2001; Behrensmeyer et al., 2007; Koch et al., 1995; Nordt et al., 2002; Alonso-Zarza and Tanner, 2006; Robinson et al., 2002; Quade et al., 1994; Ekart et al., 1999; Cerling et al., 1991; Sinha and Stott, 1994; Andrews et al., 1995; Ghosh et al., 1995; Ghosh et al., 2001; Suchecki et al., 1988; Purvis and Wright, 1991; Kenny and Neet, 1993; Mora et al., 1996; Muchez et al., 1993; Prochnow et al., 2006; Tabor et al., 2004a,b; Mack et al., 1991; Tandon et al., 1995; Retallack et al., 2004a,b; Bowen et al., 2001; Bowen et al., 2005). Numerical age data were taken directly from ages that were reported in the literature. Vertical drop lines on graph depict time boundaries for geological Epochs, Periods and Eras according to the timescale of Gradstein et al. (2004). Some numerical age dates for the calcite $\delta^{13}C$ data that are based upon biostratigraphic- and magnetostraphic- correlation to out-of-date time scales may differ slightly from numerical correlations to the timescale of Gradstein et al. (2004).

paleoatmospheric pCO_2. Negative values of pCO_2 have no physical meaning, and could be interpreted to represent calcite that formed under closed (or semi-closed) system, 1-component soil CO_2 mixing, or formation in the presence of oxidizing organic matter that is isotopically more negative than those shown in Fig. 19. Calcite $\delta^{13}C$ values that are more positive than this lower limit may be interpreted as having formed in the presence of open-system, 2-component mixing of CO_2 derived from *in situ* oxidation of organic matter and CO_2 from the global troposphere. The resulting atmospheric pCO_2 estimates are determined by the assumed concentration of soil CO_2. The thin red lines depict calcite $\delta^{13}C$ values for 2-component soils with a total soil CO_2 concentration of 5000 ppmV and atmospheric pCO_2 values of 1, 5, and 10 PAL. Within the context of the assumed variables in this model of 2-component soil CO_2 mixing, paleosol calcite $\delta^{13}C$ values suggest that atmospheric pCO_2 has ranged from modern to no greater than ~7 PAL. However, in order to highlight the importance of the assumed soil pCO_2 that is input to the model, the black stippled line depicts calcite $\delta^{13}C$ values that form in soil profiles with a total soil CO_2 of 900 ppmV, and atmospheric pCO_2 of 300 ppmV. These assumed parameters would suggest that Paleozoic and Mesozoic atmospheric pCO_2 has not been much greater than ~1 PAL. Furthermore, due to uncertainties in the values of assumed parameters, estimates of atmospheric pCO_2 from soil calcite are certainly no better than $\pm$ 300 ppmV, and probably closer to $\pm$500 ppmV to $\pm$1000 ppmV in most instances (Yapp and Poths, 1996; Ekart et al., 1999; Tabor et al., 2004a,b; Montañez et al., 2007).

The authors reiterate that Fig. 19 is provided only as an example of how atmospheric pCO_2 is related to calcite $\delta^{13}C$ values in soils characterized by mixing of 2 components of soil CO_2. In practice, atmospheric pCO_2 estimates from paleosol calcite $\delta^{13}C$ values should include organic matter $\delta^{13}C$ values from the same paleosol or a deposit in close stratigraphic proximity (e.g., Tabor et al., 2004a,b; Montañez et al., 2007), and not use summary data sets or inferred values of soil organic matter $\delta^{13}C$ values such as here.

7.4.3.2. Soil calcite $\delta^{13}C$ as a means of assessing soil pCO_2 and productivity. Although its potential has been largely ignored to date (however, see Yapp and Poths, 1996), soil and paleosol calcite $\delta^{13}C$ values may be tremendously useful as a proxy of soil pCO_2, biological productivity, and evapotranspiration in calcareous paleosols which formed prior to evolution and dominance of C_4 photosynthesizers (see Section 7.6; pre-Miocene). Recombination of Eq. (52) relates measured calcite and organic matter $\delta^{13}C$ values to soil pCO_2:

$$C_{S(cc)} = C_{A(cc)} * \frac{\delta^{13}\,C_{A(cc)} - \delta^{13}\,C_{O(cc)}}{\delta^{13}\,C_{m(cc)} - \delta^{13}\,C_{O(cc)}} \tag{53}$$

All definitions for Eq. (53) are as in Eq. (52). Considering that, in certain situations, atmospheric pCO_2 is known by independent means such as the $\delta^{13}C$ and concentration of $Fe(CO_3)OH$ in goethite (see below; Table 6), and that organic matter $\delta^{13}C$ values are available,

Table 6
Age, $\delta^{13}C$ and concentration (X_m) of $Fe(CO_3)OH$ in solid solution in goethite, and estimated atmospheric pCO_2 (PAL; PAL = 300 ppmV).

Epoch	~Age (Ma)	$\delta^{13}C$ (‰)	X_m	Atm. pCO_2	Source
Late Ordovician	440	−17.6	0.00645	16	Yapp and Poths (1993)
Late Devonian	360	−21.5	0.0175	1	Yapp and Poths (1996)
Early Permian	283	−13.5	0.0090	1	Tabor et al. (2004a,b)
Early Permian	270	−13.9	0.0083	1	Tabor et al. (2004a,b)
Early Jurassic	195	−15.3	0.0097	18	Yapp and Poths (1996)
Early Middle Jurassic	185	−15.0	0.0088	18	Yapp and Poths (1996)
Late Middle Jurassic	165	−17.2	0.0120	1	Yapp and Poths (1996)
Late Middle Jurassic	165	−17.3	0.0099	1	Yapp and Poths (1996)
Late Cretaceous	80	−19.7	0.0103	4	Yapp and Poths (1996)
Paleocene	60	−20.1	0.0067	8 ± 4	Tabor and Yapp (2005a)
Early Eocene	52	−20.1 to −15.4	0.0014–0.0064	7	Tabor and Yapp (2005a)
Late Tertiary	5	−21.7	0.0108	1	Yapp and Poths (1996)

then paleosol calcite $\delta^{13}C$ values may prove an important source of information about the concentration of total soil pCO_2, which is known to be strongly correlated with evapotranspiration and soil productivity (e.g., Brook et al., 1983). As mentioned earlier, modern soil-forming environments that are characterized by precipitation of calcite are generally low-productivity soils, with total soil pCO_2 usually no greater than ~10,000 ppmV. Note however, that this very low range of soil pCO_2 also reflects that modern tropospheric pCO_2 is low, and contributes very little (~300 ppmV) to total soil pCO_2. For times when tropospheric pCO_2 was significantly higher than modern (e.g., ~2000–3000 ppmV; Eocene, Paleocene, Cretaceous; Yapp and Poths, 1996; Yapp, 2004; Tabor and Yapp, 2005a), soil pCO_2 in calcareous soils likely had a correspondingly higher concentration. In this regard, subtraction of atmospheric pCO_2 values yields the concentration of CO_2 in the soil that is derived only from oxidation of biological materials (C_B; Yapp and Poths, 1996). Brook et al. (1983) reported a least squares variance ($R^2 = 0.81$) between soil productivity (as specified by soil pCO_2) and actual evapotranspiration, where actual evapotranspiration is the quantity of soil water that is released from the soil as water vapor through evaporation and transpiration. In this regard, paleosol calcite $\delta^{13}C$ values may prove useful as a quantitative proxy to assess aridity among populations of calcite-bearing paleosols; this includes soils that are ambiguously assigned to subhumid, semi-arid, and arid climates.

7.4.3.3. Pedogenic goethite. The common low-temperature mineral goethite (α-FeOOH) occurs in solid solution with small amounts of a ferric carbonate component ($Fe(CO_3)OH$). The molar concentration and $\delta^{13}C$ composition of the $Fe(CO_3)OH$ component in goethite are measured with an incremental vacuum dehydration–decarbonation technique that requires vacuum extraction lines with extremely low background CO_2 values (see description of high-vacuum extraction system by Yapp and Pedley, 1985). The molar fraction of $Fe(CO_3)OH$ is very low, and therefore highly susceptible to contamination from carbon sources that might be added to the goethite. Therefore, goethites undergo a strict series of chemical pre-treatments prior to incremental dehydration–decarbonation analysis. Goethites are ground in reagent-grade acetone. The <63 μm fraction is then treated with 0.5–1.0 N HCl solution in order to remove calcite and thoroughly rinsed before several treatments with 30% H_2O_2 are made in order to remove naturally occurring organics that may be sorbed to the surface of the goethite. Goethite samples that have undergone the preceding set of treatments are then analyzed in a set of incremental vacuum dehydration–decarbonation experiments, ranging from ~190 to 240 °C, and CO_2 and H_2O dehydroxylation-decarbonation products of goethite and $Fe(CO_3)OH$ are measured manometrically for their molar ratios and $\delta^{13}C$ compositions. During the dehydration process, "plateau" values of incremental H_2O:CO_2 ratios (called "*F*" ratios, which are twice that of "*X*" ratios) and $\delta^{13}C$ values emerge (Yapp and Poths, 1991, 1992, 1993; Hsieh and Yapp, 1999; Yapp, 2001a,b, 2004; Tabor et al., 2004b; Tabor and Yapp, 2005a). These plateau $\delta^{13}C$ and *F* values correspond to the $\delta^{13}C_G$ and twice the X_G values (described below), respectively.

The molar concentration (X_G) and carbon isotope value ($\delta^{13}C_G$) of the ferric carbonate component is a function of the concentration and $\delta^{13}C$, respectively, of the CO_2 present during crystallization of goethite (Yapp, 1987a,b, 2001a,b, 2004; Yapp and Poths, 1991, 1992, 1993, 1996; Tabor et al., 2004a,b). Two-component CO_2 mixing in the presence of soil goethite crystallization involves CO_2 from the atmosphere and CO_2 from oxidation of organic matter in the soil. Thus, the $Fe(CO_3)OH$ component in goethites that form in such environments may preserve information on the partial pressure of CO_2 in the Earth's atmosphere as well as the ambient pCO_2 of soil gas. Yapp and Poths (1992) presented the following Henry's law equation that relates the molar concentration of $Fe(CO_3)OH$ in solid solution in goethite to the concentration of ambient CO_2 in the soil:

$$\mathrm{Log}\, pCO_2 = \mathrm{Log}X_G + 6.04 - \frac{1570}{T} \tag{54}$$

where X_G is the mole fraction of $Fe(CO_3)OH$ in solid solution in goethite and *T* is temperature in K. If X_G and *T* are known, then atmospheric pCO_2 may be determined from Eq. (54). X_G may be determined from direct measurement of the $Fe(CO_3)OH$ in goethite, whereas temperature of goethite crystallization may be estimated from other proxies (see below). To date, reported X_G values of 2-component goethites range from 0.0014 to 0.0175 (Table 6), which corresponds to soil pCO_2 values ranging from ~20,000 to ~105,000 ppmV. Such high pCO_2 values indicate humid, biologically productive soils consistent with intense chemical weathering and development of recalcitrant pedogenic minerals such Fe-Oxides (Tardy et al., 1990a,b).

The equation that relates X_G and $\delta^{13}C_G$ values of $Fe(CO_3)OH$ in solid solution in goethites that form in the presence of two soil CO_2 components to atmospheric pCO_2 is similar to that of pedogenic calcite (Yapp and Poths, 1992, 1993, 1996):

$$\delta^{13}C_G = \left[\left(\delta^{13}C_{GA} - \delta^{13}C_{GO}\right)X_{GA}\right]\left[\frac{1}{X_G}\right] + \delta^{13}C_{GO} \tag{55}$$

The subscript "*G*" indicates goethite. $\delta^{13}C_G$ is the measured $\delta^{13}C$ value of $Fe(CO_3)OH$ in goethite, the $\delta^{13}C$ values subscripted with "*A*" and "*O*" are defined in the manner for Eq. (52). X_G is the measured mol fraction of the $Fe(CO_3)OH$ component, in the goethite, whereas the values X_{GA} would be the molar fraction of $Fe(CO_3)OH$ if atmospheric CO_2 were the only CO_2 in the soil profile.

Eq. (55) indicates that, in a plot of $\delta^{13}C_G$ vs. $1/X_G$, the $Fe(CO_3)OH$ component in goethite samples from the shallower portions of any particular soil yield a linear array with a positive slope from which an apparent pCO_2 for Earth's ancient atmosphere can be calculated (Yapp and Poths, 1992, 1993, 1996, Yapp, 2004; see Fig. 20).

To date, $Fe(CO_3)OH$ in solid solution in paleosol goethites has provided estimates of paleoatmospheric pCO_2 from 12 different paleosol profiles ranging in age from Ordovician to Miocene (Table 6). This contrasts with several hundred estimates of paleoatmospheric pCO_2 from paleosol calcite (see, for example, Fig. 19). The relative paucity of paleoatmospheric pCO_2 estimates from $Fe(CO_3)OH$ in solid solution in paleosol goethites reflects that only a few research groups have focused on this proxy method, difficulty of analysis compared to paleosol calcite, and that paleosols with 2-component Fe

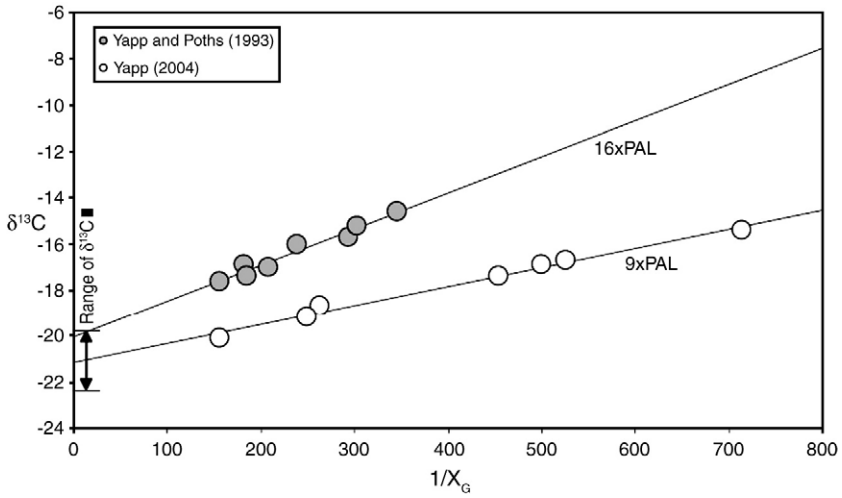

Fig. 20. $\delta^{13}C$ vs. $1/X_G$ of $Fe(CO_3)H$ component in solid solution in goethites from two different soils (Yapp and Poths, 1993; Yapp, 2004). The slope of the data array from the pedogenic goethites is related to atmospheric pCO_2 during the time of soil formation, and goethite crystallization. These data indicate atmospheric pCO_2 of 16×PAL during formation of a Late Ordovician paleosol from the Neda fm. in Wisconsin, U.S.A, and 9×PAL for a middle Eocene paleosol profile from the Ione fm. in California, U.S.A. See text for discussion.

$(CO_3)OH$ in solid solution in goethite appear to be less abundant than paleosol profiles with calcite. In spite of these limitations, estimates of paleoatmospheric pCO_2 from $Fe(CO_3)OH$ in solid solution in paleosol goethites are tremendously important because they represent the only soil mineral that provides an internal proxy of soil pCO_2, which greatly reduces the uncertainty of atmospheric pCO_2 estimates to about ±300 ppmV. It is likely significant, however, that paleoatmospheric pCO_2 estimates from paleosol goethites and calcites show the same general trends through time (Yapp and Poths, 1996; Tabor et al., 2004a,b).

7.4.4. Soil carbonates formed by mixing of three-components of soil CO_2

7.4.4.1. Calcite. As mentioned, 3-component CO_2 mixing includes CO_2 derived from (1) *in situ* oxidation of soil organic matter, (2) tropospheric CO_2 and (3) CO_2 derived from dissolution pre-existing carbonate. Soil calcite derived from 3-component soil CO_2 mixing is more likely to occur in soils and paleosols developed upon marine carbonate, because these environments have high concentrations of pre-existing carbonate. Furthermore, soil calcite formed upon marine carbonates is expected to have more positive $\delta^{13}C$ values than co-existing soils characterized by 2-component and 1-component CO_2 mixing, because marine carbonate is generally quite positive, usually greater than ~− 2‰. To date, the existence of soil calcite that records the effect of mixing of 3-components of soil CO_2 has not been demonstrated. Quade et al. (1989) isotope study of soil carbonate along an elevation and climate transect in the Great Basin, Nevada, U.S.A., included examples of pedogenic calcite from soils formed upon both siliciclastic and carbonate parent materials. That work observed a 12‰ $\delta^{13}C$ variation over a 2440 meter elevation change. Yet, the slope of calcite $\delta^{13}C$ values versus elevation was similar for samples taken from soils on carbonate and siliciclastic parent materials. The similarity of calcite $\delta^{13}C$ values among carbonate- and siliciclastic-hosted soils strongly suggests that there is complete exchange between HCO_3^- derived from dissolution of pre-existing marine calcite and CO_2 in the soil that is derived from oxidation of organic matter and tropospheric CO_2. The large variation in soil calcite $\delta^{13}C$ values that was observed in Quade et al. (1989) is interpreted to reflect principally changes in the ratio of C_3 and C_4 photosynthesizers along the elevation transect. Nevertheless, we suspect that soil calcite that is formed by mixing of three-components of soil CO_2 exists, and will likely be found in soil profiles that are (1) developed upon marine carbonate, and (2) characterized by relatively low biological productivity. The former condition reflects that marine carbonate values have positive $\delta^{13}C$ values, whereas the latter condition reflects that lower biological productivity will limit exchange with HCO_3^- derived from dissolution of pre-existing marine calcite and maintain a relatively positive $\delta^{13}C$ value of micrite. In this regard, karst surfaces developed upon marine strata in times prior to evolution of vascular plants (pre-Silurian) may be a good candidate for paleosol calcite that formed by mixing of 3 components of soil CO_2.

7.4.4.2. Goethite. Hsieh and Yapp (1999) determined that $Fe(CO_3)OH$ in solid solution in goethite from a Rhodic Paleudult in east Texas, U.S.A., preserves $\delta^{13}C$ values that range from − 13‰ to − 14‰ toward the surface of the soil (31–64 cm) to − 6‰ to − 4‰ at depths of 122 cm beneath the surface. This depth-dependent trend of $\delta^{13}C$ values is different from that expected in soils characterized by mixing of two components of soil CO_2 (Fig. 16), and was interpreted to be a result of incorporation of a fraction of dissolved carbonate that originated from dissolution of marine calcite fossils in the parent material (Eocene Weches Formation). More negative $\delta^{13}C$ values of $Fe(CO_3)OH$ towards the surface of the soil were also interpreted to represent (1) more intense and longer-duration weathering toward the top of the profile, and (2) partial to nearly complete dissolution and re-precipitation of goethite after carbonate had been removed from that portion of the soil profile. Yapp (2001a, 2002) presented the following equation to explain the $\delta^{13}C$ values of $Fe(CO_3)OH$ in solid solution in goethite from acidic soils characterized by three-component soil CO_2 mixtures:

$$\delta^{13}C_G = \left[X_{GA}\left(\delta^{13}C_{GA} - \delta^{13}C_{GO}\right) + X_{GS}\left(\delta^{13}C_{GO} - \delta^{13}C_{GCC}\right)\right]\left(\frac{1}{X_G}\right) + \delta^{13}C_{GCC} \quad (56)$$

With the exception of $\delta^{13}C_{GCC}$ and X_{GS}, all variables and subscripts are defined in the manner for Eqs. (52) and (55). $\delta^{13}C_{GCC}$ is the $\delta^{13}C$ value of $Fe(CO_3)OH$ in goethite if it were in equilibrium with aqueous CO_2 derived only from dissolution of pre-existing carbonate in the soil, whereas X_{GS} is the mole fraction of $Fe(CO_3)OH$ in goethite if it formed only from CO_2 gas in a soil with mixing of two-components of CO_2.

Eq. (56) indicates that, in a plot of $\delta^{13}C_G$ vs. $1/X_G$, the $Fe(CO_3)OH$ component in goethite samples from the soil will yield a linear array with a negative slope (Yapp, 2001a,b; 2002; Tabor et al., 2004a,b; Tabor and Yapp, 2005b). Although it is not possible at this time to estimate paleoatmospheric pCO_2 concentrations from the $\delta^{13}C$ and molar concentration of $Fe(CO_3)OH$ in goethites that formed in the presence three-component soil CO_2 mixtures, they do provide estimates of soil pCO_2.

From the perspectives of field-based morphological observations and laboratory-based mineralogical inspection, goethites that form in the presence of either 2- or 3-component soil CO_2 mixing are indistinguishable, and they are only discerned from one another by determination of Fe(CO_3)OH δ^{13}C values. That is, goethites with Fe(CO_3)OH δ^{13}C values that are too positive to be explained by two-component soil CO_2 mixing are interpreted to have formed by three component soil CO_2 mixing which included dissolution of pre-existing carbonate with very positive δ^{13}C values (Hsieh and Yapp, 1999; Tabor et al., 2004a,b; Tabor and Yapp, 2005a,c).

7.5. $\delta^{18}O$ and δD of hydroxylated minerals

Pedogenic chemical weathering products are dominantly clay-size (<2 μm), of which a large proportion are hydroxylated (e.g., Wilson, 1999). The most common hydroxylated pedogenic minerals include mica-like minerals, vermiculites, smectites, chlorites and interlayered minerals, kaolinite, halloysite, iron oxyhydroxides, aluminum oxyhydroxides, and manganese oxyhydroxides (Dixon and Weed, 1989; Wilson, 1999). If these hydroxylated minerals form in chemical equilibrium with ambient soil waters, and the oxygen and hydrogen isotope fractionation factors of these minerals are known (see Table 5 for examples pertinent to this work), then oxygen and hydrogen isotope analysis of both soil and paleosol hydroxylated minerals may provide insights into environmental and climatic conditions at the time of mineral crystallization.

The earliest isotope geochemical studies of soils focused upon the δ^{18}O and δD values of silicates and oxyhydroxides in weathering profiles that developed upon igneous and metamorphic protolith (Taylor and Epstein, 1964; Savin and Epstein, 1970a; Lawrence and Taylor, 1971, 1972). These early studies recognized an upwards enrichment of bulk silicate ^{18}O through the soil, as concentrations of clay-size alteration products become greater (Taylor and Epstein, 1964). These results were interpreted to reflect an increasing contribution of oxygen from low-temperature, pedogenically formed, minerals, and destruction of pre-existing igneous and metamorphic minerals, toward the soil surface. Lawrence and Taylor (1971, 1972) noted that although the concentration of hydroxylated minerals increases upwards through the soil profiles, there is little or no profile-scale variation in silicate δD values because the protolith from which the soils are derived contained little or no primary hydroxylated minerals (i.e., soil alteration products dominate the δD value). Furthermore, the δ^{18}O and δD values of the soil alteration products defined an array that roughly paralleled the meteoric water line (Fig. 21); clay minerals exhibited offset from the meteoric water line, in order from greatest to smallest: kaolinite, goethite, gibbsite and amorphous aluminosilicates (Savin and Epstein, 1970a,b; Lawrence and Taylor, 1971; Yapp, 1987a,b; note that this agrees with the isotope fractionation equations in Table 5). Based upon the observed relationships, those early studies hypothesized that δ^{18}O and δD values of soil-formed hydroxylated minerals approach isotope equilibrium with local meteoric waters at temperatures very near that of the mean annual surface atmosphere. Subsequent studies of soil-formed, hydroxylated- mineral δ^{18}O and δD values have utilized the basic observations outlined in those earlier studies in order to (1) differentiate supergene (low-temperature) from hypogene

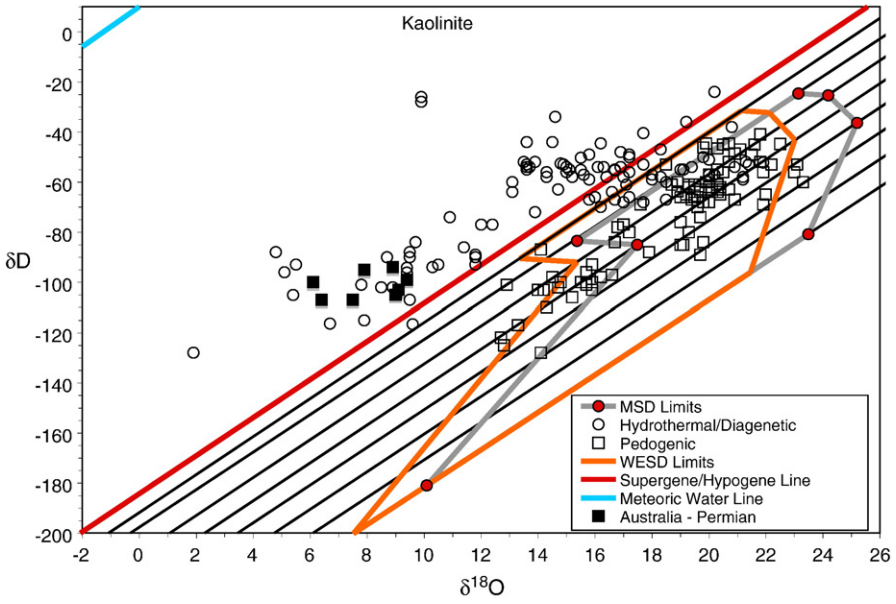

Fig. 21. Cross plot of δD versus δ^{18}O values. The blue line (upper left) represents the isotope composition of waters that lie upon the meteoric water line as defined by Craig (1961). Black lines depict 5 °C isotherms between 0 °C (right-most black line) and 35 °C (left-most black line) that represent isotope equilibrium between kaolinite and meteoric water. The red line is the 40 °C isotherm that depicts isotope equilibrium between kaolinite and meteoric water, and is the "supergene/hypogene" reference line (Sheppard et al., 1969). High-temperature hypogene processes result in kaolinite δD versus δ^{18}O values that lie to the left, whereas low-temperature supergene processes result in kaolinite δD versus δ^{18}O values that lie to the right, of the supergene/hypogene line. The gray polygon represents the modern surface domain (MSD) for kaolinite (Tabor and Montañez, 2005; see also Yapp, 1993a, 2001a,b; Savin and Hsieh, 1998), which is calculated using oxygen and hydrogen isotope fractionation equations for kaolinite (Table 5) in conjunction with the δD and δ^{18}O values of meteoric precipitation and temperature data from the IAEA data base (Rozanski et al., 1993). The orange polygon represents the Warm Earth Surface Domain (WESD) which considers global temperatures that are 5 °C warmer-than modern, and an ice-free, Earth. Open circles represent δD and δ^{18}O values for kaolinite samples that have been interpreted to originate from hydrothermal and deep-burial diagenetic processes (Sheppard et al., 1969; Sheppard and Taylor, 1974; Marumo, 1989; Macaulay et al., 1993; Stewart et al., 1994; Osborne et al., 1994; Decher et al., 1996; Hedenquist et al., 1998; Whelan et al., 1998; Matthews et al., 1999; Harris et al., 2000; Bethke et al., 2000; Parnell et al., 2000, 2004; Uysal et al., 2000; Marfil et al., 2005; Simeone et al., 2005). Open squares represent δD and δ^{18}O values for kaolinite samples that were collected from soil and paleosol profiles (Sheppard, 1977; Hassanipak and Eslinger, 1985; Bird and Chivas, 1989 [Cenozoic samples only]; Lawrence and Rashkes Meaux, 1993; Mizota and Longstaffe, 1996; Boulvais et al., 2000; Girard et al., 2000, Tabor and Montañez, 2005). For pure kaolinite samples, analytical uncertainty for δD and δ^{18}O values are ±3‰ and ±0.2‰, respectively, which corresponds to uncertainties in paleotemperature estimates of ±3 °C. Several kaolinite δ^{18}O values, however, are calculated end-member values from mixtures of kaolinite and some other silicate (e.g., quartz; Bird and Chivas, 1989; Lawrence and Rashkes Meaux, 1993), and have larger uncertainties (<± 1.1‰). With the exception of a single kaolinite from the Oligocene of Australia (Bird and Chivas, 1989), all pedogenic and paleopedogenic kaolinite samples reside within the MSD or WESD. (For interpretation of the references to colour in this figure legend, the reader is referred to the web version of this article.)

(hydrothermal) deposits, (2) delineate the paragenesis of mineral-formation in soils and paleosols, (3) determine the extent of chemical weathering in soil and paleosol profiles, (4) determine variations in the composition of soil moisture $\delta^{18}O$ and δD values, and (5) estimate the temperature of mineral crystallization.

7.5.1. Origin of residual deposits

In their study of economic copper deposits, Sheppard et al. (1969) analyzed $\delta^{18}O$ and δD values of phyllosilicates from the Idaho batholith. These workers arbitrarily selected an isotherm near 40 °C that represents equilibrium with meteoric water in order to separate minerals that formed by hypogene ($\delta^{18}O$ and δD values that correspond to >40 °C) processes from minerals that formed by supergene ($\delta^{18}O$ and δD values that correspond to <40 °C) processes (Fig. 21). This supergene/hypogene reference isotherm continues to be used with all sorts of hydroxylated minerals in order to differentiate low-temperature, from high-temperature, weathering deposits (Sheppard and Taylor, 1974; Sheppard and Gustafson, 1976; Hassanipak and Eslinger, 1985; Marumo, 1989; Cravero and Dominguez, 1992; Cravero et al., 1991, 2001; Yiu and Chang, 1999; Matthews et al., 1999; Tabor et al., 2004a,b). Fig. 21 shows the supergene/hypogene line for kaolinite. Also shown are previously reported $\delta^{18}O$ and δD values of kaolinite from hydrothermal, diagenetic and pedogenic weathering environments (see figure caption for appropriate citations). The range of kaolinite $\delta^{18}O$ and δD values indicates that many of the world's kaolinite deposits are likely derived from low-temperature, supergene weathering (e.g., Hassanipak and Eslinger, 1985; Bird and Chivas, 1989, 1993, 1995; Cravero et al., 1991; Lawrence and Rashkes Meaux, 1993; Mizota and Longstaffe, 1996; Delgado and Reyes, 1996; Harris et al., 2000; Matthews et al., 1999; Boulvais et al., 2000; Fig. 21).

In consideration of the possible origin(s) for goethite δD and $\delta^{18}O$ values, Yapp (1993a, 2001a,b) further refined the meaning of supergene processes with the concept of surface domains in order to differentiate goethite samples that formed by earth-surface processes from goethites that formed by higher-temperature processes. This concept was subsequently expanded to surface domain arrays for kaolinite (Savin and Hsieh, 1998), smectite (Tabor and Montañez, 2005) and complex mixtures of kaolinite and 2:1 phyllosilicates (Tabor and Montañez, 2005). While it is difficult, and probably impossible, to demonstrate with absolute certainty that a hydroxylated mineral formed within a soil (and remained unaltered within the paleosol) profile, surface domains are constrained by a global dataset of mean annual rainfall $\delta^{18}O$ and surface air temperatures, and thus provide a quantitative means to assess whether a mineral's $\delta^{18}O$ and δD values are consistent with environmental conditions that are expected during pedogenesis.

Specifically, the modern surface domain uses the weighted mean $\delta^{18}O$ value of precipitation ($\delta^{18}O_{precip}$) from each site in the IAEA database in order to calculate the corresponding δD of meteoric precipitation (Rozanski et al., 1993). This assumes that the meteoric water line (MWL) of Craig (1961) correctly represents the relationship between the δD and $\delta^{18}O$ of meteoric waters through time. In addition, only waters from IAEA sites with a mean annual temperature >0 °C are used to construct the MSD, as it is expected that liquid water is a requirement for crystallization of hydroxylated minerals. This treatment of the IAEA database yields 184 data points, ranging from 0 °C to ~30 °C (Fig. 15). When considering these modern IAEA data in conjunction with oxygen and hydrogen isotope fractionation factors for a given mineralogy, there is a resulting array of estimated mineral δD and $\delta^{18}O$ values that define a MSD. Fig. 21 shows the calculated MSD for kaolinite. Also shown are published kaolinite δD and $\delta^{18}O$ values (see Fig. 21 caption for references). Of the 79 different kaolinite samples taken from soil and paleosol profiles, 75 samples reside within the MSD (data points labeled "pedogenic" in Fig. 20).

The Warm Earth Surface Domain (WESD) model assumes global temperatures 5 °C warmer-than modern, and no significant continental ice sheets (Yapp, 2001a,b). This concept of the WESD array may be appropriate for "greenhouse world" intervals (Early Paleozoic, most of the Mesozoic, Early Cenozoic; e.g., Frakes et al., 1992). Using kaolinite as an example, the resultant WESD is plotted along with the MSD (Fig. 21). The WESD is somewhat more inclusive of kaolinite samples with lower $\delta^{18}O$ and δD compositions than its corresponding MSD. All but one of the 4 pedogenic kaolinites that reside outside the MSD in Fig. 21 fall within the limits of the WESD. Therefore, ~99% of paleosol kaolinite sample $\delta^{18}O$ and δD values can be adequately explained within the contexts of the MSD and WESD, and thus may provide some insights to low-temperature earth-surface processes. $\delta^{18}O$ and δD values of samples that fall outside of the surface domain arrays must be explained by other processes, such as a non-pedogenic origin, or diagenetic alteration of pedogenic minerals.

7.5.2. Variations in soil moisture $\delta^{18}O$ and δD values

Numerous studies have demonstrated that $\delta^{18}O$ and δD values of hydroxylated soil minerals reflect the isotope composition of soil water (Savin and Epstein, 1970a; Lawrence and Taylor, 1971, 1972; Yapp, 1993a, 2001a,b; 2002; Hsieh, 1997; Vitali et al., 2000, 2001). Hydroxylated soil minerals form by (1) transformation of pre-existing framework minerals in the soil by rapidly downward percolating soil waters (Beauvais and Tardy, 1991; Wilson, 1999; Bird et al., 1994b) or (2) direct precipitation from soil solutions with high Si, Al and Fe activities in poorly drained parts of soil profiles (Keller, 1963; Bourange et al., 1975; Wilson, 1999). As a result, soil waters that react to form hydroxylated soil minerals tend to have $\delta^{18}O$ and δD values which very closely reflect regional meteoric precipitation (Bird et al., 1992, 1994b; Giral-Kacmarcík et al., 1998). While the resulting $\delta^{18}O$ and δD values of the hydroxylated minerals may be offset from the true $\delta^{18}O$ and δD values of meteoric precipitation due to isotope fractionation (see Table 5), numerous studies have used the $\delta^{18}O$ and δD values of soil and paleosol hydroxylated minerals as temporal and spatial proxies for relative changes in the oxygen and hydrogen isotope composition of soil moisture and meteoric precipitation.

Lawrence and Taylor (1972) initially demonstrated that $\delta^{18}O$ and δD values of pedogenic phyllosilicate, gibbsite and amorphous aluminosilicates track regional meteoric precipitation $\delta^{18}O$ and δD values. Dutta and Suttner (1986) noted that $\delta^{18}O$ values of early diagenetic-silicate cements (kaolinite, smectite, and quartz) from arkosic sandstones of the Gondwana Supergroup in India become more positive in younger strata, a pattern which they attributed to northward migration of the subcontinent through warmer climates characterized by more positive meteoric water $\delta^{18}O$ values (e.g., see global rainfall $\delta^{18}O$ values in Fig. 15).

Bird and Chivas (1988a,b, 1989, 1993; Chivas and Bird, 1995; See also Botz et al., 1986) focused upon kaolinite $\delta^{18}O$ and δD values from Upper Paleozoic through Neogene strata of the Australian regolith. Australian kaolinites record more positive $\delta^{18}O$ values through time, from ~+6‰ in Permian strata to +18‰ in Miocene strata, which was also attributed to northward tectonic drift of the Australian continent. Collectively, these studies demonstrate the utility of hydroxylated soil-formed minerals as monitors of long-term (10^6–10^8 yr) climatic change on the time-scales of tectonic processes. Bird and Chivas (1988b) also noted that Paleozoic and Lower Mesozoic kaolinites appear to have δD values that are too positive for pedogenesis (see black squares in Fig. 21). They interpreted these results to indicate that kaolinite samples have retained their Paleozoic and Mesozoic pedogenic $\delta^{18}O$ values, but that these samples also have undergone post-formational (i.e., diagenetic) exchange of hydrogen isotopes, which has resulted in δD values that appear too positive for crystallization with meteoric water at soil temperatures (Fig. 21). Note that most of these suspect kaolinite samples have $\delta^{18}O$ values that are too negative for either the modern surface domain (MSD) or warm earth suface domain (WESD; Fig. 21). In this regard, post-formational

hydrogen isotope exchange does not seem to adequately explain the origin and isotope composition of these kaolinites. Uysal et al. (2000) suggested that the $\delta^{18}O$ and δD values of phyllosilicate from the Permian coal measures in Australia result from hydrothermal (~235 °C), rock-dominated, alteration during Late Triassic tectonic extension, and are not related to pedogenesis. The conclusions of Uysal et al. (2000) are significant because, if correct, post-formational change of hydrogen isotopes, in the absence of dissolution (and a corresponding change in $\delta^{18}O$ values), has yet to be demonstrated as an important process in hydroxylated pedogenic minerals (Yeh and Savin, 1977; Yeh and Epstein, 1978; Elsinger and Ye, 1981; Yapp, 1993a, 2000; Sheppard and Gilg, 1996; Gilg, 2000; Tabor and Montañez, 2005; Tabor, 2007; cf. O'Neil and Kharaka, 1976; Keyser and Kerrich, 1991).

At higher-resolution scales, Stern and others (1997) noted a 3–4‰ increase in $\delta^{18}O$ values of mixed smectite and kaolinite samples from Miocene paleosol profiles, over a 1–2 My interval (~8.5–6.5 Ma), in the Himalayan Molasse of Pakistan. These workers attributed the shift in phyllosilicate $\delta^{18}O$ values to be mechanistically linked to the onset of Indian Monsoon atmospheric circulation, and to diversion of isotopically heavier moisture over the Indian Ocean to interior continental sites (see also Quade et al., 1989, 1995; DeCelles et al., 2007). In their study of mixed 2:1 and 1:1 phyllosilicates from Permo-Carboniferous paleosols of the southwestern U.S.A., Tabor et al. (2002) noted that paleosol phyllosilicates record $\delta^{18}O$ values similar to those found in modern low-latitude, coastal and maritime sites. Tabor and Montañez (2002) interpreted these results to indicate a western source of meteoric precipitation, and low-latitude, reverse equatorial flow over western equatorial Pangea.

Several studies have used both δD and $\delta^{18}O$ values of hydroxylated minerals as monitors of paleo-elevation (Chamberlain and Poage, 2000; Horton et al., 2004). Chamberlain and Poage (2000) noted an ~6‰ decrease in Early Pliocene smectites from altered ashes in New Zealand, which they attributed to an ~2 km uplift of the Southern Alps. δD values of Eocene-age kaolinites that formed by alteration of auriferous gravels in California, U.S.A., indicate that the Sierra Nevada Range has remained high (>2200 m) over the past 40 to 50 million years (Mulch and Chamberlain, 2006). These studies are based upon the assumption that hydroxylated mineral $\delta^{18}O$ and δD values change with elevation. In their survey of 68 studies of meteoric waters in mountain belts, Poage and Chamberlain (2001) found that meteoric water $\delta^{18}O$ values decrease by 2.8‰ for every kilometer of elevation rise ($R^2 = 0.79$). As with other paleoelevation methods (e.g., Quade et al., 2007; Rowley and Garzione, 2007), the choice of lapse rate model greatly affects the absolute elevations predicted using pedogenic $\delta^{18}O$ values.

7.5.3. Single-mineral paleotemperature estimates

The potential of pedogenically-formed hydroxylated minerals as single-mineral geothermometers has been realized since pioneering studies of phyllosilicate $\delta^{18}O$ and δD values in soils and sediments in the early 1970 s (Savin and Epstein, 1970a,b; Lawrence and Taylor, 1971; Lawrence and Taylor, 1972). These early studies determined that $\delta^{18}O$ and δD values of soil-formed and other "supergene" hydroxylated minerals define an array that is roughly parallel with the meteoric water line. Savin and Epstein (1970a) suggested that, under conditions of chemical equilibrium with meteoric water, hydroxylated mineral $\delta^{18}O$ and δD values exhibit the following general relation:

$$\delta D_m = 8\left[\frac{{}^{D}\alpha_{m-w}}{{}^{18}\alpha_{m-w}}\right]\delta^{18}O_m + 1000\left[\left[8\times\frac{{}^{D}\alpha_{m-w}}{{}^{18}\alpha_{m-w}}\right] - 6.99\,{}^{D}\alpha_{m-w} - 1\right] \quad (57)$$

Subscript "m" denotes the mineral of interest, and the terms ${}^{D}\alpha_{m\text{-}w}$ and ${}^{18}\alpha_{m\text{-}w}$ denote the hydrogen and oxygen isotope fractionation values (α-values), respectively, between the mineral of interest and water. Given that values for ${}^{D}\alpha_{m\text{-}w}$ and ${}^{18}\alpha_{m\text{-}w}$ are temperature dependent (Table 5), and provided that temperature-dependent fractionation factors are known, these early studies speculated that measurements of δD_m and $\delta^{18}O_m$ in soil-formed hydroxylated minerals might provide information about the temperature of crystallization.

7.5.3.1. Goethite. Yapp (1987a,b, 1993a, 2000) suggested that measured $\delta^{18}O$ and δD values of ancient goethites might be useful as single-mineral paleothermometers. This paleotemperature proxy assumes chemical equilibrium with waters that lie upon Craig's (1961) Meteoric Water Line:

$$T_{(K)} = \left(\frac{1.63\times10^{6}}{\Delta^{18}O_{g-w} + 12.3}\right)^{\frac{1}{2}} \quad (58)$$

where,

$$\Delta^{18}O_{g-w} = \delta^{18}O_g - \delta^{18}O_w \approx 10_3 ln^{18}\alpha_{g-w} \quad (59)$$

and

$$\delta^{18}O_w = \left[\frac{\left(\frac{(1000 + \delta D_g)}{{}^{D}\alpha}\right) - 1010}{8}\right] \quad (60)$$

δD_g and $\delta^{18}O_g$ are the measured hydrogen and oxygen isotope composition, respectively, of goethite, and ${}^{D}\alpha_{g\text{-}w}$ is the stable hydrogen isotope fractionation factor between goethite and water (0.905; see Table 5). The analytical uncertainty of paletemperature estimates using this method is no better than ±3 °C. Using this approach, Yapp (2000) presented δD_g and $\delta^{18}O_g$ values of 31 different natural goethite samples. The goethite δD_g and $\delta^{18}O_g$ values corresponded to a range of crystallization temperatures from 6° to 69 °C, of which 16 goethites plotted within the goethite Modern Surface Domain, 8 goethites plotted within the limits of the goethite Warm Earth Surface Domain, and 7 goethites occurred outside the limits of either goethite surface domain. Tabor and others (2004a) measured δD_g and $\delta^{18}O_g$ values of −132 ± 4‰ and 2.7 ± 0.2‰, respectively, for goethite from a paleosol in Argentina that formed during the Late Triassic, at ~35–40° S paleolatitude. These values correspond to a crystallization temperature of 6 ± 3 °C; relatively cool temperatures for an interval of time that is generally associated with a Greenhouse (warm) global climate. Pleistocene-age goethites from Oklahoma, U.S.A., preserve δD_g and $\delta^{18}O_g$ values of ~ −123 ± 3‰ and ~2.9 ± 0.2‰, values which correspond to crystallization temperatures of ~9 ± 3 °C (Tabor and Yapp, 2005c). Such inferred paleotemperatures are 7 °C lower than modern mean annual temperatures in Oklahoma, U.S.A., and correspond well with independent studies that propose temperatures were ~6 °C cooler in this region during intervals of Pleistocene time (Stute et al., 1992; Stute and Schlosser, 1993).

7.5.3.2. Smectite and mixed phyllosilicates. Delgado and Reyes (1996) used oxygen (Savin and Lee, 1988) and hydrogen (Capuano, 1992) isotope fractionation equations for smectite, in conjunction with Craig's (1961) equation for the Meteoric Water Line in order to relate the $\delta^{18}O$ and δD values of smectite in paleosols to temperature of crystallization:

$$T_{(K)} = \left(\frac{3.54\times10^{6}}{\delta^{18}O_{sm} - 0.125\delta D_{sm} + 8.95}\right)^{\frac{1}{2}} (0 - 150\ ^{\circ}C) \quad (61)$$

where $\delta^{18}O_{sm}$ and δD_{sm} are the measured smectite $\delta^{18}O$ and δD values. The analytical uncertainty of paleotemperature estimates using this method is no better than ±3 °C. Delgado and Reyes observed that

$\delta^{18}O$ and δD values of altered bentonites from Cortijo de Archidona (Southeastern Spain) ranged from 21.0 to 23.0‰ and −87 to −102‰, respectively, which corresponds to temperatures of crystallization ranging from 9 ± 3 °C to 21 ± 3 °C. In their assessment of clay minerals in an Upper Triassic paleosol profile derived from basalt, Tabor and others (2004a) measured smectite $\delta^{18}O$ and δD values ranging from 14.5 to 15.6‰ and −78 to −71‰, respectively. This range of smectite $\delta^{18}O$ and δD values corresponds to temperatures of crystallization ranging from 49 to 57 °C. Such temperatures are far too high for soil formation, and were interpreted to result from hydrothermal alteration.

Tabor and Montañez (2005) adopted a similar approach to that of Delgado and Reyes (1996) in order to estimate temperature of smectite crystallization for smectite and kaolinite mixtures in Upper Pennsylvanian and Lower Permian paleosols from Texas, U.S.A. Notable differences between the approach of Tabor and Montañez (2005) and Delgado and Reyes (1996) are (1) analysis of only the <0.2 μm fraction of phyllosilicate and (2) consideration of the variability of oxygen and hydrogen isotope fractionation between smectite and water that is related to differences in the chemical composition of smectite. The range of $\delta^{18}O$ and δD values corresponds to temperatures of phyllosilicate crystallization ranging from 22 ± 3 °C to 35 ± 3 °C, where phyllosilicate $\delta^{18}O$ and δD values from Upper Pennsylvanian paleosol profiles indicated significantly lower temperatures than $\delta^{18}O$ and δD values from Lower Permian paleosol profiles.

Vitali et al. (2002) analyzed the <0.2 μm of mixed-mineral phyllosilicate fraction from a middle Cenomanian paleosol profile in the Dunvegan fm., British Columbia, Canada. Measured $\delta^{18}O$ and δD values ranged from −12.9‰ to −11.6‰ and −93‰ to −81‰, respectively, and were interpreted to correspond to paleotemperatures of phyllosilicate crystallization ranging from 9 to 16 °C. To date, very few studies have focused upon the $\delta^{18}O$ and δD values of soil and paleosol smectites and other common pedogenic minerals such as gibbsite and related aluminum hydroxides (Bird and Chivas, 1989; Vitali et al., 2000, 2001) and illite (Yeh, 1980; Capuano, 1992; Gilg, 2003; Hyeong and Capuano, 2004). Nevertheless, these hydroxylated pedogenic minerals are very common mineral products of pedogenic weathering, and these minerals have the potential to become important proxies of paleotemperature throughout much of the terrestrial Phanerozoic stratigraphic record.

7.5.3.3. Kaolinite. Much work has been done with the oxygen and hydrogen isotope compositions of soil-formed kaolinites (Sheppard, 1977; Hassanipak and Eslinger, 1985; Bird and Chivas, 1988a,b, 1989; Lawrence and Rashkes Meaux, 1993; Savin and Hsieh, 1998; Girard and Savin, 1996; Giral-Kacmarcík et al., 1989; Girard et al., 2000). The oxygen and hydrogen isotope kaolinite-water fractionation equations (Sheppard and Gilg, 1996) in conjunction with the equation for the meteoric water line of Craig (1961) relates the measured $\delta^{18}O$ and δD of kaolinite to temperature of crystallization:

$$T_{(^{\circ}K)} = \left(\frac{3.04\times10^{6}}{\delta^{18}O_{k} - 0.125\times\delta D_{k} + 7.04}\right)^{\frac{1}{2}} \quad (62)$$

As discussed earlier, only kaolinite samples from paleosol profiles with $\delta^{18}O$ and δD values that plot within the WESD and MSD should be considered viable paleotemperature proxies. For the following discussion, we also limit the dataset of kaolinite $\delta^{18}O$ and δD values to only those samples that are known to have formed within the time-frame of an individual Epoch or less in the Cenozoic. Cretaceous samples are limited to Campanian or younger kaolinites. This culling of the literature data leaves 78 kaolinite samples, which are plotted with respect to their corresponding paleolatitude of soil formation in Fig. 22.

Several observations may be made from this dataset (Fig. 22).

(1) The mid-latitudes, from ~35 to 50° N and ~30 to 62° S, are the only locations with published, pre-Pliocene kaolinite $\delta^{18}O$ and δD values. However, pedogenic kaolinite formation surely formed at lower latitude tropical sites (e.g., Wilson, 1999; Jacobs et al., 2005). Therefore, more attention should be given to determination of kaolinite $\delta^{18}O$ and δD values, as well as other potential geochemical proxy data of paleotemperature, from low-latitude sites in the future.

(2) Kaolinite $\delta^{18}O$ and δD values indicate their warmest mean temperatures (24 °C) during Cretaceous and Eocene time, followed by Paleocene (22 °C), and their lowest mean temperatures (20 °C) during Oligocene and Miocene time.

(3) Kaolinite $\delta^{18}O$ and δD values correspond to crystallization temperatures that are significantly (>3 °C) higher than mean annual surface-air temperatures at modern isolatitudinal sites. Because of the large thermal-mass of soil compared to atmosphere, subsurface temperatures are generally assumed to be approximately equivalent to that of mean annual temperature (+1 to 2 °C) with little or no seasonal change in temperature (e.g., Cerling and Quade, 1993; Buol et al., 2003). Therefore, isotope values of pedogenic isotope compositions are assumed to approximately record mean annual surface air temperatures in most studies (Yapp, 2000; Tabor, 2007; Tabor and Montañez, 2005; Tabor and Yapp, 2005c). Yet, long-term monitoring of ground and air temperatures from mid-latitude sites indicates that subsurface soil temperatures are strongly correlated with surface air temperatures, and vary seasonally, from ~0° to 22 °C, at 1.0 m depth (Bartlett et al., 2006). The rate of chemical weathering, and of crystallization of pedogenic minerals, is strongly temperature dependent. Furthermore, crystallization of soil minerals likely will not occur at 0 °C, as liquid water is necessary for chemical reaction. Therefore, it is possible that strikingly warm temperatures indicated by kaolinite $\delta^{18}O$ and δD values in Fig. 22 more accurately reflect surface-air temperatures during warm-months and growing seasons, and thus should not be compared with modern mean annual surface air-temperatures.

Note that mean annual surface air temperatures in low-latitude tropical sites do not vary annually by more than 1 or 2 °C. Therefore soil subsurface temperatures do not vary by more than 1 or 2 °C, and pedogenic mineral $\delta^{18}O$ and δD values from those sites likely provide a reasonable approximation of surface air temperatures. However, it is possible that perennially warm conditions, similar to those in the modern tropics, existed at higher mid-latitude sites during early Neogene, Paleogene and Late Cretaceous. This reflects both that paleosol profiles (Van Houten, 1961, 1982; Dury, 1971; Tardy et al., 1990a,b) and fossil floras (e.g., Dorf, 1964) that are indicative of modern, low-latitude tropical, sites (~15° N and S) occurred at paleolatitudes as high as 60°N. Furthermore, marine paleotemperature indicators suggest that mid-latitude surface oceans were significantly warmer, as high as 30 °C, during intervals of the Paleogene and Late Cretaceous (e.g., Takashima et al., 2006). In this regard, paleosol kaolinite $\delta^{18}O$ and δD values, and paleotemperature estimates shown in Fig. 22, may provide reasonable estimates of mean annual surface air paleotemperatures.

Future work of this sort should seek to (1) collect kaolinite $\delta^{18}O$ and δD values for paleotemperature estimates from places and times that are poorly represented in Fig. 22, (2) produce similar databases of $\delta^{18}O$ and δD value with other common hydroxylated pedogenic minerals, and (3) if these paleotemperatures are correct, evaluate what mechanisms (such as atmospheric pCO_2, ocean and atmospheric circulation, etc.) might contribute to such high temperatures in the mid-latitudes.

A major limitation to the application of single-mineral paleothermometers from soils and paleosols is the requisite assumption of chemical equilibrium with water $\delta^{18}O$ and δD values that lie upon the meteoric water line of Craig (1961). Changes in the position of the MWL (in hydrogen vs. oxygen isotope space) might have occurred at times during the geological past. The slope of the meteoric water line

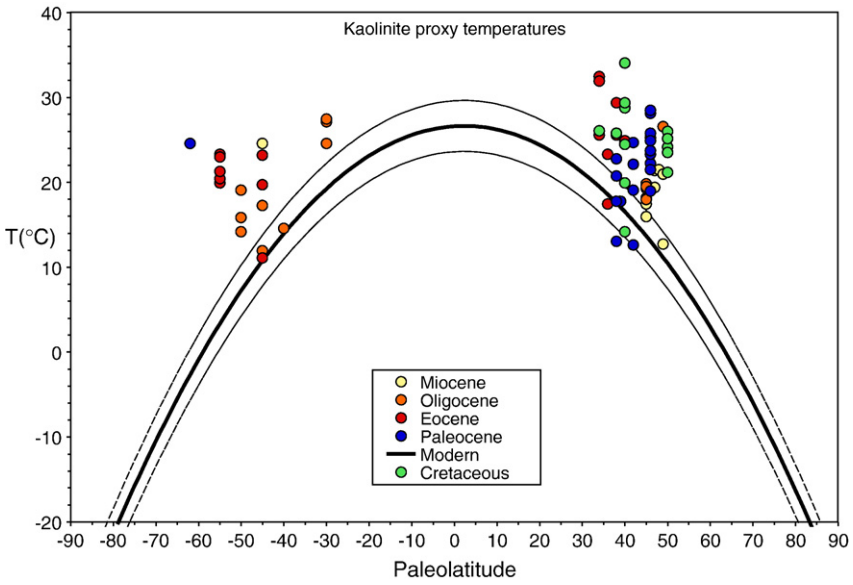

Fig. 22. Cross plot of estimated temperatures of kaolinite crystallization versus paleolatitudes of the paleosol profiles from which kaolinte samples were taken. Negative and positive values of latitude indicate positions in the southern and northern hemisphere, respectively. Paleolatitudes were determined using the "Point Tracker (v. 4) for Window" software package (developed by C.R. Scotese). Thick black line is the best-fit curve for mean annual surface air temperatures for weather station below 100 m above sea level in the International Atomic Energy Association database (Rozanski et al., 1993). Thin dashed lines represent the ±1s among the mean values for surface air temperatures. Temperature estimates for kaolinite crystallization are based upon published $\delta^{18}O$ and δD values (Sheppard, 1977; Hassanipak and Eslinger, 1985; Bird and Chivas, 1989; Lawrence and Rashkes Meaux, 1993; Mizota and Longstaffe, 1996; Boulvais et al., 2000) and are depicted as follows: green dots = Cretaceous, blue dots = Paleocene, red dots = Eocene, orange dots = Oligocene, yellow dots = Miocene. Ages for kaolinite samples are generally poorly known, and only kaolinite samples that are known to be limited to an Epoch are shown for Cenozoic data points. All Cretaceous samples are Campian or Maastrichtian. Temperature estimates are no better than ±3 °C. See text. (For interpretation of the references to colour in this figure legend, the reader is referred to the web version of this article.)

has not likely changed by more than 0.1‰ (e.g., Yurtsever and Gat, 1981) and, while the intercept of the meteoric water line is susceptible to variation that is principally related to humidity of air masses over the low-latitude tropics, it is unlikely that such changes will result in paleotemperature estimates that differ by more than ±2 °C (Delgado and Reyes, 1996). In addition, evaporation of water from the soil profile will drive soil water $\delta^{18}O$ and δD values to the right of the meteoric water line (Rozanski et al., 1993). Therefore, kaolinite which forms in equilibrium with soil waters that are offset from the meteoric water line through evaporation can result in significant overestimates of paleotemperature.

7.5.4. Mineral-pair $\delta^{18}O$ values

If two (or more) co-existing soil minerals form in chemical equilibrium, then differences in the $\delta^{18}O$ values of those two (or more) minerals may provide an estimate of temperature at the time of mineral co-precipitation. Paleotemperature estimates that are based on mineral-pair $\delta^{18}O$ values have a significant advantage over paleotemperature estimates that are based upon single-mineral $\delta^{18}O$ and δD values, in that the isotopic composition of soil water from which the minerals are derived is not important, and it is unnecessary to assume that soil water $\delta^{18}O$ and δD values lie upon the meteoric water line of Craig (1961).

There are only a few examples of paleotemperature estimates based on oxygen-isotope mineral pairs from pedogenic minerals. Yapp (1993b) estimated a paleotemperature of 23 ± 4 °C from a phosphate–goethite pair in Late Ordivician oolitic ironstone from the Neda fm., Wisconsin, USA. Yapp (1998) estimated a paleotemperature of 32 ± 4 °C from a kaolinite–goethite pair in Early Jurassic oolitic ironstone from Israel. Tabor (2007) estimated paleotemperatures from hematite–phyllosilicate pairs at five different stratigraphic horizons in Upper Pennsylvanian and Lower Permian paleosol profiles from Texas, USA. These hematite–phyllosilicate oxygen-isotope pairs indicate warming from relatively cool (24 ± 3 °C) soil temperatures in the Late Pennsylvanian to warmer soil temperatures (25 to 37 ± 3 °C) in the Early Permian. To date, all mineral-pair estimates of paleotemperature come from analysis of paleosol minerals that formed at low-latitude, tropical sites. Therefore, it is likely that these paleotemperature estimates reflect mean annual surface-air temperatures, rather than warm-season averages (see discussion of this in Section 7.5.3.3).

As mentioned above, oxygen isotope mineral-pair paleotemperature estimates are not sensitive to the isotopic composition of soil water from which the minerals co-precipitate. The temperature estimate provided by this proxy, however, does permit estimation of soil water $\delta^{18}O$ values. In the instances for the Late Ordovician and Early Jurassic examples provided in Yapp (1993b, 1998), estimated soil water $\delta^{18}O$ values are ~ −7.0‰. For the Late Carboniferous and Early Permian examples, estimated soil water $\delta^{18}O$ values range from −3.8‰ to −4.9‰. In addition, within analytical uncertainty, paleotemperature estimates from Upper Carboniferous and Lower Permian hematite-phyllosilicate mineral pairs are indistinguishable from single mineral paleotemperature estimates that are based upon $\delta^{18}O$ and δD values from paleopedogenic phyllosilicates. This represents a rare instance in which a persuasive case can be made for (1) low-temperature chemical equilibrium and (2) demonstration that very ancient soil water $\delta^{18}O$ and δD values lie upon, or very near, those defined by the modern meteoric water line (Craig, 1961).

7.6. Paleo-vegetation/paleo-photosynthesis

An additional application of isotope geochemistry in paleosols is to reconstruct past vegetative cover by estimation of the ratio of plants using C_3 and C_4 photosynthetic pathways (e.g., Quade et al., 1989, 1994; Cerling, 1992; Cerling and Quade, 1993; Cerling et al., 1993; Kingston et al., 1994; Latorre et al., 1997; Fox and Koch, 2003, 2004). The topic was recently reviewed by Tipple and Pagani (2007), so readers seeking a comprehensive review of this subject are directed there. However, a short review of the approach is appropriate here before we discuss some of the applications and results.

C_3 photosynthesis (Calvin–Benson) is the earliest developed photosynthetic pathway that is used by terrestrial plants. CO_2 diffuses into the plant and after a number of intermediate steps involving ribulose

1,5-biphosphate (RuBP) and the enzyme Rubisco, the 3-carbon sugar glyceraldhydes-3-phosphate (G3P) is produced (Tipple and Pagani, 2007). For each six G3P molecules produced, one molecule is converted to a simple sugar for cell use and the remaining five are recycled to generate more RuBP (Tipple and Pagani, 2007). Under environmentally stressful conditions such as high temperature, aridity, or high-light intensity, leaves close their stomatal openings and consequently, have lower internal CO_2 concentrations, which reduces the efficiency of C_3 photosynthesis. Two other photosynthetic pathways have evolved in terrestrial vascular plants: 1) Crassulacean acid metabolism (CAM), which is used primarily by succulents and 2) C_4 photosynthesis, which is used primarily by dry- and cold-climate grasses. Ultimately, C_4 photosynthesis uses the Calvin–Benson cycle to fix C, but a series of intermediate storage reactions increase the overall photosynthetic efficiency under environmentally stressed conditions by storing CO_2 as HCO_3^- that can be re-converted to CO_2 for use at the optimally efficient time (Tipple and Pagani, 2007).

This difference between photosynthetic pathways is recorded by paleosol carbonates and organic matter because of differences in how strongly the two pathways discriminate against ^{13}C. C_3 photosynthesis discriminates more strongly, which results in typical biomass $\delta^{13}C$ values of − 20‰ to − 33‰ (mean − 27‰), whereas C_4 photosynthesis does not discriminate strongly, which results in typical biomass $\delta^{13}C$ values of −10‰ to −14‰ (mean −13‰) (e.g., Koch, 1998; Cerling and Harris, 1999). The $\delta^{13}C$ value of soil biomass is directly related to $\delta^{13}C$ values of soil-respired CO_2 and pedogenic calcite (see Sections 7.1–7.4). Owing to a variety of factors (reviewed in Koch, 1998 and discussed above) soil calcite is typically 14‰–17‰ more positive (i.e., ^{13}C-enriched) relative to soil-respired CO_2. CAM plants are relatively rare, so most soil organic matter is derived either from C_3 or C_4 photosynthesis. Thus, using either $\delta^{13}C_{org}$ or $\delta^{13}C_{cc}$ values, it is possible to derive a simple two-component mixing line between C_3 and C_4 photosynthetic pathways, and consequently, vegetation types since C_4 plants are typically grasses (though it should be noted that there are also a number of C_3 grasses).

For pedogenic carbonates (and assuming an enrichment factor [$\Delta^{13}C$] of 15.5‰ (e.g., Fox and Koch, 2003), the proposed mixing line is between −11.5‰ (100% C_3) and +2.5‰ (100% C_4). Using this equation, or a similar one, various authors have reconstructed the balance between C_3 and C_4 plants during the Cenozoic in areas including East Africa, Pakistan, Greece, and North and South America (Quade et al., 1989, 1994; Cerling and Quade, 1993; Cerling, 1992; Cerling et al., 1993; Kingston et al., 1994; Latorre et al., 1997; Fox and Koch, 2003, 2004) and have concluded that there was a significant expansion of the amount and range of C_4 plants in the late Miocene (e.g., Fig. 19). Those results are further supported by analyses of mammal diets in many of the same areas, and which indicate a similar shift toward C_4 plants (e.g., Passey et al., 2002; Cerling et al., 1997). Though all of the studies indicated a late Miocene age for the spread of C_4 plants (at the expense of C_3 plants), the timing of the spread is regionally dependent (see Fig. 5 of Tipple and Pagani, 2007), and in North America, some component of C_4 plants was probably present much earlier in the Miocene (Fox and Koch, 2003, 2004; Sheldon, 2008).

The limitations to this approach have been discussed in various places (e.g., Koch, 1998; Fox and Koch, 2003), but there are three principle factors to consider when reconstructing the C_3–C_4 plant balance using paleosols. The first is aridity, which could potentially shift the $\delta^{13}C$ composition of C_3 biomass toward heavier values, which would give a false-positive C_4 plant result. As discussed in Section 5.5, there are various methods for reconstructing past precipitation regimes using paleosols, so it should be possible to account for this effect. Secondly, high levels of atmospheric CO_2 would result in higher concentrations of atmospheric CO_2 in the soil, a corresponding shift toward more positive $\delta^{13}C_{cc}$ values, and an overestimate of C_4 photosynthesizers. However, various marine and non-marine proxies (e.g., Royer et al., 2004) indicate at most slight elevated CO_2 levels through the Neogene above pre-industrial levels, so unless evidence for earlier C_4 plants is discovered, the entire period of time in which the C_3–C_4 balance is a viable research avenue is characterized by "low" CO_2 levels. The final potential issue is with low productivity soils, which would also have heavier $\delta^{13}C$ values, low concentrations of CO_2 derived from oxidation of soil organic matter, and a relatively greater contribution of CO_2 derived from the atmosphere owing to the influence of atmospheric CO_2 diffusion (i.e., incomplete respiration of the CO_2 that diffused into the profile). This potential problem may be examined by looking at the off-set between $\delta^{13}C_{org}$ or $\delta^{13}C_{carb}$ values for coexisting pedogenic carbonates and organic matter. If $\Delta^{13}C$ is significantly greater than 15.5‰, then low productivity may be inferred, and in that case, the $\delta^{13}C_{org}$ value is a reliable indicator of C_3–C_4 balance and the $\delta^{13}C_{carb}$ value is not (Sheldon, 2008).

8. Future approaches and challenges

8.1. Boron isotopes

There is not currently a good proxy for paleo-pH from paleosol profiles. One possible means to address this would be to look at the boron isotopic composition ($\delta^{11}B$) of paleosol carbonate nodules. Boron has two stable, non-redox dependent, isotopes: ^{10}B and ^{11}B. Boron isotopic fractionation in carbonate minerals is a pH-dependent conversion of planar boric acid, H_3BO_3, to tetrahedral borate, $B(OH)_4^-$ (Hemming and Hanson, 1992, Sanyal et al., 1996). Observations of marine carbonates have shown that borate is preferentially taken up in carbonates, preserving the isotopic fractionation of borate in the carbonate with little additional fractionation. Since borate production is pH-dependent, the final $\delta^{11}B$ isotopic composition in the carbonates ultimately depends on pH. The equilibrium expression for the conversion of boric acid to borate is:

$$K_B = \frac{(X)\left[H^+\right]}{(1-X)} \tag{63}$$

where K_B is the equilibrium constant and X is mole fraction of borate (relatively to the total B). The mass balance expression relating the isotopic composition of borate (δ_{BA}^-), boric acid (δ_B), and total boron ($\delta_{\Sigma B}$) is:

$$\delta_{\Sigma B} = \delta_{BA^-} X + \delta_B(1-X) \tag{64}$$

If Eqs. (63) and (64) are combined, the following expression relates the measured $\delta^{11}B$ composition of carbonate nodules to aH^+ ($pH = -\mathrm{Log}[aH^+]$):

$$a_{H^+} = \frac{K_B(\delta_{\Sigma B} - \delta_{BA^-})}{[(\delta_B - \delta_{BA^-}) - (\delta_{\Sigma B} - \delta_{BA^-})]} = \frac{K_B(\delta_{\Sigma B} - \delta_{BA^-})}{[\Delta_B - (\delta_{\Sigma B} - \delta_{BA^-})]} \tag{65}$$

Assuming that fractionation of boron in soils is only dependent on pH, then $\delta_{\Sigma B}$ is measured directly by measuring the $\delta^{11}B$ composition of the parent material for the soil, δ_{BA}^- is the measured $\delta^{11}B$ composition of paleosol carbonate nodules, and δ_B is 19.4 at 25 °C (Kakihana et al., 1977). K for the addition of OH^- to boric acid to form borate is $10^{5.27}$ (Kakihana et al., 1977); K_B also needs to take into account the dissociation of H_2O to provide OH^- ($10^{-13.995}$), so the overall K_B at 25 °C is $10^{-8.725}$. In marine settings, the need to estimate $\delta_{\Sigma B}$ is one of the primary difficulties in applying $\delta^{11}B$ compositions of fossils. This weakness is precisely the strength of applying this approach to paleosols, because it is possible to measure directly values for $\delta_{\Sigma B}$ if the paleosol's parent material has been preserved. In particular, this method is likely to be useful for paleosols with igneous parent materials, which typically have a more homogeneous chemical composition than alluvial parent materials.

Fig. 23 depicts the predicted pH values for a wide range of fractional values between a hypothetical paleosol and its parent material. Larger fractionations of $\delta^{11}B$ between a paleosol and its parent material correspond to more acidic pHs. It should be noted that at lower temperatures, more typical of soil formation, more acidic pH values would be predicted for the same magnitude fraction of $\delta^{11}B$. 25 °C was used primarily because it represents standard temperature for thermodynamic data, but it is possible to solve for values appropriate for lower temperatures, so this does not represent an impediment to applying this method.

One potentially exciting application of pH values calculated from $\delta^{11}B$ values of pedogenic carbonates is to address the question of what a reasonable value for $S(z)$ is in calculations of paleoatmospheric CO_2 levels (see Section 7.4.3.1), because the pH at the time of formation of the pedogenic carbonate nodules should be related to soil gas composition. For the purposes of illustration, we will consider the simplest possible case (again at 25 °C) for the formation of pedogenic carbonate:

$$CO_{2(g)} + H_2O + Ca^{2+} = 2H^+ + CaCO_3 \qquad \mathrm{Log}K_{calcite} = -9.634 \tag{66}$$

Assuming pure calcite and water (i.e., $a = 1$), the equilibrium relationship may be defined as follows:

$$\frac{\left[H^+\right]^2}{[pCO_2]\left[Ca^{2+}\right]} = K \Rightarrow \frac{\left[H^+\right]^2}{K_3\left[Ca^{2+}\right]} = pCO_2 \tag{67}$$

Because there is a 1:1 relationship between the number of moles of Ca^{2+} and CO_2, the expression may be further simplified to the following:

$$S(z) = pCO_2 = \sqrt{\frac{[a_{H^+}]^2}{K_{calcite}}} \tag{68}$$

Using pH values derived from Fig. 23 for $(\delta_{\Sigma B} - \delta_{BA^-})$ values ranging from 16 to 19 gives a range of pH from 8.05 to 7.04 (aH^+ 8.86×10^{-9} to 8.94×10^{-8}). Applying those values to Eq. (68) gives a range of $S(z)$ values of 581–5867 ppm, with the largest $\delta^{11}B$ (and lowest pH) values indicating the highest $S(z)$ as would be expected. For most calculations of paleatmospheric CO_2 levels, the predicted $S(z)$ using this method is similar to what is already being used, though somewhat lower, as only relatively acidic pH conditions would predict high $S(z)$. Using lower $S(z)$ values would predict lower atmospheric CO_2 values (Section 7.4.3.1), so this is potentially important as an additional check on those calculations.

Thus, there is considerable scope for development of new paleoproxies for pH and potentially for $S(z)$ using $\delta^{11}B$ analyses obtained from pedogenic carbonates. The main difficulties lie with $\delta^{11}B$ analysis itself, potentially poorly constrained parent material compositions, and uncertainties about paleotemperature at the time that the carbonate formed. Nonetheless, we feel that this is an area of research with considerable scope for future growth.

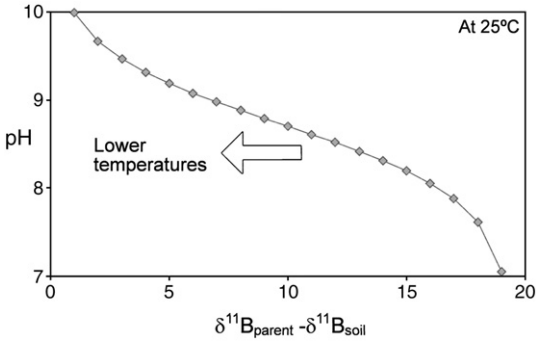

Fig. 23. Boron isotope fractionation versus pH for 25 °C. At lower temperatures, fractionation factors are smaller when boric acid is converted to borate (Kakihana et al., 1977), which shifts the curve to the left.

8.2. Energy balance models

Another recent development is a model that relates energy input into the soil system during weathering to mean annual precipitation (MAP) and temperature (MAT). Rasmussen et al. (2005) defined a new term for the energy input into a soil during pedogenesis (E_{in}); Rasmussen and Tabor (2007) refined the early framework, renaming E_{in} as effective energy and mass transfer (EEMT) and put forward a quantitative pedogenic energy model (QPEM) that relates EEMT to various quantitative measures of pedogenic properties including pedon depth, clay content, CIA-K (Eq. (5)), and the ratio of free Fe-oxides to total Fe (Fe_d/Fe_T). EEMT represents the total amount of solar energy that is available for pedogenesis and is represented by two quantities: 1) heat available to warm soil material and water and 2) reduction of C due to photosynthesis (Rasmussen and Tabor, 2007). Full derivation of the model may be found in Rasmussen et al. (2005) and Rasmusen and Tabor (2007); at least one of the relationships in the paper is potentially applicable to paleosols. Using empirical data collected for soils with igneous parent materials in the Sierra Nevadas, southern Cascades, and Sierra San Pedro Martir ranges, EEMT (kJ m^{-2} yr^{-1}) may be related to MAT and MAP as follows:

$$\mathrm{EEMT} = 347,134\ \exp^{\left(-0.5\left(\left(\frac{\mathrm{MAT}-21.5}{-10.5}\right)^2 + \left(\frac{\mathrm{MAP}-4412}{1704}\right)^2\right)\right)} \tag{69}$$

Rasmussen and Tabor (2007) also found significant differences in EEMT among different soil orders (Ultisols>Alfisols≈Andisols>Mollisols>Inceptisols>Entisols). In the form of Eq. (69), the relationship is somewhat cumbersome to apply, because while calculation of EEMT for a paleosol where MAT and MAP are known could be used to confirm a taxonomic designation, those paleoclimatic values (in particular MAT) are not that well-constrained typically. Alternatively, Rasmussen and Tabor's (2007) relationship may be re-arranged to solve for either MAT or MAP. As an example, here is the re-arranged expression for MAT:

$$\mathrm{MAT} = 21.5 + \frac{\sqrt{\left[-2\mathrm{Ln}\frac{\mathrm{EEMT}}{347,134} + \left(\frac{\mathrm{MAP}-4412}{1704}\right)^2\right.}}{-10.1} \tag{70}$$

To give a concrete example, we will apply Eq. (70) to a series of Miocene Alfisol-like paleosols (Argillisols; Sheldon, 2006d) used elsewhere in this review. EEMT for Alfisols is 25,875 ± 1781 kJ m^{-2} yr^{-1} (Rasmussen and Tabor, 2007) and the reconstructed MAP using Eq. (30) ranges from 540 to 854 mm/yr. Assuming a constant EEMT and using the MAP figures published by Sheldon (2006d), MAT figures ranging from ~12 to 20 °C are obtained (Fig. 24) and are plotted against previously obtained MAT estimates using Eq. (25). Obviously, the MAT estimates obtained using EEMT are very different than those obtained using Eq. (25), so which estimate is more reasonable?

Both equations have upper limits to the temperatures that they can predict, (17.3 °C for Eq. (25) and 21.5 °C for Eq. (70)), so Eq. (70) is potentially viable over a larger range of paleotemperatures than Eq. (25). The paleosols all correspond to the middle Miocene climatic optimum, which lead Sheldon (2006d) to question the paleotemperature results in his original study that used Eq. (25), because while the MAP estimates that he obtained matched paleobotanical results, the MAT values were only semi-consistent with estimates based on paleobotanical proxies for MAT (i.e., the highest MAT values with the full SE). Thus, based on independent lines of evidence the values obtained using Eq. (70) are perhaps more in line with expected middle Miocene MAT.

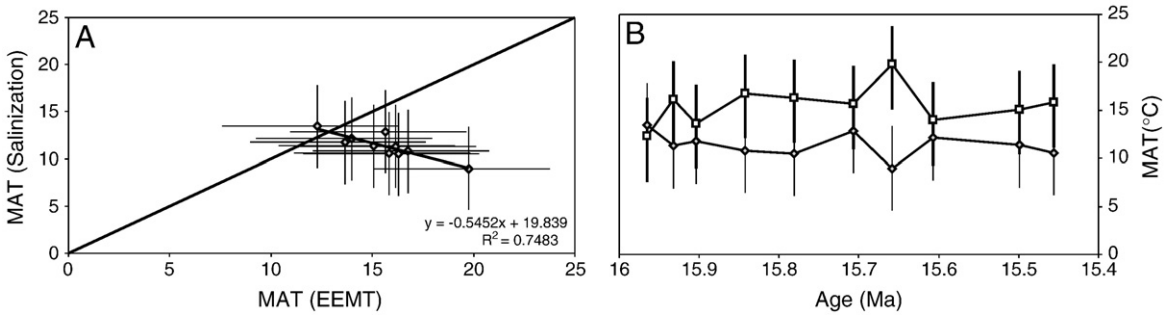

Fig. 24. Comparison of MAT derived from EEMT and Salinization. A) MAT estimates based on Salinization (*y*-axis) and EEMT (x-axis) are generally negatively correlated. B) MAT estimates from Salinization (filled diamonds) and EEMT (open squares) as a function of time show considerable overlap when errors are included, but EEMT generally predicts warmer conditions than Salinization.

However, the uncertainty on the MAT estimates using Eq. (70) are fairly large and non-linear owing to the form of Eq. (69). On average for these samples the error in MAT is +4 °C and − 4.7 °C (Fig. 24), comparable to the error on Eq. (25). Breaking it down further, the component of error due to uncertainty in EEMT is only 0.76 °C ($\pm 1\sigma$), whereas the component of the error due to the uncertainty of the MAP estimate is 3.2–3.9 °C, thus a more precise estimate for MAP would increase the precision of Eq. (70) considerably. One additional consideration is that if a fixed EEMT is assumed, then MAT and MAP are inversely related. However, the MAP and MAT data compiled by Sheldon et al. (2002) for 126 modern soils had an $R^2 = 0.54$, which though far from definitive, suggests at least some relationship between MAP and MAT, so the fixed EEMT assumption is not strictly correct. On the other hand, if one assumes that the MAT and MAP values reported by Sheldon (2006d) are correct, then applying Eq. (69) gives a mean EEMT values of 19,286 ($\pm 1\sigma$ of 4482) kJ m^{-2} yr^{-1}, which is substantially lower than the mean Alfisol EEMT value obtained by Rasmussen and Tabor (2007), but not beyond the range of error. The most likely explanation for this difference is that paleosols are all basalt-parented, whereas the equation was derived from soils with various igneous parent materials, though a secondary consideration may be the elevation variations among the soils analyzed by Rasmussen and Tabor (2007) whereas the Miocene paleosols all formed in the same relatively low elevation setting.

Thus, the QPEM model offers a lot of promise for applications ranging from taxonomy to paleoclimatic reconstruction. However, care is needed in applying it thoughtfully to paleosols given different potential sources of uncertainty. Further development may also be needed for other types of parent materials, but we think that in the long-run, these potential issues will be possible to deal with and that a QPEM that integrates both MAP and MAT (which are not really independent of one another) will be a powerful tool for paleosols research.

8.3. "Clumped isotope" paleothermometry

A recent innovation in stable isotope geochemistry that is relevant for the study of paleosols is the analysis of doubly rather than singly substituted isotopologues (Eiler, 2007). The term isotopologue refers to each possible isotopic configuration for a given compound. For example, conventional gas-source $\delta^{13}C$ analyses are measuring $^{13}C^{16}O_2$ ($z = 45$), which is one of 12 possible isotopologues for CO_2. Traditional mass-spectrometer configuration allows for measurements of $z = 44$, 45, or 46. Addition of a extra faraday cup makes the measurement of masses 47–49 possible, which in turn makes it possible to measure more isotopologues than were previously available. The abundance of the doubly substituted CO_2 isotopologue ($^{13}C^{18}O^{16}O$) produced by phosphoric acid digestion of carbonate minerals is proportional to the concentration of $^{13}C-{}^{18}O$ bonds in the reacted carbonate; that concentration is a function of the formation temperature of the carbonate minerals (Ghosh et al., 2006a,b; Eiler, 2007) and can be used as a paleothermometer (Ghosh et al., 2006a,b). $^{13}C^{18}O^{16}O$ abundance in the evolved CO_2 is measured in "per mil" relative to the expected amount of all CO_2 isotopologues in a randomized gas sample. The proportionality of the $^{13}C-{}^{18}O$ bonds is described as follows:

$$\Delta_{47} = 0.0592 \times 10^6 \times T^{-2} - 0.02 \quad (71)$$

where Δ_{47} isotopic enrichment relative to the randomized gas sample and T is the temperature (K), and where the precision due to the analytical uncertainty is ~2 °C (Ghosh et al., 2006a,b). Unlike traditional oxygen isotope-based water-carbonate paleothermometers, there is no dependence in this relationship on either the $\delta^{18}O$ of the water nor on the $\delta^{13}C$ of the dissolved inorganic carbon from which the carbonate formed (Ghosh et al., 2006a,b), therefore obviating the need for any unconstrained assumptions of either air or soil water isotopic compositions. This method has been applied successfully to pedogenic carbonates (Ghosh et al., 2006b) as a means of calculating uplift rates in the Altiplano by putting the values derived from Eq. (8) into a lapse-rate model. A thorough review of the potential applications of "clumped-isotope" paleothermometry to paleoaltimetry may be found in Quade et al. (2007).

Paleoaltimetry is just the tip of the proverbial iceberg in terms of the potential paleoclimatic and paleoenvironmental applications of this technique (e.g., Eiler, 2007) because there is no dependence on the initial $\delta^{18}O$ or $\delta^{13}C$ values of the system (which hampers many existing proxies), only on the temperature at which the doubly substituted $^{13}C^{18}O^{16}O$ isotopologue was formed. However, to reach the full potential of the technique, there is at least one outstanding issue that needs to be considered, namely the relationship between the soil temperature and the air temperature. It is not clear that these two values are necessarily the same because the soil temperature can easily exceed the air temperature in areas either with very warm temperatures (or warm seasons of the year) or where the albedo of the ground surface is low. To illustrate this, consider the difference between digging up your garden early in the spring or at the height of summer. In early spring (e.g., April in the Northern Hemisphere), the soil temperature essentially matches the air temperature, whereas in summer (e.g., August in the Northern Hemisphere) the soil temperature may be many degrees warmer than air above it. Given that pedogenic carbonates form only during certain warm times of the year (Breecker et al., 2009), un-corrected isotopologue paleotemperatures are potentially biased towards recording summer temperatures rather than mean annual temperatures. Nonetheless, the problem is likely tractable with further consideration of the timing of pedogenic carbonate formation and of the relationship between soil and air temperatures.

9. Summary

Paleopedology is still a relatively immature field, with many fundamental discoveries about processes and proxies left to be made. The shift in recent years from a largely qualitative type of analysis to a largely quantitative one has important implications both for the field itself, but also more broadly, for the reconstruction of past environmental and climatic conditions. Given that one of our best means of projecting how ongoing anthropogenic greenhouse gas additions will affect future climate is to look at how the Earth's climate has reacted during previous high CO_2 times, these new tools and proxies for making quantitative reconstructions are an important new means of addressing those effects. More specifically, though many marine proxies give broad "global" climatic information, they are indirect proxies because they are typically recording changes to a much more slowly reacting entity (i.e., ocean temperature and composition) and in the case of records derived from benthic foraminifera, one divorced from direct contact with the Earth's climate and atmosphere. Understanding how the Earth's surficial environments have changed is ultimately equally if not more important in projecting the impacts of anthropogenically-driven climate change on our lives. Paleopedology promises to be increasingly important in this endeavor. However, we would like to reiterate that, ideally, none of these proxies should stand alone as indications of paleoclimate and that our inferences about paleoclimate are only strengthened by applying multiple proxies to many paleosol profiles. Ultimately, all of these geochemical proxies should agree with other observations of the geological record and if they do not, it is the proxies that should be considered suspect.

Paleoclimatic and environmental properties that may be reconstructed using the new geochemical proxies include protolith provenance, weathering intensity, mean annual precipitation and temperature during pedogenesis, nutrient fluxes into and out of the paleosols, the atmospheric composition of important gases including CO_2 and O_2, paleosol soil gas composition and mixing relationships, soil moisture, crystallization temperature of pedogenic minerals, reconstructed vegetative covering, and paleo-altitude. Future work promises yield to other proxies for pedogenic processes, including perhaps paleo-pH and paleo-energy usage. A firm understanding of pedogenic processes and the limits of the proxies need to form the basis for applications of paleosol geochemistry, because, with all of the proxies, our applications are only as good as our understanding of the whole system.

Acknowledgements

NDS would like to acknowledge the previous support for this work from GSA, NSF, and NERC, and his very understanding fiancé Selena. NJT is supported by NSF-EAR 0617250, NSF-EAR 0545654, and NSF-EAR 0447381. This manuscript benefited from the thoughtful reviews by Greg Retallack and Carmala Garzione. In addition, the authors would like to acknowledge numerous colleagues who, through various interactions, have had an immense influence on this work: Isabel Montañez, Crayton Yapp, Doug Ekart, Greg Retallack, Jonathan Wynn, Steve Driese, and Lee Nordt.

Appendix A. Supplementary data

Supplementary data associated with this article can be found, in the online version, at doi:10.1016/j.earscirev.2009.03.004.

References

Achyuthan, H., 2003. Petrologic analysis and geochemistry of the late Neogene–early Quaternary hardpan calcretes of western Rajasthan, India. Quaternary International 106/107, 3–10.

Alonso-Zarza, A.M., Tanner, L.H., 2006. Paleoenvironmental Record and Applications of Calcretes and Palustrine Carbonates. Geological Society of America Special Paper, vol. 416. 239 pp.

Anderson, J.M., 1973. Carbon dioxide evolution from two temperate, deciduous woodland soil. Journal of Applied Ecology 10, 361–378.

Andrews, J.E., Tandon, S.K., Dennis, P.F., 1995. Concentration of carbon-dioxide in the Late Cretaceous atmosphere. Journal of the Geological Society 152, 1–3.

Arens, N.C., Jahren, A.H., Amundson, R., 2000. Can C3 plants faithfully record the carbon isotopic composition of atmospheric carbon dioxide? Paleobiology 26, 134–164.

Arkley, R.J., 1963. Calculation of carbonate and water movement in soil from climate data. Soil Science 96, 239–248.

Aslan, A., Autin, W.J., 1998. Holocene floodplain soil formation in the southern lower Mississippi Valley: implications for interpreting alluvial paleosols. Geological Society of America Bulletin 110, 433–449.

Atchley, S.C., Nordt, L.C., Dworkin, S.I., 2004. Eustatic control on alluvial sequence stratigraphy: a possible example from the K/T transition of the Tornillo Basin, Big Bend National Park, west Texas. Journal of Sedimentary Research 74, 391–404.

Bahrig, B., 1989. Stable isotope composition of siderite as an indicatory of the palaeoenvironmental history of oil shale lakes. Palaeogeography Palaeoclimatology Palaeoecology 70, 139–151.

Baker, J.C., Kassan, J., Hamilton, P.J., 1996. Early diagenetic siderite as an indicator of depositional environment in the Triassic Rewan Group, southern Syndey basin, eastern Australia. Sedimentology 43, 77–88.

Bao, H.M., Koch, P.L., 1999. Oxygen isotope fraction in ferric oxide-water systems: low temperature synthesis.

Bárdossy, G., White, J.L., 1979. Carbonate inhibits the crystallization of aluminum hydroxide in Bauxite. Science 203, 355–356.

Bárdossy, G., Jonas, K., Imre, A., Solymar, K., 1977. Interrelations of bauxite texture, micromorphology, mineral individualism, and heteromorphism. Economic Geology 72, 573–581.

Barron, E.J., 1989. Studies of Cretaceous climate. In: Berger, A., Dickinson, R.E., Kidson, J.W. (Eds.), Understanding climate change. American Geophysical Union Geophysical Monograph, vol. 52, pp. 149–157.

Barron, E.J., Hay, W.W., Thompson, S.L., 1989. The hydrologic cycle: a major variable during Earth history. Global Planetary Change 1, 157–174.

Bartlett, M.G., Chapman, D.S., Harris, R.N., 2006. A decade of ground-air temperature tracking at Emigrant Pass Observatory, Utah. Journal of Climate 19, 3722–3731.

Beauvais, A., Tardy, Y., 1991. Formation et degradation des cuirasses ferrugineuses sous climat tropical humide, a la lisiere de la foret equatoriale. Comptes Rendus Serie 2, 313, 1539–1545.

Behrensmeyer, A.K., Quade, J., Cerling, T.E., Kappelman, J., Khan, I.A., Copeland, P., Roe, L., Hicks, J., Stubblefield, P., Willis, B.J., Latorre, C., 2007. The structure and rate of late Miocene expansion of C4 plants; evidence from laterial variation in stable isotopes in paleosols of the Siwalik Group, northern Pakistan. Geological Society of America Bulletin 119, 1486–1505.

Bekker, A., Holland, H.D., Wang, P.L., Rumble, D., Stein, H.J., Hannah, J.L., Coetzee, L.L., Beukes, N.J., 2004. Dating the rise of atmospheric oxygen. Nature 427, 117–120.

Berner, R.A., 1991. A model for atmospheric CO_2 over Phanerozoic time. American Journal of Science 291, 339–376.

Berner, R.A., 2002. Examination of hypotheses for the Permo-Triassic boundary extinction by carbon cycle modeling. Proceedings of the National Academy of Science 99, 4172–4177.

Berner, R.A., 2004. The Phanerozoic Carbon Cycle. Oxford University Press, New York. 150 pp.

Berner, R.A., 2005. GEOCARBSULF: a combined model for phanerozoic atmospheric O_2. Geochimica et Cosmochimica Acta 70, 5653–5664.

Berner, R.A., Kothavala, X., 2001. GEOCARBIII: a revised model of atmospheric CO_2 over Phanerozoic time. American Journal of Science 301, 182–204.

Bestland, E.A., 2000. Weathering flux and CO_2 consumption determined from palaeosol sequences across the Eocene–Oligocene transition. Palaeogeography, Palaeoclimatology, Palaeoecology 156, 301–326.

Bestland, E.A., 2002. Fossil Andisols identified with mass-balance geochemistry (Oligocene John Day Formation, Oregon, U.S.A.). Journal of Sedimentary Research 72, 673–686.

Bethke, P.M., Rye, R.O., Finkelstein, D.B., 2000. Isotopic studies of authigenic sulfides, silicates, and carbonates, and calcite and pyrite veinlets in the Creede Formation, San Juan Mountains, Southwest Colorado. In: Bethke, P.M., Hay, R.L. (Eds.), Ancient Lake Creede; Its Volcano-Tectonic Setting, History of Sedimentation, and Relation to Mineralization in the Creede Mining District. Geological Society of America Special Paper, vol. 346, pp. 267–286.

Bird, M.I., Chivas, A.R., 1988a. Oxygen-isotope dating of the Australian regolith. Nature 331, 513–516.

Bird, M.I., Chivas, A.R., 1988b. Stable isotope evidence for low-temperature weathering and post-formation hydrogen-isotope exchange in Permian kaolinites. Chemical Geology (Isotope Geoscience Section) 72, 249–265.

Bird, M.I., Chivas, A.R., 1989. Stable isotope geochronology of the Australian regolith. Geochimica et Cosmochimica Acta 53, 3239–3256.

Bird, M.I., Chivas, A.R., 1993. Geomorphic and palaeoclimatic implications of an oxygen-isotope geochronology for Australian deeply weathered profiles. Australian Journal of Earth Sciences 40, 345–358.

Bird, M.I., Longstaffe, F.J., Fyfe, W.S., Bildgen, P., 1992. Oxygen-isotope systematics in a multiphase weathering system in Haiti. Geochimica et Cosmochimica Acta 56, 2831–2838.

Bird, M.I., Longstaffe, F.J., Fyfe, W.S., Tazaki, K., Chivas, A.R., 1994a. Oxygen-isotope fractionation in gibbsite – synthesis experiments versus natural samples. Geochimica et Cosmochimica Acta 58, 5267–5277.

Bird, M.I., Quade, J., Chivas, A.R., Fifield, L.K., Allan, G.L., Head, M.J., 1994b. The carbon-isotope composition of organic-matter occuled in iron nodules. Chemical Geology 114, 269–279.
Birkeland, P.W., 1999. Soils and Geomorphology, (3rd Ed.). Oxford University Press, New York. 448 pp.
Bockheim, J.G., Gennadiyev, A.N., 2000. The role of soil-forming processes in the definition of taxa in Soil Taxonomy and the World Soil Reference base. Geoderma 95, 53–72.
Borchardt, G., 1989. Smectites. In: Dixon, J.B., Weed, S.B. (Eds.), Soil Science Society of America, pp. 675–727. Madison, Wisconsin U.S.A.
Bottinga, Y., 1968. Calculation of fractionation factors for carbon and oxygen in the system calcite–carbon dioxide–water. Journal of Physical Chemistry 72, 800–808.
Botz, R.W., Hunt, J.W., Smith, J.W., 1986. Isotope geochemistry of minerals in Australian bituminous coal. Journal of Sedimentary Petrology 56, 99–111.
Boulvais, P., Vallet, J.M., Esteoule-Choux, J., Fourcade, S., Martineau, F., 2000. Origin of kaolinization in Brittany (NW France) with emphasis on deposits over granite; stable isotopes (O, H) constraints. Chemical Geology 168, 211–223.
Bourange, B., Paquet, H., Bocquier, G., 1975. The role of clay in the migration and accumulation of the alumina of certain tropical bauxites. Comptes Rendus, Serie D, 280, 2783–2786.
Bowen, G.J., Beerling, D.J., 2004. An integrated model for soil organic carbon and CO_2: implications for paleosol carbonate pCO_2 paleobarometry. Global Biogeochemical Cycles 18, GB1026.
Bowen, G.J., Koch, P.K., Gingerich, P.D., Norris, R.D., Bains, S., Corfield, R.M., 2001. Refined isotope stratigraphy across the continental Paleocene-Eocene boundary on Polecat Bench in the Northern Bighorn Basin. In: Gingerich, P.D. (Ed.), Paleocene-Eocene Stratigraphy and Biotic Change in the Bighorn and Clarks Fork Basins, Wyoming. University of Michigan Papers on Paleontology, vol. 33, pp. 73–88.
Bowen, G.J., Koch, P.L., Meng, J., Ye, J., Ting, S., 2005. Stratigraphy and correlation of fossiliferous late Paleocene-early Eocene strata of the Erlian Basin, Inner Mongolia, China. American Museum Novitates 3474, 1–26.
Bown, T.A., Kraus, M., 1987. Integration of channel and floodplain suites: I. Developmental sequence and lateral relations of alluvial paleosols. Journal of Sedimentary Petrology 57, 587–601.
Boynton, D., Compton, O.C., 1944. Normal seasonal changes of oxygen and carbon dioxide percentages in gas from the larger pores of three orchard subsoils. Soil Science 57, 107–117.
Boynton, D., Reuther, W., 1938. A way of sampling gases in dense subsoils and some of its advantages and limitations. Proceedings of the Soil Science Society of America 3, 37–42.
Braun, J.J., Viers, J., Dupre, B., Polve, M., Ndam, J., Muller, J.P., 1998. Solid/liquid REE fractionation in the lateritic system of Goyoum, East Cameroon: the implication for the present dynamics of the soil covers of the humid tropical regions. Geochimica et Cosmochimica Acta 62, 273–299.
Breecker, D.O., Sharp, Z.D., McFadden, L.D., 2009. Seasonal bias in the formation and stable isotopic composition of pedogenic carbonate in modern soils from central New Mexico, USA. Geological Society of America Bulletin 121, 630–640.
Brewer, R., 1976. Fabric and Mineral Analysis of Soils. Krieger, New York.
Brewer, R.C., 1964. Fabric and Mineral Analysis of Soils. Wiley, New York.
Brimhall, G.H., Dietrich, W.E., 1987. Constitutive mass balance relations between chemical composition, volume, density, porosity, and strain in metasomatic hydrochemical systems: results on weathering and pedogenesis. Geochimica et Cosmochimica Acta 51, 567–587.
Brook, G.A., Folkoff, M.E., Box, E.O., 1983. A world model of soil carbon dioxide. Earth Surface Processes and Landforms 8, 79–88.
Brown, G.H., Kingston, D.M., 1993. Early Diagenetic spherulitic siderites from Pennsylvanian palaeosols in the Boss Point Formation, Maritime Canada. Sedimentology 40, 467–474.
Buck, B.J., Mack, G.H., 1995. Latest Cretaceous (Maastrichtian) aridity indicated by paleosols in the McRae Formation, south-central New Mexico. Cretaceous Research 16, 559–572.
Buck, B.J., Wolff, K., Merkler, D., McMillan, N., 2006. Salt mineralogy of Las Vegas Wash, Nevada: morphology and subsurface evaporation. Soil Science Society of America Journal 70, 1639–1651.
Buol, S.W., Southard, R.J., Graham, R.C., McDaniel, P.A., 2003. Soil Genesis and Classification. Iowa State Press, Ames, Iowa, USA.
Calvert, C.S., 1984. Simpilified, complete CsCl-hydrazin-dimethylsulfoxide intercalation of kaolinte. Clays and Clay Minerals 323, 125–130.
Came, R.E., Eiler, J.M., Veizer, J., Azmy, K., Brand, U., Weidman, C.R., 2007. Coupling of surface temperatures and atmospheric CO_2 concentrations during the Palaeozoic era. Nature 449, 198–202.
Capo, R.C., Whipkey, C.E., Blachere, J.R., Chadwick, O.A., 2000. Pedogenic origin of dolomite in a basaltic weathering profile, Kohala peninsula, Hawaii. Geology 28, 271–274.
Capuano, R.M., 1992. The temperature-dependence of hydrogen isotope fractionation between clay-minerals and water-evidence from a geopressured system. Geochimica et Cosmochimica Acta 56, 2547–2554.
Carothers, W.C., Adami, L.H., Roenbauer, R.J., 1988. Experimental oxygen isotope fractioantion between siderite-water and phosphoric acid liberated CO_2-Siderite. Geochimica et Cosmochimica Acta 52, 2445–2450.
Caudill, M.R., Driese, S.G., Mora, C.I., 1997. Physical compaction of vertic paleosols: implications for burial diagenesis and palaeo-precipitation estimates. Sedimentology 44, 673–685.
Cerling, T.E., 1984. The stable isotopic composition of modern soil carbonate and its relationship to climate. Earth and Planetary Science Letters 71, 229–240.
Cerling, T.E., 1991. Carbon dioxide in the atmosphere: evidence from Cenozoic and Mesozoic paleosols. American Journal of Science 291, 377–400.
Cerling, T.E., 1992. Development of grasslands and savannas in East Africa during the Neogene. Palaeogeography, Palaeoclimatology, Palaeoecology 97, 241–247.
Cerling, T.E., 1999. Stable carbon isotopes in paleosol carbonates. In: Thirty, M., Coincon, R. (Eds.), Palaeoweathering, Palaeosurfaces, and Related Continental Deposits. International Association of Sedimentologist Special Publication, vol. 27, pp. 43–60. Oxford.
Cerling, T.E., Harris, J.M., 1999. Carbon isotope fractionation between diet and bioapatite in ungulate mammals and implications for ecological and paleoecological studies. Oecologia 120, 347–363.
Cerling, T.E., Quade, J., 1993. Stable carbon and oxygen isotopes in soil carbonates. In: McKenzie, J.A., Savin, S. (Eds.), Climate Change in Continental Isotopic Records. Geophysics Monograph, vol. 78. American Geophysical Union, Washington (DC), pp. 217–231.
Cerling, T.E., Solomon, D.K., Quade, J., Bowman, J.R., 1991. On the isotopic composition of carbon in soil carbon dioxide. Geochimica et Cosmochimica Acta 55, 3403–3405.
Cerling, T.E., Wang, Y., Quade, J., 1993. Expansion of C4 ecosystems as an indicator of global ecological change in the late Miocene. Nature 361, 344–345.
Cerling, T.E., Harris, J.M., MacFadden, B.J., Leakey, M.G., Quade, J., Eisenmann, J., Ehleringer, J.R., 1997. Global vegetation change through the Miocene and Pliocene. Nature 389, 153–158.
Chacko, T., Cole, D.R., Horita, J., 2001. Equilibrium oxygen, hydrogen and carbon isotope fractionation factors applicable to geologic systems. Reviews in Mineralogy and Geochemistry 43, 1–81.
Chadwick, O.A., Brimhall, G.H., Hendricks, D.M., 1990. From a black to a gray box — a mass balance interpretation of pedogenesis. Geomorphology 3, 369–390.
Chadwick, O.A., Derry, L.A., Vitousek, P.M., Huebert, B.J., Hedin, L.O., 1999. Changing sources of nutrients during four million years of ecosystem development. Nature 397, 491–497.
Chamberlain, C.P., Poage, M.A., 2000. Reconstructing the paleotopography of mountain belts from the isotopic composition of authigenic minerals. Geology 28, 115–118.
Chivas, A.R., Bird, M.I., 1995. Palaeoclimate from Gondwanaland clays. In: Churchman, G.J., Fitzpatrick, R.W., Eggleton, R.A. (Eds.), Clays controlling the Environment: Proceedings of the 10th International Clay Conference, pp. 333–338.
Clark, I., Fritz, 1997. Environmental Isotopes in Hydrogeology. Lewis Publishers, New York. 328 pp.
Clayton, R.N., Epstein, S., 1961. The use of oxygen isotopes in high temperature geological thermometry. Journal of Geology 69, 447–452.
Clechenko, E.R., Kelly, D.C., Harrington, G.J., Stiles, C.A., 2007. Terrestrial records of a regional weathering profile at the Paleocene–Eocene boundary in the Williston Basin of North Dakota. Geological Society of America Bulletin 119, 428–442.
Cleveland, D.M., Atchley, S.C., Nordt, L.C., 2007. Continental sequence stratigraphy of the Upper Triassic (Norian–Rhaetian) Chinle strata, northern New Mexico, USA: Allocyclic and autocyclic origins of paleosol-bearing alluvial successions. Journal of Sedimentary Research 77, 909–924.
Clyde, W.C., Sheldon, N.D., Koch, P.L., Gunnell, G.F., Bartels, W.S., 2001. Linking the Wasatchian/Bridgerian boundary to the Cenozoic Global Climate Optimum: new magnetostratigraphic and isotopic results from South Pass, Wyoming. Palaeogeography, Palaeoclimatology, Palaeoecology 167, 175–199.
Colman, S.M., 1982. Chemical weathering of basalts and andesites:evidence from the weathering rinds. United States Geological Survey Paper, vol. 1246. Washington.
Condie, K.C., Dengate, J., Cullers, R.L., 1995. Behavior of rare earth elements in a paleoweathering profile on granodiorite in the Front Range, Colorado, USA. Geochimica et Cosmochimica Acta 59, 279–294.
Coney, L., Reimold, W.U., Hancox, P.J., Mader, D., Koeberl, C., McDonald, I., Struck, U., Vajda, V., Kamo, S.L., 2007. Geochemical and mineralogical investigation of the Permian–Triassic boundary in the continental realm of the southern Karoo basin, South Africa. Palaeoworld 16, 67–104.
Craig, H., 1961. Isotopic variations in meteoric waters. Science 133, 1702–1708.
Cravero, M.F., Dominguez, E.A., 1992. Kaolin deposits in the Lower Cretaceous Baquero Formation (Santa Cruz Province, Patagonia, Argentina). Journal of South American Earth Sciences 6, 223–235.
Cravero, M.F., Dominguez, E., Murray, H.H., 1991. Valores δO^{18} y δD en Caolinitas, indicadores de un clima templado moderado durante el Jurasico Superior-Certacico Inferior de la Patagonia, Argentina. Rev. Assoc. Geol. Argent. (RAGA) XLVI, 1–2, pp. 20–25.
Cravero, F., Dominguez, E., Iglesias, C., 2001. Genesis and applications of the Cerro Bubio kaolin deposit, Patagonia (Argentina). Applied Clay Science 18, 157–172.
Criss, R.E., 1999. Principles of Stable Isotope Distribution. Oxford University Press, New York. 264 pp.
Currie, B.S., Rowley, D.B., Tabor, N.J., 2005. Middle Miocene paleoaltimetry of southern Tibet: implications for the role of mantle thickening and delamination in the Himalayan orogen. Geology 33, 181–184.
Dansgaard, W., 1964. Stable isotopes in precipitation. Tellus 16, 436–468.
Darmody, R.G., Thorn, C.E., Allen, C.E., 2005. Chemical weather and boulder mantles, Kärkevagge, Swedish Lapland. Geomorphology 67, 159–170.
Datta, S., Thibault, Y., Fyfe, W.S., Powerll, M.A., Hart, B.R., Martin, R.R., Tripthy, S., 2002. Occurrence of trona in alkaline soils of the Indo-Gangetic Plains of Uttar Pradesh (UP), India. Episods 25, 236–239.
de Jong, E., Schappert, H.J.V., 1972. Calculation of soil respiration and activity from CO_2 profiles in the soil. Soil Science 113, 28–33.
DeCelles, P.G., Quade, J., Kapp, P., Fan, M., Dettman, D.L., Ding, L., 2007. High and dry in central Tibet during the Oligocene. Earth and Planetary Science Letters 253, 389–401.
Decher, A., Bechtel, A., Echle, W., Friedrich, G., Hoernes, S., 1996. Stable isotope geochemistry of bentonites from the island of Milos (Greece). Chemical Geology 129, 101–113.

Delgado, A., Reyes, E., 1996. Oxygen and hydrogen isotope compositions in clay minerals: a potential single-mineral geothermometer. Geochimica et Cosmochimica Acta 60, 4285–4289.
Deutz, P., Montanez, I.P., Monger, H.C., Morrison, J., 2001. Morphology and isotope heterogeneity of late Quaternary pedogenic carbonates; implications for paleosols carbonates as Paleoenvironmental proxies. Palaeogeography Palaeoclimatology Palaeoecology 166, 293–317.
Deutz, P., Montanez, I.P., Monger, H.C., 2002. Morphology and stable and radiogenic isotope composition of pedogenic carbonates in late Quaternary relict soils, New Mexico, U.S.A.; an integrated record of pedogenic overprinting. Journal of Sedimentary Research 72, 809–822.
Dever, L., Durand, R., Fontes, J.Ch., 1988. The isotopic and chemical composition of secondary calcite in saturated zone as palaeoclimatic indicators. Chemical Geology 70, 114–121.
Dixon, J.B., 1989. Kaolin and serpentine group minerals, In: Dixon, J.B., Weed, S.B. (Eds.), Minerals in Soil Environments, 2nd Ed. Soil Science Society of America Book Series, vol. 1, pp. 467–526.
Dixon, J.B., Weed, S.B., 1989. Minerals in soil environments. Soil Science Society of America. Madison, Wisconsin, U.S.A.
Dorf, E., 1964. The use of fossil plants in paleoclimatic interpretations. In: Nairn, A.E.M. (Ed.), Problems in palaeoclimatology. Interscience Publishers, pp. 13–31.
Driese, S.J., 2004. Pedogenic translocation of Fe in modern and ancient Vertisols and implications for interpretations of the Hekpoort paleosol (2.25 Ga). Journal of Geology 112, 543–560.
Driese, S.G., Ober, E.G., 2005. Paleopedologic and paleohydrologic records Precipitation Seasonality from Early Pennsylvanian "Underclay" paleosols, U.S.A. Journal of Sedimentary Research 75, 997–1010.
Driese, S.G., Mora, C.I., Stiles, C.A., Joeckel, R.M., Nordt, L.C., 2000. Mass-balance reconstruction of a modern Vertisol: implications for interpreting the geochemistry and burial alteration of paleo-Vertisols. Geoderma 95, 179–204.
Driese, S.G., Jacobs, J.R., Nordt, L.C., 2003. Comparison of modern and ancient Vertisols developed on limestone in terms of their geochemistry and parent material. Sedimentary Geology 157, 49–69.
Driese, S.G., Nordt, L.C., Lynn, W., Stiles, C.A., Mora, C.I., Wilding, L.P., 2005. Distinguishing climate in the soil record using chemical trends in a Vertisol climosequence from the Texas Coastal Prairie, and application to interpreting Paleozoic paleosols in the Appalachian basin. Journal of Sedimentary Research 75, 340–353.
Driese, S.G., Medaris Jr., G., Ren, M., Runkel, A.C., Langford, R.P., 2007. Differentiating pedogenesis from diagenesis in early terrestrial paleoweathering surfaces formed on granitic composition parent materials. Journal of Geology 115, 387–406.
Droser, M.L., Bottjer, D.J., 1986. A semiquantitative field classification of ichnofabric. Journal of Sedimentary Petrology 56, 558–559.
Dury, G.H., 1971. Relict deep weathering and duricrusting in relation to palaeoenvironments of middle latitudes. Geographic Journal 137, 511–522.
Dutta, P.K., Suttner, L.J., 1986. Alluvial sandstone composition and paleoclimate; II, Authigenic mineralogy. Journal of Sedimentary Petrology 56, 346–358.
Dworkin, S.I., Nordt, L., Atchley, S., 2005. Determining terrestrial paleotemperatures using the oxygen isotopic composition of pedogenic carbonate. Earth and Planetary Science Letters 237, 56–68.
Eiler, J.M., 2007. "Clumped-isotope" geochemistry — the study of naturally-occurring multiply-substituted isotopologues. Earth and Planetary Science Letters 262, 309–327.
Ekart, D.D., Cerling, T.E., Montanez, I.P., Tabor, N.J., 1999. A 400 million year carbon isotope record of pedogenic carbonate: implications for paleoatmospheric carbon dioxide. American Journal of Science 299, 805–827.
Elsinger, E.V., Ye, H., 1981. Mineralogy, $^{18}O/^{16}O$ and D/H ratios of clay rich sediments from Deep Sea Drilling Project site 180, Aleutian Trench. Clays and Clay Minerals 29, 309–315.
Epstein, S., Buchsbaum, R., Lowenstam, H.A., Urey, H.C., 1953. Revised carbonate-water isotopic temperature scale. Geology Society of America Bulletin 64, 1315–1326.
Eugster, H.P., Chou, I.M., 1973. The depositional environments of precambrian banded iron-formations. Economic Geology and the Bulletin of the Society of Economic Geologists 68, 1144–1168.
Fang, C., Moncrief, J.B., 2001. The dependence of soil CO_2 efflux on temperature. Soil Biology and biogeochemistry 33, 155–165.
Faure, K., Harris, C., Willis, J.P., 1995. A profound meteoric water influence on Genesis in the Permian Waterberg coalfield, South Africa: evidence from stable isotopes. Journal of Sedimentary Research A65, 605–613.
Fang, C., Moncrieff, J.B., Gholz, H.L., Clark, K.L., 1998. Soil CO_2 efflux and its spatial variation in a Florida Slash pin plantation. Plant and Soil 205, 135–146.
Feakes, C.R., Holland, H.D., Zbinden, E.A., 1989. Ordovician paleosols at Arisaig, Nova Scotia, and evolution of the atmosphere. In: Bronger, A., Catt, J.A. (Eds.), Paleopedology: Nature and Application of Paleosols. Catena Supplement, vol. 16, pp. 207–232.
Fedo, C.M., Nesbitt, H.W., Young, G.M., 1995. Unraveling the effects of potassium metasomatism in sedimentary rocks and paleosols, with implications for paleoweathering conditions and provenance. Geology 23, 921–924.
Feng, J., Hsieh, Y.P., 1998. wetlands and aquatic processes; sulfate reduction in freshwater wetland soils and the effects of sulfate and substrate loading. Journal Environmental Quality 27, 968–972.
Feng, W., Yapp, C.J., 2008. Experimental tests of the effects of Al substitution on the goethite-water D/H fractionation factor. Geochimica et Cosmochimica Acta 72, 1295–1311.
Ferguson, K.M., Gregory, R.T., Constantine, A., 1999. Lower Cretaceous (Aptian–Albian) secular changes in the oxygen and carbon isotope record from high paleolatitude, fluvial sediments, southeast Australia: comparisons to the marine record. In: Barrera, E., Jonson, C.C. (Eds.), Evolution of the Cretaceous Ocean-Climate System. Geological Society of America Special Paper, vol. 332, pp. 59–72.
Fox, D.L., Koch, P.L., 2003. Tertiary history of C4 biomass in the Great Plains, U.S.A. Geology 31, 809–812.
Fox, D.L., Koch, P.L., 2004. Carbon and oxygen isotopic variability in Neogene paleosol carbonates: constraints on the evolution of C_4-grasslands of the Great Plains, USA. Palaeogeography, Palaeoclimatology, Palaeoecology 207, 305–329.
Frakes, L.A., Francis, J.E., Syktus, J.I., 1992. Climate Modes of the Phanerozoic. University Press, Cambridge, UK.
Franzmeier, F.P., Bryant, R.B., Steinhardt, G., 1985. Characteristics of Wisconsinan glacial tills in Indiana and their influence on Argillic horizon development. Soil Science Society of America Journal 49, 1481–1486.
Freytet, P., Verrecchia, E.P., 2002. Lacustrine and palustrine carbonate petrography: an overview. Journal of Paleolimnology 27, 221–237.
Fritz, S.J., Toth, T.A., 1997. An Fe-berthierine from a Cretaceous laterite: Part II, estimation of Eh, pH and pCO_2 conditions of formation. Clays and Clay Minerals 45, 580–586.
Garzione, C.N., Dettman, D.L., Quade, J., DeCelles, P.G., Butler, R.F., 2000. High times on the Tibetan Plateau: paleoelevation of the Thakkhola graben, Nepal. Geology 28, 339–342.
Garzione, C.N., Dettman, D.L., Horton, B.K., 2004. Carbonate oxygen isotope paleoaltimetry: evaluating the effect of diagenesis on paleoelevation estimates for the Tibetan plateau. Palaeogeography, Palaeoclimatology, Palaeoecology 212, 119–140.
Gat, J.R., Bowser, C.J., 1991. The heavy isotope enrichment of water in coupled evaporative systems. Geochemical Society Special Publication 3, 159–168.
Genise, J.F., Bellosi, E.S., Gonzalez, M.G., 2004. An approach to the description and interpretation of ichnofabrics in palaeosols. Geological Society Special Publications 228, 355–382.
Ghosh, P., Bhattacharya, S.K., Jani, R.A., 1995. Paleoclimate and palaeovegetation in central India during the Upper Cretaceous based on stable-isotope composition of paleosol carbonates. Palaeogeography, Palaeoclimatology, Palaeoecology 114, 285–296.
Ghosh, P., Ghosh, P., Bhattacharya, S.K., 2001. CO_2 levels in the Late Palaeozoic and Mesozoic atmosphere from soil carbonate and organic matter, Satpura Basin, central India. Palaeogeography, Palaeoclimatology, Palaeoecology 170, 219–236.
Ghosh, P., Adkins, J., Affek, H., Balta, B., Guo, W.F., Schauble, E.A., Schrag, D., Eiler, J.M., 2006a. C-13-O-18 bonds in carbonate minerals: a new kind of paleothermometer. Geochimica et Cosmochimica Acta 70, 1439–1456.
Ghosh, P., Garzione, C.N., Eiler, J.M., 2006b. Rapid uplift of the Altiplano revealed through C-13-O-18 bonds in paleosol carbonates. Science 311, 511–515.
Gile, L.H., Peterson, F.F., Grossman, R.B., 1966. Morphological and genetic sequences of carbonate accumulation in desert soils. Soil Science 101, 347–360.
Gilg, H.A., 2000. D–H evidence for the timing of kaolinitization in Northeast Bavaria, Germany. Chemical Geology 170, 5–18.
Gilg, H.A., 2003. Isotope geochemistry and origin of illite–smectite and kaolinite from the Seilitz and Kemmlitz kaolin deposits, Saxony, Germany. Clay Minerals 38, 95–112.
Gilg, G.A., Sheppard, S.M.F., 1996. Hydrogen isotope fractionation between kaolinite and water revisited. Geochimica et Cosmochimica Acta 60, 529–533.
Gill, S., Yemane, K., 1996. Implications of a Lower Pennsylvanian Ultisol for equatorial Pangean climates and early, oligotropic, forest ecosystems. Geology 24, 905–908.
Giral-Kacmarcík, S., Savin, S.M., Nahon, D.B., Girard, J.P., Lucas, Y., Abel, L.J., 1998. Oxygen isotope geochemistry of kaolinite in laterite-forming processes, Manaus, Amozonas, Brazil. Geochimica et Cosmochimica Acta 62, 1865–1879.
Girard, J.P., Savin, S.M., 1996. Intracrystalline fractionation of oxygen isotopes between hydroxyl and non-hydroxyl sites in kaolinite measured by thermal dehydroxylation and partial fluorination. Geochimica et Cosmochimica Acta 60, 469–487.
Girard, J.P., Fryssinet, P., Gilles, C., 2000. Unraveling climatic changes from intraprofile variation in oxygen and hydrogen isotopic composition of goethite and kaolinite in laterites; an integrated study from Yaou, French Guiana. Geochimica et Cosmochimica Acta 64, 409–426.
Glinski, J., Stepniewski, W., 1985. Soil aeration and its role for plants. CRC, Boca Raton, Florida, USA.
Gluyas, J.G., 1984. Early carbonate diagenesis within Phanerozoic shales and sandstones of the NW European shelf. Clay Minerals 19, 309–321.
Gonfiantini, R., 1986. Environmental isotopes in lake studies. In: Fritz, P., Fontes, J.C. (Eds.), Handbook of Environmental Geochemistry, v. 2, The terrestrial Environment. B. Elsevier, Amsterdam, pp. 113–168.
Gradstein, F.M., Ogg, J.G., Smith, A.G., Bleeker, W., Lourens, L.J., 2004. A new geologic time scale, with special reference to the Precambrian and Neogene. Episodes 27, 83–100.
Graham, A., 1999. Late Cretaceous and Cenozoic history of North American vegetation. Oxford University Press, New York.
Gregory, R.T., 1991. Oxygen isotope history of seawater revisited: time scales for boundary event changes in the oxygen isotope composition of seawater. In: Taylor, H.P., O'Neil, J.R., Kaplan, I.R., I.R. (Eds.), Stable Isotope Geochemistry: A Tribute to Samuel Epstein. The Geochemical Society, San Antonio, U.S.A., pp. 65–76.
Hamer, J.M.M., Sheldon, N.D., Nichols, G.J., 2007a. Global aridity during the Early Miocene? A terrestrial paleoclimate record from the Ebro Basin, Spain. Journal of Geology 115, 601–608.
Hamer, J.M.M., Sheldon, N.D., Nichols, G.J., Collinson, M.E., 2007b. Late Oligocene–Early Miocene palaeosols of distal fluvial systems, Ebro Basin, Spain. Palaeogeography, Palaeoclimatology, Palaeoecology 247, 220–235.
Harnois, L., 1988. The CIW index: a new chemical index of weathering. Sedimentary Geology 55, 319–322.

Harris, C., Compton, J.S., Bevington, S.A., 2000. Oxygen and H isotopes composition of kaolinite deposits, Cape Peninsula, South Africa; low temperature, meteoric origin. Journal of African Earth Sciences 94, 1353–1366.
Hartley, A.J., May, G., 1998. Miocene gypcretes in the Calama Basin, northern Chile. Sedimentology 45, 351–364.
Hasiotis, S.T., 2004. Reconnaissance of Upper Jurassic Morrison Formation ichnofossils, Rocky Mountain Region, USA; paleoenvironmental, stratigraphic, and paleoclimatic significance of terrestrial and freshwater ichnocoenoses. Sedimentary Geology 167, 177–268.
Hassanipak, A.A., Eslinger, E., 1985. Mineralogy, crystallinity, O^{18}/O^{16}, and D/H of Georgia kaolins. Clays and Clay Minerals 33, 99–106.
Hedenquist, J.W., Arribas, A., Reynolds, T.J., 1998. Evolution of an intrusion-centered hydrothermal system; far southeast-Lepanto porphyry and epithermal Cu–Au deposits, Philippines. Economic Geology and the Bulletin of the Society of Economic Geology 93, 373–404.
Hemming, N.G., Hanson, G.N., 1992. Boron isotopic composition and concentration in modern marine carbonates. Geochimica et Cosmochimica Acta 56, 537–543.
Herbillon, A.J., Mestdagh, M.M., Vielvoye, L., Derouane, E.G., 1976. Iron in kaolinites with special reference to kaolinites from tropical soils. Clay Minerals 16, 195–220.
Hessler, A.M., Lowe, D.R., Jones, R.L., Bird, D.K., 2004. A lower limit for atmospheric carbon dioxide levels 3.2 billion years ago. Nature 428, 736–738.
Hill, I.G., Worden, R.H., Meighan, I.G., 2000. Geochemical evolution of a paleolaterite: the Interbasaltic Formation, Northern Ireland. Chemical Geology 166, 65–84.
Hoefs, J., 1997. Stable isotope geochemistry. Springer, Berlin. 201 pp.
Holland, H.D., Zbinden, E.A., 1988. Paleosols and the evolution of the atmosphere: part I. In: Lerman, A., Meybeck, M. (Eds.), Physical and Chemical Weathering in Geochemical Cycles. New York, Kluwer Academic Publishers.
Horton, T.W., Sjostrom, D.J., Abruzzese, M.J., Poage, M.A., Waldbauer, J.R., Hren, M.T., Wooden, J.L., Chamberlain, C.P., 2004. Spatial and temporal variation of Cenozoic surface elevation in the Great Basin and Sierra Nevada. American Journal of Science 304, 862–888.
Hsieh, J.C.C., 1997. An oxygen isotopic study of soil water and pedogenic clays in Hawaii. California Institute of Technology, unpublished Ph.D. Dissertation, 181 pp.
Hsieh, J.C.C., Yapp, C.J., 1999. Stable carbon isotope budget of CO_2 in a wet, modern soil as inferred from $Fe(CO_3)OH$ in pedogenic goethite: possible role of calcite dissolution. Geochimica et Cosmochimica Acta 63, 767–783.
Hyeong, K., Capuano, R.M., 2004. Hydrogen isotope fractionation factor for mixed-layer illite-smectite at 60 degree C to 150 degrees C: new data from the northeast Texas Gulf Coast. Geochimica et Cosmochimica Acta 68, 1529–1543.
Irwin, H., Curtis, C., Coleman, M., 1977. Isotopic evidence for source of diagenetic carbonates fromed during burial of organic-rich sediments. Nature 269, 209–213.
Jackson, M.L., 1964. Chemical composition of soil. In: Bear, F.E. (Ed.), Chemistry of the soil. Reinhold Publishing Corporation, New York, U.S.A., pp. 71–141.
Jackson, M.L., Abdel-Kader, F.H., 1978. Kaolinite intercalation procedure for all sizes and types with X-ray diffraction spacing distinctive from other phyllosilicates. Clays and Clay Minerals 26, 81–87.
Jacobs, B.F., Tabor, N., Feseha, M., Pan, A., Kappelman, J., Rasmussen, T., Sanders, W., Wiemann, M., Crabaugh, J., Massini, J.L.G., 2005. Oligocene terrestrial strata of northwestern Ethiopia: a preliminary report on paleoenvironments and paleontology. Palaeotologia Electronica 8, 25A.
Janis, C.M., Damuth, J., Theodor, J.M., 2002. The origins and evolution of the North American grassland biome: the story from the hoofed mammals. Palaeogeography, Palaeoclimatology, Palaeoecology 177, 183–198.
Jenny, H.J., 1941. Factors of Soil Formation. McGraw-Hill, New York. 281 pp.
Jenny, H.J., Leonard, C.D., 1935. Functional relationships between soil properties and rainfall. Soil Science 38, 363–381.
Johnson, J.W., Oelkers, E.H., Helgeson, H.C., 1992. SUPCRT92: a software package for calculating the standard molal thermodynamic properties of minerals, gases, aqueous species, and reactions from 1 to 5000 bar and 0 to 1000 °C. Computers and Geosciences 18, 899–947.
Kah, L.C., Riding, R., 2007. Mesoproterozoic carbon dioxide levels inferred from calcified cyanobacteria. Geology 35, 799–802.
Kahmann, J.A., Seaman III, J., Driese, S.G., 2008. Evaluating trace elements as paleoclimate indicators: multivariate statistical analysis of late Mississippian Pennington Formation Paleosols, Kentucky, USA. Journal of Geology 116, 254–268.
Kakihana, H., Kotaka, M., Satoh, S., Nomura, M., Okamoto, M., 1977. Fundamental studies on the ion-exchange separation of boron isotopes. Bulletin of the Chemical Society of Japan 50, 158–163.
Kasting, J.F., 1993. Earth's early atmosphere. Science 259, 920–926.
Kasting, J.F., 2004. Archaean atmosphere and climate. Nature 432. doi:10.1038/nature03166.
Keeling, C.D., Whorf, T.P., Wahlen, M., Plikcht, J., 1995. Interannual extremes in the rate of rise of atmospheric carbon dioxide since 1980. Nature 375, 666–670.
Keller, W.D., 1963. Diagenesis in clay minerals; a review. Clays and Clay Minerals 13, 136–157.
Kemp, R.A., Zarate, M., Toms, P., King, M., Sanabria, J., Arguello, G., 2006. Late Quaternary paleosols, stratigraphy and landscape evolution in the Northern Pampa, Argentina. Quaternary Research 66, 119–132.
Kenny, R., Neet, K.E., 1993. Upper Pennsylvanian-Permian (Naco Group) paleosols (north-Central Arizona): field and isotopic evidence. Geoderma 58, 131–148.
Keyser, T.K., Kerrich, R., 1991. Retrograde exchange of hydrogen isotopes between hydrous minerals and water at low temperatures. In: Taylor, H.P., O'Neil, J.R., Kaplan, I.R. (Eds.), Stable Isotope Geochemistry: A Tribute to Samuel Epstein. The Geochemical Society, San Antonio, U.S.A., pp. 409–422.
Kim, S.-T., O'Neil, J.R., 1997. Equilibrium and nonequilibrium oxygen isotope effects in synthetic carbonates. Geochimica et Cosmochimica Acta 61, 3461–3475.
Kingston, J.D., Marino, B.D., Hill, A., 1994. Isotopic evidence for Neogene hominid paleoenvironments in the Kenya Rift Valley. Science 264, 955–959.
Kirkland, J.I., 2006. Fruita paleontological area (Upper Jurassic, Morrison Formation), western Colorado: an example of terrestrial taphofacies analysis. In: Foster, J.R., Lucas, S.G. (Eds.), Paleontology and Geology of the Upper Jurassic Morrison Formation. New Mexico Museum of Natural History, vol. 36, pp. 67–95.
Kisakürek, B., Widdowson, M., Jame, R.H., 2004. Behaviour of Li isotopes during continental weathering: the Bidar laterite profile, India. Chemical Geology 212, 27–44.
Knapp, A.K., Conrad, S.L., Blair, J.M., 1998. Determinants of soil CO_2 flux from a sub-humid grassland: effect of fire and fire history. Ecological Applications 8, 760–770.
Koch, P.L., 1998. Isotopic reconstruction of past continental environments. Annual Reviews of Earth Planetary Sciences 26, 573–612.
Koch, P.L., Zachos, J.C., Dettman, D.L., 1995. Stable isotope stratigraphy and paleoclimatology of the Paleogene Bighorn Basin (Wyoming, USA). Palaeogeography Palaeoclimatology Palaeoecology 115, 61–89.
Koch, P.L., Clyde, W.C., Hepple, R.P., Fogel, M.L., Wing, S.L., Zachos, J.C., 2003. Carbon and oxygen isotope records from paleosols spanning the Paleocene–Eocene boundary, Bighorn Basin, Wyoming. In: Wing, S.L., Ginerich, P.D., Schmitz, B., Thomas, E. (Eds.), Causes and Consequences of Globally Warm Climates in the Early Paleogene. Geological Society of America Special Paper, vol. 369, pp. 49–64. Boulder, Colorado.
Kohur, C., Muehlenbachs, K., Dudas, M.J., 1995. Authigenic dolomite in a saline soil in Alberta, Canada. Soil Science Society of America Journal 59, 1499–1504.
Koppi, A.J., Edis, R., Field, D.J., Geering, H.R., Klessa, D.A., Cockayne, D.J.H., 1996. Rare earth element trends and cerium–uranium–manganese associations in weathered rock from koongarra, Northern Territory, Australia. Geochimica et Cosmochimica Acta 60, 1695–1707.
Koster, H.M., Ehricher, U., Gilg, H.A., Jordan, R., Murad, E., Onnich, K., 1999. Mineralogical and chemical characteristic of five nontronites and Fe-rich smectites. Clay Minerals 34, 579–599.
Kraus, M.J., 1987. Integration of channel and floodplain suites: II. Lateral relations of alluvial paleosols. Journal of Sedimentary Petrology 57, 602–612.
Kraus, M.J., 1997. Lower Eocene alluvial paleosols; pedogenic development, stratigraphic relationships, and paleosol/landscape associations. Palaeogeography, Palaeoclimatology, Palaeogeography 129, 387–406.
Kraus, M.J., 1999. Paleosols in clastic sedimentary rocks: their geologic applications. Earth-Science Reviews 47, 41–70.
Kraus, M.J., Aslan, A., 1993. Eocene hydromorphic paleosols: significance for interpreting ancient floodplain processes. Journal of Sedimentary Petrology 63, 453–463.
Kraus, M.J., Hasiotis, S.J., 2006. Significance of different modes of rhizolith preservation to interpreting paleoenvironmental and paleohydrologic settings: examples from Paleogene paleosols, Bighore Basin, Wyoming, U.S.A. Journal of Sedimentary Research 76, 633–646.
Kraus, M.J., Riggins, S., 2007. Transient drying during the Paleocene–Eocene Thermal Maximum (PETM): analysis of paleosols in the Bighorn Basin, Wyoming. Palaeogeography, Palaeoclimatology, Palaeoecology 245, 444–461.
Krishnamurthy, R.V., Bhattacharya, S.K., 1991. Stable oxygen and hydrogen isotope ratios in shallow ground waters from India and a study of the role of evapotranspiration in the Indian monsoon. In: Taylor, H.P., O'Neil, J.R., Kaplan, I.R. (Eds.), Stable Isotope Geochemistry: A Tribute to Samuel Epstein. The Geochemical Society, San Antonio, U.S.A., pp. 187–193.
Krull, E.S., Retallack, G.J., 2000. $\delta^{13}C$ depth profiles from paleosols across the Permian–Triassic boundary: evidence for methane release. Geological Society of America Bulletin 112, 1459–1472.
Kürschner, W.M., Kvacek, Z., Dilcher, D.L., 2008. The impact of Miocene atmospheric carbon dioxide fluctuations on climate and the evolution of terrestrial ecosystems. Proceedings of the National Academy of Sciences 105, 449–453.
Kurtz, A.C., Derry, L.A., Chadwick, O.A., Alfano, M.J., 2000. Refractory element mobility in volcanic soils. Geology 28, 683–686.
Landuyt, C.J., 1990. Micromorphology of iron minerals from bog ores of the Belgian Campine area. In: Douglas, L.A. (Ed.), Soil Micromorphology: A basic and applied science. Developments in Soil Science, vol. 19. Elsevier, Amsterdam, pp. 289–294.
Latorre, C., Quade, J., McIntosh, W.C., 1997. The expansion of C_4 grasses and global climate change in the late Miocene: stable isotope evidence from the Americas. Earth and Planetary Science Letters 146, 83–96.
Lawrence, J.R., Taylor, H.P., 1971. Deuterium and ^{18}O correlation: clay minerals and hydroxides in Quaternary soils compared to meteoric waters. Geochimica et Cosmochimica Acta 34, 25–42.
Lawrence, J.R., Rashkes Meaux, J., 1993. The stable isotopic composition of ancient kaolinites of North America. In: Swart, P.K., Lohmann, K.C., McKenzie, J., Savin, S. (Eds.), In Climate Change in Continental Isotopic Records. Geophysical Monograph, vol. 78, pp. 249–262.
Lawrence, J.R., Taylor, H.P., 1972. Hydrogen and oxygen isotope systematics in weathering profiles. Geochimica et Cosmochimica Acta 36, 1377–1393.
Lawrence, J.R., White, J.W.C., 1991. The elusive climate signal in the isotopic composition of precipitation. In: Taylor, H.P., O'Neil, J.R., Kaplan, I.R. (Eds.), Stable Isotope Geochemistry: A Tribute to Samuel Epstein. The Geochemical Society, San Antonio, U.S.A., pp. 169–185.
Lawton, T., Buck, B.J., 2006. Implications of diapir-derived detritus and gypsic paleosols in Lower Triassic strata near the Castle Valley salt wall, Paradox basin, Utah. Geology 34, 885–888.
Laza, J.H., 2006. Termiteros del Plioceno y Pleistoceno de la provincial de Buenos Aires, Rupublica Argentina: significacion paleoambiental y paleozoogeographica (Pliocene–Pleistocene termite mounds of Buenos Aires Province, Argentina: paleoenvironmental and paleozoogeographical significance. Ameghiniana 43, 641–648.

Leckie, D.A., Fox, C., Tarocai, C., 1989. Multiple paleosols of the Late Albian Boulder Creek Formation, British Columbia, Canada. Sedimentology 36, 307–323.
Leopold, E.B., Clay-Poole, S.T., 2001. Florissant leaf and pollen floras of Colorado compared: climatic implications. Proceedings of the Denver Museum of Natural History 4, 17–69.
Levin, N.E., Quade, J., Simpson, S.W., Semaw, S., Rogers, M., 2004. Isotopic evidence for Plio-Pleistocene environmental change at Gona, Ethiopia. Earth and Planetary Science Letters 219, 92–110.
Li, Y.-H., 2000. A Compendium of Geochemistry. Princeton University Press, Princeton. 475 pp.
Loisy, C., Verrecchia, E.P., Dufour, P., 1999. Microbial origin for pedogenic micrite associated with a carbonate paleosol (Champagne, France). Sedimentary Geology 126, 193–204.
Ludvigson, G.A., Gonzalez, L.A., Metzger, R.A., Witzke, B.J., Brenner, R.L., Murillo, A.P., White, T.S., 1998. Meteoric sphaerosiderite lines and their use for paleohydrology and paleoclimatology. Geology 26, 1039–1042.
Macaulay, C.I., Fallick, A.E., Haszeldine, R.S., 1993. Textural and isotopic variations in diagenetic kaolinite from the Magnus oilfield sandstones. Clay Minerals 28, 625–639.
Machette, M.N., 1985. Calcic soils the southwestern United States. Geological Society of America Special Paper 203, 1–22.
Mack, G.H., Cole, D.R., 2005. Geochemical model of $\delta^{18}O$ of pedogenic calcite versus latitude and its application to Cretaceous palaeoclimate. Sedimentary Geology 174, 115–122.
Mack, G.H., Cole, D.R., Giordano, T.H., Schaal, W.C., Barcelos, J.H., 1991. Paleoclimatic controls on stable oxygen and carbon isotopes in caliche of the Abo Formation (Permian), south-central New Mexico, U.S.A. Journal of Sedimentary Petrology 61, 458–472.
Mack, G.H., James, W.C., Monger, H.C., 1993. Classification of paleosols. Geological Society of America Bulletin 105, 129–136.
Mack, G.H., Tabor, N.J., Zollinger, H.J., in revision. Paleosols and sequence stratigraphy of the lower Permian Abo member, south-central New Mexico. Journal of Sedimentary Research.
Macleod, K.G., Smith, R.M.H., Koch, P.L., Ward, P.D., 2000. Timing of mammal-like reptile extinctions across the Permian–Triassic boundary in South Africa. Geology 28, 227–230.
Magaritz, M., Amiel, A.J., 1980. Calcium carbonate in a calcareous soil from the Jordan Valley, Israel; its origin as revealed by the stable carbon isotope method. Soil Science Society of America Proceedings 44, 1059–1062.
Magaritz, M., Kaufman, A., Yaalon, D.H., 1981. Calcium carbonate nodules in soil; $^{18}O/^{16}O$ and $^{13}C/^{12}C$ ratios and ^{14}C contents. Geoderma 25, 157–172.
Majoube, M., 1971. Oxygen-18 and deuterium fractionation between water and steam. Journal de Chimie Physique et de Physico-Chimie Biologique 68, 1423.
Marbut, C.F., 1935. Atlas of American Agriculture, Part III, Soils of the United States. United States Department of Agriculture Advance Sheets 8. Washington (D.C.), US Government Printing Office.
Marfil, S.A., Maiza, P.J., Cardellach, E., Corbella, M., 2005. Origin of kaolin deposits in the 'Los Menucos" area, Rio Negro Province, Argentina. Clay Minerals 40, 283–293.
Markewich, H.W., Pavich, M.J., Buell, G.R., 1990. Contrasting soils and landscapes of the Piedmont and Coastal Plain, eastern United States. Geomorphology 3, 417–447.
Marumo, K., 1989. Genesis of kaolin minerals and pyrophyllite in Kuroko deposits of Japan: Implications for the origins of the hydrothermal fluids from mineralogical and stable isotope data. Geochimica et Cosmochimica Acta 53, 2915–2924.
Matsumoto, R., Iijima, A., 1981. Origin and diagenetic evolution of Ca–Mg–Fe carbonates in some coalfields of Japan. Sedimentology 28, 239–259.
Matthews, A., Ayalon, A., Ziz, A., Shaked, J., 1999. Hydrogen and oxygen isotope studies of alteration in the Timna Igneous Complex. Israel Journal of Earth Science 48, 121–131.
Maynard, J.B., 1992. Chemistry of modern soils as a guide to interpreting Precambrian paleosols. Journal of Geology 100, 279–289.
McCarthy, P.J., Plint, A.G., 2003. Spatial variability of paleosols across Cretaceous interfluves in the Dunvegan Formation, NE British Columbia, Canada: palaeohydrological and stratigraphic implications. Sedimentology 50, 1187–1220.
McCrea, J.M., 1950. On the isotope chemistry of carbonates and paleotemperature scale. Journal of Chemical Physics 18, 849–857.
McFadden, L.D., Tinsley, J.C., 1985. Rate and depth of pedognic-carbonate accumulation in soils: Formulation and testing of a compartment model. In: Wiede, D.L. (Ed.), Soils and Quaternary geology of the southwestern United States. Geological Society of America Special Paper, vol. 203, pp. 23–41.
McFadden, I.D., Amundson, R.G., Chadwick, O.A., 1991. Numerical modeling, chemical and isotopic studies of carbonate accumulation in arid regions. In: Nettleton, W.D. (Ed.), Occurrence, Characteristics and Genesis of Carbonate, Gypsum, and Silica Accumulation in Soils. Soil Science Society of America Special Publication, vol. 26, pp. 17–35.
McMillan, M., Schwertmann, U., 1988. Morphological and genetic relations between siderite, calcite and goethite in a low moor peat from southern Germany. European Journal of Soil Science 49, 283–293.
Melezhik, V.A., Fallick, A.E., Smith, R.A., Rosse, D.M., 2007. Spherical and columnar, spetarian, ^{18}O depleted, calcite concretions from Middle–Upper Permian lacustrine siltstones in northern Mozambique; evidence for very early diagenesis and multiple fluids. Sedimentology 54, 1389–1416.
Metzger, C.A., Terry III, D.O., Grandstaff, D.E., 2004. Effect of paleosol formation on rare earth element signatures in fossil bone. Geology 32, 497–500.
Mizota, C., Longstaffe, F.J., 1996. Origin of Cretaceous and Oligocene Kaolinites from the Iwaizumi clay deposit, Iwate, northeastern Japan. Clays and Clay Minerals 44, 408–416.
Montañez, I.P., Tabor, N.J., Niemeier, D., DiMichele, W.A., Frank, T.D., Fielding, C.R., Isbell, J.L., 2007. CO_2-forced climate and vegetation instability during late Paleozoic deglaciation. Science 315, 87–91.
Moore, D.M., Reynolds Jr., R.C., 1996. X-ray diffraction and the identification of clay minerals. Oxford University of Press, New York, U.S.A.
Mora, C.I., Driese, S.G., 1993. A steep mid Paleozoic to late Paleozoic decline in atmospheric CO_2 – evidence from the soil carbonate CO_2 palebarometer. Chemical Geology 107, 217–219.
Mora, C.I., Driese, S.G., Colarusso, L.A., 1996. Middle to late Paleozoic atmospheric CO_2 levels from soil carbonate and organic matter. Science 271, 1105–1107.
Mozley, P.S., 1988. Relation between depositional environment and elemental composition of early diagenetic siderite. Geology 17, 704–706.
Mozley, P.S., Carothers, W.W., 1992. Elemental and isotopic composition of siderite in the Daruk Formation, Alaska: effect of microbial activity and water-sediment interaction on early pore-water chemistry. Journal of Sedimentary Petrology 62, 681–692.
Mozley, P.S., Wersin, P., 1992. Isotopic composition of siderite as an indicator of depositional environment. Geology 20, 817–820.
Muchez, P., Peeters, C., Keppens, E., Viaene, W.A., 1993. Stable isotopic composition of paleosols in the Lower Visean of eastern Belgium – evidence of evaporation and soil-gas CO_2. Chemical Geology 106, 389–396.
Mulch, A., Chamberlain, C.P., 2006. Stable isotope paleoaltimetry in orogenic belts; the silicate record in surface and crustal geological archives. In: Kohn, M.J. (Ed.), Paleoaltimetry; geochemical and thermodynamic approaches. Reviews in Mineralogy and Geochemistry, vol. 66, pp. 89–118.
Muller, J., 1995. Oxygen isotopes in iron (III) oxides: a new preparation line; mineral-water fractionation factors and paleoenvironmental considerations. Isotopes and Environmental Health Studies 31, 301–302.
Munsterman, D., Kerstholt, S., 1996. Sodium polytungstate, a new non-toxic alternative to bromoform in heavy liquid separation. Review of Paleobotany and Palynology 91, 417–422.
Murakami, T., Ito, J.-I., Utsunomiya, S., Kasama, T., Kozai, N., Ohnuki, T., 2004. Anoxic dissolution processes of biotite: implications for Fe behavior during Archean weathering. Earth and Planetary Science Letters 224, 117–129.
Nadon, G.C., Issler, D.R., 1997. The compaction of floodplain sediments: timing, magnitude and implications. Geoscience Canada 24, 37–43.
Nakamura, N., 1974. Determination of REE, Ba, Fe, Mg, Na and K in carbonaceous and ordinary chondrites. Geochimica et Cosmochimica Acta 38, 757–775.
Nash, V.E., Pettry, D.E., Mohd Noor Sudin, 1988. Mineralogy and chemical properties of two Ultisols formed in glauconitic sediments. Soil Science 145, 270–277.
Nesbitt, H.W., Markovics, G., 1997. Weathering of granodioritic crust, long term storage of elements in weathering profiles, and petrogenesis of siliclastic sediments. Geochimica et Cosmochimica Acta 61, 1653–1670.
Nesbitt, H.W., Young, G.M., 1982. Early Proterozoic climates and plate motions inferred from major element chemistry of lutites. Nature 299, 715–717.
Nordt, L., Atchley, S., Dworkin, S.I., 2002. Paleosol barometer indicates extreme fluctuations in atmospheric CO_2 across the Cretaceous-Tertiary boundary. Geology 30, 703–706.
Nordt, L., Atchley, S., Dworkin, S., 2003. Terrestrial evidence for two greenhouse events in the latest Cretaceous. Geological Society of America Today 13, 11, 4–9.
Nordt, L., Orosz, M., Driese, S., Tubbs, J., 2006. Vertisol carbonate properties in relation to mean annual precipitation: implications for paleoprecipitation estimates. Journal of Geology 114, 501–510.
O'Geen, A.T., Busacca, A.J., 2001. Faunal burrows as indicators of paleo-vegetation in eastern Washington, USA. Palaeogeogeography, Palaeoclimatology, Palaeoecology 169, 23–37.
O'Neil, J.R., Kharaka, Y.K., 1976. Hydrogen and oxygen isotope exchange reactions between clay minerals and water. Geochimica et Cosmochimica Acta 40, 241–246.
O'Neil, J.R., Clayton, R.N., Mayeda, T.K., 1969. Oxygen isotope fractionation in divalent metal carbonates. Journal of Chemical Physics 51, 5547–5558.
Ohmoto, H., Watanabe, Y., Kumazawa, K., 2004. Evidence from massive siderite beds for a CO_2-rich atmosphere before ~1.8 billion years ago. Nature 429, 395–399.
Osborne, M., Haszeldine, R.S., Fallick, A.E., 1994. Variation in kaolinite morphology with growth temperature in isotopically mixed pore fluids, Brent Group, UK North Sea. Clay Minerals 29, 591–608.
Pagani, M., Freeman, K.H., Arthur, M.A., 1999. Late Miocene atmospheric CO_2 concentration and the expansion of C_4 grasses. Science 285, 876–878.
Palandri, J.L., Reed, M.H., 2001. Reconstruction of in situ composition of sedimentary formation waters. Geochimica et Cosmochimica Acta 65, 1741–1767.
Parnell, J., Baron, M., Boyce, A., 2000. Controls on kaolinite and dickite distribution; Highland boundary fault zone; Scotland and Northern Ireland. Journal of the Geological Society 157, 635–640.
Parnell, J., Watt, G., Chen, H., Wycherley, H., Boyce, A., Elmore, D., Blumstein, R., Engel, M., Green, P., 2004. Kaolin polytype evidence for a hot-fluid pulse along Caledonian thrusts during rifting of the European margin. Mineralogical Magazine 68, 419–432.
Passey, B.H., Cerling, T.E., Perkins, M.E., Voorhies, M.R., Harris, J.M., Tucker, S.T., 2002. Environmental change in the Great Plains: an isotopic record from fossil horses. Journal of Geology 110, 123–140.
Pavlov, A.A., Hurtgen, M.T., Kasting, J.F., Arthur, M.A., 2003. Methane-rich Proterozoic atmosphere? Geology 31, 87–90.
Pavlov, A.A., Kasting, J.F., Brown, L.L., Rages, K.A., Freedman, R., 2000. Greenhouse warming by CH_4 in the atmosphere of early Earth. Journal of Geophysical Research 105, 11,981–119,990.
Pearson, M.J., 1979. Geochemistry of the Hepworth Carboniferous sediment sequence and origin of the diagenetic iron minerals and concretions. Geochimica et Cosmochimica Acta 43, 927–941.

Pedro, G., 1982. The conditions of formation of secondary constituents. In: Bonneau, M., Souchier, B. (Eds.), Constituents and properties of soils. Academic Press, London, pp. 63–81.
Perez-Huerta, A., Sheldon, N.D., 2006. Pennsylvanian sea level cycles, nutrient availability, and brachiopod community structure. Palaeogeography, Palaeoclimatology, Palaeoecology 230, 264–279.
Peters-Kottig, W., Strauss, H., Kerp, H., 2006. The land plant $\delta^{13}C$ record and plant evolution in the Late Palaeozoic. Palaeogeography, Palaeoclimatology, Palaeoecology 240, 237–252.
Pett-Ridge, J.C., Monastra, V.M., Derry, L.A., Chadwick, O.A., 2007. Importance of atmospheric inputs and Fe-oxides in controlling soil uranium budgets and behavior along a Hawaiian chronosequences. Chemical Geology 244, 691–707.
Poage, M.A., Chamberlain, C.P., 2001. Empirical relationships between elevation and the stable isotope composition of precipitation and surface waters: considerations for studies of paleoelevation change. American Journal of Science 301, 1–15.
Postma, D., 1981. Formation of siderite and vivianite and the pore-water composition of a recent bog sediment in Denmark. Chemical Geology 31, 225–244.
Postma, D., 1982. Pyrite and siderite formation in brackish and freshwater swamp sediments. American Journal of Science 282, 1151–1183.
Postma, D., 1983. Pyrite and siderite oxidation in swamp sediments. European Journal of Soil Science 34, 163–182.
Poulsen, C.J., 1999. The mid-Cretaceous ocean circulation and its impact on greenhouse climate dynamics (Ph.D. thesis): University Park, Pennsylvania State University, 219 p.
Prochnow, S.J., Nordt, L.C., Atchley, S.C., Hudec, M.R., 2006. Multi-proxy paleosol evidence for middle and late Triassic climate trends in eastern Utah. Palaeogeography, Palaeoclimatology, Palaeoecology 232, 53–72.
Purvis, K., Wright, V.P., 1991. Calcretes related to phreatic vegetation from the Middle Triassic Otter Sandstone of south west England. Sedimentology 38, 539–551.
Pye, K., Dickson, J.A.D., Schiavon, N., Coleman, M.L., Cox, M., 1990. Formation of Siderite-Mg-Calcite-iron sulphide concretions in intertidal marsh and sandflat sediments, north Norfolk, England. Sedimentology 37, 325–343.
Quade, J., Cerling, T.E., 1995. Expansion of C4 grasses in the late Miocene of northern Pakistan: evidence from stable isotopes in paleosols. Palaeogeography, Palaeoclimatology, Palaeoecology 115, 91–116.
Quade, J., Cerling, T.E., Bowman, J.R., 1989. Development of Asian monsoon revealed by marked ecological shift during the latest Miocene in northern Pakistan. Nature 342, 162–166.
Quade, J., Solounias, N., Cerling, T.E., 1994. Stable isotopic evidence from paleosol carbonates and fossil teeth in Greece for forest or woodlands over the past 11 Ma. Palaeogeography, Palaeoclimatology, Palaeoecology 108, 41–53.
Quade, J., Cater, J.M.L., Ojha, T.P., Adam, J., Harrison, T.M., 1995. Late Miocene environmental change in Nepal and the northern Indian sub-continent: Stable isotopic evidence from paleosols. Geology Society of America Bulletin 107, 1381–1397.
Quade, J., Levin, N., Semaw, S., Stout, D., Renne, R., Rogers, M., Simpson, S., 2004. Paleoenvironments of the earliest stone toolmakers, Gona, Ethiopia. Geological Society of America Bulletin 116, 1529–1544.
Quade, J., Garzione, C., Eiler, J., 2007. Paleoelevation reconstruction using pedogenic carbonates. Reviews in Mineralogy and Geochemistry 66, 53–87.
Rabenhorst, M.C., Wilding, L.P., West, L.T., 1984. Identification of pedogenic carbonates using stable carbon isotope microfabric analysis. Soil Science Society of America Journal 48, 125–132.
Rasmussen, C., Tabor, N.J., 2007. Applying a quantitative pedogenic energy model across a range of environmental gradients. Soil Science Society of America Journal 71, 1719–1729.
Rasmussen, C., Southard, R.J., Horwath, W.R., 2005. Modeling energy inputs to predict pedogenic environments using regional environmental databases. Soil Science Society of America Journal 69, 1266–1274.
Retallack, G.J., 1976. Triassic palaeosols in the Upper Narrabeen Group of New South Wales. Part I: features of the palaeosols. Journal of the Geological Society of Australia 23, 383–399.
Retallack, G.J., 1983. Late Eocene and Oligocene paleosols from Badlands National Park, South Dakota. Geological Society of America Special Paper 193 82 pp.
Retallack, G.J., 1986. Reappraisal of a 2200 Ma-old paleosol from near Waterval Onder, South Africa. Precambrian Research 2, 195–232.
Retallack, G.J., 1991. Untangling the effects of burial alteration and ancient soil formation. Annual Review of Earth Planetary Sciences 19, 183–206.
Retallack, G.J., 1994. The environmental factor approach to the interpretation of paleosols. In: Amundson, R., et al. (Ed.), Factors in soils formation: A fiftieth anniversary retrospective. Soil Science Society of America Special Publication, vol. 33, pp. 31–64.
Retallack, G.J., 1997a. Early forest soils and their role in Devonian global change. Science 276, 583–585.
Retallack, G.J., 1997b. Neogene expansion of the North American prairie. Palaios 12, 380–390.
Retallack, G.J., 1997c. Palaeosols in the upper Narrabeen Group of New South Wales as evidence of Early Triassic palaeoenvironments without modern analogues. Australian Journal of Earth Sciences 44, 185–201.
Retallack, G.J., 1999. Post-apocalyptic greenhouse paleoclimate revealed by earliest Triassic paleosols in the Sydney Basin, Australia. Geological Society of America Bulletin 111, 52–70.
Retallack, G.J., 2000. Depth to pedogenic carbonate horizon as a paleoprecipitation indicator? comment and reply. Geology 28, 572–573.
Retallack, G.J., 2001a. Cenozoic expansion of grasslands and climatic cooling. The Journal of Geology 109, 407–426.
Retallack, G.J., 2001b. Soils of the past. Blackwell, Oxford. 600 pp.
Retallack, G.J., 2002. Carbon dioxide and climate over the past 300 million years. Philosophical Transations of the Royal Society of London 360, 659–673.
Retallack, G.J., 2005a. Earliest Triassic claystone breccias and soil-erosion crisis. Journal of Sedimentary Research 75, 679–695.
Retallack, G.J., 2005b. Pedogenic carbonate proxies for amount and seasonality of precipitation in paleosols. Geology 33, 333–336.
Retallack, G.J., 2007. Cenozoic paleoclimate on land in North America. Journal of Geology 115, 271–294.
Retallack, G.J., Feakes, C.R., 1987. Trace fossil evidence for Late Ordovician animals on land. Science 235, 499–502.
Retallack, G.J., Germán-Heins, J., 1994. Paleosol evidence for the geological antiquity of rain forests. Science 265, 499–502.
Retallack, G.J., Jahren, H., 2008. Methane release from igneous intrusion of coal during late Permian extinction events. Journal of Geology 116, 1–20.
Retallack, G.J., Krinsley, D.H., 1993. Metamorphic alteration of a Precambrian (2.2 Ga) paleosol from South Africa revealed by backscattered electron imaging. Precambrian Research 63, 27–41.
Retallack, G.J., Krull, E.S., 1999. Landscape ecological shift at the Permian–Triassic boundary in Antarctica. Australian Journal of Earth Sciences 46, 785–812.
Retallack, G.J., Mindszenty, A., 1994. Well preserved Late Precambrian paleosols from northwest Scotland. Journal of Sedimentary Research A64, 264–281.
Retallack, G.J., Veevers, J.J., Morante, R., 1996. Global coal gap between Permian-Triassic extinction and Middle Triassic recovery of peat-forming plants. Geological Society of America Bulletin 108, 195–207.
Retallack, G.J., Bestland, E.A., Fremd, T., 2000. Eocene and Oligocene paleosols and environmental change in central Oregon. Geological Society of America Special Paper 344 192 pp.
Retallack, G.J., Jahren, H., Sheldon, N.D., Chakrabarti, R., Metzger, C.A., Smith, R.M.H., 2005. The Permian–Triassic boundary in Antarctica. Antarctic Science 17, 241–258.
Retallack, G.J., Smith, R.M.H., Ward, P.D., 2003. Vertebrate extinction across Permian–Triassic boundary in Karoo basin, South Africa. Geological Society of American Bulletin 115, 1133–1152.
Retallack, G.J., Orr, W.N., Prothero, D.R., Duncan, R.A., Kester, P.R., Ambers, C.P., 2004a. Eocene–Oligocene extinction and climate change near Eugene, Oregon. Geological Society of America Bulletin 116, 817–839.
Retallack, G.J., Wynn, J.G., Fremd, T.J., 2004b. Glacial–interglacial scale paleoclimatic change without large ice sheets in the Oligocene of central Oregon. Geology 32, 297–300.
Robertson, J.A., Gazis, C.A., 2005. An oxygen isotope study of seasonal trends in soil water fluxes at two sites along a climate gradient in Washington State (USA). Journal of Hydrology 328, 375–387.
Robinson, S.A., Andrews, J.E., Hesselbo, S.P., Radley, J.D., Denni, P.F., Harding, I.C., Allen, P., 2002. Atmospheric pCO_2 and depositional environment from stable-isotope geochemistry of calcrete nodules (Barremian, Lower Cretaceous, Wealden Beds, England). Journal of the Geological Society 159, 215–224.
Rolston, D.E., 1986. Gas diffusivity. In methods of soil analysis, Part 1. Physical and mineralogical methods, second edition. In: Klute, A. (Ed.), American Society of Agronomy and Soil Science Society of America, Madison, Wisconsin, USA. Agricultural Monograph, vol. 9, pp. 1089–1102.
Rowley, D.B., Currie, B.S., 2006. Palaeo-altimetry of the late Eocene to Miocene Lunpola Basin, central Tibet. Nature 439, 677–681.
Rowley, D.B., Garzione, C.N., 2007. Stable isotope-based paleoaltimetry. Annual Review of Earth and Planetary Sciences 35, 463–508.
Royer, D.L., 1999. Depth to pedogenic carbonate horizon as a paleoprecipitation indicator? Geology 27, 1123–1126.
Royer, D.L., Berner, R.A., Beerling, D.J., 2001a. Phanerozoic atmospheric CO_2 change; evaluating geochemical and paleobiological approaches. Earth Science Reviews 54, 349–392.
Royer, D.L., Wing, S.L., Beerling, D.J., Jolley, D.W., Koch, P.L., Hickey, L.H., Berner, R.A., 2001b. Paleobotanical evidence for near present day levels of atmospheric CO_2 during part of the Tertiary. Science 292, 2310–2313.
Royer, D.L., Berner, R.A., Montañez, I.P., Tabor, N.J., Beerling, D.J., 2004. CO_2 as a primary driver of Phanerozoic climate change. GSA Today 14 (3), 4–10.
Rozanski, K., Araguas-Araguas, L., Gonfiantini, R., 1993. Isotopic patterns in modern global precipitation. In: Swart, P.K., Lohmann, K.C., McKenzie, J., Savin, S. (Eds.), Climate Change in Continental Isotopic Records. Geophysical Monograph, vol. 78, pp. 1–36.
Ruskin, B.G., Jordan, T.E., 2007. Climate change across continental sequence boundaries: paleopedology and lithofaces of the Iglesia Basin, northwestern Argentina. Journal of Sedimentary Research 77, 661–679.
Ruxton, B.P., 1968. Measures of the degree of chemical weathering of rocks. Journal of Geology 76, 518–527.
Rye, R., Holland, H.D., 1998. Paleosols and the evolution of atmospheric oxygen: a critical review. American Journal of Science 298, 621–672.
Rye, R., Holland, H.D., 2000. Geology and geochemistry of paleosols developed on the Hekpoort Basalt, Pretoria Group, South Africa. American Journal of Science 300, 85–141.
Rye, R., Kuo, P.H., Holland, H.D., 1995. Atmospheric carbon dioxide concentrations before 2.2 billion years ago. Nature 378, 603–605.
Salomons, W., Goudie, A.S., Mook, W.G., 1978. Isotopic composition of calcrete deposits from Europe, Africa and India. Earth Surface Processes 3, 43–47.
Sanyal, A., Hemming, N.G., Broecker, W.S., Lea, D.W., Spero, H.J., Hanson, G.N., 1996. Oceanic pH control on the boron isotopic composition of foraminifera: evidence from culture experiments. Paleoceanography 11, 513–517.
Sanyal, P., Bhattacharya, S.K., Kumar, R., Ghosh, S.K., Sangode, S.J., 2004. Mio-Pliocene monsoonal record from Himalayan foreland basin (Indian Siwalik) and its relation

to vegetational change. Palaeogeography, Palaeoclimatology, Palaeoecology 205, 23–41.
Sarkar, A., Sarangi, S., Bhattacharya, S.K., Ray, A.K., 2003. Carbon isotopes across the Eocene-Oligocene boundary sequence of Kutch, western India: implications from oceanic productivity and pCO2 change. Geophysical Research Letters 30, 42-1–42-4.
Savin, S.M., Epstein, S., 1970a. The oxygen and hydrogen geochemistry of clay mineral. Geochimica et Cosmochimica Acta 34, 25–42.
Savin, S.M., Epstein, S., 1970b. The oxygen and hydrogen isotope geochemistry of ocean sediments and shales. Geochimica et Cosmochimica Acta 34, 43–63.
Savin, S.M., Hsieh, J.C.C., 1998. The hydrogen and oxygen isotope geochemistry of pedogenic lay minerals; principles and theoretical background. Geoderma 82, 227–253.
Savin, S.M., Lee, M., 1988. Isotopic studies of phyllosilicates. Reviews in Mineralogy 19, 189–223.
Sayyed, M.R., Hundekari, S.M., 2006. Preliminary comparison of ancient bole beds and modern soils developed upon the Deccan volcanic basalts around Pune (India): potential for paleoenvironmental reconstruction. Quaternary International 156–157, 189–199.
Schaetzl, R.J., Anderson, S., 2005. Soils; genesis and geomorphology. Cambridge University Press, New York. 817 pp.
Schlesinger, W.H., 1985. The formation of caliche soils in the Mojave Desert, California. Geochimica et Cosmochimica Acta 49, 57–66.
Schlesinger, W.H., 1997. Biogeochemistry: an analysis of global change. Academic Press, San Diego. 588 pp.
Schroeder, P.A., Melear, N.D., 1999. Stable carbon isotope signatures preserved in authigenic gibbsite from a forested granitic-regolith: Panola Mt., Georgia, USA. Geoderma 91, 261–279.
Schroeder, P.A., Austin, J.C., Dowd, J.F., 2006. Estimating long-term soil respiration rates from carbon isotopes occluded in gibbsite. Geochimica et Cosmochimica Acta 70, 5692–5697.
Sclater, J.G., Christie, P.A.F., 1980. Continental stretching: an explanation of post-mid-Cretaceous subsidence of the central North Sea basin. Journal of Geophysical Research 85, 3711–3939.
Scotchman, I.C., 1991. The geochemistry of concretions from the Kimmeridge Clay Formation of southern and eastern England. Sedimentology 38, 79–106.
Semeniuk, V., Meagher, T.D., 1981. Calcrete in Quaternary coastal dunes in southwestern Australia; a capillary-rise phenomenon associated with plants. Journal of Sedimentary Research 51, 47–68.
Sharp, Z., 2007. Principles of Stable isotope Geochemistry. Prentice Hall, New York. 360 pp.
Sheldon, N.D., 2003. Pedogenesis and geochemical alteration of the picture gorge subgroup, Columbia River Basalt, Oregon. Geological Society of America Bulletin 115, 1377–1387.
Sheldon, N.D., 2005. Do red beds indicate paleoclimatic conditions? a Permian case study. Palaeogeography, Palaeoclimatology, Palaeoecology 228, 305–319.
Sheldon, N.D., 2006a. Abrupt chemical weathering increase across the Permian–Triassic boundary. Palaeogeography, Palaeoclimatology, Palaeoecology 231, 315–321.
Sheldon, N.D., 2006b. Precambrian paleosols and atmospheric CO_2 levels. Precambrian Research 147, 148–155.
Sheldon, N.D., 2006c. Quaternary glacial–interglacial climate cycles in Hawaii. Journal of Geology 114, 367–376.
Sheldon, N.D., 2006d. Using paleosols of the picture Gorge Basalt to reconstruct the middle Miocene climatic optimum. Paleobios 26, 27–36.
Sheldon, N.D., 2008. C_4 ecosystems in Montana throughout the Neogene. Geological Society of America Abstracts with Programs 40 (7), 126–127.
Sheldon, N.D., 2009. Non-marine records of climatic change across the Eocene-Oligocene transition. In: Koeberl, C., Montanari, A. (Eds.), The Late Eocene Earth - Hothouse, Icehouse, and Impacts: Geological Society of America Special Paper, vol. 452, pp. 241–248.
Sheldon, N.D., Retallack, G.J., 2001. Equation for compaction of paleosols due to burial. Geology 29, 247–250.
Sheldon, N.D., Retallack, G.J., 2002. Low oxygen levels in earliest Triassic soils. Geology 30, 919–922.
Sheldon, N.D., Retallack, G.J., 2003. Low oxygen levels in earliest Triassic soils: Comment and Reply. Geology 31, e20–21.
Sheldon, N.D., Retallack, G.J., 2004. Regional Paleoprecipitation Records from the Late Eocene and Oligocene of North America. Journal of Geology 112, 487–494.
Sheldon, N.D., Retallack, G.J., 2007. Non-marine records of climatic change across the Eocene–Oligocene transition. Geological Society of America Penrose Conference: The Late Eocene Earth, pp. 66–68.
Sheldon, N.D., Retallack, G.J., Tanaka, S., 2002. Geochemical climofunctions from North America soils and application to paleosols across the Eocene–Oligocene boundary in Oregon. Journal of Geology 110, 687–696.
Sheldon, N.D., Mitchell, R.L., Collinson, M.E., Hooker, J.J., 2009. Eocene-Oligocene transition paleoclimate record from paleosols, Isle of Wight (UK). In: Koeberl, C., Montanari, A. (Eds.), The Late Eocene Earth - Hothouse, Icehouse, and Impacts: Geological Society of America Special Paper, vol. 452, pp. 241–248.
Sheppard, S.M.F., 1977. The Conubian Bathoith, SW England; D/H and $^{18}O/^{16}O$ studies of kaolinite and other alteration minerals. Journal of the Geological Society London 133, 573–591.
Sheppard, S.M.F., Gilg, H.A., 1996. Stable isotope geochemistry of clay minerals; the story of sloppy, sticky, lumpy and tough, Cairns–Smith (1971). Clay Min. 31, 1–24.
Sheppard, S.M.F., Gustafson, L.B., 1976. Oxygen and hydrogen isotopes in porphyry copper-deposit at El Salvador, Chile. Economic Geology 71, 1549–1559.
Sheppard, S.M.F., Taylor, H.P., 1974. Hydrogen and oxygen isotope evidence for the origins of water in the Boulder batholith and the Butte Ore deposits, Montana. Economic Geology and Bulletin of the Society of Economic Geology 69, 926–946.
Sheppard, S.M.F., Nielsen, R.L., Taylor Jr., H.P., 1969. Oxygen and hydrogen isotope ratios of clay minerals fro porphyry copper deposits. Economic Geology 64, 755–777.
Simeone, R., Dilles, J.H., Padalino, G., Palomba, M., 2005. Mineralogical and stable isotope studies of kaolin deposits; shallow epithermal systems of western Sardinia, Italy. Economic Geology and Bulletin of the Society of Economic Geology 100, 115–130.
Sinha, A., Stott, L.D., 1994. New atmospheric pCO_2 estimates from paleosols during the late Paleocene early Eocene global warming interval. Global and Planetary Change 9, 297–307.
Sinha, R., Tandon, S.K., Sanyal, P., Gibling, M.R., Stuben, D., Berner, Z., Ghazanfari, P., 2006. Calcretes from a Late Quaternary interfluve in the Ganga Plains, India: carbonate types and isotopic systems in a monsoonal setting. Palaeogeography, Palaeoclimatology, Palaeoecology 242, 214–239.
Sleep, N.H., 2004. Archaean palaeosols and Archaean air. Nature 432. doi:10.1038/nature03167.
Smith, R., Botha, J., 2005. The recovery of terrestrial vertebrate diversity in the South African Karoo Basin after the end-Permian extinction. Comptes Rendus Paleovol 4, 623–636.
Soil Survey Staff, 1975. Soil Taxonomy: United States Department of Agriculture Handbook no. 436. Washington D.C., 754 pp.
Soil Survey Staff, 2003. Keys to Soil Taxonomy, 9th ed. USDA-ARS, Washington, DC.
Soil Survey Staff, 2006. Keys to Soil Taxonomy, 10th ed. USDA-Natural Resources Conservation Service, Washington, D.C. 341 pp.
Soloman, D.K., Cerling, T.E., 1987. The annual carbon dioxide cycle in a montane soil: observations, modeling, and implications for weathering. Water Resources Research 23, 2257–2265.
Sparks, D.L., 2003. Environmental Soil Chemistry. Academic Press, San Diego. 352 pp.
Spencer, E., 1925. On some occurrences of spherulitic siderite and other carbonates in sediments. Journal of the Geological Society London 81, 667–705.
Srivastava, P., 2001. Paleoclimatic implications of pedogenic carbonate in Holocene soils of the Gangetic Plains. Palaeogeography Palaeoclimatology Palaeoecology 172, 207–259.
Srivastava, P., Bhattacharyya, T., Pal, D.K., 2002. Significance of the formation of calcium carbonate minerals in the pedogenesis and management of cracking clay soils (Vertisols) of India. Clays and Clay Research 50, 111–126.
Srodon, J., 1999. Use of clay minerals in reconstructing geological processes; recent advances and some perspectives. Clay Minerals 34, 27–37.
Stern, L.A., Chamberlain, C.P., Reynolds, R.C., Johnson, G.D., 1997. Oxygen isotope evidence of climate change from pedogenic clay minerals in the Himalayan molasses. Geochimica et Cosmochimica Acta 61, 731–744.
Stewart, R.N.T., Fallick, A.E., Haszeldine, R.S., 1994. Kaolinite growth during pore-water mixing – isotopic data from Paleocene sands, North-Sea, UK. Clay Minerals 29, 627–636.
Stiles, C.A., Stensvold, K.A., 2008. Loess contribution to soils forming on dolostone in the Driftless Area of Wisconsin. Soil Science Survey of America Journal 72, 650–659.
Stiles, C.A., Mora, C.I., Driese, S.G., 2001. Pedogenic iron-manganese nodules in Vertisols: a new proxy for paleoprecipitation? Geology 29, 943–946.
Stiles, C.A., Mora, C.I., Driese, S.G., 2003. Pedogenic processes and domain boundaries in a Vertisol climosequence: evidence from titanium and zirconium distribution and morphology. Geoderma 116, 279–299.
Stoops, G., 1983. SEM and light microscopic observations of minerals in bog-ores of the Belgian Campine. Geoderma 30, 179–186.
Strauss, H., Peters-Kottig, W., 2003. The Paleozoic to Mesozoic carbon cycle revisited: the carbon isotopic composition of terrestrial organic matter. Geochemistry, Geophysics, Geosystems 4, 1–12. doi:10.1029/2003GC000555.
Strömberg, C.A.E., 2002. The origin and spread of grass-dominated ecosystems in the Late Tertiary of North America: preliminary results concerning the evolution of hypsodonty. Palaeogeography Palaeoclimatology Palaeoecology 177, 59–75.
Stute, M., Schlosser, P., 1993. Principles and applications of the nobel gas paleothermometer. In: Swart, P.K., Lohmann, K.C., McKenzie, J., Savin, S. (Eds.), Climate Change in Continental Isotopic Records. Geophysical Monograph, vol. 78, pp. 89–100.
Stute, M., Schlosser, P., Clark, J.F., Broecker, W.S., 1992. Paleotemperatures in the southwestern United States derived from noble gas measurements in groundwater. Science 256, 1000–1003.
Suchecki, R.K., Hubert, J.F., Dewet, C.C.B., 1988. Isotopic imprint of climate and hydrogeochemistry on terrestrial strata of the Triassic-Jurassic Hartford and Fundy Rift Basins. Journal of Sedimentary Petrology 58, 801–811.
Suzuoki, T., Epstein, S., 1976. Hydrogen isotope fractionation between OH-bearing minerals and water. Geochimica et Cosmochimica Acta 40, 1229–1240.
Tabor, N.J., 2007. Permo-Pennsylvanian palaeotemperatures from Fe-Oxide and phyllosilicate $\delta^{18}O$ values. Earth Planetary Science Letters 253, 159–171.
Tabor, N.J., Montañez, I.P., 2002. Shifts in late Paleozoic atmospheric circulation over western equatorial Pangea: insights from pedogenic mineral $\delta^{18}O$ compositions. Geology 30, 1127–1130.
Tabor, N.J., Montañez, I.P., 2004. Morphology and distribution of fossil soils in the Permo-Pennsylvanian Wichita and Bowie Groups, north-central Texa, USA: implications for western equatorial Pangean palaeoclimate during the icehouse-greenhouse transition. Sedimentology 51, 851–884.
Tabor, N.J., Montañez, I.P., 2005. Oxygen and hydrogen isotope compositions of Permian pedogenic phyllosilicates: development of modern surface domain arrays and implications for paleotemperature reconstructions. Palaeogeography, Palaeoclimatology, Palaeoecology 223, 127–146.
Tabor, N.J., Yapp, C.J., 2005a. Coexisting goethite and gibbsite from a high-paleolatitude (55°N) Late Paleocene laterite: concentration and $^{13}C/^{12}C$ ratios of occluded CO_2 and associated organic matter. Geochimica et Cosmochimica Acta 69, 5495–5510.

Tabor, N.J., Yapp, C.J., 2005b. Incremental vacuum dehydration–decarbonation experiments on a natural gibbsite (α-$Al(OH)_3$): CO_2 abundance and $\delta^{13}C$ values. Geochimica et Cosmochimica Acta 69, 519–527.
Tabor, N.J., Yapp, C.J., 2005c. Juxtaposed Permian and Pleistocene isotopic archives: Surficial environments recorded in calcite and goethite from the Wichita Mountains, Oklahoma. Geological Society of America Special Paper 395, 55–70.
Tabor, N.J., Montañez, I.P., Southard, R.J., 2002. Mineralogical and stable isotopic analysis of pedogenic proxies in Permo-Pennsylvanian paleosols: Implications for paleoclimate and paleoatmospheric circulation. Geochimica et Cosmochimica Acta 66, 3093–3107.
Tabor, N.J., Montañez, I.P., Zierenberg, R., Currie, B.S., 2004a. Mineralogical and geochemical evolution of a basalt-hosted fossil soil (Late Triassic, Ischigualasto Formation, northwest Argentina); Potential for paleoenvironmental reconstruction. Geological Society of America Bulletin 116, 1280–1293.
Tabor, N.J., Yapp, C.J., Montañez, I.P., 2004b. Goethite, calcite, and organic matter from Permian and Triassic soils: carbon isotopes and CO_2 concentrations. Geochimica et Cosmochimica Acta 68, 1503–1517.
Tabor, N.J., Montanez, I.P., Kelso, K.A., Currie, B.S., Shippman, T.A., 2006. A late Triassic soil catena: landscape controls on paleosol morphology across the Carnian–Age Ischigualasto–Villa Union Basin, Northwestern Argentina. In: Alonso-Zarza, A.M., Tanner, L.H. (Eds.), Paleoenvironmental Record and Applications of Calcretes and Palustrine Carbonates. Geological Society of America Special Paper, vol. 416, pp. 17–41.
Tabor, N.J., Montanez, I.P., Steiner, M., Schwindt, D., 2007. The $\delta^{13}C$ values of Permo-Triassic carbonates from South Africa reflect a stinking, sulfurous swamp, not atmospheric conditions. Palaeogeography, Palaeoclimatology, Palaeoecology 225, 370–381.
Takashima, R., Nishi, H., Huber, B.T., Leckie, R.M., 2006. Greenhouse world and the Mesozoic Ocean. Oceanography 19, 82–93.
Takeuchi, A., Larson, P.B., Suzuki, K., 2007. Influence of paleorelief on the Mid-Miocene climate variation in southeastern Washington, northeastern Oregon and western Idaho, USA. Palaeogeography, Palaeoclimatology, Palaeoecology 254, 462–476.
Tandon, S.K., Sood, A., Andrews, J.E., Dennis, P.F., 1995. Paleoenvironments of the dinosaur-bearing Lameta Beds (Maastrichtian), Narmada Valley, central India. Palaeogeography, Palaeoclimatology, Palaeoecology 117, 153–184.
Tardy, Y., Kobilsek, B., Roquin, C., Paquet, H., 1990a. Influence of Periatlantic climates and paleoclimates on the distribution and mineralogical composition of bauxites and ferricretes. Chemical Geology 84, 179–182.
Tardy, Y., Koilsek, B., Roquin, C., Paquet, H., 1990b. Influence of Periatlantic climates and paleoclimates on the distribution and mineralogical composition of bauxites and ferricretes. Geochemistry of the Earth's Surface and of Mineral Formation 2, 179–181.
Taylor Jr., H.P., Epstein, S., 1964. Comparison of Oxygen Isotope Analysies of Tektites, Soils, and Impactite Glasses, Chapter 14. North-Holland Publishing, Amsterdam, pp. 181–199.
Terry, D.O., 2001. Paleopedology of the Chadron Formation of northwestern Nebraska: implications for paleoclimatic change in the North American mid-continent across the Eocene–Oligocene boundary. Palaeogeography, Palaeoclimatology, Palaeoecology 168, 1–38.
Thornthwaite, C., 1948. An approach toward a rational classification of climate. Geographical Reviews 38, 55–94.
Tipple, B.J., Pagani, M., 2007. The early origins of terrestrial C_4 photosynthesis. Annual Reviews of Earth and Planetary Sciences 35, 435–461.
Trueman, C.N., 1999. Rare earth element geochemistry and taphonomy of terrestrial vertebrate assemblages. Palaios 14, 555–568.
Tyler, G., 2004. Rare earth elements in soil and plant systems – a review. Plant and Soil 267, 191–206.
Ufnar, D.F., Gonzalez, L.A., Ludvigson, G.A., Brenner, R.L., Witzke, B.J., 2002. The mid-Cretaceous water bearer: isotope mass balance quantification of the Albian hydrologic cycle. Palaeogeography, Palaeoclimatology, Palaeoecology 188, 51–71.
Ufnar, D.F., Ludvigson, G.A., Gonzalez, L.A., Brenner, R.L., Witzke, B.J., 2004. High latitude meteoric ^{18}O compositions: Paleosol siderite in the Middle Cretaceous Nanushuk Formation, North Slope, Alaska. Geological Society of America Bulletin 16, 463–473.
Uhl, D., Klotz, S., Traiser, C., Thiel, C., Utescher, T., Kowalski, E., Dilcher, D., 2007. Cenozoic paleotemperatures and leaf physiognomy: a European perspective. Palaeogeography, Palaeoclimatology, Palaeoecology 248, 24–31.
Utescher, T., Mosbrugger, V., 2007. Eocene vegetation patterns reconstructed from plant diversity: a global perspective. Palaeogeography, Palaeoclimatology, Palaeoecology 247, 243–271.
Uysal, I.T., Golding, S.D., Baublys, K., 2000. Stable isotope geochemistry of authigenic clay minerals from Late Permian coal measures, Queensland, Australia; implications for the evolution of the Bowen Basin. Earth Planetary Science Letters 180, 149–162.
Valley, J.W., Taylor Jr., H.P., O'Neil, J.R., 1986. Stable isotopes in high temperature geological processes. Reviews in Mineralogy 16 570 pp.
van der Weijden, C.H., van der Weijden, R.D., 1995. Mobility of major, minor and some redox-sensitive trace elements and rare-earth elements during weathering of four granitoids in central Portugal. Chemical Geology 125, 149–167.
Van Houten, F.B., 1961. Climatic significance of red beds. In: Nairn, A.E.M. (Ed.), Descriptive paleoclimatology. Interscience Publishers, pp. 89–139.
Van Houten, F.B., 1982. Ancient soils and ancient climates. Climate in Earth History, U.S. National Research Council, Geophysics Study Committee, pp. 112–117.
Vepraskas, M.J., 1992. Redoximorphic features for identifying aquic conditions:North Carolina Agricultural Research Service, Raleigh, North Carolina. Technical Bulletin, vol. 301. 33 pp.
Vinogradov, A.P., 1959. Geochemistry of Core and Dispersed Chemical Elements in Soils. Translated by Consultants Bureau, New York. 209 pp.
Vitali, F., Longstaffe, F.J., Bird, M.I., Caldwell, W.G.E., 2000. Oxygen-isotope fraction between aluminum-hydroxide phases and water at < 60 degree C: results of decade-long synthesis experiments. Clay and Clay Minerals 48, 230–237.
Vitali, F., Longstaffe, F.J., Bird, M.I., Gage, K.L., Caldwell, W., Glen, E., 2001. Hydrogen-isotope fractionation in aluminum hydroxides; synthesis products versus natural samples from bauxites. Geochimica et Cosmochimica Acta 65, 1391–1398.
Vitali, F., Longstaffe, F.J., McCarthy, Plint, P.J., Guy, A., Caldwell, W., Glen, E., 2002. Stable isotopic investigation of clay minerals and pedogenesis in an interfluve paleosol from the Ceonomanian Dunvegan Formation, N.E. British Columbia, Canada. Chemical Geology 192, 269–287.
Volk, T., 1987. Feedbacks between weathering and atmospheric CO_2 over the last 100 million years. American Journal of Science 287, 263–279.
Walter, A.V., Nahon, D., Flicoteaux, R., Girard, J.P., Melfi, A., 1995. Behaviour of major and trace elements and fractionation of REE under tropical weathering of typical apatite-rich carbonatite from Brazil. Earth and Planetary Science Letters 136, 591–601.
Whelan III, T., Roberts, H.H., 1973. Carbon isotope composition of diagenetic carbonate nodules from freshwater swamp deposits. Journal of Sedimentary Petrology 43, 54–58.
Whelan, J.F., Cobb, J.C., Rye, R.O., 1998. Stable isotope geochemistry of sphalerite and other mineral matter in coal beds from the Illinois and Forest City basins. Economic Geology and the Bulletin of the Society of Economic Geology 83, 990–1007.
Whipkey, C.E., Capo, R.C., Hsieh, J.C.C., Chadwick, O.A., 2002. Development of magnesian carbonates in Quaternary soils on the Island of Hawaii. Journal of Sedimentary Research 72, 138–165.
White, T., Gonzalez, L., Ludvigson, G., Poulsen, C., 2001. Middle Cretaceous greenhouse hydrologic cycle of North America. Geology 29, 363–366.
White, T., Witzke, B., Ludvigson, G., Brenner, R., 2005. Distinguishing base-level change and climate signals in a Cretaceous alluvial sequence. Geology 33, 13–16.
Whiticar, M.J., Faber, E., Schoell, M., 1986. Biogenic methane formation in marine and freshwater environments: CO_2 reductions vs. acetate fermentation — isotope evidence. Geochimica et Cosmochimica Acta 50, 693–709.
Wilson, J.J., 1999. The origin and formation of clay minerals in soil; past, present and future perspectives. Clay Mineralogy 34, 7–25.
Wimpenny, J., Gannoun, A., Burton, K.W., Widdowson, M., James, R.H., Gíslason, S.R., 2007. Rhenium and osmium isotope and elemental behaviour accompanying latering formation in the Deccan region of India. Earth and Planetary Science Letters 261, 239–258.
Wolfe, J.A., 1994. Tertiary climatic changes at middle latitudes of western North America. Palaeogeography, Palaeoclimatology, Palaeoecology 108, 195–205.
Wood, W.W., Petraitis, M.J., 1984. Origin and distribution of carbon dioxide in the unsaturated zone of the southern high plains of Texas. Water Resources 20, 1193–1208.
Yamaguchi, M., Flocker, W.J., Howard, F.D., 1967. Soil atmosphere as influenced by Temperature and Moisture. Soil Science Society of America Proceedings 31, 164–167.
Yapp, C.J., 1987a. Oxygen and hydrogen isotope variations among goethites (α-FeOOH) and the determination of paleotemperatures. Geochimica et Cosmochimica Acta 51, 945–957.
Yapp, C.J., 1987b. A possible goethite-iron (III) carbonate solid solution and the determination of CO_2 partial pressures in low temperature geologic systems. Chemical Geology 64, 259–268.
Yapp, C.J., 1990. Oxygen isotopes in iron (III) oxides 1. mineral-water fractionation factors. Chemical Geology 85, 329–355.
Yapp, C.J., 1993a. The stable isotope geochemistry of low temperature Fe(III) and Al "Oxides" with implications for continental paleoclimates. In: Swart, P.K., Lohmann, K.C., McKenzie, J., Savin, S. (Eds.), Climate Change in Continental Isotopic Records. Geophysical Monograph, vol. 78, pp. 285–294.
Yapp, C.J., 1993b. Paleoenvironment and oxygen isotope geochemistry of ironstone of the Upper Orovician Neda Formation, Wisconsin, USA. Geochimica et Cosmochimica Acta 57, 2319–2327.
Yapp, C.J., 1998. Paleoenvironmental interpretations of oxygen isotope ratios in oolitic ironstones. Geochimica et Cosmochimica Acta 62, 2409–2420.
Yapp, C.J., 2000. Climatic implications of surface domains in arrays of δD and $\delta^{18}O$ from hydroxyl minerals: Geothite as an example. Geochimica et Cosmochimica Acta 64, 2009–2025.
Yapp, C.J., 2001a. Mixing of CO_2 in surficial environments as recorded by the concentration and $\delta^{13}C$ values of the $Fe(CO_3)OH$ component in goethite. Geochimica et Cosmochimica Acta 65, 4115–4130.
Yapp, C.J., 2001b. Rusty relics of earth history: Iron (III) oxides, isotopes, and surficial environments. Annual Review of Earth and Planetary Sciences 29, 165–199.
Yapp, C.J., 2002. ERRATUM. Geochim. Cosmochim. Acta 66, 1497.
Yapp, C.J., 2004. Fe(CO)OH in goethite from a mid-latitude North American Oxisol: estimate of atmospheric CO_2 concentration in the Early Eocene "climatic optimum". Geochim. Cosmochim. Acta 68, 935–947.
Yapp, C.J., Pedley, M.D., 1985. Stable hydrogen isotopes in iron oxides. II. D/H variations among natural goethites. Geochimica et Cosmochimica Acta 49, 487–495.
Yapp, C.J., Poths, H., 1991. $^{13}C/^{12}C$ ratios of the Fe(III) carbonate component in natural goethites. In: Taylor, H.P., O'Neil, J.R., Kaplan, I.R., I.R. (Eds.), Stable Isotope Geochemistry: A Tribute to Samuel Epstein. The Geochemical Society, San Antonio, U.S.A., pp. 257–270.
Yapp, C.J., Poths, H., 1992. Ancient atmospheric CO_2 pressures inferred from natural goethites. Nature, 355, 342–344.
Yapp, C.J., Poths, H., 1993. The carbon isotope geochemistry of gtoethite (α-FeOOH) in ironstone of the Upper Ordovician Neda Formation, Wisconsin, USA: implications for early Paleozoic continental environments. Geochimica et Cosmochimica Acta, 57, 2599–2611.

Yapp, C.J., Poths, H., 1996. Carbon isotopes in continental weathering environments and variations in ancient atmospheric CO_2 pressure. Earth Planetary Science Letters 137, 71–82.

Yeh, H.W., 1980. D/H ratios and late-stage dehydration of shale during burial. Geochimica et Cosmochimica Acta 44, 341–352.

Yeh, H.-W., Epstein, S., 1978. Hydrogen isotope exchange between clay minerals and sea water. Geochimica et Cosmochimica Acta 42, 140–143.

Yeh, H.-W., Savin, S.M., 1977. Mechanism of burial metamorphism on argillaceous sediments, 3. Oxygen isotope evidence. Geological Society of America Bulletin 88, 1321–1330.

Yemane, K., Siegenthaler, C., Kelts, K., 1989. Lacustrine environment during Lower Beaufort (Upper Permian) Karoo deposition in northern Malawi. Palaeogeography Palaeoclimatology Palaeoecology 70, 165–178.

Yiu, T.F., Chang, S.S., 1999. Formation conditions of vesicle/fissure-filling smectites in Penghu basalts; a stable isotope assessment. Clay Minerals 34, 381–393.

Yurtsever, Y., Gat, J.R., 1981. Atmospheric waters. In: Gat, J.R., Gonfiantini, R. (Eds.), Stable Isotope Hydrology: Deuterium and Oxygen-18 in the Water Cycle. IAEA Technical Reprint Series, vol. 210, pp. 103–142.

Zbinden, E.A., Holland, H.D., Feakes, C.R., 1988. The Sturgeon Falls paleosol and the composition of the atmosphere 1.1 Ga BP. Precambrian Research 42, 141–163.

Zhang, G.-L., Pan, J.-H., Huang, C.-M., Gong, Z.-T., 2007. Geochemical features of a soil chronosequence developed on basalt in Hainan Island, China. Revista Mexicana de Ciencias Geológicos 24, 261–269.

Ziegler, C.L., Murray, R.W., Hovan, S.A., Rea, D.K., 2007. Resolving eolian, volcanogenic, and authigenic components in pelagic sediment from the Pacific Ocean. Earth and Planetary Science Letters 254, 416–432.